DOCTOR OF PHILOSOPHY

On the mechanical properties of bast fibre reinforced thermosetting polymer matrix composites.

Hughes, John Mark

Award date:
2000

Awarding institution:
Bangor University

On the Mechanical Properties of Bast Fibre Reinforced Thermosetting Polymer Matrix Composites

A thesis submitted for the degree of Doctor of Philosophy of the University of Wales

by

John Mark Hughes

School of Agricultural and Forest Sciences
University of Wales,
Bangor, Gwynedd, United Kingdom

May 2000

Acknowledgements

Firstly, I would like to thank my supervisors Drs Jamie Hague and Callum Hill, for their invaluable guidance, support, and enthusiasm throughout the course of this work.

I would also like to thank the many other members of staff whose help and assistance made it possible for me to complete the experimental part of the project. In particular I would like to thank Mr Duncan Easter, Mr John Evans, Mr Jim Frith, Dr Mike Hale, Mr Gwyn Lloyd Jones, Mr Dick Salisbury, Mrs Helen Simpson, Ms Becky Snell and Dr Richard Quinney.

Furthermore, I would like to thank all those staff and colleagues who have, in one way or another been involved in this work and with whom varied and useful discussions have helped shape this thesis. I would, in particular like to mention Dr James Bolton, Dr Martin Breese, Dr Pat Denne, Professor John Dinwoodie, Dr Laurence Mott, Mr Gary Newman and Dr Gilles Sèbe.

I would like to acknowledge the financial support given by Messrs. Watkin Jones Ltd. and The BioComposites Centre by way of a University studentship.

I would also like to thank all my friends and colleagues, who have made this period of study such an enjoyable experience for me: Shaheen Akhter, Nihat Cetin, George Goroyias, Andy Horne, José Lima, Lokmal, Steve Mallon, Khalil Shawtakaly and Morwenna Spear.

Finally, I would like to thank Saija and my parents and family for their love, support and encouragement.

Abstract

Bast fibre reinforced, unsaturated polyester matrix composites were fabricated using non-woven mats of hemp or jute fibre as reinforcement. Composites were also prepared using chopped strand mat glass fibre as reinforcement. The short-term mechanical properties of the laminates were assessed. It was observed that at equivalent fibre volume fractions the stiffness of the glass fibre reinforced material only marginally exceeded that of the two, unmodified bast fibre, reinforced materials. At equivalent fibre volume fractions, however, the strength of the glass fibre reinforced composite was found to be significantly greater than that of the bast fibre reinforced materials. It was noted that in the bast fibre reinforced composites, the onset of non-linear behaviour occurred at relatively low applied stresses. Work of fracture in static three-point flexure and Charpy impact strength tests, indicated that the toughness of the plant fibre reinforced material was as much as an order of magnitude less than that of the glass fibre reinforced material. Fracture mechanics techniques were used to further quantify toughness and confirmed this to be so. Furthermore, these tests indicated that the microstructure of the bast fibre reinforced material should be examined more closely. Microscopy conducted on the fibres revealed that these were often subject to extensive micro-compressive damage. It was postulated that uneven fibre straining characteristics could lead to compromised interfacial properties, which might in turn detrimentally affect the macroscopic behaviour of the composite. A technique known as half fringe photoelasticity was used to investigate the stress-field in the matrix surrounding the fibre defects. It was observed that not only did concentrations of stress occur in the vicinity of these, but also that the shear stress distribution along the length of the fibre was interrupted by the presence of the defects. The implications of fibre defects upon composite properties are discussed.

Table of Contents

List of Papers

Publications:

Hughes, M., Hill, C., Sèbe, G., Hague, J., Spear, M. and Mott, L. (2000). An Investigation into the Effects of Microcompressive Defects on Interphase Behaviour in Hemp-Epoxy Composites Using Half Fringe Photoelasticity. *Composite Interfaces* **7**(1): 13-30.

Sèbe, G., Cetin, N.S., Hill, C.A.S. and Hughes, M. (2000). RTM Hemp Fiber-reinforced Polyester Composites. *Applied Composite Materials (in press).*

Eichhorn, S.J., Hughes, M., Snell, R. and Mott, L. (2000). Raman Shifts in the Spectra of Natural Cellulose Fibres. *J. Mat. Sci. Letters* **19**(8): 721-723.

Communications:

Hughes, M., Mott, L., Hague, J. and Hill, C.A.S. (1999). The Toughness of Vegetable Fibre Reinforced Unsaturated Polyester Composites. *In: Proceedings of the 5th International Conference on Woodfiber-Plastic Composites, May 26-27, 1999, Madison, WI, USA.* Forest Products Society, Madison, WI, USA.

List of Figures

List of Tables

List of Plates

Nomenclature

Symbol	*Units*	*Parameter*
a	(m)	half crack length
a	(m)	amplitude
c	(m s^{-1})	velocity of light
c	(m^2 N^{-1})	stress optic coefficient
C	(m^2 N^{-1})	relative stress optic coefficient
E_1	(GN m^{-2})	axial laminate modulus
E_2	(GN m^{-2})	transverse laminate modulus
E_f	(GN m^{-2})	fibre Young's modulus
E_m	(GN m^{-2})	matrix Young's modulus
E_r	(GN m^{-2})	laminate Young's modulus for random reinforcement
f	(Hz)	frequency
f_σ	(N m^{-1})	material fringe value
G	(kJ m^{-2})	strain energy release rate
G_C	(kJ m^{-2})	critical strain energy release rate
h	(m)	thickness of wave retarder
I	(-)	light intensity
J	(kJ m^{-2})	experimental J
J_C	(kJ m^{-2})	critical J
K	(MN $m^{-3/2}$)	stress intensity factor
K_C	(MN $m^{-3/2}$)	critical stress intensity factor
K_{IC}	(MN $m^{-3/2}$)	plane strain fracture toughness
K_J	(MN $m^{-3/2}$)	equivalent K
K_{JC}	(MN $m^{-3/2}$)	equivalent critical K
L	(m)	fibre half-length
M	(kg)	mass
M_c	(kg)	mass of composite
M_f	(kg)	mass of fibre

n	(-)	index of refraction
N	(-)	fringe order
r	(m)	fibre radius
r_y	(m)	plastic zone radius
s	(-)	fibre aspect ratio
s_c	(-)	critical fibre aspect ratio
t	(s)	time
V_f	(-)	fibre volume fraction
$V_{f\,\min}$	(-)	minimum fibre volume fraction
V_m	(-)	matrix volume fraction
V	(m^{-3})	volume
V_c	(m^{-3})	volume of composite
x	(m)	axial distance from fibre mid-point
X_c	(-)	composite property
X_f	(-)	fibre property
X_m	(-)	matrix property
Z	(-)	video response (grey level value)
Δ	(-)	angular phase shift
ε_1	(-)	applied composite strain
ε_{fu}	(-)	fibre strain at failure
ε_{mu}	(-)	matrix strain at failure
ε_{uc}	(-)	composite strain at failure
ϕ	(^{O})	loading angle
$\Delta\Phi$	(^{O})	average misorientation angle of reinforcing element
γ	(-)	log linear sensitivity curve
γ_S	(J m^{-2})	surface energy
γ_{sv}	(J m^{-2})	surface energy of solid-vapour interface
γ_{sl}	(J m^{-2})	surface energy of solid-liquid interface
γ_{lv}	(J m^{-2})	surface energy of liquid-vapour interface
λ	(m)	wavelength of light

θ	(^{O})	contact angle
ρ	(kg m^{-3})	density
ρ_c	(kg m^{-3})	composite density
ρ_f	(kg m^{-3})	fibre density
ρ_r	(kg m^{-3})	density of cured resin
σ	(MN m^{-2})	stress
σ_{app}	(MN m^{-2})	nominal applied stress
σ_{1u}	(MN m^{-2})	laminate axial ultimate stress
σ_{2u}	(MN m^{-2})	laminate transverse ultimate stress
σ_{ru}	(MN m^{-2})	planar-random laminate ultimate stress
σ_c	(MN m^{-2})	composite applied stress
σ_{comp}	(MN m^{-2})	composite axial compressive strength
σ_{uc}	(MN m^{-2})	composite ultimate stress
σ_f	(MN m^{-2})	axial fibre stress
σ_ϕ	(MN m^{-2})	laminate off-axis ultimate tensile stress
$\overline{\sigma}_f$	(MN m^{-2})	volume averaged fibre stress
σ_{fu}	(MN m^{-2})	fibre ultimate tensile strength
σ_{fmu}	(MN m^{-2})	fibre stress at onset of matrix cracking
σ_m	(MN m^{-2})	matrix stress
σ_{mu}	(MN m^{-2})	matrix ultimate tensile strength
σ_{mfu}	(MN m^{-2})	matrix stress at onset of fibre fracture
$\overline{\sigma}_m$	(MN m^{-2})	volume averaged matrix stress
σ_{ys}	(MN m^{-2})	yield stress (0.2% proof stress)
σ_F	(MN m^{-2})	fracture stress (Griffith's criterion)
τ_{12u}	(MN m^{-2})	laminate shear strength
τ_i	(MN m^{-2})	interfacial shear stress
τ_{if}	(MN m^{-2})	frictional interfacial shear stress
τ_s	(MN m^{-2})	matrix plastic shear strength
ν_m	(-)	matrix Poisson's ratio
ω	(Hz)	angular frequency of light

1 Introduction

1.1 Background

Artificial composites, particularly polymer matrix composites such as the ubiquitous 'fibreglass', form an important class of engineering materials. It has been estimated that the growth in the use of polymer matrix composites has been running at between 5% and 10% annually - in excess of that of the polymers themselves (Matthews & Rawlings, 1994). These materials are often found in applications in which their excellent specific properties may be exploited, for example in transportation and aerospace (Ivens *et al.*, 1997). However, it should be remembered that man-made composites are by no means a new phenomenon, but have been in use for thousands of years; from the reinforced mud bricks of the Ancients to the composite bows of Medieval times (Gordon, 1976).

By far the greatest use of composite materials is made by nature; wood, bone and teeth being just a few examples of naturally occurring composites. The diversity of these natural materials is a reflection of the manner in which composites can be engineered for certain properties. Indeed, it could be argued that nature has 'selected' composites through evolutionary processes because of their excellent properties and their ability to be 'fabricated' by biosynthetic means. Further, it seems plausible that the high strength, stiffness and toughness of these materials combined with their low weight may have contributed to the development of highly dynamic life forms (including mankind) as well as to large structures such as trees.

1.2 Composite materials

Composites might be thought to consist of two (or more) distinct constituents or *phases*, which when married together, result in a material with entirely different

properties to those of the individual components. Typically, an artificial composite would consist of a *reinforcement* phase of stiff, strong material, frequently fibrous in nature, embedded in a continuous *matrix* phase. The latter is often weaker and less stiff than the former. Two of the main functions of the matrix are to transmit externally applied loads, via shear stresses at the *interface*, to the reinforcement and to protect the latter from environmental and mechanical damage (Matthews & Rawlings, 1994). The advantage of such a coupling is that the high strength and stiffness of the fibres, which would, in most practical situations be unable to transmit loads, may be exploited. Naturally occurring composites (such as bone and wood) are also reinforced with fibrous material. In the case of bone, for example, the hard crystalline mineral, hydroxyapatite ($(Ca_{10}(PO_4)_6OH)_2$) forms the reinforcement phase, embedded in a matrix of the protein, collagen (Currey, 1984; Bonfield, 1994).

An interesting feature of composites is that the different phases often act synergistically, lending improved properties to the resultant material (Norwood, 1994). By way of example, the fracture toughness (G_c) of a typical glass fibre-epoxy composite is in the region of 40-100 kJ m^{-2} and as such would be classified as a tough material. On the other hand, glass with a G_c of around 0.01 kJ m^{-2} and epoxy resin with a G_c of around 0.1 kJ m^{-2} would both be regarded as brittle (Hull & Clyne, 1996). Thus two essentially brittle substances, when brought together in the form of a composite can result in an extremely tough material (Gordon, 1976).

1.3 Polymer matrix composites

The matrices of artificial composites are often synthetic polymers derived from petrochemicals. These polymer matrix composites (PMCs) are generally reinforced with man-made fibre. Glass fibre, which accounts for some 99% of all reinforcement used in PMCs, is by far the most widely used (Owens Corning, 1996). In applications requiring especially good specific properties, however, other inorganic fibres such as boron or carbon may be utilised. Alternatively, synthetic organic fibres such as aramid might be employed (Hull & Clyne, 1996). Certain naturally occurring fibres

are also sometimes used commercially, to reinforce composite products. 'Tufnol' (composites of cotton fabric reinforced epoxy or phenolic resin), is perhaps one of the best known materials in this category, having been produced for over sixty years (Tufnol, 1991, 1992). Some typical values for the mechanical properties of several reinforcing fibres are given in Table 1.1.

Table 1.1 Mechanical properties of some synthetic and natural (plant) fibres (*Sources:* Hull & Clyne, 1996, Ivens *et al.*, 1997).

Fibre type	*Density* ($Mg\ m^{-3}$)	*Young's modulus* ($GN\ m^{-2}$)	*Tensile strength* ($MN\ m^{-2}$)	*Failure strain* (%)
Synthetic fibres				
E-glass	2.56	76	2000	2.6
high strength carbon	1.75	230	3400	3.4
Kevlar™ (aramid)	1.45	130	3000	2.3
boron	2.6	400	4000	1.0
Natural fibres				
flax	1.4-1.5	50-70	500-900	1.3-3.3
hemp	1.48	30-60	310-750	2-4
jute	1.4	20-55	200-450	2-3
sisal	1.45	9-22	80-840	3-14
cotton	1.5	6-10	300-600	6-8

Broadly speaking, the polymers comprising the matrices of PMCs may be classified as either thermosetting or thermoplastic.

1.3.1 Thermosetting polymers

These are initially liquid resins that harden into brittle solids at room temperature when cured. Curing involves chemical cross-linking, which is achieved by the application of heat and/or pressure and/or the addition of a catalyst to complete the process. Because they are initially relatively low viscosity liquids, thermosetting

resins are very versatile and can be used to produce composites of complex shape and large size (Norwood, 1994). It is estimated that in excess of 75% of all matrices in PMCs are thermosetting (Matthews & Rawlings, 1994). Examples of thermosetting polymers include; polyester, vinlyester, epoxy and phenolic resins.

1.3.2 Thermoplastic polymers

These are polymers that flow readily under the effects of heat and stress. Unlike thermosetting resins which are chemically cross-linked, bonding between the polymer chains of thermoplastics is due to Van der Waal's forces which are easily overcome, allowing for relatively easy movement between adjacent chains. Examples of thermoplastic polymers include nylon (polyamide), polyethylene, polypropylene and polyetheretherketone (PEEK) (Matthews & Rawlings, 1994). Unlike thermosetting polymers, which are relatively brittle, thermoplastic polymers can undergo considerable plastic deformation prior to failure and as such are comparatively tough (Hull & Clyne, 1996). A summary the mechanical properties of a number of polymers is presented in Table 1.2.

Whilst the utility of composite materials based on synthetic polymers reinforced with man-made fibres cannot be seriously disputed, there are a number of potentially serious environmental issues associated with their use. In recent years, this has helped focus attention on the potential for replacing one or both of the synthetic phases with alternative materials derived from renewable resources.

Table 1.2 Selected properties for different polymers (*Source:* Hull & Clyne, 1996).

Matrix	*Density* ($Mg\ m^{-3}$)	*Young's modulus* ($GN\ m^{-2}$)	*Tensile strength* ($MN\ m^{-2}$)	*Failure strain* (%)
Thermosets				
epoxy resins	1.1-1.4	3-6	35-100	1-6
polyesters	1.2-1.5	2.0-4.5	40-90	2
Thermoplastics				
Nylon 6.6	1.14	1.4-2.8	60-70	40-80
polypropylene	0.9	1.0-1.4	20-40	300
PEEK	1.26-1.32	3.6	170	50

1.4 Natural fibre reinforced PMCs

Whilst the ultimate aim might be to manufacture structural composites entirely from renewable resources (i.e. both reinforcement and matrix), a number of environmental issues could be dealt with by realising the substitution of synthetic (primarily glass) fibres with natural fibres. In recent years a significant number of articles have appeared in the literature which discuss the environmental (and other) benefits of utilising various plant fibres as reinforcement in both thermoplastic and thermosetting PMCs (e.g. Rowell, 1992; Robson *et al.*, 1993; Bolton, 1994, 1995; Carruthers, 1994; Hill, 1997; Ivens *et al.*, 1997; Olesen & Plackett, 1999; Schuh, 1999). No attempt will be made here to extensively review all the issues pertaining to the substitution of synthetic fibres with naturally derived ones. Nevertheless, it is appropriate to mention some of the more salient points which have been raised.

1.4.1 Environmental considerations

Glass fibre, which forms by far the greatest proportion of reinforcement used in PMCs, has a high embodied energy content of around 30 GJ/tonne. This compares with around 4 GJ/tonne for plant fibre material (Bolton, 1995). However, with the

latter, this embodied energy may be partially recovered, either by composting or incineration. Neither of these options are available for glass fibre. This raises the question of the disposal of a product or structure at the end of its working life. With glass fibre reinforced material, the only sensible option is to landfill the material, since recycling (only really relevant to thermoplastics) may be problematic. With plant fibre reinforced material, however, the possibility exists to either compost or incinerate, thereby avoiding the necessity to landfill and at the same time recover some of the aforementioned energy content of the fibre (and that of the matrix too).

Plant fibres are CO_2 neutral. Only atmospheric carbon dioxide is used to produce the fibres in the plant, which is subsequently liberated upon incineration or composting. Thus, the net change in the CO_2 balance is zero. Although glass fibres themselves contain no CO_2, the energy required for their manufacture doubtless accounts for a net increase in atmospheric carbon dioxide (due to the burning of fossil fuels).

Today, one of the problems being faced (particularly in Europe) is that of food over production. Certain fibre crops, notably flax and hemp have traditionally been grown in Europe (Dempsey, 1975). If new, high added value, industrial applications could be found for these fibres then this could help solve these problems by switching land usage to annually harvested fibre crops.

Although not environmental issues, it is worthwhile noting that plant fibres are potentially less hazardous to health, they are more pleasant to work with and furthermore, since they are less abrasive than glass fibres, they do not blunt tools to the same extent.

1.4.2 Economic viability

Cost is potentially an area in which natural fibres could score highly over their synthetic counterparts. Table 1.3 shows a comparison between the prices of three synthetic fibres and three natural fibres (Ivens *et al.*, 1997). As may be noted, the prices of all three plant fibres are less than that of E-glass and significantly less than either carbon or aramid fibres. Nevertheless, it should be borne in mind that there is

often considerable variation in the price of natural fibre depending upon factors such as the type and extent of processing (Ivens *et al.*, 1997) and whether the fibre is to be used in any high added value products, such as textiles (Robson *et al.*, 1993; Ivens *et al.*, 1997). For instance, the price of flax can increase approximately ten-fold after spinning and still further after weaving (Sharma, 1999).

Table 1.3 Comparison between the costs of artificial and natural fibres (*Source:* Ivens *et al.*, 1997).

Fibre type	*Cost (ECU/kg)*
E-glass	1.5-2.5
Carbon fibre	30-50
Aramid	20-35
Flax	0.5-1
Hemp	0.5-1
Jute	0.5

Additional costs would undoubtedly be incurred in making natural fibres suitable for composite manufacture. These might include cleaning to improve adhesion to the matrix or further breakdown processes, for instance steam explosion (Kessler & Kohler, 1996). Alternatively, some form of chemical modification or surface treatment may be required (Chum & Power, 1992). In addition, it may be necessary to process the fibres (for example by weaving or using non-woven technology) into a form suitable for use as reinforcement in composite fabrication (Ivens *et al.*, 1997).

1.4.3 Technical aspects

As may be noted from Table 1.1, the tensile properties of the vegetable fibre, in general, do not compare particularly favourably with the synthetics, even glass fibre. However, when density is taken into account and the specific properties, especially stiffness, are compared (Table 1.4), then vegetable fibres start to look more attractive.

Table 1.4 Specific tensile properties of reinforcing fibres (*Source:* Ivens *et al.*, 1997).

Fibre	*Specific tensile strength (MN m^{-2})*	*Specific Young's modulus (GN m^{-2})*
E-glass	980-1367	27-29
Flax	345-620	34-48
Hemp	210-510	20-41
Jute	140-320	14-39
Sisal	55-580	6-15

As will be discussed more fully in the following chapter, however, it should be borne in mind that the mechanical properties of composites are governed to a large extent by the volume, rather than mass, fraction of reinforcement used (Mathews & Rawlings, 1994). Consequently, it will be the absolute, rather than the specific, properties that will have the greatest impact upon the ultimate performance of the composite. Nevertheless, for a given volume loading of fibre, the density of a plant fibre reinforced composite will be lower than that of a glass fibre reinforced equivalent, leading to enhanced specific composite properties.

On a purely performance or cost basis, the suitability of vegetable fibres as reinforcement in PMCs is open to question. However, if environmental concerns are to be addressed, then plant fibres offer a potentially attractive alternative to manmade fibres.

1.5 Fibre selection

1.5.1 Fibre technical specification

For fibres to act effectively as reinforcement in polymeric matrices, they must possess good tensile stiffness and strength as well as failure strains similar to those of the matrices (Riedel, 1999; Riedel *et al.*, 1999). If the strain to failure is very much

greater than that of the matrix, insufficient stress build-up in the fibre would be achieved prior to matrix failure, resulting in poor reinforcing efficiency. In addition to this, it would be of benefit if the fibres were relatively thin and possessed high aspect ratios; that is to say they were long in comparison to their diameter. This would provide the greatest possible surface area for adhesion between the phases, as well making preferential alignment of the fibres possible, allowing for some scope in tailoring composite properties. In addition to this thin, high aspect ratio fibres are typically easier to process (*cf.* the spinning of cotton and flax).

From a techno-economic standpoint, it would also be advantageous if the fibres were derived from an established and widely used industrial crop, with a good understanding of growth factors and fibre isolation procedures.

In a European context, the fibre types which would appear to most closely "fit the bill" are flax (*Linum usitatissimum*) and hemp (*Cannabis sativa*). Flax is still widely cultivated and processed for textiles in Europe (Franck, 1992; Mackie, 1992), whilst until fairly recent times hemp was grown for textiles, cordage etc. and is now enjoying something of a revival. Jute (*Corchorus capsularis*), another potentially suitable fibre, is generally widely available in Europe, imported from Asia. The work presented herein concentrates (but not exclusively) on hemp. This is primarily because of the resurgent interest in the U.K. and Europe in this fibre type, for industrial applications. As will be discussed in the forthcoming chapters, it is believed that many of the findings may well be applicable to flax, because of the similar ultrastructural organisation of these two fibre types. A certain amount of work utilising jute as reinforcement was also conducted, and is presented herein.

1.5.2 Reinforcement processing

As noted above, the cost of woven material (e.g. linen) is significantly higher than that of the raw fibre, which might preclude this as suitable reinforcement. Air laid non-woven technology does, however, provide a potentially cost effective means of arranging fibres into a mattress structure which could be used as a basis for composite fabrication (Newman, 1999). For this reason, non-woven, needle-punched, felted fibre (hemp and jute) mats were utilised as reinforcement pre-forms in the laminates fabricated in this work.

1.6 Matrix polymer

It is perhaps worthwhile noting at this stage that, at the outset, the aim of this project was to develop a plant fibre reinforced polymer composite, suitable for commercial production. The types of products envisaged were those that might have been fabricated by hand lay-up or by resin transfer moulding (see Chapter 2). These fabrication techniques require the use of thermosetting polymers. Because of its extensive use in the type of products envisaged, the matrix polymer chosen for this study was an unsaturated polyester.

1.7 Background and rationale of the study

1.7.1 Background

The initial aim of the programme was, as noted above, to produce a plant fibre reinforced thermosetting polymer matrix material suitable for commercial production. The hope was to achieve a direct substitution of glass fibre (in the form of a random chopped strand mat) with a non-woven, needle-punched plant fibre felt. The results of preliminary investigations, however, indicated that the short-term mechanical properties of the bast fibre reinforced composites fell far short of their glass fibre

reinforced counterparts. Since this would, undoubtedly, have a direct bearing upon the potential applications for which these materials might be suitable, it was believed that the project should focus on more 'fundamental' issues concerning the material behaviour and the underlying mechanisms controlling these.

As noted in Section 1.2, one of the attributes of composite materials (particularly certain natural composites such as wood) is their excellent toughness. That is to say they possess good resistance to the propagation of cracks or 'crack-like' defects which could ultimately lead to failure of the material or structure (Gordon, 1976). Preliminary tests suggested that, for an equivalent level of reinforcement (on a volume for volume basis), the toughness of plant fibre reinforced unsaturated polyester laminates was substantially less than that of their synthetic fibre reinforced counterparts. Furthermore, it was found that chemical modification (acetylation) of the fibre, aimed at improving the environmental stability of the resultant composites, only made matters worse. This was unfortunate, since it had been originally believed that chemical or surface modification could be used to improve composite properties (see Section 2.6.2). Although this was achieved to some extent (particularly with regard to long-term exposure to wet and biologically aggressive environments), the loss in toughness was deemed to be of overriding concern. As a result, whilst the use of chemical modification was studied (although none of the results are presented herein) it was felt that a far more profitable approach would be that of a thorough appraisal of the material itself. This, it was believed, should be conducted at several levels of organisation, from the laminates themselves, to the fibres and the interaction between the two phases. It was believed that such an approach would highlight factors limiting composite performance and thereby help identify ways in which performance improvements might be gained.

After preliminary studies, this work took shape as an investigation into the mechanical properties of plant fibre reinforced thermosetting PMCs and was effectively split into three sections. Firstly, the mechanical properties of the laminates themselves were considered, secondly the reinforcing fibres were investigated and finally the interaction between the fibre and matrix at the interface or interphase was studied.

1.7.2 Structure of thesis

The following chapter provides, by way of a literature review, relevant theoretical background in support of the remainder of the thesis. This includes a brief description of the biology and ultrastructure appropriate to hemp, flax and jute fibres as well as describing the biochemistry and technology of the fibre isolation process. In addition to this, the chemistry of unsaturated polyester and epoxy resins is briefly reviewed. A short overview of the main composite fabrication methods employed is presented. Some relevant aspects of composite materials science and mechanics are also included. In addition to the foregoing, Chapter 2 contains a review of the literature pertaining to plant fibre reinforced thermosetting PMCs.

Chapter 3 encompasses the mechanical properties of laminates reinforced with non-woven, needle punched felts. Selected preliminary results as well as those of more extensive tensile, flexural, Charpy impact strength, and fracture toughness tests are presented. Also included are the results and findings of an examination of the fracture surfaces using scanning electron microscopy.

Chapter 4 presents the findings of a microscopical study of the fibres. In Chapter 5, the results of an investigation into the micromechanics of deformation and fracture of 'model' single fibre composites are presented. Chapter 6 draws together the main findings of the work in an attempt to explain some of the observed macroscopic material behaviour, in relation to its microstructure. Finally, Chapter 7, reviews the main conclusions of the work and its perceived deficiencies and makes recommendations as to areas in which it is believed further research would be beneficial.

2 Literature Review

2.1 Composite materials

2.1.1 Introduction

As noted in the previous chapter, composite materials are composed of two or more phases, usually a *reinforcement* of strong stiff material, embedded in a weaker, more compliant *matrix*. By combining these phases a material is produced which, in general, possesses properties entirely different from that which might be expected from a consideration of the individual constituents. The example cited in Chapter 1, to demonstrate this phenomenon, was toughness. In this section, a brief review of the salient aspects of composites science and technology is conducted. This review has been based upon a number of standard text books covering the topic of composite materials. These include: Piggott (1980), Matthews and Rawlings (1994) and Hull and Clyne (1996), together with more specific literature.

2.1.2 Reinforcement processes

2.1.2.1 Load sharing

Key to the understanding of the mechanical behaviour of fibre reinforced composite materials is the concept of load sharing between fibre and matrix. Whilst stress may vary sharply from point to point along the fibre (particularly in short fibres), the proportion of the external load carried by each of the individual constituents can be assessed by volume-averaging the loads associated within them (Hull & Clyne, 1996). This gives rise to the following condition:

$$\sigma_c = V_f \bar{\sigma}_f + (1 - V_f)\bar{\sigma}_m \qquad (2.1)$$

Where: σ_c is the composite applied stress

$\bar{\sigma}_f$ is the volume averaged fibre stress

$\bar{\sigma}_m$ is the volume averaged matrix stress

V_f is the *volume fraction* of reinforcement. This is the volume of fibre present in the composite as a fraction of the total volume of the composite (expressed as a percentage throughout this text).

For a two phase composite, it may be observed that a certain proportion of the load will be carried by the fibre and the remainder by the matrix. Provided the response of the composite remains elastic, the proportion of the load carried by each constituent will depend upon:

- the volume fraction of reinforcement
- the shape and orientation of the reinforcement
- the elastic properties of the constituents.

The reinforcement may be considered to be acting efficiently if it carries a relatively large proportion of the externally applied load. A high reinforcing efficiency can lead to greater composite strength and stiffness, since the reinforcement is usually both stronger and stiffer than the matrix (Hull & Clyne, 1996).

2.1.2.2 Elastic stress transfer

A necessary aspect of the reinforcement process is the transfer of externally applied stresses to the main load bearing constituent (reinforcement) of the composite. This transfer of stress is accomplished by shear stresses, τ_i, acting across the interface between matrix and fibre. If it is initially assumed that the bonding between the phases is perfect (i.e. there is no slippage at the interface) and that the system behaves elastically, then the transfer of stress may be rationalised as follows. As the composite is strained, the matrix deforms around the fibre as depicted in Figure 2.1. Shear strains induced in the matrix lead to shear stresses (τ_i) at the interface. As may be noted from Figure 2.1, the distortion is greatest at the fibre ends and thus it follows that τ_i will be greatest in these regions. In a similar manner, it may be reasoned that, at the fibre ends, the axial stress in the fibre, σ_f, will be zero and will build up as a

result of τ_i, with increasing distance from the fibre end to a maximum point, some distance away. This is the basis for the shear-lag model of stress transfer first proposed by Cox (1952).

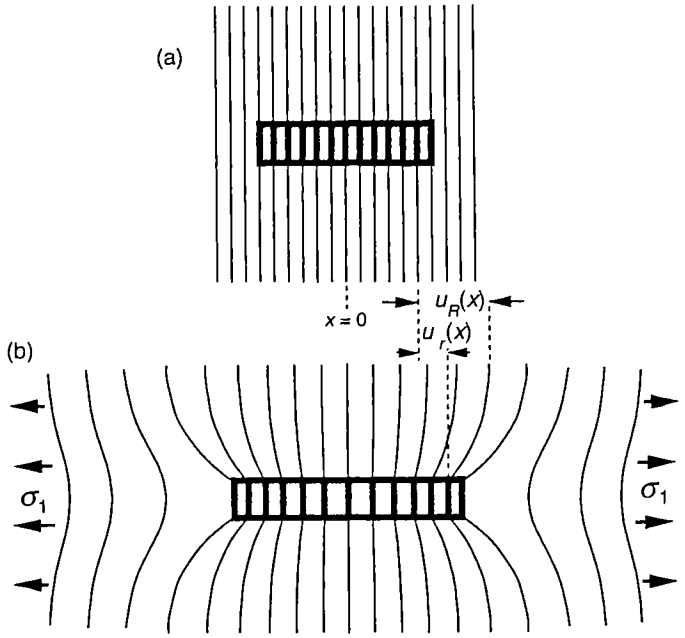

Figure 2.1 Schematic representation of a 'Cox-type' shear-lag distortion in the matrix surrounding a reinforcing fibre (*Source:* Hull & Clyne, 1996).

By considering the balance of forces acting on an element of the fibre, it may be shown that:

$$\frac{d\sigma_f}{dx} = -\frac{2\tau_i}{r} \qquad (2.2)$$

Where: x is the axial distance from the fibre mid-point

r is the fibre radius

By utilising this approach, it may be shown that the axial stress distribution, due to elastic stress transfer in a fibre, may be given by (Hull & Clyne, 1996):

$$\sigma_f = E_f \varepsilon_1 \left[1 - \cosh(nx/r)\,\mathrm{sech}(ns)\right] \qquad (2.3)$$

Where: E_f is the fibre Young's modulus

ε_1 is the applied composite strain

s is the fibre aspect ratio, defined as L/r (where L is the fibre half length)

n is a dimensionless constant given by:

$$n = \left[\frac{2E_m}{E_f(1+\nu_m)\ln(1/V_f)}\right]^{1/2}$$

Where: E_m is the matrix Young's modulus

ν_m is the matrix Poisson's ratio

Furthermore, it may be shown that the variation of τ_i along the fibre can be given by (Hull & Clyne, 1996):

$$\tau_i = \frac{n\varepsilon_1}{2} E_f \sinh\left(\frac{nx}{r}\right)\mathrm{sech}\,(ns) \qquad (2.4)$$

The interesting features of these relationships are that they predict that stress transfer is dependent upon the elastic properties of the phases, the applied strain and the aspect ratio of the reinforcement. Equation 2.3, predicts that the maximum axial fibre stress will depend upon its stiffness as well as the applied strain, and that the build-up of stress is related to the difference between the fibre and matrix moduli. Similarly, from Equation 2.4, it may be noted that the distribution of τ_i is dependent upon the same parameters. For a composite system (based upon a hypothetical plant fibre reinforced thermosetting polymer) in which the fibre modulus is taken to be 50 GN m^{-2} and the matrix modulus to be 3.5 GN m^{-2}, with different aspect ratios (s = 5, 25,

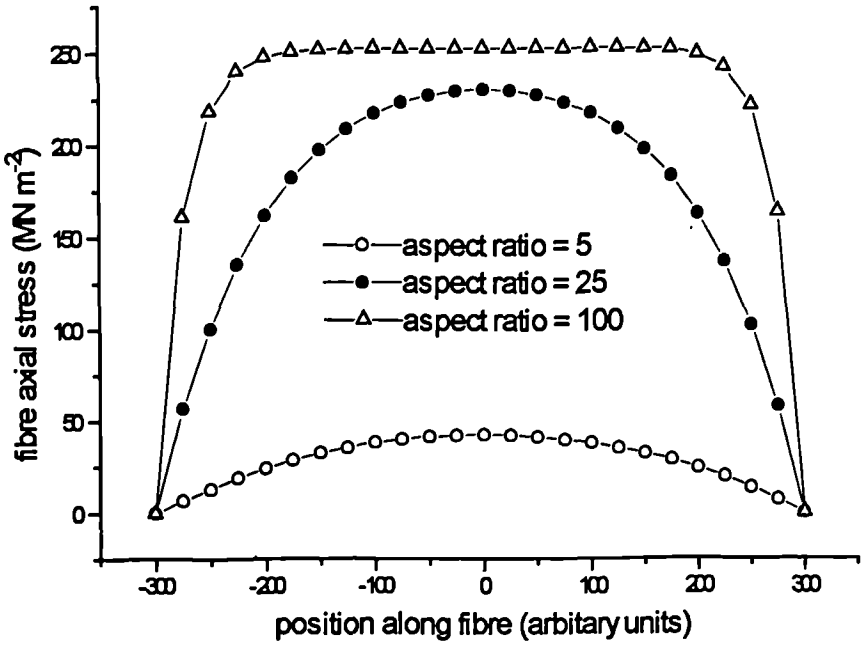

Figure 2.2 Theoretical shear-lag prediction of the variation of σ_f along the fibre length, assuming fibre aspects ratios of 5, 25 and 100 and an applied strain of 0.5%.

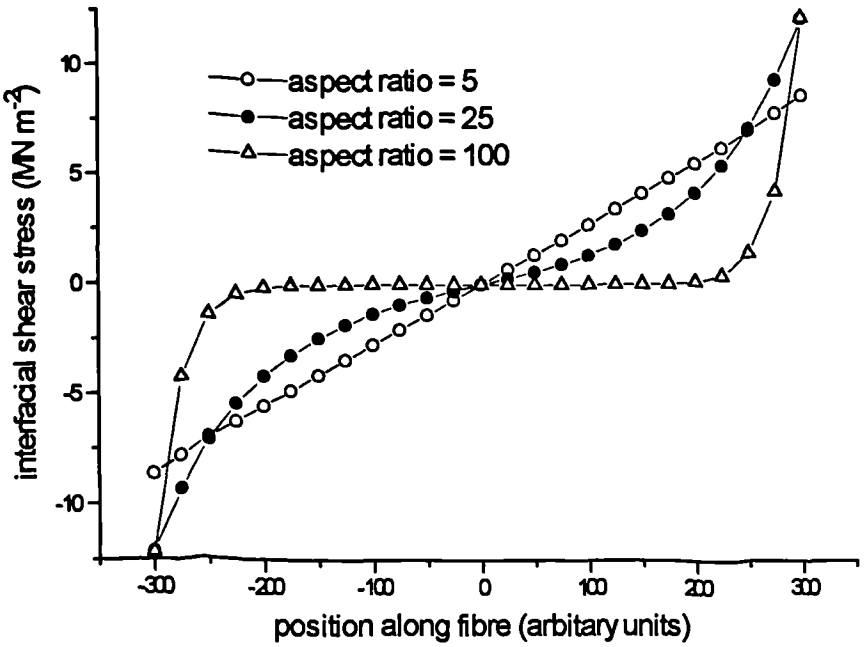

Figure 2.3 Theoretical shear-lag prediction of the variation of τ_i along the fibre length, assuming fibre aspects ratios of 5, 25 and 100 and an applied strain of 0.5%.

100) predicted distributions of σ_f and τ_i (utilising Equations 2.3 and 2.4 and assuming $n = 0.125$) along the fibre for an applied strain of 0.5% are shown in Figures 2.2 and 2.3 respectively.

2.1.2.3 Stress transfer aspect ratio

It may be noted from Figure 2.2, that there is a build-up of axial fibre stress with increasing distance from the fibre end. However, as may be observed, it is only when the fibre aspect ratio exceeds something of the order of 30 that the maximum axial stress is achieved (i.e. the fibre strain is equal to matrix strain and a plateau is reached - this is clearly noted when $s = 100$). For this theoretical system, therefore, there is an ineffective length in the region of the fibre ends where the stress is gradually building-up. This gives rise to the concept of a critical value for the stress transfer length, at which value of s the axial fibre stress builds up to a maximum, corresponding to the strain being imposed on the composite (Hull & Clyne, 1996). It follows that fibres below this critical value aspect ratio will be less efficient in terms of reinforcement than longer fibres. This is clearly observed in the fibre with an aspect ratio of 5, in which the axial fibre stress barely reaches 10% of the maximum plateau stress of 250 MN m^{-2} for the same applied strain. Figure 2.3 shows the theoretical interfacial shear stress distribution. It may be noted that when s equals 100, τ_i has zero value over much of the fibre length.

2.1.2.4 Inelastic processes

The above scenario assumes that the bonding between fibre and matrix is perfect, i.e. no slippage takes place between fibre and matrix during straining of the composite, in other words the system remains elastic. However, if a critical value of τ_i is exceeded, localised failure may result. This might be due to rupture of the fibre-matrix bond (see Chapter 6) or to shear failure of the matrix, if such bonding is particularly good. If it is assumed that fibre-matrix debonding occurs rather than matrix shear failure (probable in PMCs - Piggott, 1980) and that following debonding, stress transfer at the interface takes place through friction (which is constant) then a shear and axial stress distribution similar to that shown in Figures 2.4 might be expected. This model assumes that τ_{if} is constant near the ends of the fibre and zero at the centre. Again,

using a balance of forces argument, it may be shown that the axial stress in the fibre varies, linearly, as shown in Equation 2.5 (Piggott, 1980).

$$\sigma_f = \frac{2\tau_{if}}{r}(L - x) \qquad (2.5)$$

Where: τ_{if} is the frictional interfacial shear stress

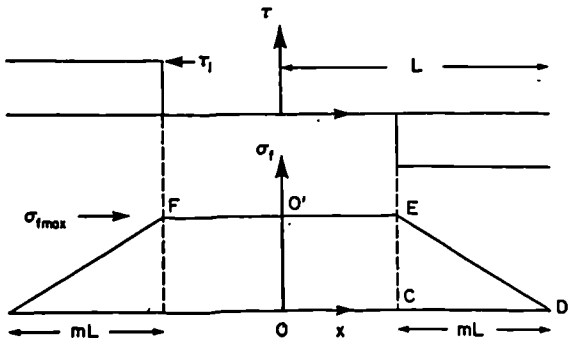

Figure 2.4 Variation of axial fibre stress σ_f and frictional interfacial shear stress τ_{if} along a single fibre (*Source:* Piggott, 1980).

For a given composite system, intermediate situations may well exist in which stress transfer takes place through a combination of elastic and inelastic processes. In the region of the fibre ends, for example, fibre-matrix debonding may well be stimulated by high interfacial shear stresses, whereas in the central portion of the fibre bonding remains intact. Indeed, this form of stress distribution has been observed in the vicinity of broken fibre ends in real composite systems, consisting of single or multiple fibre microcomposites (Van den Heuvel *et al.*, 1997).

If elastic stress transfer is compared with transfer by friction (Figures 2.2 and 2.4) it is evident that whilst the form of the stress distribution differs between these processes, a critical value of aspect ratio can be identified. At this point, the axial stress at the mid-point reaches the ultimate tensile stress of the fibre σ_{fu}, resulting in fibre fracture (assuming that fibre fracture takes place at a defined and constant value). The aspect

ratio of the fibre at which this occurs is known as the critical aspect ratio (s_c). If stress transfer by friction only is considered, then it may be shown that the fibre critical aspect ratio is given by (Piggott, 1980; Hull & Clyne, 1996):

$$s_c = \frac{\sigma_{fu}}{2\tau_{if}} \tag{2.6}$$

Thus far, only an idealised situation has been considered, in which only stress transfer parallel to the fibre axis has been considered. Nevertheless, in most "real" materials, some degree of off-axis loading will take place. In such cases, the reinforcing efficiency will be reduced and when loading is normal (or nearly so) to the fibre axis, then the matrix may actually be weakened by the presence of the reinforcing fibres (Chou, 1994; Hull & Clyne, 1996).

2.1.3 Interface

From the foregoing, it is evident that the integrity of the bonding between fibre and matrix plays a major role in the determination of composite properties (Hull & Clyne, 1996). Whilst adequate fibre-matrix adhesion is required to ensure the integrity of the composite, it is also necessary that uncoupling of the two phases occurs under certain conditions (for example to ensure that various toughening mechanisms come into play). In view of the importance of the interface in controlling composite properties, it is appropriate to briefly review adhesion related to fibre composites.

The first, but not only, requirement for good adhesion is that the liquid polymer should adequately wet the substrate to which it is to bond. This is necessary since the distances over which inter-atomic and inter-molecular forces operate are exceedingly small. In addition, it is important that air entrapment or voids be excluded from the system, since these can result in compromised mechanical properties. For instance, it has been estimated that a void volume of only 1% can lead to a 7% reduction in composite strength (Matthews & Rawlings, 1994). Wetting will occur if the viscosity of the liquid polymer is not too high and when it results in a decrease in the total

energy of the system. When considering the thermodynamics of the wetting process, equilibrium is dictated by the Young equation (Kinloch, 1987):

$$\gamma_{sv} = \gamma_{sl} + \gamma_{lv}\cos\theta \qquad (2.7)$$

Where:

γ_{sv}	is the surface energy of the solid-vapour interface
γ_{sl}	is the surface energy of the solid-liquid interface
γ_{lv}	is the surface energy of the liquid-vapour interface
θ	is the contact angle

Equation 2.7 implies that complete wetting (i.e. $\theta = 0$) will occur if the surface energy of the solid-vapour interface is equal to or greater than the sum of the liquid-vapour surface energy and the solid-liquid interface surface energy. Systems where the surface energy of the solid-vapour interface exceeds that of the liquid-vapour interface by a good margin are likely to wet easily (Hull & Clyne, 1996). Once intimate contact with the substrate has been established, a number of mechanisms have been proposed to explain adhesion between the two phases. These include (Kinloch, 1987):

- mechanical interlocking
- diffusion theory
- electronic theory
- adsorption theory.

Of these, the adsorption theory is the most widely applicable. Adsorption theory proposes that, provided sufficiently intimate molecular contact is achieved at the interface, the phases will adhere because of the inter-atomic and inter-molecular forces which are established between the atoms and molecules in the surface of the polymer and substrate. It is believed that the most common such forces are van der Waals forces, but may also include other secondary forces such as hydrogen bonds. It is also considered that primary (ionic, covalent and metallic) bonds as well as donor-acceptor interactions may contribute to the bonding process (Kinloch, 1987). Table

2.1 summarises the bond types (and typical bond energies) thought to be implicated in adsorption theory.

Table 2.1 Summary of bond types and bond energies thought to be implicated in the adsorption theory of adhesion (*Source:* Kinloch, 1987).

Type	*Bond energy (kJ mol^{-1})*
Primary bonds	
ionic	600-1000
covalent	60-700
metallic	110-350
Donor-acceptor bonds	
Bronstead acid-base interactions	Up to 1000
Lewis acid-base interactions	Up to 80
Secondary bonds	
hydrogen bonds	Up to 40
Van der Waals bonds	0.08-40

In addition to adsorption theory, and as will be discussed in more detail later in the text (Section 6.6.4.1), mechanical interlocking may also be an important mechanism of interfacial adhesion in bast fibre reinforced PMCs. The mechanical interlocking theory attributes adhesion to a 'lock and key' effect, provided by the surface roughness of the substrate. This form of bonding is likely to be more effective under shear, rather than tensile, loading (Hull & Clyne, 1996). A greater resistance to tensile failure is likely if some re-entrant angles are present.

2.1.4 Fibre microstructure

2.1.4.1 Volume fraction

Many factors combine to affect composite properties. However, in the opinion of Matthews and Rawlings (1994), the relative proportions of the phases, expressed as a volume fraction (V_f), is the single most important parameter. The volume weighted average of the properties of each constituent comprising the composite can be used to

describe a number of material properties. In general terms, this relationship is known as the 'Rule of Mixtures' (ROM) and may be expressed as follows:

$$X_c = V_f X_f + V_m X_m \tag{2.8}$$

Where:

X_c is the composite property

X_f is the fibre property

X_m is the matrix property

V_m is the volume fraction of matrix. This is the volume of matrix in the composite as a fraction of the total volume of the composite. Assuming that the composite consists of two phases only (with no voids), V_m may be expressed alternatively as $\left(1 - V_f\right)$.

Equation 2.1 is an example of a ROM relationship. Equation 2.8 can be used to predict, say, the density of a composite from a prior knowledge of the densities of each phase. It may also be used to predict some mechanical properties in certain instances. For example, the ROM, can be used to predict the axial stiffness of unidirectional long-fibre composites and has been used, by extrapolation, to predict the strength and stiffness of natural fibres (Bisanda & Ansell, 1991).

Since the strength and stiffness of the reinforcement are generally far greater than that of the matrix, it is apparent from Equation 2.8 that, in general, it is of benefit to have as high a volume fraction of reinforcement as possible. This, however, has limitations since there is an upper ceiling to V_f. For a uniaxially aligned composite containing fibres of circular cross section, the theoretical upper value lies between around 75% and 90% depending upon the packing arrangement (Hull & Clyne, 1996). In commercial PMCs, V_f generally lies in the range 10% to 70%.

2.1.4.2 Fibre architecture

As intimated in Section 2.1.2, the orientation and the aspect ratio of the reinforcement (since this affects the efficacy of stress transfer between phases) is important in terms

of the mechanical response of the material. The orientation of long fibres is frequently in the form of a unidirectional *lamina* (or *plies*) consisting of many fibres lying parallel to one another as shown in Figure 2.5. Many *laminae* are often stacked up upon one another to form a *laminate*, possibly in either a cross-ply or angle-ply configuration (Figure 2.5). The stacking sequence is denoted by the angle made with respect to the x direction of each ply in the laminate. For example, in the laminate shown in Figure 2.5(a), the stacking sequence is $0^0/90^0/0^0/0^0/90^0/0^0$ which simplifies to $[0/90/0]_s$ (Hull & Clyne, 1996). The laminate structure referred to above is generally only applicable to high performance materials. Often, woven, braided or knitted fibre fabrics are used as convenient reinforcement configurations. A commonly used form of fibre distribution, particularly for low-cost applications is chopped strand mat (CSM). In CSM, relatively long bundles of fibres are distributed in a planar-random sense. This form of reinforcement results in *planar-isotropic* laminate properties, but is limited to fairly low values of V_f (Hull & Clyne, 1996).

2.1.5 Elastic deformation of laminates

2.1.5.1 Axial stiffness

In the case of a unidirectional long-fibre laminate loaded parallel to the fibre axis, axial stiffness may be expressed, as indicated above, by the ROM relationship. In this instance, the axial modulus of the composite can be given by:

$$E_1 = V_f E_f + \left(1 - V_f\right) E_m \tag{2.9}$$

Where:

- E_1 is the axial modulus of the laminate
- E_f is the modulus of the fibre (assuming that the fibre possesses isotropic properties)
- E_m is the modulus of the matrix

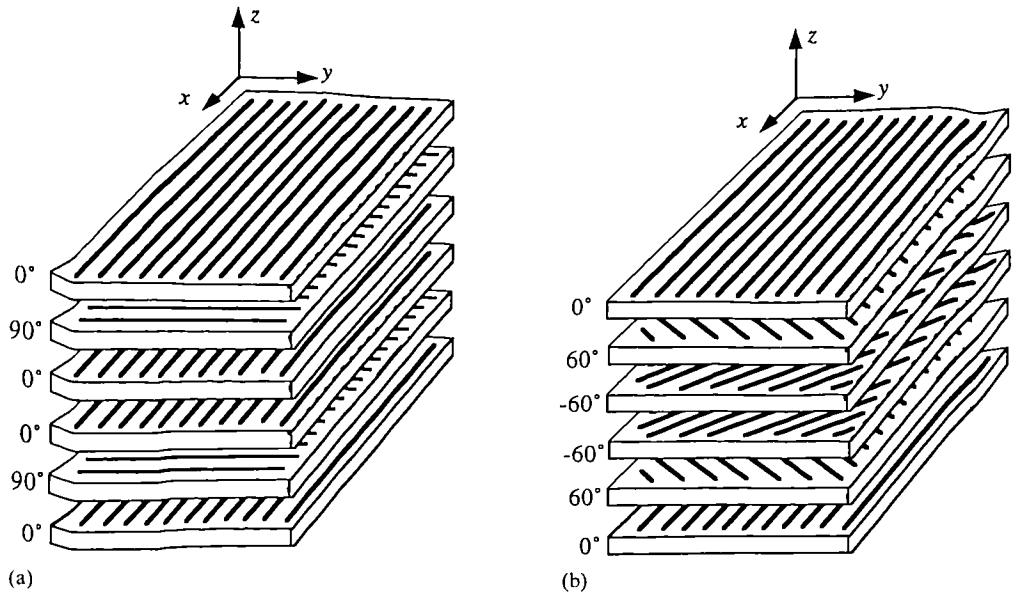

Figure 2.5 Schematic representation of the stacking sequence in a multiply laminate (*Source:* Hull & Clyne, 1996).

This analysis is based upon the premise that both fibre and matrix strains are equal (the overall composite strain, ε_1) and that the composite can be treated as two 'slabs', one of 'reinforcement' and the other of 'matrix', constrained to deform to the same extent. This type of equal strain model is also known as a 'Voigt model'.

2.1.5.2 Transverse stiffness

Whereas, under uniaxial loading in long-fibre composites both matrix and fibre undergo equal strain, under transverse loading the situation is complicated by the perturbation of the matrix due to the presence of fibres. The effect of this is to introduce regions within the matrix which undergo relatively greater strain. In effect, the fibres act as stress concentrators which may simulate localised inelastic behaviour arising from, say, interfacial debonding, plastic deformation of the matrix and microcracking, at relatively low levels of applied stress (Hull & Clyne, 1996).

Because of this, a slab model approach which assumes equal stress (rather than equal strain as in the model described above), does not yield such satisfactory predictions for transverse stiffness. According to Hull and Clyne (1996), the most successful semi-empirical prediction is that due to Halpin and Tsai (1967), which broadly takes into account enhanced fibre load bearing, relative to the equal stress assumption. Transverse stiffness E_2, is given by:

$$E_2 = \frac{E_m\left(1+\xi\eta V_f\right)}{\left(1-\eta V_f\right)} \tag{2.10}$$

Where $$\eta = \frac{\left(\frac{E_f}{E_m}-1\right)}{\left(\frac{E_f}{E_m}+\xi\right)}$$

E_2 is the transverse laminate modulus

ξ is an adjustable parameter generally of the order of unity.

For the hypothetical composite system described in Section 2.1.2 (E_f = 50 GN m^{-2}; E_m = 3.5 GN m^{-2}), the axial and transverse moduli, predicted from Equations 2.9 and 2.10 respectively are represented graphically in Figure 2.6 (assuming that $\xi = 1$).

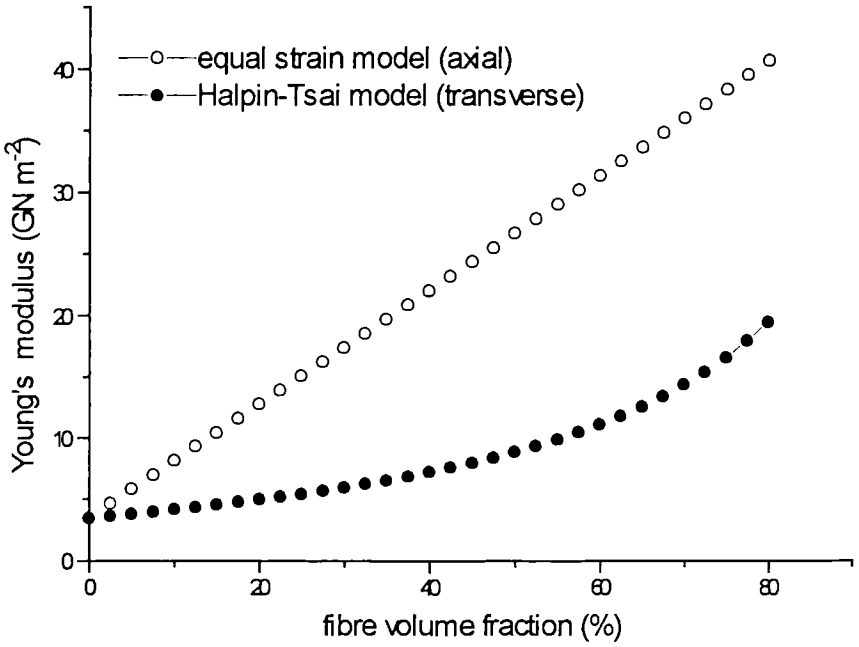

Figure 2.6 Predicted variation of axial and transverse laminate moduli with V_f.

The off-axis elastic deformation of unidirectional laminates will not be considered herein. However, one particular case (namely that of a random configuration) warrants mention in view of the importance of this reinforcement arrangement in this work.

2.1.5.3 Young's modulus of planar-random oriented fibre

As noted previously and as will be discussed more fully later in this chapter, the reinforcement utilised in the production of laminates in this work was in the form of a non-woven felt. The orientation of the fibres within this fabric might best be described as 'pseudo planar-random'. The fibre distribution cannot be regarded as being wholly planar-random since some preferred fibre alignment is undoubtedly imparted during manufacture. However, it is appropriate to consider the stiffness of a planar-random fibre reinforced laminate since this would probably be the closest approximation in this instance (especially considering that it was proposed to compare

the properties of the bast fibre reinforced laminates with that of a CSM glass fibre reinforced material).

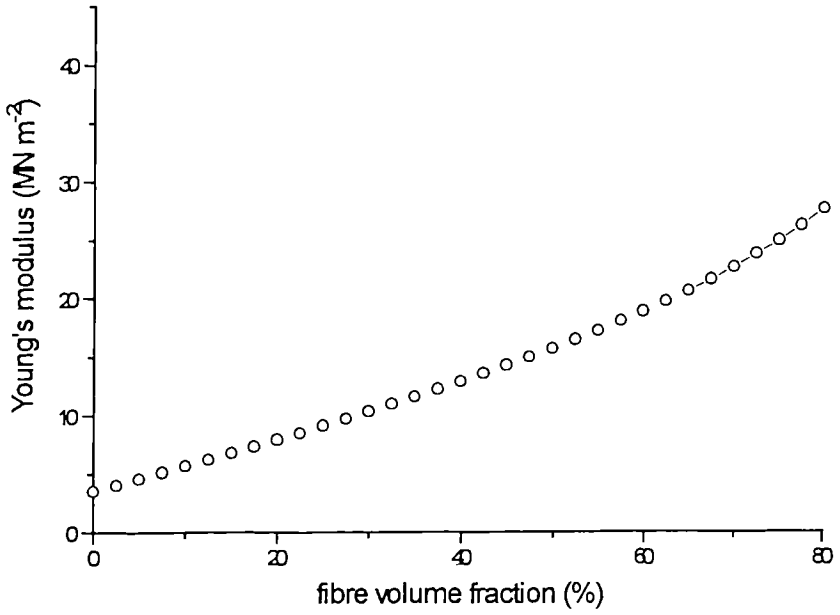

Figure 2.7 Theoretical relationship between E and V_f for a planar-random reinforced laminate.

By assuming the laminate to be composed of an infinite number of micro-laminae, it may be shown that the in-plane Young's modulus, E_r, of a random fibre reinforced laminate may be given by (Piggott, 1980):

$$E_r \cong \frac{3}{8}E_1 + \frac{5}{8}E_2 \qquad (2.11)$$

By substituting Equations 2.9 and 2.10 into Equation 2.11, it is possible to derive a theoretical expression for the variation of Young's modulus with V_f, for a planar-random array of fibres. This is presented graphically in Figure 2.7 (based upon the same hypothetical laminate used previously). It may be observed that up to around

40% to 45%, the relationship between Young's modulus and V_f shows an almost linear relationship.

2.1.6 Strength and failure of composites

If a unidirectional lamina subject to an arbitrary state of stress is considered, failure may occur as a result of critical values of axial tensile (σ_{1u}), transverse tensile (σ_{2u}) or shear stresses (τ_{12u}) being exceeded (or a combination thereof), as depicted in Figure 2.8 (Hull & Clyne 1996).

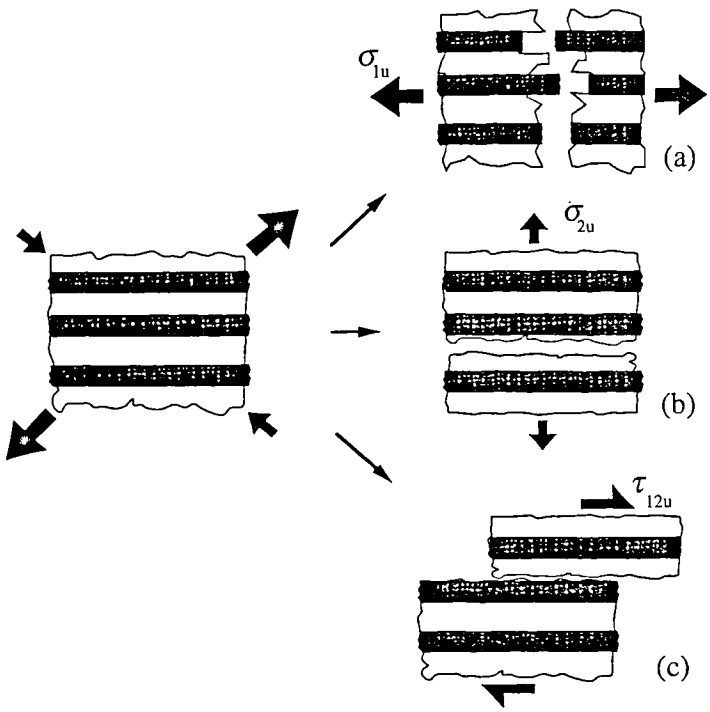

Figure 2.8 Schematic representation of the failure modes of a unidirectional lamina due to (a) axial tensile stress, (b) transverse tensile stress and (c) shear stress (*Source:* Hull & Clyne, 1996).

2.1.6.1 Axial tensile failure

If it is assumed that both reinforcement and matrix behave in a brittle manner (i.e. neither phase undergoes yielding prior to fracture) then, for a unidirectionally aligned long-fibre composite loaded parallel to the fibre axis, two distinct failure scenarios may be envisaged. The first occurs when the fibre strain to failure, ε_{fu}, is less than that of the matrix failure strain, ε_{mu}. The second occurs when the failure strain of the matrix is less than that of the fibre. Simplified models for the prediction of axial laminate strength (σ_{1u}) have been developed utilising this approach (Hull & Clyne, 1996).

In the first instance, fibre failure precedes matrix fracture (i.e. $\varepsilon_{fu} < \varepsilon_{mu}$). In this situation, it may be shown that the failure stress of the lamina can be expressed as follows (Hull & Clyne, 1996; Piggott, 1980):

$$\sigma_{1u} = V_f \sigma_{fu} + (1 - V_f)\sigma_{mfu} \qquad (2.12)$$

Where: σ_{mfu} is the matrix stress at the onset of fibre fracture

When the fibre failure strain exceeds that of the matrix, cracking of the latter occurs prior to axial composite failure. As the composite is loaded, matrix cracking initiates once the failure strain ε_{mu} is reached. As cracking continues, load is progressively transferred to the fibres. If the load is carried entirely by the fibres, then the failure stress σ_{1u} is given by:

$$\sigma_{1u} = V_f \sigma_{fu} \qquad (2.13)$$

If, however, matrix cracking is incomplete before all the load has been transferred to the fibres then the composite axial strength can be given by:

$$\sigma_{1u} = V_f \sigma_{fmu} + (1 - V_f)\sigma_{mu} \qquad (2.14)$$

Where: σ_{fmu} is the fibre stress at the onset of matrix cracking

As indicated above, these models are simplifications. In reality, the situation is complicated by the fact that residual loads continue to be carried by the phases even after one or other has failed and that a certain amount of stress transfer also takes place. In addition to this, it is assumed that the strength of a fibre is constant along its length and that failure takes place in isolation; neither assumption is likely to be true (Hull & Clyne, 1996).

2.1.6.2 Transverse failure

The nature of the interfacial bonding, the fibre distribution and the presence of voids combine to influence failure under transverse loading. As noted in Section 2.1.5, under transverse loading, stress concentrations are stimulated in the matrix and in such regions of high local stress, interfacial debonding can (for example) occur. The result is that the laminate stress and strain to failure under transverse loading is often significantly less than that of the unreinforced resin itself (Hull & Clyne, 1996).

2.1.6.3 Shear strength

According to Hull and Clyne (1996), there is no simple analytical expression to predict the effect of V_f on the shear strength of laminates. It is, nevertheless, worthwhile noting that failure may occur in any one of the six directions depicted schematically in Figure 2.9. It should be noted that in Figure 2.9, the designation of the shear stresses are as follows. A shear stress designated τ_{ij} refers to a stress acting in the *i*-direction on a plane with a normal in the *j*-direction. For example τ_{12} acts in the 1-direction, along a plane perpendicular to the 2-direction.

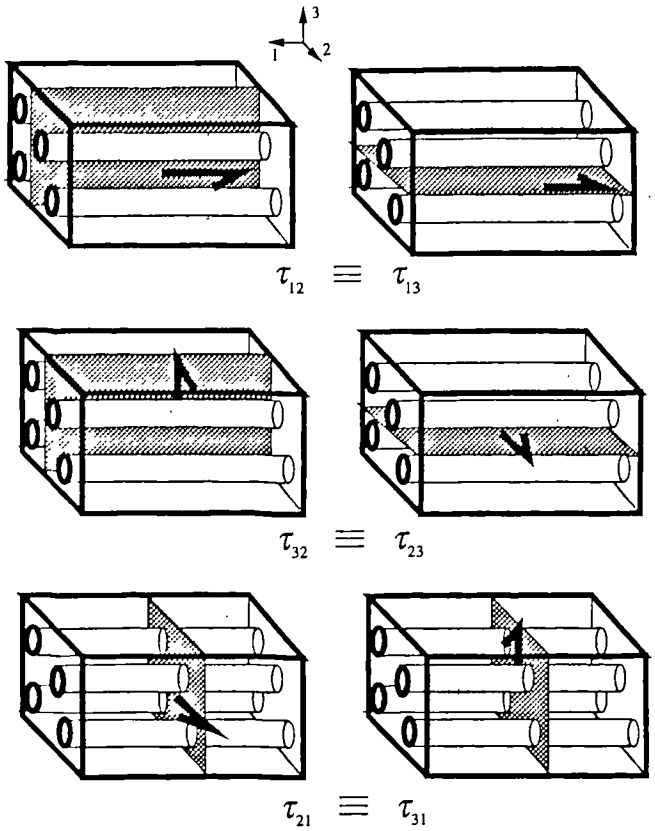

Figure 2.9 Possible directions of shearing in a unidirectional fibre composite (*Source:* Hull & Clyne, 1996).

2.1.6.4 Failure of laminates under off-axis loading

From the foreging, it is clear that the strength of a unidirectional lamina is highest when it is loaded parallel to the fibre direction (axial tensile strength) and lowest when it is loaded perpendicular to this direction (transverse tensile strength). At intermediate angles, failure may occur by a combination of axial tensile, transverse tensile or shear loads. The 'Tsai-Hill' criterion (Equation 2.15) can be used to predict the failure of a unidirectional laminate under off-axis loading and furthermore can provide, by inspection of the relative magnitudes of the terms, an indication of the likely failure mode (Hull & Clyne, 1996).

$$\sigma_\phi = \left[\frac{\cos^2\phi\left(\cos^2\phi - \sin^2\phi\right)}{\sigma^2_{1u}} + \frac{\sin^4\phi}{\sigma^2_{2u}} + \frac{\cos^2\phi\sin^2\phi}{\tau^2_{12u}} \right]^{-1/2} \qquad (2.15)$$

Where: σ_ϕ is the off-axis tensile failure stress of the lamina

ϕ is the loading angle

σ_{1u} is the axial tensile strength of the lamina

σ_{2u} is the transverse tensile strength of the lamina

τ_{12u} is the shear strength of the lamina

2.1.6.5 Strength of a planar-random arrangement of fibres

For a planar-random reinforcement, a laminate might be thought to consist of multiple unidirectional sub-laminae, each oriented at differing angles, ϕ, to the applied stress (Piggott, 1980). For such an arrangement, it may be shown that the ultimate strength, σ_{ru}, for a random arrangement of fibres may be given by an expression analogous to that for the stiffness (Equation 2.11), as follows:

$$\sigma_{ru} = \frac{3}{8} V_f \sigma_{fu} + (1 - V_f)\sigma_{mu} \qquad (2.16)$$

2.1.7 Toughness

For many engineering materials, adequate toughness (or work of fracture) is essential for their safe use in practical situations. Toughness may be regarded as the resistance a material possesses to the propagation of cracks or crack-like defects which might ultimately lead to failure. These cracks may, for example, be macroscopic, 'stress raisers' such as bolted joints, or sharp changes in section, or alternatively pre-existing crack-like defects in the material itself. These cracks result in localised stress concentrations, the magnitude of which depend upon the size and shape of the crack. If the stress concentrations are high enough, the material in the vicinity of the crack-tip may fail. Under certain conditions a crack may propagate catastrophically, leading to sudden failure of the material. The crack-tip may, therefore, be viewed as a mechanism whereby local stresses in the material are raised sufficiently for fracture to occur. However, for the crack to propagate, it must be energetically favourable for it to do so. The energy to drive the crack forward is provided by the release of stored

strain energy in the material, together with any external work done by the loading system. Thus, if a material possesses mechanisms whereby significant amounts of energy can be absorbed as the crack advances or if, by some contrivance, the stress concentration at the crack-tip can be relieved, then it is likely to be tough.

Brittle materials such as glass have little means of energy absorption or crack-blunting and hence fail in a catastrophic manner, exhibiting low fracture energies of around 0.01 kJ m^{-2}. Ductile metals such as mild steel, on the other hand, absorb large quantities of energy by plastic deformation. Typically, tough engineering materials such as steel exhibit fracture energies of around 100 kJ m^{-2} (Hull & Clyne, 1996). As indicated in Section 1.1, many composites exhibit very good toughness, albeit the constituents are essentially brittle. The reason for this may be the heterogeneous nature of composite materials (Gordon, 1976), in that they possess a number of crack-blunting and energy absorption mechanisms.

2.1.7.1 Interface

As noted in Section 2.1.3, the interface is of great importance. Whilst sufficient adhesion between fibre and matrix is desirable so as to ensure adequate composite integrity, fibre-matrix uncoupling under certain circumstances is necessary in order to stimulate toughening mechanisms within the composite. For example, for a composite to have high toughness, it is necessary that a crack travelling through the matrix is repeatedly deflected and blunted. This occurs when an advancing crack meets an interface which subsequently ruptures, resulting in the crack being blunted or deflected. Cook and Gordon (1964), proposed a mechanism whereby crack-deflection would take place at an interface if the interface 'strength' was approximately 20% of that of the matrix. Crack-deflection criteria based on energetic considerations have also been proposed (e.g. Kendall, 1975). Interfacial fracture energies have been measured experimentally for single filament polymer matrix composites (e.g. Pegoretti *et al*, 1996; Hampe & Marotzke, 1997).

Energy is dissipated in the debonding process, through the creation of new crack surfaces. In addition to this, debonding provides a means by which fibres may pull-out from the matrix sockets and in the process a substantial amount of energy is

absorbed through frictional sliding (Hull & Clyne, 1996). Thus, the conditions under which debonding and crack-deflection take place are of significance in terms of composite toughness. This aspect will be discussed more fully in Chapter 6.

Interfacial bond strength, therefore, has implications for the overall toughness of the composite. If interfacial adhesion is too great, a crack propagating through the matrix will not be deflected along the interface, as a result of which, the crack may traverse the fibre without the energy absorbing mechanisms (save for the energy required to fracture the fibre) of interfacial debonding (see below) and fibre pull-out being stimulated. This would undoubtedly lead to poor composite toughness. There are a number of energy absorbing mechanisms implicated in PMCs.

2.1.7.2 Energy absorbing mechanisms

The contribution that each of the energy absorbing mechanisms makes to the overall toughness of the composite varies, depending upon the composite system involved and the properties of the phases. The various mechanisms can, nevertheless, be summarised as follows:

- **Matrix deformation and fracture.** With brittle thermoset polymers, the contribution from matrix deformation and fracture to the overall fracture energy of the composite is likely to be small. Typically, fracture energies of thermosetting polymers are of the order of 0.1 kJ m^{-2} (Hull & Clyne, 1996).

- **Fibre fracture.** Brittle fibres such as glass exhibit very low fracture energies of the order 0.01 kJ m^{-2}. The contribution to the overall work of fracture of the composite is likely, therefore, to be small (Hull & Clyne, 1996). Wood fibres can, however, exhibit high fracture energies. It has been observed that these fibres can deform in a 'pseudo-plastic' manner, when strained parallel to the fibre axis (Page *et al*, 1971). It has been postulated that the high work of fracture, or toughness, observed in wood is a result of its structural organisation (Gordon & Jeronomidis, 1974, Jeronomidis, 1976, Jeronomidis, 1980). This contention has been borne out by the manufacture of artificial composites which mimic the structure of natural composites. In this way it has been found that it is possible to obtain fracture

energies comparable with those of ductile metals and higher than that of other artificial composites (Gordon & Jeronomidis, 1980). Thus fibre fracture could, potentially, contribute greatly to the toughness of a composite.

- **Interfacial debonding.** The debonding energy in composites is generally quite small, ~0.01 kJ m^{-2} (Hull & Clyne, 1996; Piggott, 1980) and the resulting contribution to the overall work of fracture is generally low (~0.5 kJ m^{-2}). As discussed above, if the interfacial fracture energy is increased too much, debonding is hindered.

- **Frictional sliding and fibre pull-out.** Potentially, this mechanism can absorb large amounts of energy (~100 kJ m^{-2}). Frictional energy dissipation during pull-out is dependent upon interfacial roughness, contact pressure and sliding distance (Hull & Clyne, 1996).

In summary, adequate toughness is a prerequisite of an engineering material. Many PMCs often exhibit very good works of fracture, particularly when viewed on a specific basis. Toughness is dependent upon interfacial effects and the material properties of the constituents. A number of energy absorbing mechanisms are thought to contribute to the overall work of fracture of composites, of which fibre pull-out is the most significant. However, with natural fibres as a reinforcement, fibre fracture may offer a potential additional mechanism for toughness enhancement.

2.2 Composite manufacture

As noted in the previous chapter, the most frequently used matrices are thermosetting polymers, with glass fibre being the most commonly employed reinforcement. Since the properties of a composite are largely governed by the volume fraction of reinforcement and the orientation thereof, which in turn are parameters controlled by the manufacturing process, a review of these is appropriate. The manufacture of

thermosetting PMCs can be conveniently divided into open-mould and closed-mould processes.

2.2.1 Open-mould processes

2.2.1.1 Hand laminating

Because of the flexibility of the method and low capital outlay in moulds and equipment, hand laminating is widely used to produce composite products of large size and complex shape. The production of sailing craft, motor boats and canoes is typically by this method.

Essentially, the process involves the application of a layer of neat resin, the 'gel coat', to a female mould which has been sprayed with release agent to facilitate the removal of the finished component. Once the gelation of this primary coat has taken place, alternate layers of resin and reinforcement are applied until the desired thickness is achieved. A ribbed roller is used to ensure full impregnation of the reinforcement by the resin. Once cured, the component is removed from the mould and finished.

2.2.1.2 Spray-up

In this process both resin and fibre are delivered simultaneously onto the mould. Continuous strands of reinforcement are chopped into short lengths by a chopper unit and carried onto the mould surface by a stream of catalysed resin.

2.2.1.3 Filament winding

Continuous fibre strands are fed through a resin bath and thence onto a rotating male former. The fibre feed and resin bath are mounted on a traversing head in such a way that by manipulating the relative speed of the traversing head and the speed of rotation of the former, the desired winding angle may be achieved. Filament winding is used in the production of pressure vessels, gas bottles, pipes, rocket motors etc.

Other forms of open-mould processes exist, many of which are variations on the ones described above. A summary of the open-mould processes detailed is given in Appendix 1.

Closed-mould processes

2.2.2.1 Vacuum bag

In this process, reinforcement and resin are applied by hand lamination techniques to a female mould. The laminate is then covered with a release film and a rubber bag, clamped to the edges of the mould, placed over the laminate. The air in the space between the bag and the laminate is evacuated so that atmospheric pressure is applied over the surface of the composite, aiding consolidation of the laminate and impregnation of the fibre by the resin. External hand rolling is still required to ensure the full penetration of the fibres.

A variation on the vacuum bag theme is known as pressure bag moulding. In this, a positive pressure is applied rather than atmospheric pressure alone, resulting in improved consolidation and higher fibre volume fractions.

2.2.2.2 Autoclave

This is a vacuum bag assembly as described above, placed within a pressure vessel. The laminate is subjected to vacuum, positive external pressure and heat simultaneously, resulting in very good consolidation, curing and high volume fractions.

2.2.2.3 Cold press

Good dispersion and impregnation of the fibres by the resin can be achieved by the use of the high pressures obtained using rigid moulds mounted in hydraulic presses. Dry reinforcement is loaded into the mould and resin poured on top. The mould is then closed and pressure applied, distributing the resin and impregnating the reinforcement. Once the resin has hardened, the pressure is released and the component removed from the mould.

2.2.2.4 Hot press

This process is similar to the cold press method. However, production rates are improved substantially by the application of heat. Because of this, metal moulds must be used, adding to the expense of the process.

2.2.2.5 Resin transfer moulding

This process again has similarities with cold pressing, in that reinforcement is loaded into a matched male/female mould. However, rather than introducing the resin before the mould is closed and pressed, the resin is pumped into the mould through injection ports, after closure.

2.2.2.6 Vacuum-assisted resin injection

This process is a development of resin transfer moulding. The closed mould is first sealed around the edges after which it is partially evacuated; resin is then injected by pump or gravity feed. The advantages of this system are that better consolidation of the laminate and lower void content in the composite are achieved, as well as a higher volume fraction.

2.2.2.7 Injection moulding

A technique similar to the one used to process thermoplastics is used to manufacture high volume goods such as electric plugs and sockets.

The open- and closed-mould techniques described above are only capable of producing one component at a time. Continuous processes such as pultrusion, continuous lamination and continuous filament winding are able to produce composites without interruption. However, the range of shapes which can be achieved is limited. A summary of the closed-mould processes described above, is given in Appendix 2.

In summary, a number of manufacturing methods can be utilised to produce PMCs. The system employed will depend upon many factors including, the size of the composite, fibre volume fraction, orientation and morphology and the shape and complexity of the component etc. Tooling and equipment costs are also important criteria.

2.3 Bast fibres: biology, chemistry, ultrastructure and properties

2.3.1 Bast fibres

Flax (*Linum usitatissimum*), hemp (*Cannabis sativa*) and jute (*Corchorus capsularis*) are dicotyledonous plants containing long vegetable fibres known as *bast* fibres. These are obtained from the bark, or *bast*, of the plant stem. Figure 2.10 shows the location of these fibres in the stem of the flax plant (Catling & Grayson, 1982). Flax and hemp fibres have similar characteristics and end uses and the plants have long been cultivated by mankind (Weindling, 1947). Whereas flax and hemp grow well in temperate climates, jute is a tropical species (Weindling, 1947).

The bast fibres that are separated from the plant stem during retting and decortication (see below) are referred to as *technical* fibres or *fibre bundles*. It is these which are subsequently used in textiles, or other applications. The length of these fibres varies considerably. In flax, for instance, the length of the technical fibres might be from 0.3-0.6 metres whilst in hemp they range from 0.9-1.8, but can attain lengths of up to 4.5 metres (Weindling, 1947). The thickness of the technical fibres vary from around 50 to 500 μm in flax to 0.5 to 5 mm in hemp. The fibre bundles are, in turn, composed of many individual cells. These too vary in length and diameter. In flax, for example, cell length varies from 5 to 50 mm, averaging around 25 mm, whilst the diameter ranges from 15 to 35 μm, giving the fibres an average aspect ratio of 1200 (Weindling, 1947). Hemp cells range from 5 to 55 mm in length, averaging around 20 mm and are between 0.125 and 0.375 mm in diameter (Weindling, 1947). The average aspect ratio for hemp cells is 1000 (Weindling, 1947).

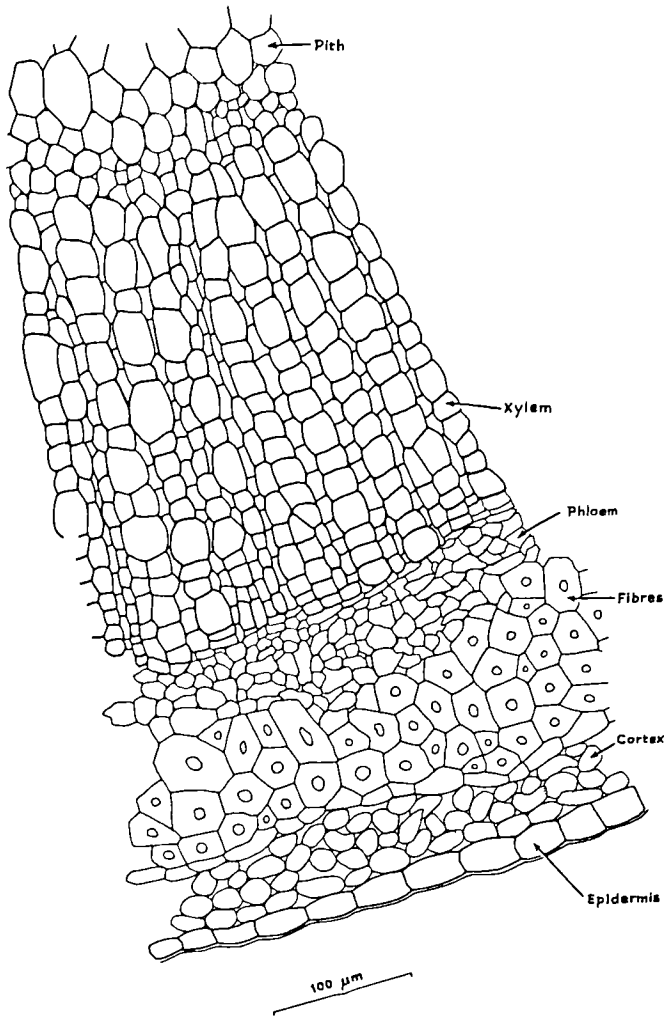

Figure 2.10 Cross-section of a flax stem, showing the location of the fibres (*Source:* Catling & Grayson, 1982).

2.3.2 Chemical composition of lignocellulosic fibres

Plant fibres are, themselves, composite structures of considerable complexity and elegance. Since the mechanical performance of composites is heavily dependent upon the properties of the reinforcement, it is appropriate to consider, briefly, the chemical composition and ultrastructure of bast fibres since this has a direct bearing upon their mechanical behaviour. Bast fibres are *lignocellulosic* fibres which consist of three main polymers: *cellulose*, *lignin* and *matrix polysacharides* (such as *pectins* and *hemicelluloses*) associated with cellulose and lignin in the cell wall. In addition to

these, a number of non-structural components such as waxes, inorganic salts and nitrogenous substances are also present (Desch & Dinwoodie, 1996; Focher, 1992). A summary of the main chemical constituents of bast fibres, compiled from a number of sources, is presented in Table 2.2. It may be noted that there is a significant degree of variation due, no doubt, to fibre variability and different analysis methods. Nevertheless, it is possible to distinguish general trends and it is possible to derive an 'average' or typical composition for a hypothetical bast fire (based upon a flax or hemp fibre ultimate). This might consist of around 85% (by mass) cellulose, 10% hemicellulose and 5% lignin.

Table 2.2 Summary of the main chemical constituents of flax, hemp and jute (*Various sources*).

Fibre type	*Cell-ulose (%)*	*Hemi-cellulo-se (%)*	*Pectin (%)*	*Lignin (%)*	*Extra-ctives (%)*	*Reference*
flax	80-90	-	2-6*	-	3-4	Weindling, 1947
	79	20.7	2.6	2.4	1.9	Bledzki *et al.*, 1996
	71.2	18.6	1.1	2.2	6	Gassan & Bledzki, 1996
	81	14	2	3	-	Robson *et al.*, 1993
hemp	85.7	-	10.2*	-	5.3	Weindling, 1947
	83.4	20.1	1.0	4.1	0.9	Bledzki *et al.*, 1996
	74	18	1	4	-	Robson *et al.*, 1993
jute	59.9	12.1	-	17.5	9.9	Lilholt & Bjarre, 1997
	70-83	-	23-28*	-	1.5-6.9	Weindling, 1947
	69.8	23.3	0.2	14.9	0.6	Bledzki *et al.*, 1996
	71.6	13.3	0.2	13.1	1.8	Gassan & Bledzki, 1996
	72	13	<1	13	-	Robson *et al*, 1993

*Includes "pectose bodies, lignin", "pectose and gummy substances" and "incrusting and pectin matter". These include hemicellulose, pectin and lignin.

2.3.2.1 Cellulose

In flax, hemp and jute, cellulose accounts for around three quarters of the cell wall material (Weindling, 1947). Cellulose may be described as a high molecular weight, long chain molecule, consisting of β-D anhydroglucopyranose units, bound with $\beta-(1\rightarrow 4)$ glycosidic linkages, as represented schematically in Figure 2.11 (Desch & Dinwoodie, 1996; Fengel & Wegener, 1984; Focher, 1992). Every alternate unit ($C_6H_{10}O_5$) is rotated through 180^{O} (Desch & Dinwoodie, 1996). Two anhydroglucopyranose molecules form the smallest repeating unit in the chain, known as the *cellobiose* unit. The number of anhydroglucopyranose units (the degree of polymerisation - DP) in plant cellulose lies in the range 7,000-15,000 (Fengel & Wegener, 1984). In retted (see below) flax fibre the DP is of the order of 2,500-3,000 depending upon the growing factors and retting conditions (Focher, 1992).

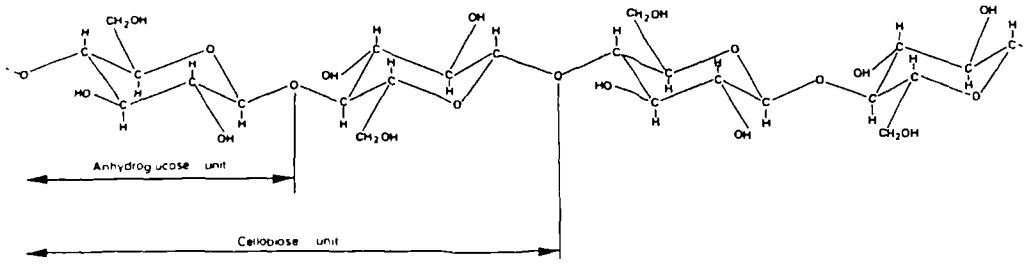

Figure 2.11 Schematic representation of part of a cellulose chain. (*Source:* Desch & Dinwoodie, 1996).

The structure of the anhydroglucopyranose unit is not flat, but bent in the form of a chair (this is the lowest energy configuration - Fengel & Wegener, 1984). Ribbon-like cellulose molecules pack together to form a crystal structure with neighbouring cellulose chains displaced by one quarter of a repeating unit. The existence of hydroxyl (-OH) groups facilitates intra- and inter-molecular hydrogen bonding, which binds adjacent molecules and imparts rigidity to the structure. Individual anhydroglucopyranose units are joined covalently, giving rise to a very strong

molecular chain along its length (Desch & Dinwoodie, 1996). This packing arrangement is shown schematically in Figure 2.12.

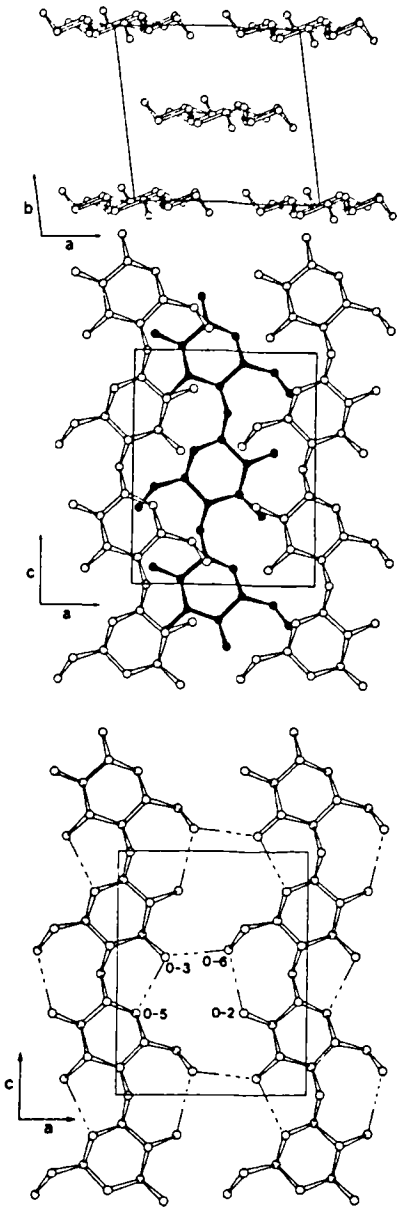

Figure 2.12 Schematic representation of the packing arrangement of cellulose chains, showing inter- and intra- molecular bonding (*Source:* Focher, 1992).

Further aggregation of the cellulose molecules, gives rise to the crystalline 'backbone' of what may be regarded as the basic fibrous building element of all lignocellulosic fibres – the *microfibril*. The diameter of this unit is generally of the order of 10-30 nm. Nevertheless, even smaller units, termed *elementary fibrils* have been detected,

having average diameters of between 2 and 4 nm (Fengel & Wegener, 1984). As will be discussed further in Section 2.3.3 this cellulose 'core' is surrounded by para- and amorphous cellulose as well as other polymeric material (Fengel & Wegener, 1984). In a longitudinal sense, the cellulose 'core' of the fibril is thought to consist of crystalline regions (the *crystallites*) interspersed with less ordered domains. The exact nature of this structure has not been fully elucidated and a number of models have been proposed (Fengel & Wegener, 1984; Chanzy, 1990). The length of the crystallites varies from around 50 to 100 nm, depending upon the origin of the cellulose (Chanzy, 1990; Desch & Dinwoodie, 1996). Between 70% and 80% of the cellulose present in bast fibres is crystalline (Fengel & Wegener, 1984). It should be noted that a significant proportion of this non-crystalline cellulose corresponds to the surface chains (Chanzy, 1990).

2.3.2.2 Hemicelluloses

These are heterogeneous polysaccharides, composed of various monomeric units such as D-glucose, D-mannose, D-galactose, D-xylose, L-arabinose and small amounts of L-rhamnose in addition to D-glucuronic acid, 4-O-methyl-D-glucuronic acid and D-galacturonic acid (Sjöström, 1993). Structurally, hemicelluloses are branched molecules having a low degree of crystallinity (Fengel & Wegener, 1984; Desch & Dinwoodie, 1996). Typically, DP is only around 200 (Sjöström, 1993). In wood, hemicelluloses are thought to account for some 20% to 30% of the dry weight of wood (Sjöström, 1993) whereas in bast fibres this is considerably less (see Table 2.2). According to Fengel and Wegener (1984), there is most probably a linkage between polysaccharides and lignin, the so called 'lignin-carbohydrate complex'. It seems highly probable therefore that hemicelluloses function as 'interfacial coupling agents', linking the cellulose 'core' to the surrounding lignin.

2.3.2.3 Pectins

Pectins are present in plant tissue to varying degrees, being found predominantly in fruit peel and gums (Fengel & Wegener, 1984). Unretted flax contains between 3% and 4% pectins (Kertesz, 1951). In flax, pectins are to be found in the cells surrounding fibre bundles, especially those separating bast fibres from core tissue (Akin *et al.*, 1996). High concentrations of pectins occur in the primary cell wall and

middle lamella of fibres (Fengel & Wegener, 1984; Focher, 1992; Sjöström, 1993; Akin *et al.*, 1996). Here, in conjunction with hemicelluloses, their function is that of a cementing material (Focher, 1992). Because of their importance as a binding material, removal of pectins during the retting process (see below) is of particular importance in the production of technical fibre.

The main building block of pectin is a linear chain of $\alpha-(1\rightarrow 4)$ linked D-galacturonic acid units (Kertesz, 1951; Stephen, 1983; Aspinall, 1980; Fengel & Wegener, 1984; Sjöström, 1993). The predominant galacturonan backbone of pectin is, however, modified by the insertion, at intervals, of α-L-rhamnopyranose units (Aspinall, 1980). Other neutral sugars such as D-galactose and L-arabinose (Sjöström, 1993; Aspinall, 1980) are present in extended side chains, whilst D-xylose; L-fucose; D-glucuronic acid are present in short side chains (Aspinall, 1980).

The uronan chain is ordered into blocks of unbranched, unesterified segments and heavily branched, esterified blocks (Jarvis, 1984). The latter are frequently interrupted by rhamnose units, linked by $\alpha-(1\rightarrow 2)$ and $\alpha-(1\rightarrow 4)$ bonds to adjacent galacturonic acid units (Fengel & Wegener, 1984). Many of the rhamnose units carry arabinan and galactan side chains. The rhamnose units introduce 'kinks' into the chain. The unbranched, unesterified blocks are rarely interrupted by rhamnose units. The chains are thus able to aggregate together along the unbranched lengths and form junctions, through bonding together non-covalently by co-ordinated calcium ions. This enables gel formation to take place. High ester pectic polysaccharides are able to form acid gels (Jarvis, 1984).

2.3.2.4 Lignin

Lignin is an amorphous, highly cross-linked aromatic polymer resulting from the dehydrogenative radical polymerisation of *p*-coumaryl, coniferyl and synapyl alcohols, which are the precursors and building blocks of all lignins (Focher, 1992). By mass, lignin accounts for some 20% to 40% of the cell wall in wood (Fengel & Wegener, 1984; Focher, 1992). In flax this figure lies between 2% and 5% depending upon the degree of retting (Focher, 1992).

2.3.3 Structural organisation of the cell wall

Broadly speaking, lignocellulosic fibres are analogous to synthetic fibre reinforced composites, in which cellulose forms the reinforcement with other polysaccharides and lignin, the matrix. The basic fibrous building element of the cell wall may be regarded the microfibril. The microfibril can itself be viewed as a composite, in which crystalline cellulose forms the 'reinforcement' core, surrounded by a 'matrix' of para- and amorphous cellulose, hemicellulose and pectins. These are, in turn, sheathed in lignin. Several models of the association of the cell wall components have been proposed by various authors. Figure 2.13(a), shows a schematic representation of the cross-section of the microfibril. As may be noted, in this model a single crystalline 'core' is surrounded by a 'matrix' of other polysaccharides and lignin. Figure 2.13(b) depicts, not only the supramolecular structure of the microfibril, but also takes into account, smaller elementary fibrils. Nevertheless, in both these models, it may be observed that there is a close association between the cellulose 'core' and the surrounding hemicelluloses and lignin.

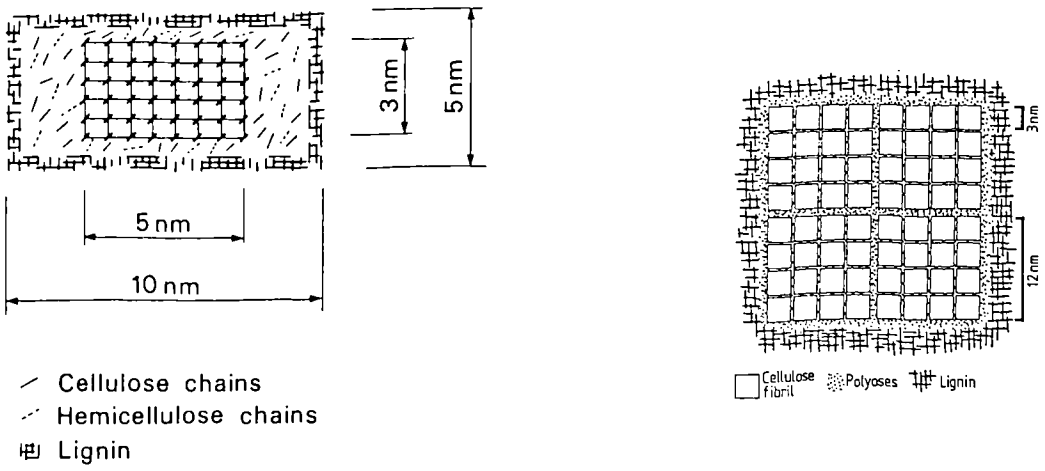

(a) (b)

Figure 2.13 Schematic representation of the cross-section of an individual microfibril (*Sources: a)* Desch & Dinwoodie, 1996; *b)* Fengel & Wegener, 1984).

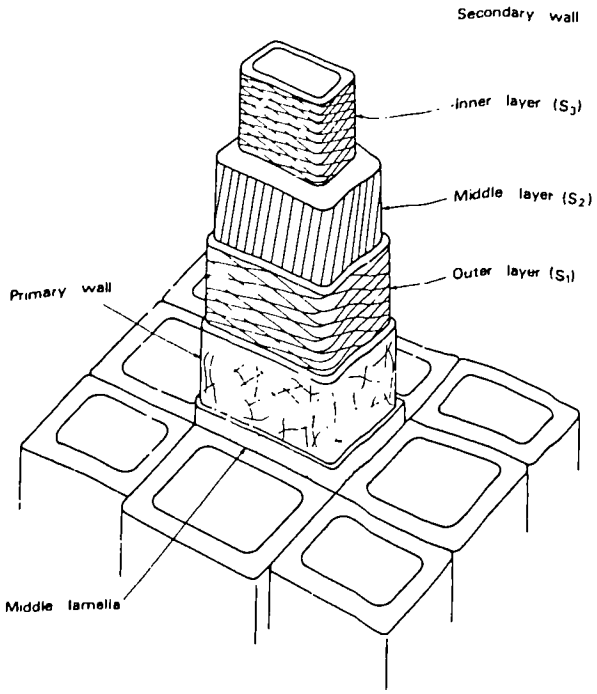

Figure 2.14 Schematic representation of the cell wall structure of a typical lignocellulosic fibre (*Source:* Desch & Dinwoodie, 1996).

In detail, the structure of an individual lignocellulosic fibre consists of a *primary* and *secondary* cell wall, with the arrangement of the microfibrils within each of these varying as depicted schematically in Figure 2.14. The very thin primary wall, lying at the outside of the fibre, adjacent to the *middle lamella* (the interstitial region between adjacent cells), consists of a more or less random arrangement of microfibrils (Desch & Dinwoodie, 1996). The secondary wall may be further sub-divided into S_1, S_2 and S_3 layers. The microfibrils within the outermost S_1 layer, which forms around 10% of the wall thickness, are arranged in two distinct spirals; one left handed and the other right handed ('Z' and 'S' helices). The microfibrils in this layer lie at angles of between 50° and 70° to the fibre long axis (Desch & Dinwoodie, 1996). The angle formed between the microfibril axis and the fibre axis is referred to as the *microfibrillar angle*. The microfibrils in the middle, S_2, layer which comprises some 85% of the total wall thickness, are aligned parallel to one another in a steeply inclined helix. In wood, the microfibrillar angle of the S_2 layer lies between 10° and 30° (Desch & Dinwoodie, 1996). In bast fibres, the microfibrillar angle of the S_2

layer is generally low; in hemp for instance, this has been reported to lie between 2^{O} and 2.3^{O} (depending upon the measurement technique used) and in jute at 7.9^{O} (Preston, 1974). The mechanical properties of the fibre are closely linked to the microfibrillar angle of the S_2 layer (see Figure 2.15); low angles being associated with higher strength and stiffness (Mark, 1967). The S_3 layer in wood fibres accounts for only around 1% of the wall thickness (Desch & Dinwoodie, 1996).

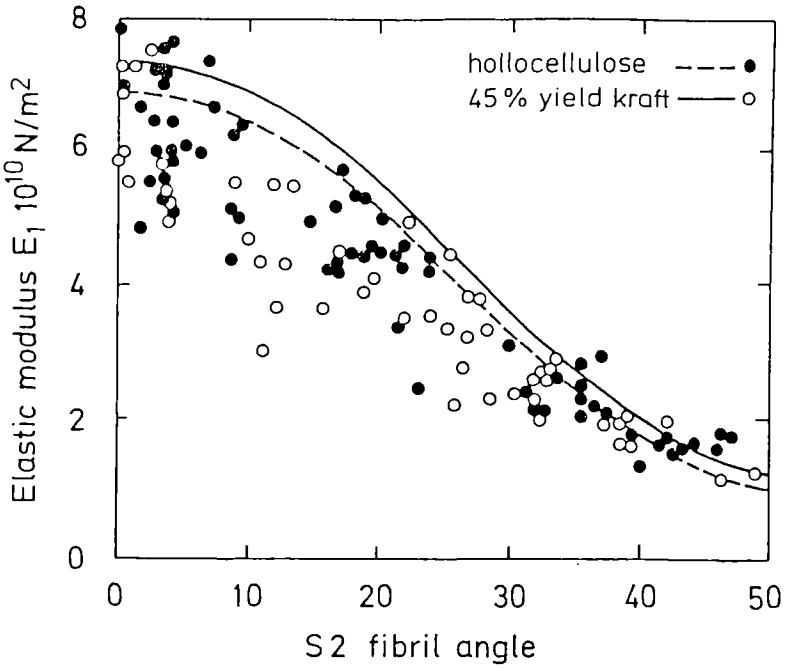

Figure 2.15 Variation of the fibre tensile (Young's) modulus with the microfibrillar angle of the S_2 layer (*Source:* Page *et al.*, 1977).

2.4 Fibre extraction, processing and properties

2.4.1 Introduction

Flax and hemp, as well as other bast fibres such as jute, are extracted from the stem in a decortication process which involves several operations. Firstly, the mature plant is

either cut or pulled from the ground. Pulling is preferred to cutting as it preserves as much of the fibre length as possible (Searle & Tuck, undated). Nevertheless at present, harvesting in the UK is by cutting. The straw is then *retted.* In this operation the technical fibres are loosened from the surrounding stem tissue in a form of controlled rotting. Enzymes, secreted by micro-organisms, degrade the non-cellulosic substances, mainly pectins, which are in abundance in the surrounding tissue, thereby liberating the intact fibre bundles (Dempsey, 1975; Chesson, 1978, 1980; Sharma, 1987b). Once retting is complete, the straw is dried, usually by spreading in the field and when it is dry it is *scutched.* This involves the straw being broken up mechanically with extraneous woody material, the shives, being removed from the fibre bundles. The final operation is termed *hackling.* This involves the fibres being pulled through a set of pins to align them and to remove any remaining woody material. Short or broken fibres known as *tow* are also separated from the long fibres (Dempsey, 1975).

According to Dempsey (1975), fibre quality is very sensitive to the retting operation and whilst ultimately fibre quality is dependent upon the quality of the straw, poor retting can lower the quality of the resultant fibre. In view of the influence of retting upon fibre quality, it is appropriate to briefly review the methods of retting. Traditionally, dew or field retting and water retting have been employed (Dempsey, 1975). Recently, however, attention has been directed towards retting procedures involving chemical or enzymatic degradation of pectins (Sharma, 1987c; Vilppunen *et al.*, 1992).

As indicated, retting involves the liberation of the fibres in the straw by the action of enzymes capable of decomposing pectins. Much of the literature cited in the forthcoming sections concerns the retting of flax, since a considerable amount of research has been carried out on this fibre due to its commercial importance. Nevertheless, the same principals apply to the retting of other bast fibres, in particular hemp, which, according to Dempsey (1975) has traditionally been retted in much the same way.

2.4.2 Dew retting

Dew retting involves laying pulled straw on the ground when the temperatures are above $0^{O}C$ and turning occasionally during the retting period. The retting period generally lasts for between 25 and 30 days in summer and between 50 and 100 days in winter (Dempsey, 1975). According to Dempsey (1975), the quality of fibre produced by this method is inferior to that of water retted fibre (see below). The principal micro-organisms involved in dew retting are fungi and although bacteria have been reported to be present they are often suppressed by the former (Sharma *et al.*, 1989; Sharma & Van Sumere, 1992). A major disadvantage of dew retting is that it is totally dependent upon weather conditions, which can sometimes lead to the loss of a whole crop. Further, the labour costs involved are high (Sharma & Van Sumere, 1992).

2.4.3 Water retting

Although water retting used to be carried out in ditches, ponds and slow moving rivers, this practice has been largely discontinued in many countries due to pollution problems (Dempsey, 1975). Most water retting nowadays is undertaken in purpose built retting tanks (Dempsey, 1975; Chesson, 1978; Sharma & Van Sumere, 1992). Pollution by rettery effluents, however, continues to be problematic and has led to the decline of flax retting in many countries (Sharma & Van Sumere, 1992).

In this process, the straw is firstly given a preliminary leaching for 2-24 hours (Chesson, 1978; Sharma & Van Sumere, 1992) after which the leach water is drained off, fresh water added and the ret commenced. Retting is completed in between 3 and 7 days at water temperatures of between $30^{O}C$ and $35^{O}C$ (Sharma & Van Sumere, 1992). The retting action is carried out by enzymes secreted by a population of mainly anaerobic bacteria. (Dempsey, 1975; Chesson, 1978; Sharma, 1987a; Majumdar *et al.*, 1990; Sharma & Van Sumere, 1992).

2.4.4 Novel retting methods

2.4.4.1 Enzyme retting

One of the drawbacks of retting as an industrial process, particularly dew retting, is the lack of control over the process. Furthermore, the length of time taken to complete the ret is comparatively long. In addition to this, the organic by-products of the process lead to pollution which can be problematic (Dempsey, 1975; Sharma & Van Sumere, 1992). The use of commercial enzyme preparations has been explored as an alternative method of retting to overcome these problems (Sharma, 1987a, 1987b; Sharma & Van Sumere, 1992; Majumdar *et al.*, 1990; Vilppunen *et al.*, 1992).

Enzymatic retting is similar in concept to tank retting. However, rather than enzymes secreted by micro-organisms being responsible for the retting action, commercially prepared enzymes are used. To date, most studies on the enzymatic retting of bast fibres have been carried out on a laboratory or semi-industrial scale. Nevertheless, it has been demonstrated that the retting time can be dramatically reduced. Majumdar *et al.* (1990), for example, reported that the retting of jute can be completed in 48 hours, whilst the ret time of flax has been reduced to 20-24 hours (Sharma, 1987a, 1987b). Vilppunen *et al.* (1992) claim to have reduced the ret time to 3-6 hours for flax.

Sharma (1987b) found that there was no significant difference between the strength of enzyme retted fibre and that of water retted material, whilst Majumdar *et al.* (1990), reported that the strength of enzyme retted jute was higher than that of conventionally retted fibre. However, Sharma and Van Sumere (1992) state that the strength of enzyme retted fibre is not as good as that of the best quality water retted fibre. This was attributed to the inability to control the enzyme action during retting; the enzyme concentration being higher, and the end point of the ret being reached faster than in water retting. Owing to this, it is possible to 'overshoot' and over-ret the fibre, leading to a loss in fibre strength. Furthermore, after retting is complete, there is a tendency for the residual enzymes to continue to act and weaken the fibre. Methods have now been developed to overcome these problems (Sharma & Van Sumere,

1992). Recently, excellent quality flax fibre has been produced on a semi-commercial scale utilising this retting method (Vilppunen, *et al.*, 1999).

2.4.4.2 Chemical retting

Pectins may be degraded by chelating agents for calcium (Aspinall, 1980). The use of chelating agents as a novel method for the retting of flax straw has been patented (Sharma, 1987c). By chelating metal ions from the pectin complex, plant pectins and hemicelluloses can be extracted with an alkaline solution of chelating agents, leaving the fibre free from pectins and hemicelluloses (Sharma, 1987c). On a semi-industrial scale, flax stems have been retted successfully using ethylene diamine tetra acetic acid (EDTA) sodium salt (Sharma, 1987b). The quality and strength of the fibre were not significantly different from either water or enzymatically retted fibre but chemical retting did remove a high percentage of hemicellulose and pectin (sharma, 1987b).

Once retting (by whichever method) has been completed, the fibres may be separated from the remaining woody material by scutching. Thereafter the material may be hackled.

Following retting and decortication, the fibre bundles may then be further refined into individual cells. A technique which has received a significant amount of attention in this respect is steam explosion treatment (Kessler & Kohler, 1996; Kohler & Kessler, 1999).

2.4.5 Felting

The cost advantage of using plant fibre material as a reinforcement in PMCs was noted in Chapter 1. However, whilst the cost of the raw material may be comparatively low, further processing could add significantly to the total cost of processing the fibres into a useful reinforcement arrangements. Air-laid, needle-punched, non-woven technology offers a means of forming fibres into felted mats potentially suitable for use as reinforcement in PMCs (Olesen & Plackett, 1999).

Essentially, the felting process can be split into three steps. The first involves taking chopped, decorticated fibre and teasing this into a fine web. During this mechanical process, known as *carding*, the fibres are repeatedly combed between rotating drums or rollers equipped with numerous fine 'teeth'. Multiple layers of the web are subsequently built-up, one upon the other, to form a light mattress, in the second, *cross-lapping*, stage. Finally, the bulky mass is squeezed with rollers and *needle-punched.* This effectively locks together the compressed mattress to form a felted material. A schematic representation of the felting process is shown in Appendix 3. By this method, felts of varying areal density, or 'grammage' may be produced.

2.4.6 Mechanical properties of fibres

Ultimately, the mechanical properties of a composite depend upon the properties of the phases and in particular those of the fibre reinforcement. A summary of the reported tensile properties of flax, hemp and jute fibre is presented in Table 2.3. As with chemical composition (Table 2.2) a great deal of variability exists between the values reported for any particular fibre type. The cause of this variability may be the result of any one or more of a large number of factors. The following are some examples of factors which might contribute to variability in the mechanical properties of the fibres:

- Type of fibre; whether it is the technical fibre or fibre ultimate that is being tested.
- Fibre variability; arising from ultrastructural organisation, growth conditions, fibre maturity or the degree of retting.
- Fibre damage; whether the fibres have been carefully removed from the stem in the laboratory or whether they have been decorticated industrially.
- Testing; the accuracy of the testing equipment, the type of test, measurement of specimen cross section, number of replicates, gauge length, ambient humidity and temperature of test etc.

Although there is a great deal of variability both within each fibre type and between different fibre types, 'typical' values for tensile strength, stiffness and strain to failure may be identified for each. If an ideal flax fibre, only, is considered, then based upon

the figures given in Table 2.3 a fibre modulus of, say, 90 GN m^{-2}, might reasonably be expected for an ultimate fibre (possibly somewhat less for a fibre bundle). Further, if a strain to failure of say 2% is assumed (again not unreasonable considering the figures shown in Table 2.3) and that the fibres behave as Hookean materials (Davies & Bruce, 1998), then a fibre ultimate tensile strength of around 1800 MN m^{-2} would be expected. Again, this would not seem implausible for a fibre ultimate (tensile strengths in excess of 2 GN m^{-2} have been recorded for individual flax ultimate specimens - Bos, 1999). As will be discussed in detail in Chapter 4, fibre damage may well play a significant role in determining the mechanical properties of bast fibres.

Table 2.3 Mechanical properties of flax, hemp and jute fibre bundles and fibre ultimates.

Fibre type	*Young's modulus (GN m^{-2})*	*Ultimate tensile strength (MN m^{-2})*	*Strain to failure (%)*	*Reference*
flax	-	814	-	Brown, 1947
	-	1500*	-	Bos *et al.*, 1997
	103	690	-	McMullen, 1984
	85	2000*	-	Bolton, 1994
	50-70	500-900	1.3-3.3	Ivens *et al.*, 1997
	28	345-1035	2.7-3.2	Sridhar *et al.*, 1982
	100	1100	2.4	Bledzki *et al.*, 1996
	52	621	1.33	Davies & Bruce, 1998
hemp	-	690	-	Brown, 1947
	25	895	-	Bolton, 1994
	30-60	310-750	2-3	Ivens *et al.*, 1997
	-	690	1.6	Bledzki *et al.*, 1996
	57	-	-	McMullen, 1984
jute	-	455	-	Brown, 1947
	8	538	-	Bolton, 1994
	10-78	-	-	Wells *et al.*, 1980
	27.6	393-773	1.7-1.8	Sridhar *et al.*, 1982
	13	550	-	Bledzki *et al.*, 1996

* denotes fibre ultimates

2.5 Thermosetting polymers

Two thermosetting polymers frequently used as matrices in PMCs are unsaturated polyesters and epoxies. These resins are initially relatively low viscosity liquids, which cure to form a three-dimensional cross-linked polymer of essentially infinite molecular weight (Restaino & James, 1994). The inherent three-dimensional network of thermosets results in significant advantages over thermoplastic matrices including, for example, better dimensional stability and less flow under stress (Restaino & James, 1994). Nevertheless, these polymer glasses are brittle, exhibiting fracture energies of the order of a few hundred J m^{-2}. This contrasts with many thermoplastics which have fracture energies of several kJ m^{-2} (Hull & Clyne, 1996).

2.5.1 Unsaturated polyesters

The general reaction scheme for producing an unsaturated polyester resin is shown in Figure 2.16. Polyester resins are the reaction products of the esterification of di- or poly-hydric alcohols with di- and poly-basic acids or anhydrides (Hare, 1996). The resins that are of greatest interest in composites are polyesters containing maleate/fumarate unsaturation (Restaino & James, 1994). The resulting polyester moiety is dissolved in a polymerisable solvent, usually styrene. During the cure, styrene co-polymerises with the polyester through the unsaturated (R_3) portion of the molecule to give a cross-linked resin (Restaino & James, 1994). Co-polymerisation during cure relies largely on the free radical-induced opening of the unsaturated bonds (Hare, 1996).

2.5.2 Epoxies

Epoxy resins are prepared by the ring-opening polymerisation of compounds containing, on average, more than one epoxy group per molecule (Restaino & James, 1994). Typically, these resins are formed by the reaction of epichlorohydrin and a dihydroxy compound; the latter usually being a diphenol, for example, bisphenol A

(Turner, 1988). According to Turner (1988) two reactions with the phenolic hyroxyl brings about polymerisation; *a)* condensation with chlorine to eliminate hydrochloric acid and *b)* addition to epoxide, opening the ring (this produces one hydroxyl group). This type of epoxy resin contains a maximum of two epoxide rings at either end of the molecule (Turner, 1988). Figure 2.17 shows the chemical structure of an epoxide based upon epichlorohydrin and bisphenol A. The curing agent ring opens the epoxide groups and, since each molecule of the curing gent can react with several epoxide groups, a cross-linked structure is formed by the curing agent acting as multi-functional bridge between epoxide moieties (Restaino & James, 1994).

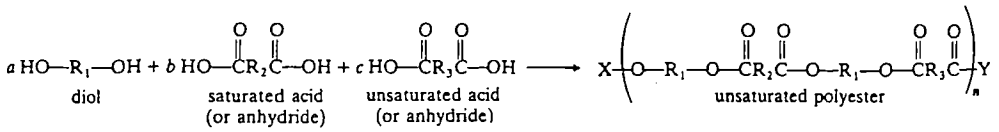

Figure 2.16 Representation of the general reaction scheme for producing an unsaturated polyester resin (*Source*: Restaino & James, 1994).

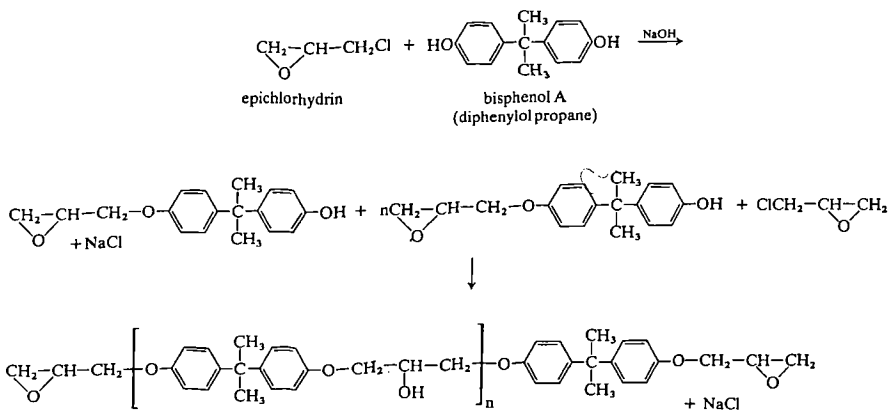

Figure 2.17 Schematic representation of an epoxide based on epichlorohydrin and bisphenol A (*Source*: Turner, 1988).

2.6 Review of work on thermosetting polymer-plant fibre composites

The history of natural fibre reinforced polymers can be traced back almost to the advent of synthetic polymers in the early part of the 20th Century. However, following the introduction of glass fibre during WW II, research into the use of natural fibres as a reinforcement in structural composites rapidly declined. Nevertheless, as noted in Chapter 1, in more recent times there has been a resurgence of interest in natural fibre reinforced polymers. It is perhaps not surprising that this renewed interest occurred during the 1970's and 80's when rapid increases in oil prices prevailed. So as to place in context the work presented herein, it seems appropriate to give a short account of the history of vegetable fibre reinforced polymer composites and to review some of the early work undertaken in this area. The main purpose of this section, however, is to review the more recent scientific work undertaken in this sphere. It should be noted that this is not intended to be an exhaustive survey of the literature, but will concentrate on the more salient work relating to the mechanical properties of vegetable fibre reinforced thermosetting PMCs.

2.6.1 Historical background

2.6.1.1 Introduction

The roots of synthetic polymer matrix composites can be traced back to as early as 1909, with the invention of Bakelite. Soon after, this was mixed with wood flour and later with string and waste rag to form the earliest synthetic PMCs (McMullen, 1984). Although pioneering work was carried out in 1924 by Messrs Caldwell and Clay, into the use of fabric reinforced synthetic resins for airscrews (De Bruyne, 1937), it was not until the 1930's that any significant interest was shown in the potential of synthetic composites as structural materials (McMullen, 1984). Much of this early work on natural fibre reinforcement for synthetic resins was spurred on by the search for lighter materials for use in aircraft primary structures (McMullen, 1984).

One of the first, true, man-made composites, potentially capable of being used in structural applications was "Gordon-Aerolite". This was a composite consisting of unidirectionally aligned unbleached flax thread impregnated with phenolic resin (McMullen, 1984). The development of this material began in 1936 with work undertaken by De Bruyne to utilise cotton fabric, as reinforcement in phenolic mouldings (Bishopp, 1997). Indeed, in 1936 De Bruyne in conjunction with The De Havilland Aircraft Company Ltd., with whom De Bruyne had a consultancy (Bishopp, 1997) took out a patent entitled "Improvements relating to the Manufacture of Material and Articles from Resinous Substances" (patent specification [No. 470,331], 1936). From Gordon-Aerolite, a number of prototype aircraft structural components were produced. One of the first of these was a wing spar for the Bristol *Blenheim* (Bishopp, 1997). As well as this, was the production of an experimental fuselage for the Supermarine *Spitfire* fighter (Aero Research Ltd., 1945). This development was instigated by a threatened shortage of bauxite for the production of duralumin. However, this threat did not materialise and so this line or research was discontinued (Aero Research Ltd., 1945).

Other cellulose-based composites, employing paper impregnated with adhesives were, however, used successfully in a number of wartime applications. The most notable of these was probably a composite pilot seat for the *Spitfire* (McMullen, 1984). It is interesting to note, however, that apart from this and possibly drop-tanks (for fuel), no use was made of cellulose-based composites for aircraft primary structures (McMullen, 1984).

By the mid 1940's, the use of cellulosic fibre (either as fabric or in paper form) reinforced polymers was quite well established and much interest was being shown in the use of these materials for structural parts (Livingston Smith, 1945). Indeed, Brown in his 1947 book stated (with reference to research being carried out at the time) that, "the beneficial results of work.....will result in a great extension in the application of this material." However, with the advent of strong and stable synthetic fibres and liquid polymers such as polyesters and epoxies, the use of cellulose fibre reinforced composites in structural applications was superceeded by wholly synthetic

composites. The properties of these early cellulose based composites, nevertheless, remain extremely impressive.

2.6.1.2 Properties of Gordon-Aerolite and other early cellulose-based composites

As noted above, Gordon-Aerolite, was a composite consisting of unidirectional flax thread in a matrix of phenolic resin. Skeins of this material, approximately 15 cm in width would be placed next to one another and over laid by others placed at right angles (i.e. a $[0/90/0]_s$ laminate), to build up the required thickness. The pack of strips was then hot pressed to consolidate the laminate (Aero Research Ltd., 1945).

The ultimate tensile strength and Young's modulus of a longitudinally loaded unidirectional skein of this material were around 480 MN m^{-2} and 48 GN m^{-2} respectively, with a density of 1363 kg m^{-3} (Aero Research Ltd., 1945). It was stated by the authors of this work that for a cross-ply laminate, "The material had approximately equal strength and stiffness along and across the sheet, but the strength and stiffness at 45^{O} to the grain was only one-half that along the fibres". Furthermore, "The specific tensile strength at 0^{O} and 90^{O} was approximately the same as that of duralumin, while the specific stiffness (tensile at 0^{O} and 90^{O} and shear at 45^{O}) was about three-quarters that of duralumin." The fibre volume fraction of these composites was around 75% (Livingston Smith, 1945). This is approaching the theoretical maximum for a unidirectionally aligned fibre composite. The compressive strength of "Gordon-Aerolite" was found to be 200 MN m^{-2}, parallel to the fibres and 95 MN m^{-2}, perpendicular to them; shear strength parallel to the fibres was 38 MN m^{-2} (Livingstone Smith, 1945). Unfortunately, no figures were quoted for the impact properties of this material.

At this time, much of the reinforcement was of cotton fabric, either in sheet form or as diced, chopped or shredded material (Brown, 1947). In 1937, De Bruyne, gave a lecture to the Royal Aeronautical Society entitled "Plastic Materials for Aircraft Construction". In this he presented details of the properties of a material referred to as "Cord-Aerolite". This was a woven cotton fabric in which the number of 'cords' in the warp direction formed around 90% of the total. This fabric was embedded in a bakelite matrix. It was found that the compressive strength of the reinforced laminate

was no greater than that of the unreinforced bakelite, but the nature of the stress-strain relationship was altered, as was the failure mode, which occurred predominantly in shear. Similar findings were reported elsewhere for other fabric reinforced laminates (Brown, 1947). The cord reinforcement was, however, found to have "a remarkable effect on the properties in tension". The tensile strength was reported to be 180 MN m^{-2} and Young's modulus around 13.8 GN m^{-2}. It was noted that the ultimate strength of the laminate was equal to that of the cords alone, which was interpreted to mean that the cord reinforcement had pulled away from the surrounding resin prior to failure. It was believed that the point at which the fibres started to pull away from the resin was related to the moulding pressure. Furthermore, it was observed that in this (and in laminates bound with urea formaldehyde or methyl methacrylate) material the initial moulding pressure affected the stress-strain response. Higher moulding pressures were observed to result in a higher initial Young's modulus as well as a more linear stress-strain response. Interestingly, when transverse sections of the material were viewed under crossed polariser and analyser, " round each cord there is a line of bright light suggesting that a high adhesion stress in the resin such as might be produced if resin and cord were in a state of initial stress relative to one another."

Although it was found that maximum strength was obtained using paper-based laminates, composites reinforced with textiles (either in sheet form or chopped, diced or shredded) were attributed with high "shock resistance" (Brown, 1947). In other words, the use of fabrics conferred toughness to an otherwise brittle resin. Whilst it is difficult to compare data on impact strength, it may be noted that the addition of sheet fabric resulted in a twenty-fold increase in this property over that of the unreinforced phenolic resin alone (Brown, 1947). The addition of chopped, diced or shredded material resulted in a twelve-fold increase and the laminated paper a ten-fold increase over that of the neat polymer (Brown, 1947). To give this some perspective, the sheet fabric reinforced laminates were found to possess an impact strength two and a half times that of spruce (Brown, 1947). It should be noted, however, that no details were given of the test type nor conditions. It is interesting to record that Brown (1947) states categorically that; "if the highest impact resistance is required the fibrous reinforcement must be present as a fabric."

According to Brown (1947) scouring, to remove sizing agents used in weaving, increased penetration of the resin into the fabric. It was found that following scouring, the average tensile strength was 1.5 times higher than the unscoured reinforcement and impact strength increased by a factor of 1.65. Scouring also improved shear strength and Young's modulus, but had little effect on compressive strength.

Finally, before leaving this early work on cellulose fibre reinforced laminates, it is interesting to note that Brown (1947), summarised the factors which he believed gave rise to high strength in textile reinforced polymers. These were:

- The fibre of which the textile is composed has a high Young's modulus and a high tensile strength.
- The yarn has a minimum twist.
- The fabric is constructed to allow the threads to lie as straight as possible with minimum crimp.
- The fabric is scoured.
- The resin has high tensile strength.
- The resin is able to penetrate the yarns to the maximum possible extent.
- The moulding pressure is high.
- Care is taken to avoid overbaking the plastic.

2.6.2 Recent work on plant-fibre reinforced thermosetting PMCs

Whilst the mechanical properties of the early composite laminates are extremely impressive and serve as a benchmark, it must be noted that their manufacture necessitated high temperatures and moulding pressures. For this, heavy and expensive equipment was required. Furthermore, the shape of the laminates produced thus were extremely limited. According to McMullen (1984), it was J.E. Gordon who first proposed that fibre reinforced composite materials should be used to low-pressure mould large, one-piece monocoque shells, rather than using the laminates as a direct substitute for existing materials. It is this approach - moulding complicated structures

at low pressures - which would, presumably, be the most (cost) effective means of utilising plant fibres in composites. There must, nevertheless, still be a number of applications for which high-pressure moulding would be appropriate. Much of the more recent work has, however, involved the use of thermosetting resins not requiring high moulding temperatures or pressures to form the laminate.

Some early work was conducted in the 1970's on the use of sisal and jute, to reinforce epoxy and polyester matrices, with the aim of producing low-cost housing units as well as other common structures (Paramasivam & Abdul Kalam, 1974; Winfield & Winfield, 1974). Paramasivam and Abdul Kalam (1974) found that tensile strengths of between 245 and 295 MN m^{-2} could be achieved from unidirectional sisal reinforced epoxy - nearly half the strength of a similar glass fibre-epoxy laminate. The stiffness of the unidirectional laminates was around 8.3 GN m^{-2}. No further details regarding this work were, however, published. Other experimental jute fibre reinforced polyester composites were produced for low-cost housing units as well as grain silos and fishing boats during this period (Winfield, 1979). Much of this work was, however, directly related to applications rather than to an evaluation of material properties.

More recently, Wells *et al.* (1980), studied the use of unmodified jute as reinforcement in an epoxy matrix. Unidirectional laminates were prepared from jute sliver (parallel stands of retted jute fibre), a non-twist experimental yarn, crimped warp fibre from hessian fabric, low-twist yarn, untwisted yarn and an experimental 'unidirectional' fabric. It was found that at a V_f of 70%, the non-twist experimental yarn resulted in the stiffest laminates (flexural modulus 38 GN m^{-2}), whilst the strongest laminates were the non-twist experimental yarn and untwisted yarn (at 395 and 384 MN m^{-2} respectively). These results are in accordance with the observation made by Brown (1947) that the threads should "lie as straight as possible with minimum crimp". The authors attributed the lower properties of laminates containing twisted or crimped fibres to orientation effects, rather than to fibre damage sustained during spinning or weaving. They also derived, by extrapolation, the Young's modulus for the fibres. These varied between 53 and 66 GN m^{-2}, depending upon species. Flexural strength was also derived by extrapolation and found to vary

between 570 and 640 MN m^{-2}. No data was presented on the relative impact properties of these laminates.

Roe and Ansell (1985) measured the tensile strength, Young's modulus, work of fracture (determined by Charpy impact) and inter-laminar shear strength of unidirectionally aligned, unmodifed jute fibre-polyester composites at a number of V_f. They found that Young's modulus, tensile strength, work of fracture and interlaminar shear strength all increased linearly with V_f. They also evaluated, by extrapolation, the fibre tensile modulus and found this to be 55.5 GN m^{-2} (which is in close agreement with that found by Wells *et al.*, 1980). The fibre tensile strength obtained, again by extrapolation, was 442 MN m^{-2}. The authors noted that above a V_f of around 60%, incomplete wetting of the fibres occurred and at a V_f of 70%, failure of the laminates occurred at low stresses. Strain to failure was observed to rise with increasing volume fraction, levelling off at around 1%. The work of fracture of the composites was evaluated using a notched Charpy test. It was noted that at volume fractions greater than 30%, the composites were "tough". This was accompanied by a change in the failure mode of the laminates; from tension, to tension plus shear. At a V_f of 60 %, the work of fracture rose to in excess of 20 kJ m^{-2}, for a crack propagating normal to the fibre direction.

Sanadi *et al.* (1985), fabricated unidirectional sunhemp (another bast fibre) fibre reinforced polyester resin composites. They found that both Young's modulus and ultimate tensile strength followed a linear ROM relationship with volume fraction. A fibre modulus derived from the ROM was found to be approximately 35 GN m^{-2}. They concluded that the specific stiffness of a unidirectional sunhemp reinforced composite of 40% V_f was higher than that of a glass fibre composite of 20% V_f. In their study on the origins of toughness of natural fibre-polyester composites, Sanadi *et al.* (1986a) measured the notched Izod impact strength of unidirectional sunhemp-polyester composites. They found that at a V_f of 24%, the work of fracture measured in this way was 21.54 kJ m^{-2}, some 15 times greater than that of the unreinforced polymer alone (1.37 kJ m^{-2}). It was noted that following fracture, some of the fibres had undergone fibrillation and splitting, and that the paths of propagating

cracks were not straightforward. For instance, it was observed that an advancing crack may have entered the fibre but, may then have been deflected along the interface between fibre ultimates and thereafter, deflected again across the fibre, resulting in a "step-fracture". Pull-out aspect ratios were noted to be of the order of 3. They concluded that the main fibre fracture mechanisms included "fibril" pull-out, plastic flow of the lignin-hemicelluose matrix, plastic deformation of the fibrils, fibre splitting and crack diversion at the fibril-fibril interface. It was believed that these mechanisms were partially responsible for the high toughness of these materials.

Later, Sanadi *et al.* (1986b) analysed the tensile and impact properties of sunhemp fibre-reinforced polyester unidirectional composites, as well as the tensile properties of the fibres themselves. Ultimate tensile strength and Young's modulus of approximately 390 MN m^{-2} and 35 GN m^{-2} respectively were obtained for the fibres. The fibre strain to failure was noted to be 1.1%. Once again, the Young's modulus and tensile strength of the laminates varied linearly with V_f, following closely the theoretical predictions of the ROM. In addition, they predicted the frictional interfacial shear stress from the observed pull-out lengths of the fibres and found this to be 4.34 MN m^{-2}. They noted that the effectiveness of the fibre-matrix bond is dependent upon the chemical compatibility and the presence of mechanical "keying" between fibre and matrix.

Their analysis of the toughness of the composites included a comparison with theoretical predictions. It was found that for the composite systems under investigation, the experimental works of fracture were only around a half those predicted from the theory. By way of explanation they noted, for instance, that the fibres may well permanently contract during pull-out (as evidenced by the "considerable 'clearance' between the fibres and the matrix"), resulting in reduced frictional energy absorption. Furthermore, they believed that variations in the frictional interfacial shear stress, caused by the fibres twisting and turning as they pull-out from the matrix socket, might well affect the work of fibre pull-out. In addition, they believed that the estimate for the interfacial fracture energy they had used for the theoretical prediction was on the high side, which had the effect of increasing the total

work of fracture. They also commented that the phenomenon of fibre fracture was quite complex.

Kumar (1986), prepared unidirectional jute fibre-epoxy laminates with a 29% fibre volume fraction, using a hand lay-up technique. These laminates were tested to determine the longitudinal and transverse moduli, Poisson's ratio and shear modulus. The average longitudinal modulus was found to be 16.8 GN m^{-2} (this compared with 13.5 GN m^{-2} for the modulus predicted from the ROM). The ultimate tensile strength was found to be 119.2 MN m^{-2}. It was found that the average strain to failure of the laminates was 0.71%. In tests conducted on the fibres themselves, these workers found the average tensile strength of jute fibre to be 271 MN m^{-2} and Young's modulus to be 39.1 GN m^{-2}. The stress-strain behaviour of the fibres was linear to failure. Average transverse modulus and strength were found to be 3.47 GN m^{-2} and 10.2 MN m^{-2} respectively. Under both longitudinal and transverse loading the stress-strain behaviour of the laminates was linear to failure. The in-plane shear modulus and Poisson's ratio were found to be 1.5 GN m^{-2} and 0.32 respectively.

O'Dell (1997), prepared resin transfer moulded (RTM) laminates to a volume fraction of between 10% and 15%, using a non-woven jute fabric to reinforce an unsaturated polyester matrix. The properties of these were compared with those of laminates reinforced with a random continuous glass fibre mat. It was found that both the tensile and flexural strength, and stiffness of the jute laminates, were generally less than half that of the glass fibre reinforced material. Notched and un-notched Izod tests, showed that the impact strength of the jute reinforced material, was an order of magnitude lower than that of the glass fibre reinforced material.

Like O'Dell (1997), Sèbe *et al.* (1999) also studied the properties of RTM laminates consisting of non-woven fabric reinforced unsaturated polyester. Rather than jute, however, hemp was the fibre of choice in this work. It was found that flexural strength and modulus increased with V_f. Un-notched Charpy impact strength, on the other hand, was found to decrease initially with low fibre content, but then increase on the addition of further fibre. The poor impact properties were attributed to the introduction of "a disproportionately high degree of critical defects to the composite

structure, perhaps in the form of voids or poorly bonded interface regions". It was also thought that this phenomenon might be partially explained by the presence of many pre-existing fibre microcompressive defects.

Munikenche Gowda *et al.* (1999) studied the mechanical properties of untreated jute fabric-reinforced polyester composites. Woven jute fabric was hand laminated with polyester resin to form composites with a fibre volume fraction of around 45%. The average longitudinal tensile strength and modulus of this laminate was found to be 60 MN m^{-2} and 7 GN m^{-2} respectively. The same properties under transverse loading were 35 MN m^{-2} and 3.5 GN m^{-2} respectively. The discrepancy was attributed to differing numbers of yarns in the warp and weft directions of the reinforcing fabric. Under compression, the addition of reinforcement was found to improve the compressive modulus around twofold over that of the unreinforced resin. The compressive strength of the laminate was, however, almost the same as the pure resin; this is in agreement with the findings of De Bruyne (1937) for "Cord-Aerolite". In flexure, the laminates exhibited average strengths and moduli of 92.5 MN m^{-2} and 5.1 GN m^{-2} respectively. The authors reported that in the flexural tests, no specimen failed through delamination and that the failure mode exhibited little or no fibre pull-out. Charpy impact tests were conducted and it was found that at this fibre volume fraction, the average impact strength of the laminates was 29 kJ m^{-2}, approximately 16 times greater than that of the pure resin alone. An average interlaminar shear strength of 10 MN m^{-2} was reported for these laminates. In-plane shear strengths and moduli for this material were found to be 16.6 MN m^{-2} and 2.2 GN m^{-2} respectively.

Oksman (1999), studied the mechanical properties of RTM flax fibre reinforced-epoxy matrix composites. The flax fibre used in this study was enzymatically retted, in a semi-industrial process, and thought to be of superior quality to conventionally retted fibre. The mechanical properties of unidirectional composites reinforced with these fibres and with traditionally (field) retted flax as well as with glass fibres were compared. It was found that for equivalent V_f, the strength (both absolute and specific values) of the enzymatically retted fibre reinforced material was better than the conventionally retted fibre; but that neither reached that of the glass fibre laminate. The stiffness of the unidirectional enzymatically retted flax-reinforced laminates was

found to be superior to that of the glass fibre reinforced laminates, for equal V_f. The strain to failure of the enzymatically retted flax-reinforced epoxy was found to lie between 0.8% and 0.9%, which compared with around 2.8% for the glass fibre reinforced material. The stress-strain behaviour was found to be approximately linear. A derived fibre strength for the enzymatically retted material of 700 MN m^{-2} was obtained. A fibre modulus of between 80 and 100 GN m^{-2} was estimated for the enzymatically retted flax. It was thought that the adhesion between fibre and matrix was not "as strong as expected", as evidenced by visible fibre pull-out and the fact that the fibres were "not covered with the epoxy matrix". It was noted, however, that the void content was low. No data on toughness was presented.

Bos and Van den Oever (1999) studied the influence of fibre structure on the mechanical properties of pultruded flax-polyester and flax-epoxy laminates. These materials were tested in tension and in compression. Interestingly, whilst the tensile strength of flax-polyester composites increased with V_f, following a ROM relationship, their compressive strength did not show any increase, but stayed at the level of the compressive strength of the pure polymer. It was noted that adhesion between the fibre and polymer was "very poor" and was attributed to the thin waxy layer surrounding the fibres, which it was thought prevented bonding. However, removal of this layer did not result in an improvement in compressive strength. Several regimes designed to improve the compatibility between the two phases were tried, but without success. It was speculated that fibre damage in the form of kink bands may have contributed to the low compression strength of the laminates. Similar effects were observed with the flax-epoxy system. An increase in tensile strength was observed with V_f, whilst compressive strength was unaffected. A slight increase in the compressive strength (~16%) was noted upon removal of the waxy layer. Again, however, it was concluded that adhesion was poor. Addition of melamine-formaldehyde (MF) as a compatibiliser did improve compressive strength, but at the expense of tensile strength. It was postulated that the MF stabilised kink bands in the fibre, thereby improving compressive strength, rather than simply acting as a compatibiliser. The authors believed that kink band damage, present in scutched

fibres, hindered optimisation of the compressive strength of these laminates and might "seriously hamper the use of flax fibres in more structural applications".

It may be noted that the more recent work reviewed above considered the use of bast fibres only as reinforcement. For completeness, however, it should be noted that a number of other agro-fibres have been considered in the capacity of reinforcement in PMCs. These include, for example, straw (White & Ansell, 1983), sisal (Bisanda & Ansell, 1991), bamboo (Jain *et al.*, 1992), wood cellulose (Zadorecki, *et al.*, 1986; Zadorecki & Michell, 1989) and coir (Prasad *et al.*, 1983).

As noted by Sanadi *et al.* (1985), moisture absorption and poor bonding between fibre and matrix "have been identified as the major bottlenecks in large scale use of these composites". Lignocellulosic material is inherently hydrophilic. This is due to the abundant hydroxyl functionality present in the cell wall polysaccharides (Desch & Dinwoodie, 1996). Accessible -OH groups, not mutually satisfied, are able to hydrogen bond with available water molecules. This results in the absorption of moisture, leading to swelling of the cell wall material. Conversely, desorption leads to shrinkage. In addition to dimensional instability, the presence of -OH groups on the fibre surface render this hydrophilic, giving rise to potential problems of compatibility with (more) hydrophobic synthetic polymers (Bolton, 1995). This is a particular issue with thermoplastics (Ivens *et al.*, 1997) and a significant volume of work has been published on the means of achieving an improvement in the compatibility between the two phases (e.g. Myers *et al.*, 1990; Kolosick *et al.*, 1990; Maldas & Kokta, 1991a,b; Liang *et al.*, 1994). The situation with thermosetting resins is somewhat different, however, in that these polymers are generally more hydrophilic. For example, epoxy resins often contain -OH functionality, rendering them somewhat polar (Turner, 1988) and are thus likely to be more compatible with lignocellulosic material.

Nevertheless, a combination of fibre dimensional instability coupled with relatively poor adhesion between the phases, can lead to compromised composite properties (Zadorecki & Flondin, 1986), as well as to dimensional instability of the laminates themselves. Indeed, dimensional instability was noted to be one of the problems

associated with the early flax-phenolic materials (Gordon, 1976). Whilst no work is presented herein on the use of either surface or fibre modification to improve composite properties, it is worthwhile noting that a good deal of work has been published in this area. It is appropriate, therefore, to note some of the general findings obtained, particularly with regard to the effects of fibre modification on the mechanical properties of the composites.

Zadorcki and Flondin (1986), for instance, conducted a microscopical study of the formation of debonding cracks in cellulose fibre based unsaturated polyester composites. The reinforcing fibre was in the form of a bleached kraft paper. This was used in unmodified form and modified by the introduction of coupling agents based on trichloro-*s*-triazine. Three coupling agent were utilised. Two were considered to result in covalent bonds forming across the interface whilst the other was thought to lead to improved molecular contact. Initially, all composites were "translucent", indicating that no voids were present in the material. Following soaking and redrying, however, "whitening" occurred in the untreated fibre-polyester specimens as well as in composites reinforced with fibres modified in such a way as to lead to improved molecular contact. In the composites formed from fibres modified so as to form covalent bonds across the interface, no such debonding cracks were noted. The authors postulated a mechanism of crack formation, based upon the stresses induced across the interface when the fibres dried out; in poorly bonded material this occurs relatively easily, in well bonded laminates rather less so.

Hua *et al.* (1987), investigated the use of formaldehyde and melamine compounds to modify cellulose fibre with the aim of producing composites with reduced moisture sensitivity. Laminates, prepared from modified and unmodified bleached kraft paper reinforced polyester resin, were tested for moisture absorption and wet and dry mechanical properties. Although the dry mechanical properties were little affected by the method of modification and were somewhat better than the untreated fibre-reinforced material, the wet strength of some of the modified fibre reinforced material was markedly superior to others and to the untreated fibre laminates. It was believed that not only was interfacial adhesion enhanced but also the fibre strength was improved by modification (using 5% formaldehyde and 5% dimethylolmelamine).

Bisanda and Ansell (1991), studied the effect of silane treatment on the mechanical and physical properties of unidirectional sisal-epoxy composites. They found that silane treatment (following mercerisation) resulted in an improved resistance to water absorption (after 72 hours immersion). In moist environments, all mechanical properties (compressive strength, flexural modulus and flexural strength) were improved with the silane treated sisal-reinforced laminates. Interestingly, they found that, apart from compressive strength, the dry mechanical properties were unaffected by use of the coupling agent. The compressive strength of the laminates was improved following mercerisation. This was attributed to an "improvement in the interfacial bonding by giving rise to additional sites of mechanical interlocking, hence promoting more resin/fibre interpenetration at the interface". No additional improvement was gained after silane treatment. It was noted that the failure of the untreated fibre composites was "predominently by cleavage in the loading planes with little bulging and shear buckling". It was considered that the waxy surface of the untreated fibre allowed an easy mode of failure, which the strongly bonded material was able to resist. The modified fibre-reinforced composites on the other hand, underwent "considerable lateral deformation before finally failing by shear deformation, usually indicated by a zone of kinked fibres making an inclination of about 45^{O} to the loading axis".

Ogano-silane treated fibre was used as reinforcement (orientation unspecified) in RTM jute-epoxy composites by Gassan and Bledzki (1996). The composites were manufactured with a fibre volume fraction of about 40%. It was noted that following modification, tensile strength became independent of laminate moisture content, but modulus fell with increasing moisture levels. At the maximum attainable moisture content (~5.2%), Young's modulus was around 30% lower than the dry value. With unmodified fibre reinforcement, tensile strength fell to around 65% at the maximum moisture content, whilst modulus only retained around 25% of its dry value. Dry properties, however, appeared to be little affected by surface modification.

Sèbe *et al.* (2000), in their studies on RTM hemp fibre reinforced polyester, observed that the introduction of strong interfacial adhesion, by modification with methacrylic anhydride, did not result in an increase in the dry flexural properties of the laminates.

However, it was noted that the mode of failure changed, with modification causing the composites to become embrittled. Subsequent unnotched Charpy impact tests confirmed this to be so. It was noted that fibre pull-out was suppressed in the case of the modified fibre reinforced composites. It has been shown conclusively that such modification leads to the formation of covalent bonds with the matrix (Hill & Cetin, 2000).

The above represents a brief review of some of the literature concerned with the use of surface or chemical treatments to improve the performance of vegetable fibre reinforced thermosetting PMCs. Broadly speaking, whilst improved interfacial bonding enhances the wet strength and stiffness of lignocellulosic fibre reinforced composites, the dry properties are less affected, with at best only fairly minor improvements in performance being recorded. On the other hand it has been intimated that toughness (measured as impact strength), may well be compromised by the introduction of strong interfacial adhesion.

A summary of some of the main mechanical properties of the plant fibre reinforced thermosetting PMCs reviewed herein (arranged in chronological order) are presented in Table 2.4.

2.7 Approach

As may be noted, most of the work reviewed in the preceding section has focused on evaluating the properties of finished laminates and the effects of either, *a)* fibre type, *b)* fibre loading fraction, *c)* orientation of reinforcement or *d)* the use of coupling agents or chemical modification, to improve either the short-term mechanical properties of the material, or their environmental performance.

Table 2.4 A summary of some of the mechanical properties of a number of plant fibre reinforced thermosetting PMCs.

Reference	*Fibre type*	*Matrix type*	V_f (%)	*Reinforcement geometry*	*Fibre treatment*	*Tensile modulus* ($GN\ m^{-2}$)	*Flexural modulus* ($GN\ m^{-2}$)	*Tensile strength* ($MN\ m^{-2}$)	*Flexural strength* ($MN\ m^{-2}$)	*Work of fracture* ($kJ\ m^{-2}$)	*Failure strain* (%)
Aero Research Ltd. (1945)	flax (spun)	phenolic	75	UD 'Gordon-Aerolite'	none	48.0	-	480.0	-	-	-
Paramasivan & Abdul Kalam (1974)	sisal	epoxy	-	UD	none	8.3	-	245.0-295.0	-	-	-
Wells *et al.* (1980)	jute	epoxy	70	UD 'retted'	none	-	43.5	-	450.0	-	-
	"	"	"	UD 'sliver'	"	-	28.0	-	320.0	-	-
	"	"	"	UD 'expt. yarn'	"	-	38.5	-	395.0	-	-
	"	"	"	UD 'untwisted yarn'	"	-	28.7	-	384.0	-	-
	"	"	"	UD 'fabric'	"	-	24.0	-	305.0	-	-
	"	"	50	'hessian'	"	-	8.0	-	90.0	-	-
	"	"	60	'felt'	"	-	10.0		100.0	-	-
White & Ansell (1983)	straw	polyester	61	UD	none	8.2	5.5	-	53.0	3.8	-
Prasad *et al.* (1983)	-	-	0	-	-	-	3.1	-	48.5	8.3	-
	coir	polyester	20	'random mat'	none	-	2.5	-	33.0	7.4	-
	"	"	"	"	'NaOH'	-	3.4	-	42.3	11.3	-
Roe & Ansell (1985)	-	polyester	0	-	-	4.0	-	20.0	-	-	-
	jute	"	60	UD	none	35.0	-	250.0	-	22.0 (notch-ed Charpy)	~1.0

Table 2.4 Continued.

Sanadi *et al.* (1986b)	sunn-hemp	polyester	24	UD	none	11.2	-	125.0	-	21.0 (notch-ed Izod)	-
Kumar (1986)	jute	epoxy	29	UD 'longitudinal'	none	16.8	-	119.2	-	-	0.71
	"	"	"	UD 'transverse'	"	3.5	-	10.2	-	-	-
Zadorecki *et al.* (1986)	wood pulp	polyester	0	-	-	3.3	-	78.5	-	-	4.7
		"	40*	'planar isotropic'	none	6.7-8.5	-	66-79	-	-	1.1-1.7
Hua *et al.* (1987)	wood pulp	polyester	45	'planar isotropic'	none	4.8	-	129.8	-	-	-
		"	"	"	DMM[1]	5.1	-	139.6	-	-	-
Bisanda & Ansell (1991)	-	epoxy	0	-	-	-	3.1	-	95.0	-	-
	sisal	"	40	UD	none	-	15.9	-	266.5	-	-
	"	"	"	"	mercerised	-	17.6	-	262.1	-	-
	"	"	"	"	silane	-	17.4	-	244.5	-	-
Jain *et al.* (1992)	bamboo	epoxy	50	UD	none	-	-	175.3	151.8	45.6 (kJ m^{-2}) (35% V_f)	-
Uma Devi *et al.* (1997)	pine-apple	polyester	0*	-	none	0.6	-	20.6	2.0	1.6	
	"	"	10*	'random orientation'	"	1.8	-	17.1	3.6	1.3	
	"	"	20*	(30mm fibre length)	"	1.8	-	40.0	12.0	3.0	
	"	"	30*	"	"	2.3	-	52.9	24.2	3.6	
	"	"	40*	"	"	2.5	-	63.3	-	5.0	
O'Dell (1997)	jute	polyester	10-15	air-layed non-woven 'longitudinal'	none glycol	3.7	3.1	45.8	61.7	38.7 (J m^{-1})	-
	"	"				3.2	3.2	43.5	63.1	32.4 (J m^{-1}) (unnotched Izod)	-

Table 2.4 Continued.

Zimmerman & Losure (1998)	-	epoxy	0	-	none	2.6	-	57.0	-	0.8 (J cm^{-1})	-
	kenaf	"	24	non-woven	"	1.8	-	26.0	-	0.5 (")	-
	"	"	35	"	"	1.8	-	40.0	-	0.6 (")	-
	"	"	44	"	"	3.5	-	39.0	-	0.5 (")	-
Bos & van den Oever (1999)	flax	polyester	30*	UD 'pultruded'	none	-	-	285.0	-	-	-
	"	epoxy	"	"	"	-	-	250.0	-	-	-
Munikenche Gowda *et al.* (1999)	-	polyester	-	-	-	1.4	2.2	12.1	48.0	-	-
	jute	"	45	woven 'longitudinal'	none	7.0	5.1	60.0	92.5	29.0	-
	"	"	"	woven 'transverse'	"	3.5	-	35.0	-	-	-
Oksman (1999)	flax	epoxy	21	UD 'enzyme retted'	none	22.0	-	193.0	-	-	0.9
	"	"	42	"	"	35.0	-	280.0	-	-	0.9
	"	"	47	"	"	39.0	-	279.0	-	-	0.8
	"	"	32	UD 'field retted'	"	15.0	-	132.0	-	-	1.2
Sèbe *et al.* (1999)	-	polyester	0	-	-	-	3.7	-	33.0	8.5	-
	hemp	"	26	air-layed non-woven	none	-	5.3	-	80.0	8.8	-
	"	"	"	'random'	pyridine	-	5.4	-	77.0	8.8	-
	"	"	"	"	methylme-thacrylate	-	6.5	-	74.0	3.0	-

Notes: *Weight fraction. [1]DMM – dimethylolmelamine. UD – unidirectionally aligned fibre composite

As far as thermosetting PMCs reinforced with bast fibre are concerned, very little work appears to have been undertaken with regard to the fundamental mechanics of the interaction between fibre and matrix and the effect that this has upon the mechanical behaviour of the material. It was noted in Section 2.1.7 that toughness is a particularly important mechanical property, required of an engineering material. It seems likely, therefore, that if bast fibre reinforced composites are to be used in structural or semi-structural applications, then due account will need to be taken of this important property.

Whilst an improvement in properties over those of the unreinforced polymer have, quite rightly, been emphasised, relatively little work appears to have been conducted on the mechanical properties relative to their most likely synthetic competitor - glass fibre. It would seem appropriate, therefore, that in any work undertaken the properties of bast fibre reinforced materials should be compared directly (on a volume for volume basis) with their glass fibre reinforced equivalents.

In view of the foregoing, it was believed that this work should consist of a thorough appraisal of the short-term mechanical properties of the material, with particular emphasis on toughness, since this aspect does not appear to have been as rigorously assessed as the other properties. In conjunction with this, it was felt that it was important to investigate both the fibres themselves, particularly with regard to any features which might affect the mechanical properties of the composite properties, and the interaction between fibre and matrix - the composite micromechanics.

3 Physical and Mechanical Properties of Laminates

3.1 Introduction

Whilst the environmental benefits of substituting the synthetic fibres, currently used as reinforcement in thermosetting PMCs, with natural fibres would appear clear, it is also evident that the resultant composite materials must be able to compete in performance terms too. The work presented in this and the following two chapters was undertaken in order to gain a more fundamental understanding, at various levels of organisation, of the mechanisms controlling the mechanical behaviour of these materials. At this stage, no chemical or surface modification of the fibres was considered as a means of improving the short-term performance of the composites. It was believed that a better starting point would be a thorough investigation into factors which might contribute to the mechanical response of bast fibre reinforced thermosetting PMCs. This approach was adopted in the belief that a more thorough understanding of material behaviour could help pinpoint any limiting factors and possibly highlight ways in which performance might be improved.

In this chapter, the physical and macro-mechanical properties of laminates prepared from non-woven, un-modified bast fibre (jute and hemp) reinforced unsaturated polyester are considered. Throughout, these properties are compared with those of equivalent (on a volume for volume basis of reinforcement) materials reinforced with glass fibre. During an extensive programme of preliminary tests (some of the results of which are presented in Section 3.3.2), it became clear that the natural fibre reinforced material appeared to lack the toughness, that is to say the crack stopping ability, of their glass fibre reinforced equivalents. In view of this, a significant proportion of this chapter is given over to the quantification, utilising fracture mechanics techniques, of this property. In addition to this, other, short-term mechanical (tensile, flexural and impact) properties of the laminates are presented.

3.2 Materials and method

3.2.1 Fibre

Two bast fibre types were utilised in this part of the work, namely jute *(Corchorus capsularis)* and hemp (*Cannabis sativa*). Jute, grown, retted, decorticated, chopped and baled in Bangladesh, was supplied by Sidlaws of Dundee. Hemp, grown in the UK, was supplied by Hemcore Ltd. This fibre had been dew retted and mechanically decorticated, prior to chopping and baling. The length of both fibre types was approximately 50 mm. No further fibre treatment had been carried out. The fibres were processed into a non-woven felt, in the manner described in Chapter 2, by J.B. Plant Fibres Ltd. of Holyhead, Gwynedd. The areal density of the material used for composite fabrication varied from approximately 350 g.s.m (grams per square metre), to around 1100 g.s.m. Prior to use, the fibre felts were refluxed in a mixture of toluene, acetone and industrial methylated spirit (in the proportions 4:1:1 by volume) for ½ hour to remove waxes and other extractable material.

In addition to the natural fibre reinforcement, glass fibre was utilised for comparative studies. This was supplied in the form of chopped strand mat (CSM), manufactured by Scott Bader.

3.2.2 Matrix resin

A general purpose unsaturated polyester resin (Synolite 0593-T-1, manufactured by DSM resins) of 40% styrene content was used for the matrix. This required accelerator (N,N-diethylaniline, 10% in aliphatic ester) and initiator (dibenzoylperoxide) for curing at room temperature (~20^{o}C). Accelerator and initiator, added at a rate of 3% (by weight) each, were found to give a gel time of approximately 1 hour which was adequate for completion of the fabrication process.

3.2.3 Laminate fabrication

Laminates were prepared as flat plaques, approximately 30 cm square and of nominal thickness 4.5 mm. These dimensions were found to be suitable for a variety of test specimen sizes.

The investigation into the effect of fibre volume fraction on mechanical properties necessitated the fabrication of laminates containing various fibre loadings. A single layer of non-woven material, lightly clamped to a pressure of approximately 0.5 bar, produced laminates with a V_f in the region of 16%. Higher volume fractions were achieved by pre-pressing multiple layers of felt in a hot press at 105°C to a thickness of 4.5 mm. The press was held closed for 5 minutes. It was found that when the pressure was released a permanent 'set' had been imparted to the fibre felts. Little 'spring back' was noted after removal of the clamping pressure. After pressing, the felts were allowed to recondition at 65% R.H. and 20°C. Very little further 'spring back' was evident. Preliminary tests on the laminates containing single layers of felt showed that there was a degree of anisotropy (see Section 3.3.2) which was attributed to a preferred fibre orientation imparted to the felts during manufacture. Because of this, in laminates requiring several plies, multiple felts were stacked with the same orientation and subsequent testing undertaken bearing this in mind. The lamination procedure was as follows:

3.2.3.1 Resin preparation

Accelerator was first added to the resin and mixed thoroughly with a mechanical stirrer for approximately 5 minutes (for a 1 kg charge). Subsequently, the initiator was added and mixing continued (a further 5 minutes). Prior to use, the resin was degassed under vacuum for 5 minutes.

3.2.3.2 Felt impregnation

The felt impregnation process essentially involved drawing, by means of vacuum, catalysed resin through a plastic tube in which the reinforcement was situated. A schematic representation of the process in shown in Figure 3.1.

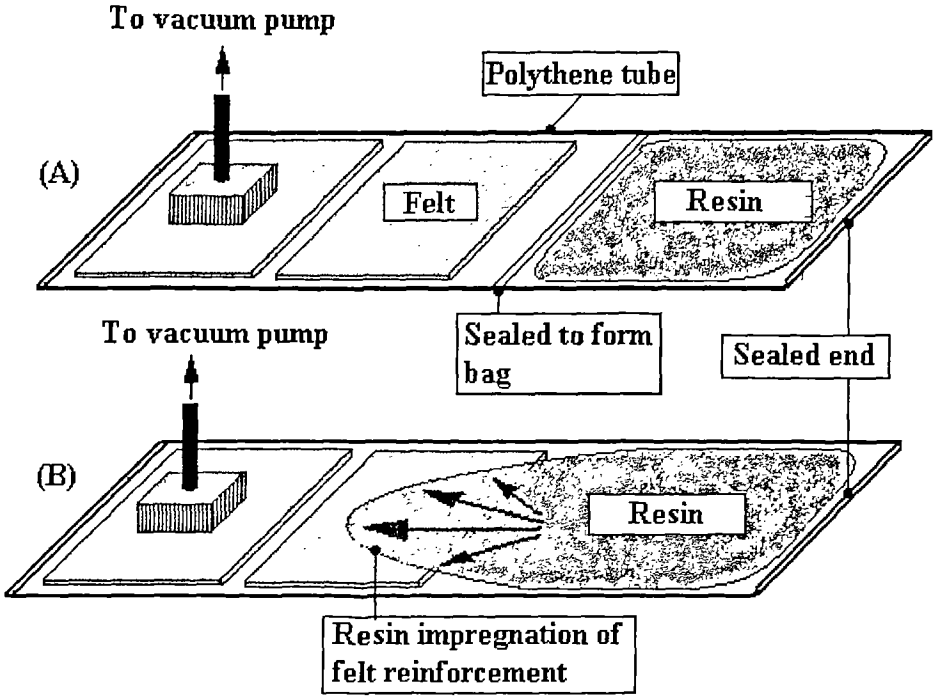

Figure 3.1 Resin vacuum impregnation process.

Squares of felt reinforcement (either single 'ply' or pre-pressed 'multi-ply') were inserted into heavy duty industrial polythene tubing which, when laid flat, was of a width such that the felts formed a 'snug' fit when inside (in practice the tubing was approximately 10 cm wider than the felt; the width of the tubing was reduced by folding over and taping). A tight fit was necessary to prevent the resin bypassing the felts, leaving resin starved regions. An additional, 'sacrificial' felt was inserted at the head of the tube, to prevent resin entering the suction head (attached to a vacuum pump) or collapsing the tube when under vacuum. This end was then sealed with tape. At the other end of the tube, a bag was formed with the aid of 'bulldog' clips, into which the catalysed resin was poured. Once the resin was in the bag formed at the end of the tube, this end too was sealed with tape. The clips separating the resin and reinforcement were subsequently removed and the catalysed polymer allowed to slowly impregnate the felt. Impregnation was assisted mechanically by means of a roller. As soon at the felts were fully loaded with resin, the vacuum was removed, the tube cut open and the impregnated felts taken out for moulding.

3.2.3.3 Moulding

The impregnated felts were placed between toughened glass plates (400 mm x 400 mm by 15 mm thick) to which had previously been applied a film of wax release agent (M700/C-WAX; Oskar's, Pflegemittel GmbH, D-47059 Duisburg, Germany) in accordance with the manufacturers instructions. Mild steel spacers, 4.5 mm thick (7.0 mm thick for fracture toughness specimens) were inserted at each corner and the plates clamped.

3.2.3.4 Preparation of CSM reinforced laminates

The vacuum impregnation technique could not be used for the CSM reinforcement, due to excessive 'washing' of the reinforcement during the process, resulting in very uneven laminates. Instead, the laminates were prepared by careful hand lay-up directly onto the glass plates. Once the desired thickness had been built up, another plate was placed on top, with spacers between the plates, and clamped as described above.

3.2.3.5 Casting of resin without reinforcement

Unreinforced resin laminates were prepared by pouring catalysed resin onto a glass plate, children's modelling clay ('Plasticine') being used to prevent resin overflow. A second plate was placed on top with spacers between the two and clamped.

3.2.3.6 Laminates for fracture toughness testing

In order to attempt an estimation of the toughness of the material using fracture mechanics techniques, thicker specimens were utilised. These were prepared in the same manner as described above save that several additional layers of felt were required to attain comparable fibre volume fractions. These laminates were prepared to a nominal thickness of 7.0 mm.

3.2.4 Curing

Gelation was allowed to proceed at room temperature (~20^{o}C) for approximately 20 hours, after which the laminates were removed from the plates and placed in an oven to post cure for 6 hours at 90^{o}C. This temperature was chosen so as to minimise

thermal degradation of the fibre. To reduce distortion of the laminates during this stage of the operation they were placed between 4 mm thick aluminium plates and clamped. The laminates were separated by 'grease-proof' baking paper to prevent contact with one another and the plates.

3.2.5 Specimen preparation

A number of mechanical tests were performed, each requiring specimens of differing dimensions; nevertheless, the preparation procedure was similar for all. The tests conducted included the following:

- tensile (Young's) modulus and tensile strength
- flexural modulus and strength
- Charpy impact strength
- fracture toughness.

Coupons for the tensile, flexural and Charpy impact strength tests were prepared from the natural fibre reinforced laminates by cutting with a circular cross-cut saw. By this method it was found that samples could be prepared with minimal damage to the cut surfaces. The cut surfaces were, however, gently abraded to remove artefacts. Initial testing showed that acceptably low standard deviations were achievable, indicating that the effect of preparation damage was minimal. All CSM and un-reinforced polymer laminates, as well as those specimens destined for fracture toughness testing were, however, cut with a water lubricated diamond saw. This method gave an excellent surface finish.

Starter notches for the fracture toughness specimens were cut centrally in an 'edgewise' plane using the diamond saw (see Figure 3.2). To obtain a sufficiently sharp starter crack at the root of the notch, razor sawing, as described in Anderson (1995), was utilised. Plate 3.1 shows a sharp notch 'sawn' in a polyester resin specimen. This method proved satisfactory for all laminate types.

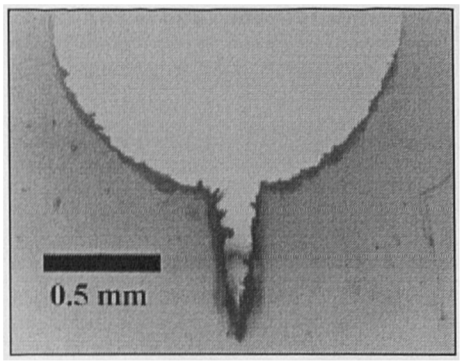

Plate 3.1 Transmitted light micrograph of a sharp 'starter crack' sawn at the root of a notch stress concentrator in an un-reinforced polymer laminate.

3.2.6 Conditioning

Prior to testing, all specimens were conditioned for a minimum of one week at 65% relative humidity and a temperature of 20^{O}C.

3.2.7 Testing

Tensile tests were conducted on an Instron 1195 universal testing machine, fitted with a 100 kN load cell. Load versus extension (measured either as cross-head movement or independently by means of an extensometer) data were acquired by PC, which also facilitated machine control. Flexural and fracture toughness tests were carried out on an Instron model 4301, universal testing machine fitted with a 5 kN load cell. This instrument too was PC controlled.

3.2.7.1 Tensile tests

Tensile testing was conducted in accordance with BS 2782: Part 10: Method 1003:1977. (EN 61). A cross-head speed of 2 mm min.$^{-1}$ was used. Modified type II specimens were utilised; the modification lay in specimen dimensions and clamping. The standard specifies a specimen length of at least 250 mm. In view of the size of the laminates, however, this was not possible and thus this was reduced to 200 mm, with a width of 20 mm, thereby maintaining the same specimen aspect ratio. Furthermore, rather than utilising pin jointed ends, the specimens were clamped using

self tightening jaws. To prevent damage to the specimen where clamped, removable 'U' shaped aluminium tags were fitted over the ends of the specimen prior to clamping. A slight abrading of the ends ensured that the specimens did not slip in the jaws. During testing, fracture of the specimens (even the brittle resin) rarely occurred within or near to the grips. Every care was taken to ensure correct alignment of the specimens in the jaws, prior to final tightening. Strain was measured with an extensometer, attached to the central portion of the test specimen with clips. During testing, this was removed at a pre-determined point (0.3% strain) to prevent damage when the specimen failed.

3.2.7.2 Flexural tests

Testing was conducted in accordance with BS 2782: Part 10: Method 1005: 1977 (EN 63) - Determination of Flexural Properties. Three Point Method. Specimen coupons of nominal dimensions 100 mm x 15 mm x 4.5 mm were utilised. The cross-head speed was 10 mm $min.^{-1}$.

3.2.7.3 Impact tests

The Charpy method (BS EN ISO 179:1997 - Determination of Charpy impact strength) was used to assess the flat-wise impact properties of un-notched type 1 specimens. The nominal specimen dimensions were 80 mm x 10 mm x 4.5 mm. An analogue Zwick instrument, equipped with either a 0.5 J or a 4 J pendulum was used.

3.2.7.4 Fracture toughness

The procedure adopted for the determination of fracture toughness was based upon the method described in BS 7448: Part 1: 1991. This standard describes a procedure to determine the opening mode plane strain fracture toughness (K_{IC}), the critical crack-tip opening displacement (CTOD) fracture toughness, and the critical J fracture toughness of metallic materials.

Rectangular section, single edge notched (SEN) specimens were loaded in three point flexure. The load-line displacement rate (cross-head speed) was 5 mm $min.^{-1}$. The loading fixture and nominal specimen dimensions are shown schematically in Figure 3.2. In addition to noting the overall dimensions of the specimen, the depth of the

notch was accurately measured, prior to testing, by means of a dial micrometer (accurate to 0.01mm) equipped with a sharp edge (razor blade) which 'sat' in the sawn notch. Control of the loading device and data capture were via PC. The data capture rate was set at 20 points sec^{-1}. Specimens were loaded until a maximum force reading was attained. Captured data was saved in 'ASCII' format to facilitate subsequent analysis in 'ORIGIN' software.

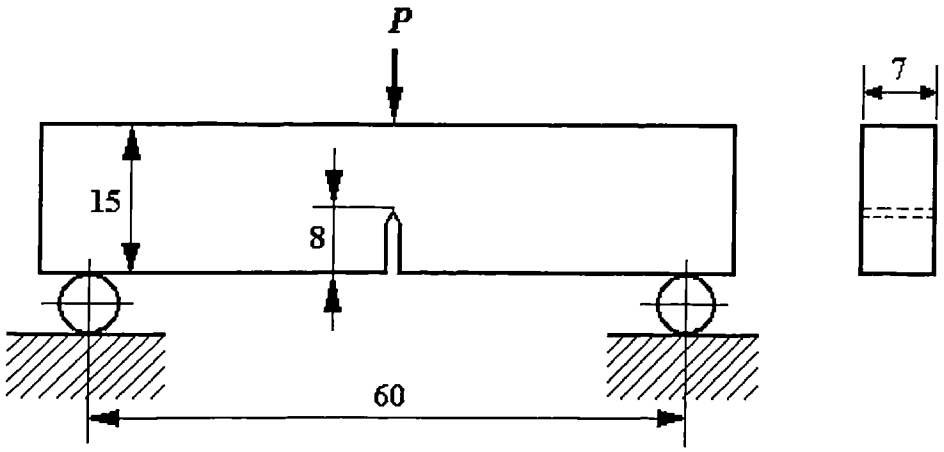

Figure 3.2 Three point bending specimen for fracture toughness determination (*all dimensions are in millimetres*).

3.2.8 Evaluation of physical properties

3.2.8.1 Measurement of density

The dimensions of all specimen coupons were accurately measured and their weight recorded. From these the composite density, ρ_c, was calculated using the well known relationship:

$$\rho_c = M_c/V_c \qquad (3.1)$$

Where: M_c is the mass of the composite

V_c is the volume of the composite

3.2.8.2 Measurement of fibre volume fraction

Fibre volume fraction may be calculated utilising Equation 3.2, provided the density of the fibre is known.

$$V_f = M_f / V_c \rho_f \tag{3.2}$$

Where: M_f is the mass of fibre

ρ_f is the bulk density of the fibre

Estimates of V_f were made using literature values for the bulk density of jute and hemp fibres. However, as will be discussed below, this method is potentially inaccurate due to a number of factors. Therefore, in addition, V_f was calculated from the following expression which does not require a prior knowledge of the fibre density (Roe & Ansell, 1985):

$$V_f = \left(V_c - \left(M_c - M_f\right)/\rho_r\right)/V_c \tag{3.3}$$

Where: ρ_r is the density of the cured polymer

This method accounts for any porosity of the fibre in the calculation and has the advantage that a value for the effective bulk density of the fibre can be derived. As stated by Roe and Ansell (1985), the value for V_f thus obtained is not strictly a true fibre volume fraction but, as will be discussed below, is probably more representative as a factor controlling mechanical behaviour than a derived volume fraction which assumes the fibre to be a solid mass.

3.2.9 Fractography

The modes of failure of the specimens tested were noted. Broken specimens from the Charpy tests were prepared for scanning electron microscopy by cutting, with a hacksaw, a small portion of the test specimens, in the region of the fracture surface

and securing to aluminium stubs with an epoxy adhesive. The samples were dried over silica gel, under vacuum, for at least 48 hours prior sputter coating with gold. Examination was conducted with a Hitachi S-520 scanning electron microscope (SEM).

3.3 Results and discussion

3.3.1 Physical properties

3.3.1.1 Appearance

The surface finish of the laminates produced was extremely smooth and defect free; this was attributed to the good surface finish of the plate glass used to mould the composite. The colour of the laminates depended upon that of the reinforcing material. Jute reinforced material was a rather light brown colour, whilst the hemp reinforced material was somewhat darker in appearance. Both natural fibre reinforced laminates were of a pleasing colour, being somewhat akin to varnished tropical hardwood. The CSM reinforced laminates were an off-white colour.

3.3.1.2 Fibre volume fraction

As discussed in Chapter 2, fibre volume fraction is probably the single most important parameter influencing composite properties (Matthews & Rawlings, 1994) and therefore it is essential to establish this as accurately as possible so that comparisons between, fibre types can be made. Fibre volume fraction may be evaluated by utilising Equation 3.2, which requires a value for the bulk density of the fibre. Natural fibres are, however, variable materials and jute and hemp are no exception. As such, figures quoted for their bulk density should be treated with caution. Variability arises from factors such as fibre maturity, which affects the cell wall thickness and consequently the density of the fibres. Figures vary considerably but typically lie in the region 600-1200 kg m^{-3} (Bolton, 1994), with values as high as 1480 kg m^{-3} having been reported (Ivens *et al.*, 1997). From Equation 2.8 it can be shown that, (assuming the density of the composite and resin remain constant), V_f varies as the inverse of fibre density. Since the upper threshold for fibre density occurs when it reaches the density of the

cell wall material (~1500 kg m^{-3}) a lower limiting value for V_f can be established for a given weight of fibre. This condition will be reached either when the fibres are solid, in other words they do not possess any lumen space whatsoever, or, if the lumena are completely filled with resin. It should be noted that this argument assumes that there are no additional voids present in the composite structure. Table 3.1 compares V_f derived by: *a)* assuming that the density of the fibres is that of the cell wall material, *b)* using literature values for fibre density (Ivens *et al.*, 1997) and *c)* using the expression in Equation 3.3. As expected, the volume fraction derived by assuming the fibre density to be 1500 kg m^{-3} (column A), in the most part, provides the lowest estimate of V_f (with the exception of 6 and 9 ply hemp laminates).

Table 3.1 Calculated volume fractions of laminates.

reinforcement type	*A.* V_f *(%) assuming* ρ_{fibre} $=1500\ kg\ m^{-3}$	*B.* V_f *(%)* $\rho_{jute}=1450\ kg\ m^{-3}$ $\rho_{hemp}=1480\ kg\ m^{-3}$	*C.* V_f *(%) (derived from Equation 3.3)*
2 ply jute	18.8	19.5	19.3
4 ply jute	34.8	36.6	36.3
6 ply jute	39.0	40.4	40.4
3 ply hemp	14.7	14.9	15.1
6 ply hemp	31.6	32.0	31.4
9 ply hemp	44.7	45.4	44.3
CSM*	20.0	20.0	25.3

*Density of E glass fibre taken to be 2560 kg m^{-3} (Hull & Clyne, 1996).

The calculation of V_f by the remaining methods (columns B and C) both assume a certain degree of fibre porosity and result in higher estimates for V_f. The volume fraction figures obtained by utilising the bulk density of the fibre (column B), makes no allowance for the fact that during fabrication, resin enters the lumen space. On the other hand, derivation of V_f from Equation 3.3 implicitly takes this factor into account.

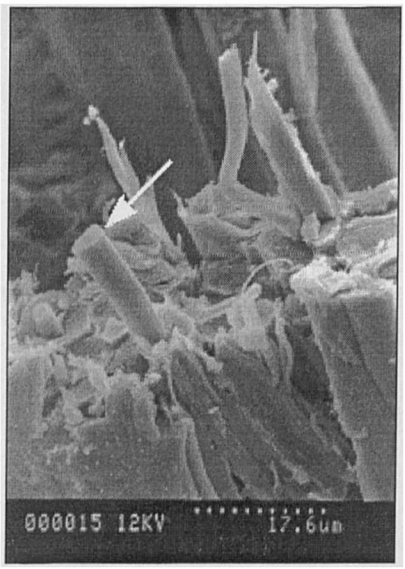

Plate 3.2 SEM micrograph of the fracture surface of a jute reinforced polyester laminate, showing the cured polymer projecting from the fractured fibre.

In reality, SEM micrographs (Plate 3.2) clearly show resin to have entered the lumena of jute fibres and although this phenomenon was not observed directly in hemp, it cannot be ruled out. It is, however, not known what proportion of the total lumen space might be occupied by the polymer in this manner. The literature values taken for the bulk densities of the fibres are in fact very close to the assumed density of the cell wall material itself and therefore little difference is observed in V_f. Erroneous estimates of V_f may well arise, however, regardless of the value assumed for the bulk density of the fibre, since the lumena are likely to be at least partially filled with polymer. In reality, however, this method might be the more representative, since it is debatable what function resin included in the lumen space would play in controlling fibre mechanical properties (see below). The difference, however, observed between V_f calculated by assuming the cell wall density to be 1500 kg m^{-3} and Equation 3.3 is small (generally < 2%) and probably within the range of experimental error, indicating that void space (whether the lumena or otherwise) is minimal. Since no independent measurements of the fibre bulk density were undertaken in this work to verify literature figures, the method of calculating V_f from Equation 3.3 was utilised, with the exception of the CSM glass fibre reinforcement. With the glass fibre, V_f was determined utilising Equation 3.2. As can be seen from Table 3.1, there is an

approximately 25% difference between the V_f calculated via Equation 3.3 and that derived directly from the fibre density. Since the former takes into account included voids, it might be implied that these laminates contain around 5% void space. However, since the density of glass fibre is known with some accuracy, the figure of 20% for V_f is probably realistic. It is worthwhile noting that many included air bubbles were visible in the CSM laminate, believed to be a result of the fabrication process.

The apparent lack of void space in the bast fibre reinforced laminates is indicative of good wetting of the fibres by the resin. As noted previously, Roe and Ansell (1985) concluded that an intimate bond between fibre and polyester was achieved up to a volume fraction of around 60%. Beyond this level of fibre addition, they found that incomplete wetting occurred, resulting in compromised composite properties. This may point to potentially good adhesion between the two phases, since the first requirement for good adhesion, namely that the substrate is adequately wetted, would seem to be fulfilled. However, as noted in Section 2.1.3, this requirement being met in itself does not guarantee good adhesion. It is likely, however, that the relatively low viscosity of the resin (although quantitatively measured, no problems were experienced with the wetting out of the laminates) coupled with the vacuum forming technique aided this.

It was noted previously that systems in which the surface energy of the solid interface exceeds that of the liquid interface by a good margin are likely to wet easily (Equation 2.7). The surface energy of liquid polyester resin (γ_{lv}) is quoted as being of the order 35 mJ m^{-2} (Hull & Clyne, 1996). The surface energy of wood has been reported to be around 50 mJ m^{-2} for many species (Liptáková & Kúdela, 1994) and that of untreated sisal fibre to be similar (Singh, *et al.*, 1998). It seems likely, therefore, that in other lignocellulosic materials such as bast fibres, the surface energy will be greater than that of the resin, making good wetting probable. Furthermore, it is likely that the removal of oils, waxes and other extraneous material from the surface of the fibre through refluxing would have the effect of increasing the surface energy.

The appearance of the cured polymer within the lumena of jute fibres would certainly seem to lend weight to the argument that good wetting occurs. Nevertheless, it is interesting to note that in some instances what appear to be columns of cured resin (Plate 3.2) are seen projecting from the fractured fibres. This may indicate that although the liquid polymer is able to penetrate the cell, presumably through the cut ends of the fibres, through pits (apertures connecting adjacent cells for the purpose of transporting water) or other fissures, it is not intimately bonded to the fibre. During curing, thermosetting resins undergo volumetric shrinkage, which in polyesters is of the order 4-8% (Hull & Clyne, 1996). This cure shrinkage is likely to lead to normal stresses acting across the interface between lumen surface and polymer which could, if adhesion is poor, result in the two being relatively easily separated. It is also likely that during curing, the elevated temperatures (due either to the exotherm from the curing polymer or to post-curing) cause moisture to be driven from the fibres, causing them to shrink also.

It is interesting to speculate upon the influence that the polymer cured within the lumen has upon the mechanical properties of the laminate. Firstly, if adhesion is non-existent, then the resin within the matrix could not take part in any load sharing operation since the interface shear strength would be zero. However, the resin could act as mechanical restraint preventing the cell collapsing, either because of radial loads applied on the fibre, or due to any contraction of the cell when subject to a tensile stress. When adhesion is finite, no doubt some load sharing would take place, but this is likely to be governed by the elastic behaviour of the fibre (i.e. how the strain distribution varies between the outside of the fibre and the lumen surface) and the efficacy of the bonding between fibre and cured polymer. As discussed above, it is likely that normal stresses acting across the interface could well result in debonding taking place at low stress levels. This would lead to the conclusion that the contribution to the overall mechanical response of the material made by the lumen resin is negligible. It could therefore be argued that when defining V_f for plant fibre reinforced material, lumen resin should be ignored. Bearing this in mind, the V_f utilised in this study could under-estimate slightly the 'effective' fibre volume fraction of the composite, but the effect is likely to be almost insignificant.

3.3.1.3 Density

The densities of the bast fibre reinforced laminates as a function of volume fraction are presented in Figures 3.3 and 3.4. As can be seen, density increases with V_f for both fibre types. Nevertheless, unlike the theoretical prediction made by the ROM (Equation 2.8), the relationship is not linear. A comparison with the theoretical prediction shows that, at all volume fractions studied (> 0), the experimentally determined densities lie below the theoretical line. Extrapolation of the regression curves to a fibre V_f of 100% leads to theoretical fibre densities well in excess of 1500 kg m^{-3} (2114 kg m^{-3} and 1659 kg m^{-3} for jute and hemp respectively) which are clearly unrealistic.

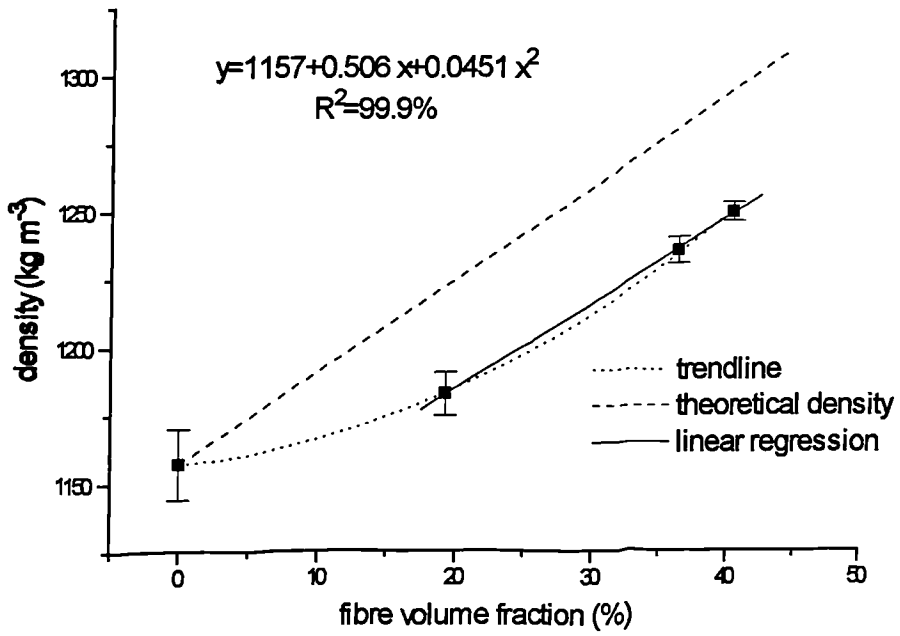

Figure 3.3 Variation of laminate density with V_f - jute fibre reinforced laminate.

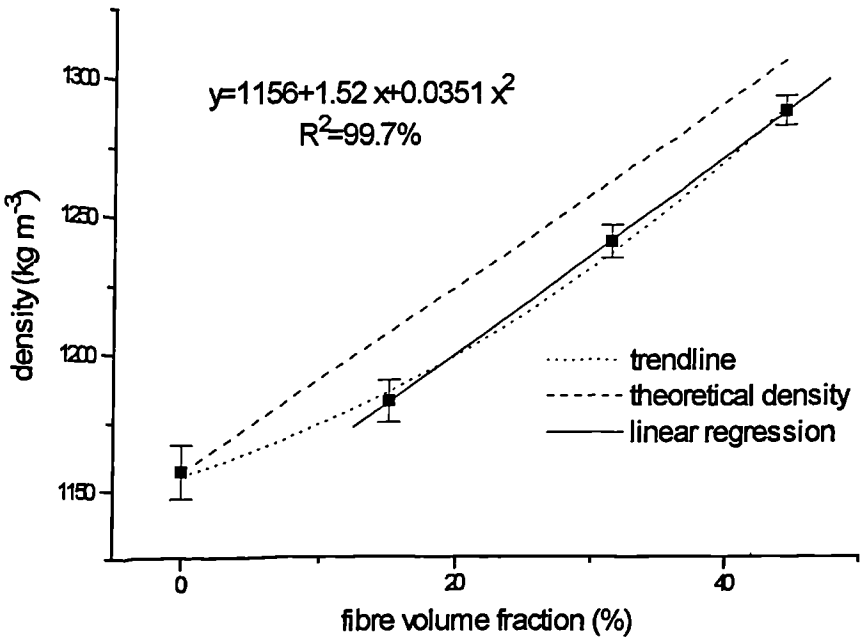

Figure 3.4 Variation of laminate density with V_f - hemp fibre reinforced laminate.

If, however, it is assumed that the void content of the resin itself remains constant, then the differential observed between the theoretical prediction of density and the experimentally determined values may be attributed to void space included by the addition of fibre (i.e. lumen space and other voids). If, because of this, the first data point (un-reinforced resin) is ignored and a linear regression performed on the remaining data then excellent fits are achieved (R^2 values of better than 99% for both fibre types). The fibre densities obtained by extrapolation of these regression lines were then found to be 1438 kg m^{-3} and 1494 kg m^{-3} for jute and hemp respectively. It is believed that these are probably realistic values for the apparent density of the fibre and are in good agreement with the literature values (Ivens *et al.*, 1997) utilised to determine V_f in Table 3.1.

In comparing the trends of the regression lines with the theoretical predictions, it is evident in the case of jute reinforcement that the regression line appears to lie almost parallel with the theoretical line, at a value of about 75 kg m^{-3} lower at all values of

V_f. In the case of hemp, the two lines would appear to converge; at a volume fraction of ~20% the calculated density is only around 25 kg m^{-3} lower than the theoretical prediction. It would seem, therefore, that up to the volume fractions studied, a proportionate increase in void space is not observed with increasing fibre loading, from which it might be inferred that wetting of the fibre by the liquid polymer during fabrication remains good even at higher V_f. Indeed, if the hemp reinforcement only is considered, it would appear that void space actually decreased at higher fibre loading. This is probable since the method employed to attain higher volume fractions involved pre-pressing the fibre mats in a hot press. This may well have resulted in some collapse of thin walled fibres, thereby reducing lumen space. As a consequence there would probably be less lumen space for the resin to occupy in the first instance. Alternatively, pressing may induce some longitudinal splitting of the fibre, thereby exposing any lumena to resin ingress.

At a V_f of 20%, the densities of the glass, jute and hemp fibre reinforced laminates were 1358 kg m^{-3}, 1185 kg m^{-3} and 1200 kg m^{-3} respectively (the densities of the bast fibre laminates were determined by interpolation, utilising the regression equations shown in Figures 3.3 and 3.4).

3.3.2 Preliminary investigations

During the initial stages of this work a number of parameters with the potential to influence the mechanical properties of the laminates were explored by means of three point flexural tests. These included, fibre type, volume fraction, fibre architecture and the effect of various surface and chemical treatments. Since several of these parameters have a direct influence upon the mechanical properties discussed in the reminder of this chapter, it is appropriate to present selected results from these preliminary investigations at this juncture. Results from investigations into the effects of; *a)* fibre microstructure (e.g. felt orientation and the number and areal density of plies) and *b)* the effect of extraction are presented.

3.3.2.1 Microstructure - anisotropy due to felt orientation

During the felting process a 'preferred' orientation is imparted to the fibres. Since this occurs during 'carding', which is followed by 'cross lapping', the preferred orientation lies perpendicular to the machine direction. Furthermore, the line of needle punching is also perpendicular to that of the preferred fibre direction. In view of this, it was believed that a degree of anisotropy would be imparted to any laminates reinforced with such a felt and should therefore be investigated. Table 3.2 provides a comparison of the orthogonal flexural properties of three laminate types as determined from coupons cut from the material in mutually perpendicular directions. A two sample *t*-test (at the 95% confidence level) performed on the data showed that, for each laminate type, significant differences in both flexural strength and stiffness arose as a result of the testing orientation. Since all other parameters remain unchanged, it may be concluded that this anisotropy was due to the felt (and hence to some extent fibre) orientation. Throughout the remainder of this section of the work, due account was taken of the anisotropic nature of the laminate reinforcement.

Table 3.2 Comparison of flexural properties tested parallel and perpendicular to the preferred fibre orientation (i.e. perpendicular and parallel to the machine direction).

Laminate type	*Flexural modulus (GN m^{-2})*		*Flexural strength (MN m^{-2})*	
	parallel to fibre direction	*perpendicular to fibre direction*	*parallel to fibre direction*	*perpendicular to fibre direction*
jute	7.36 (*0.25*)	5.35 (*0.058*)	104.4 (*7.6*)	78.2 (*2.2*)
hemp	8.71 (*0.35*)	5.29 (*0.002*)	143.2 (*2.3*)	100.9 (*2.0*)
flax	5.39 (*0.28*)	4.52 (*0.16*)	100.3 (*4.0*)	88.2 (*2.2*)

Notes: A) The V_f of both the jute and flax laminates was ~35%. The V_f of the hemp laminate was ~40%. B) Standard deviations are in parentheses.

3.3.2.2 Microstructure - effect of the number of 'plies'

Following the discussion above, it is a reasonable assumption that a certain degree of 'in plane' fibre orientation also takes place. During felting, fine webs of carded fibre are laid one upon the other, forming a thick 'fluffy' mattress of fibres. This mattress is subsequently pressed by nip rollers and needle punched to 'intertwine' the fibres,

thus locking the structure together. Prior to needle punching, it is probably reasonable to assume that the majority of fibres are aligned in the X-Z plane within the felt (see Figure 3.5).

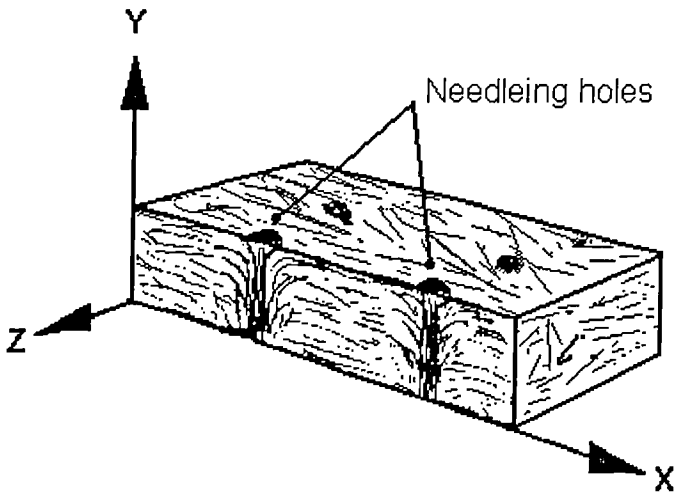

Figure 3.5 Schematic representation of the structure of the needled, non-woven felted fabric, showing misalignment of fibres in the vicinity of needle holes.

Following needle punching, it was apparent from an examination of the felts that a good proportion of the fibres were subsequently oriented in the Y direction. It is likely that the proportion of fibres oriented in the Y direction will depend upon the degree of needle punching and/or the thickness and grammage of the felts. In order to test this hypothesis, laminates were prepared to the same V_f, but with different grammage of reinforcement. The results are presented in Table 3.3.

Table 3.3 The influence of different felt densities on the flexural properties of laminates (V_f ~13.5%).

Laminate type	*Flexural modulus (GN m^{-2})*	*Flexural strength (MN m^{-2})*
2 x 350 g.s.m. hemp	3.55 (0.27)	72.68 (5.95)
1 x 700 g.s.m. hemp	3.21 (0.31)	55.32 (7.51)

Note: Differences between means are significant at the 95% confidence level.

It was observed that both the strength and stiffness of the laminates reinforced with two layers of 350 g.s.m hemp were greater than those of the laminate reinforced with only a single layer of 700 g.s.m. material. This may be explained as follows. The 350 g.s.m. felt, being thinner would, in all probability, consist of a greater number of fibres oriented in a planar-random sense (i.e. in the X-Y plane – Figure 3.5) than in the 700 g.s.m. felt. Although the needling density was similar for both non-wovens the likelihood is that in the denser felt, a greater proportion of the fibres would be engaged in 'locking together' the structure of the fabric. In other words in the 700 g.s.m. felt, a relatively greater proportion of the fibres would be oriented in the Z direction than in the lighter materials. Consequently, in the laminate containing two layers of 350 g.s.m. felt it seems highly probable that there was, in total, a greater proportion of fibres oriented in the X-Y plane than in the laminates reinforced with a single layer of 700 g.s.m. felt. This would undoubtedly result in more efficient reinforcement which could well explain the higher flexural strength and stiffness of the laminate reinforced with two layers of 350 g.s.m. felt.

An examination of the fracture of the laminates reinforced with a single layer of felt revealed an interesting feature of needling, namely that failure invariably occurred at these points. In this respect, needle punching may be likened to a row of perforations, critically weakening the laminate.

3.3.2.3 Effect of extraction

Lignocellulosic material contains a proportion of non-bonded material. In addition to this, during processing, lubricating oils and other debris undoubtedly contaminate the fibre surfaces. To minimise the influence of these substances on composite properties (primarily interface performance), the fibre was solvent washed by refluxing prior to lamination. To assess the effect of this upon composite performance, the properties of laminates prepared with extracted and 'loom state' fibre were evaluated (Table 3.4).

Table 3.4 Effect of prior extraction of reinforcing fibre on laminate properties (V_f ~22%).

Reinforcement	*Density* ($kg\ m^{-3}$)	*Flexural modulus* ($GN\ m^{-2}$)	*Flexural strength* ($MN\ m^{-2}$)*
un-extracted hemp fibre	1185 (*3*)	4.70 (*0.14*)	98.6 (*4.8*)
extracted hemp fibre	1192 (*7*)	4.84 (*0.10*)	95.0 (*5.1*)

Note: *Difference between means not significant at the 95% confidence level.

As can be seen, there are slight increases in both the density and the flexural modulus of the laminate reinforced with extracted hemp fibre (<1% and <3% respectively). Whilst there would appear to be a small drop in strength, this difference was not found to be statistically significant.

Both the apparent increase in density and stiffness may be explained by improved fibre to matrix interaction. Removal of waxes, oils and other debris could have the effect of changing the surface free energy of the fibre, rendering it more readily wettable by the resin. If this were so, then it is likely that fewer void spaces would be present, thereby increasing the density of the laminate. As discussed in Section 3.3.1, the voids may be either unfilled lumena or other cavities in the structure of the composite. Improved wetting may also promote interfacial adhesion, either as a result of more intimate contact between the phases leading to better mechanical interlocking, or to enhanced secondary force interactions (see Section 2.1.3). An improved interface may result in more efficient stress transfer between the matrix and fibre, leading to enhanced composite stiffness.

3.3.3 Tensile properties

As outlined above, preliminary tests confirmed that laminates reinforced with non-wovens were anisotropic. In view of this, all specimens were prepared and tested with the preferred fibre orientation aligned parallel to the major axis of the specimen. The results presented for the mechanical properties of the bast fibre reinforced laminates therefore probably overestimate the properties which might be expected if

the reinforcement was truly randomly planar in nature. Furthermore, all laminates were prepared from multiple felts of low areal density (~350 g.s.m for the hemp laminates and ~500 g.s.m for the jute laminates). In view of the discussion in the previous section, it was believed that the adoption of multiple 'plies' would minimise the effects of out of plane fibre alignment and needle punching.

3.3.3.1 Nature of stress-strain behaviour

Typical tensile stress versus tensile elongation records for the various laminates investigated are presented in Figure 3.6. The stress-strain behaviour of the un-reinforced resin is essentially linear until fracture. The inclusion of fibre was observed to increase Young's modulus (steeper initial part of the curve) and to impart a certain amount of non-linear 'plastic' behaviour to the laminate, regardless of fibre type.

For all laminate types, it was observed that failure occured in a brittle manner upon the attainment of the first peak stress. Almost without exception, this form of fracture occurred for all the specimens tested. Tensile elongation to failure (which is equivalent to strain, since all specimens were of the same gauge length) was seen to increase with the addition of glass fibre, but at similar V_f was reduced with both jute and hemp, when compared with the un-reinforced polymer. This may, in part at least, be explained by the differing failure strains of the various constituents.

The failure strain of the polyester resin used in this work, determined from these experiments, was found to be around 1.7%. The failure strain of E-glass fibre is approximately 2.6% (Hull & Clyne, 1996), whilst that of flax, similar in structure to hemp (see Chapter 4), has been reported to be <1.5% (Davies & Bruce, 1998). It would seem that the failure strains of the organic and inorganic fibres straddle that of

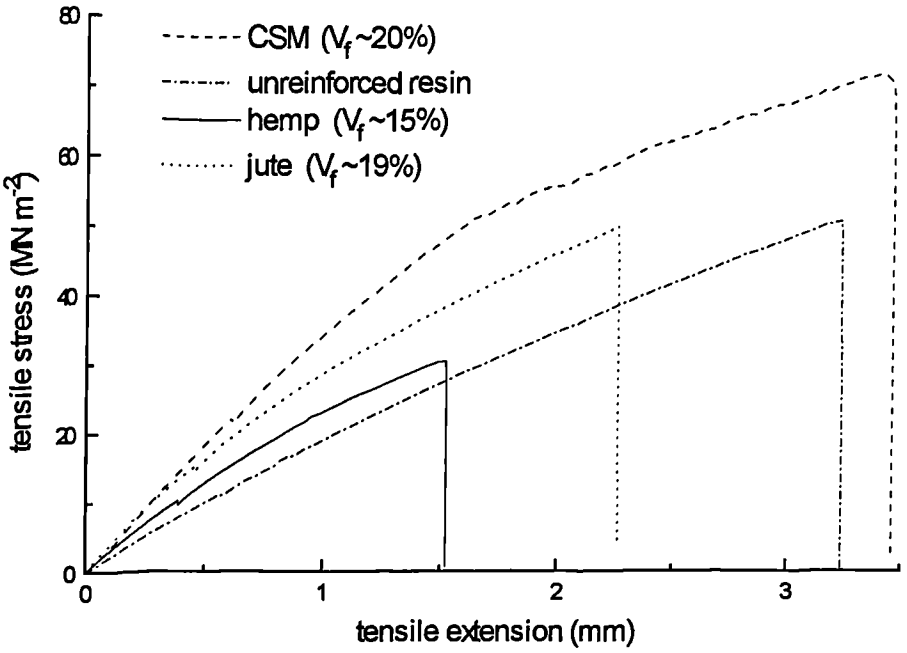

Figure 3.6 Typical tensile stress versus tensile extension records for un-reinforced polymer, CSM, jute and hemp reinforced specimens.

the polymer and the behaviour of the laminates appear to reflect this. Thus at relatively low V_f (< 20%), the difference in failure strain may be explained by the fact that the bast fibres fail at relatively low strain, leaving the matrix un-reinforced; changes to the microstructure, such as stress concentrations at the broken fibre ends may then promote fracture of the matrix, leading to overall failure of the laminate at strains below that of the un-reinforced polymer itself. The converse may be true of the glass fibre reinforced material, in that matrix cracking precedes fibre failure. Since the tensile strength of the fibre is very much greater than that of the polymer itself, it is reasonable that the fibres will continue to support significant loads after matrix cracking has initiated. This is borne out by an examination of the failed laminates; the CSM reinforced material exhibiting a substantial amount of transverse micro-cracking (observed as fine bands across the specimen), whereas at these volume fractions none was evident whatsoever in either bast fibre reinforced laminate. Nevertheless, as will be discussed below, higher V_f resulted in increased strains to failure for the bast fibre reinforced composites which are probably a reflection of different failure mechanisms.

The stress-strain curve for the CSM reinforced laminate shows a distinct 'knee' occurring at around 50 MN m^{-2}. Similar behaviour has been noted in cross-ply laminates (Chou, 1994) and is probably due to the onset of transverse micro-cracking, initiating where the fibres are locally aligned perpendicular to the applied stress (analogous to rupture in transverse plies). The behaviour of the bast fibre reinforced composites appeared to be similar. However, the 'knee' in the curve was not as distinct, but was nevertheless discernible. It does, however, appear as though non-linear behaviour was initiated at significantly lower stress levels in the bast fibre reinforced materials.

Figures 3.7 and 3.8 show typical stress-tensile elongation curves for jute and hemp respectively, at three different V_f, together with that of the un-reinforced polymer (as noted previously, these are equivalent to stress-strain curves, since the guage lengths were the same). As can be seen, the addition of both bast fibre types in increasing proportion had the effect of increasing both stress and strain to failure. The difference between the 36.3% and 40.4% V_f jute reinforcement was marginal, but then the difference in V_f was small, and furthermore the curves are simply representative and cannot therefore be treated quantitatively. Interestingly, in the case of jute reinforcement, at all V_f, the failure strain of the laminates was below that of the polymer itself. In the case of hemp, however, at a V_f of 44.3% the failure strain exceeded that of the resin. This increase in strain to failure of both laminate types may be explained by a change in the mode of failure. At higher volume fractions, extensive transverse micro-cracking becomes visible. Presumably this occurs because, with a higher percentage of fibre, concentrations of stress at the fibre matrix-interface make it more likely for the matrix to rupture prematurely. However, with a greater proportion of fibre, the laminate remains bound together by the fibres bridging the matrix cracks.

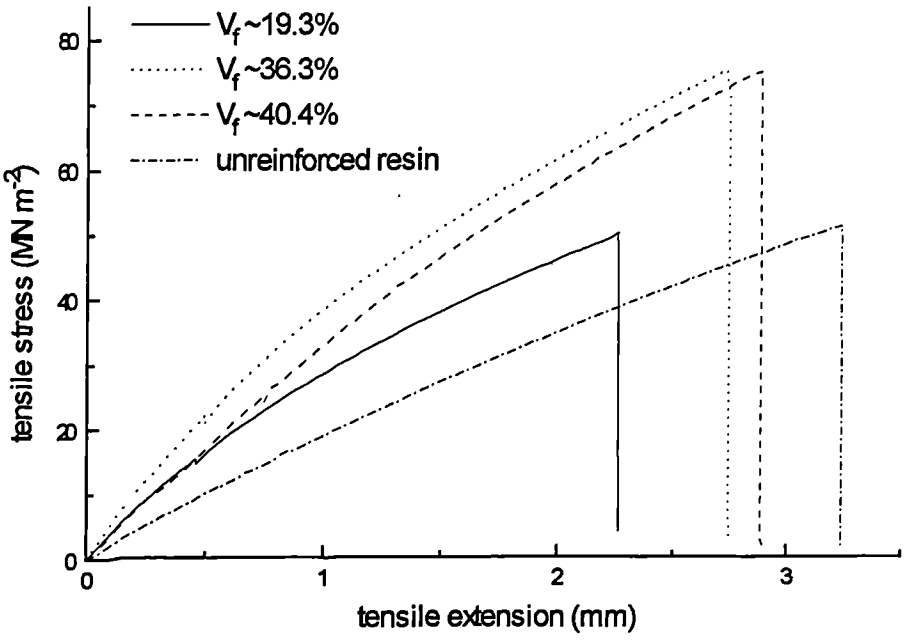

Figure 3.7 Typical tensile stress versus tensile extension records for jute reinforced laminates.

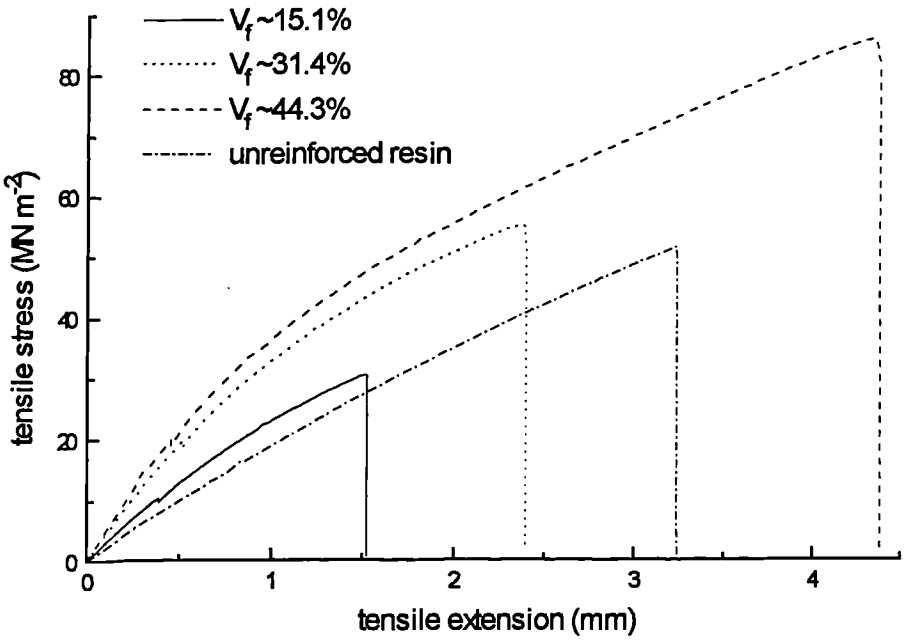

Figure 3.8 Typical tensile stress versus tensile extension records for hemp reinforced laminates.

Although it is difficult to deduce from the curves, it appeared as though there was significantly more non-linear, 'plastic', behaviour in the hemp reinforced laminates than the jute reinforced material, particularly at higher V_f. To investigate this phenomenon, the yield stress or rather (since these laminates do not possess a distinguishable yield point), the 0.2% proof stress (Timings, 1989) of the laminates was determined and compared with the ultimate tensile strength of the laminates (see below). It did, however, seem evident that in both bast fibre reinforced materials, incipient non-linear behaviour occured at relatively low stress levels (possibly <20 MN m^{-2}). Although not directly tested in this part of the work, it is believed that this non-linear behaviour is irreversible and most probably due to micro-structural damage. A fuller discussion of this aspect of the work is conducted in Chapter 6.

An estimate of the work of fracture is provided by the area under a force-displacement record (Jeronomidis, 1980). Since it may be observed that the areas under the stress-elongation curves increase with V_f (Figures 3.7 and 3.8), this may be indicative of improved toughness resulting from higher fibre loading. The issue of composite fracture toughness is considered in Section 3.3.6.

3.3.3.2 Young's modulus

Figures 3.9 and 3.10 show Young's modulus, E, as a function of V_f for jute and hemp fibre reinforced polyester respectively. As might be expected, increasing V_f resulted in an increase of stiffness. In both instances, there appeared to be an almost linear relationship between E and V_f. Regression analysis confirmed this, with excellent 'goodness of fits' being achieved (R^2 values of better than 99%).

Such a relationship might well be expected from the theory. As noted in Section 2.1.5, the theoretical prediction (Equation 2.11) for a planar-random reinforcement configuration (Figure 2.7) shows an almost linear relationship between Young's modulus and volume fraction up to a value for V_f of around 40-45%.

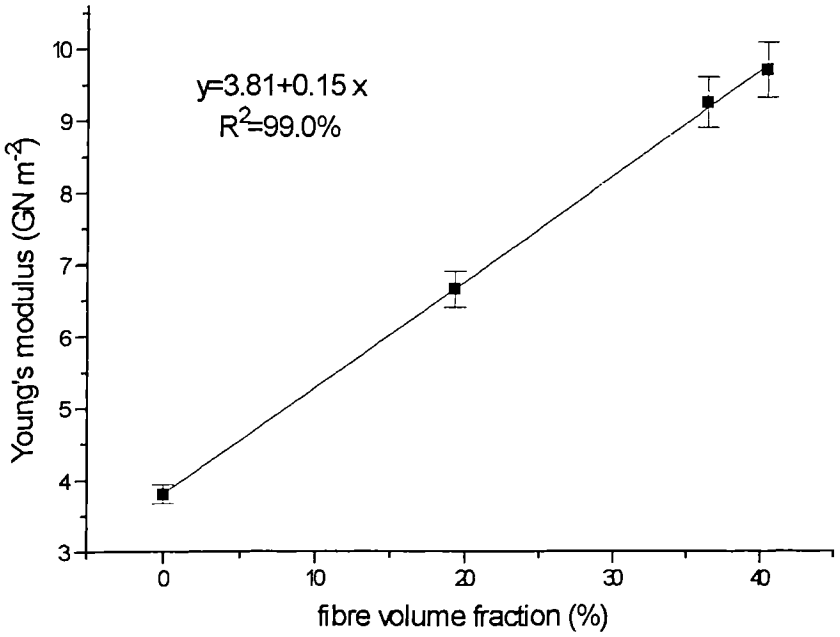

Figure 3.9 Young's modulus versus volume fraction. Jute fibre reinforcement.

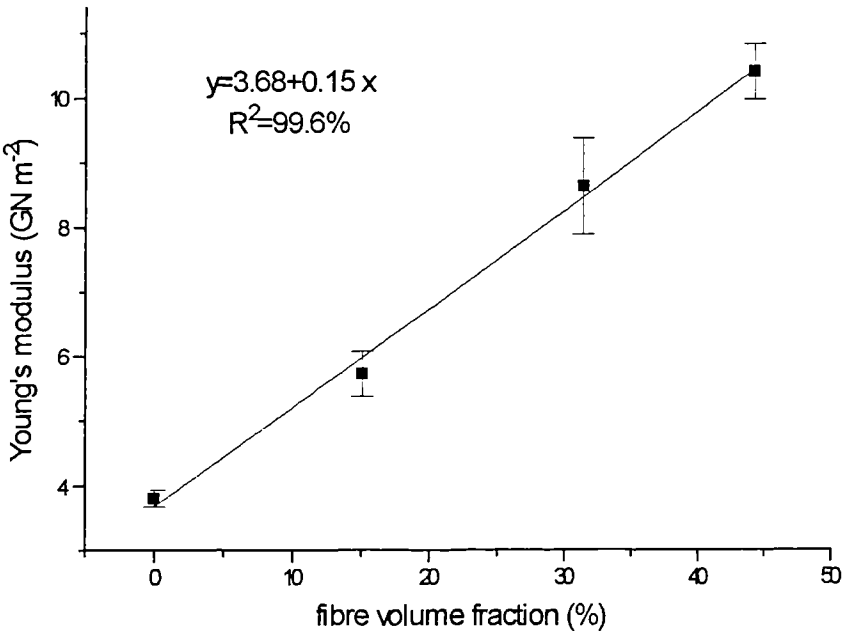

Figure 3.10 Young's modulus versus volume fraction. Hemp fibre reinforcement.

A comparison of the tensile stiffness of the three laminate types versus V_f is presented in Figure 3.11. It can be observed that the plots for the two bast fibre reinforced composites almost coincide with each other. This is an interesting phenomenon, given that reported values for the tensile stiffness of hemp generally exceed those of jute (see Table 1.1). This difference may, however, be explained by variations in fibre achitecture, since different areal weights (with different needling densities) of felt were utilised for the different fibres types.

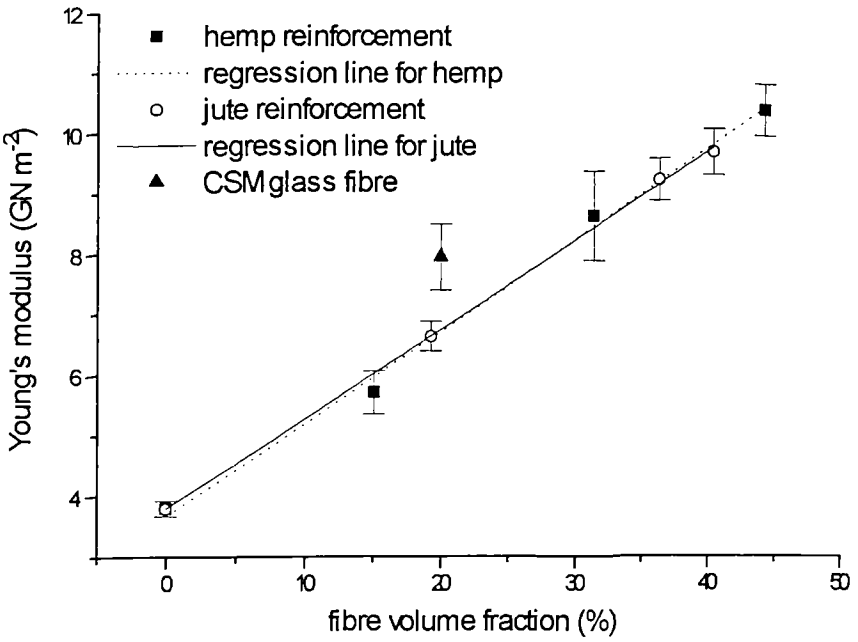

Figure 3.11 Variation of Young's modulus with V_f for jute, hemp and CSM glass fibre reinforced laminates.

At equivalent V_f (20%), the Young's modulus of the glass fibre reinforced laminate only marginally exceeded that of the bast fibre reinforced material. It should, however, be remembered that the moduli for the bast fibre reinforced materials are probably a 'best case' scenario for this reinforcement architecture, and thus the 'real' difference is probably somewhat greater. Young's modulus at 20% V_f for the bast

fibre reinforced laminates has been derived from the regression equations shown in Figures 3.9 and 3.10, and a comparison with the CSM reinforced material is shown in Table 3.5. Also shown are the specific values (E/ρ). Viewed in this manner, the stiffness values of the plant fibre reinforced material looks very encouraging!

Table 3.5 Comparison of absolute and specific Young's moduli (V_f = 20%).

Laminate type	*Young's modulus (GN m^{-2})*	*E/ρ (MN m^{-2}/kg m^{-3})*
Jute	6.81	5.75
Hemp	6.68	5.57
CSM glass fibre	7.95	5.85

The superior tensile stiffness of the glass fibre reinforced material may be accounted for by the greater modulus quoted for this fibre type (Ivens *et al.*, 1997). Further, the configuration of the bast fibres themselves may well influence the elastic properties of the laminate, for whilst glass fibres in CSM are generally straight, the bast fibres are decidedly 'curly' where they pass over, under and between one another. The type of structure seen in a needled non-woven is probably more akin to paper than to a CSM reinforcement. This 'curliness' of the fibres would no doubt present problems in modelling the elastic properties of laminates reinforced with such material.

In view of the above, no attempt was made in this work to model the elastic behaviour of the non-woven plant fibre reinforced laminates. The empirical relationships derived for E as a function of V_f, will, of course only be valid within the range of volume fractions studied and for the particular non-woven felts utilised.

3.3.3.3 Tensile strength

Tensile stress at break, σ_{uc}, as a function of V_f for the two bast fibre reinforced laminates are shown in Figures 3.12 and 3.13.

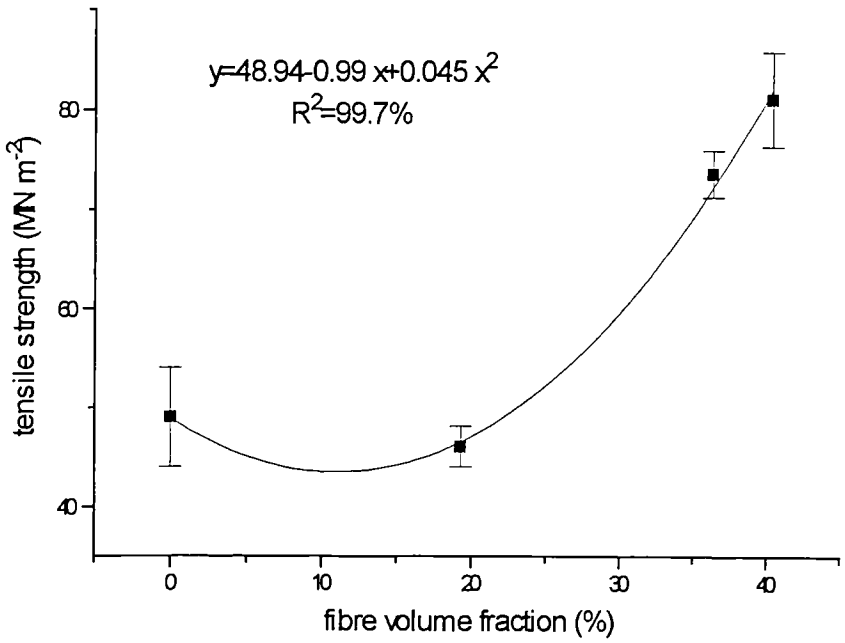

Figure 3.12 Tensile stress at break versus fibre volume fraction. Jute reinforcement.

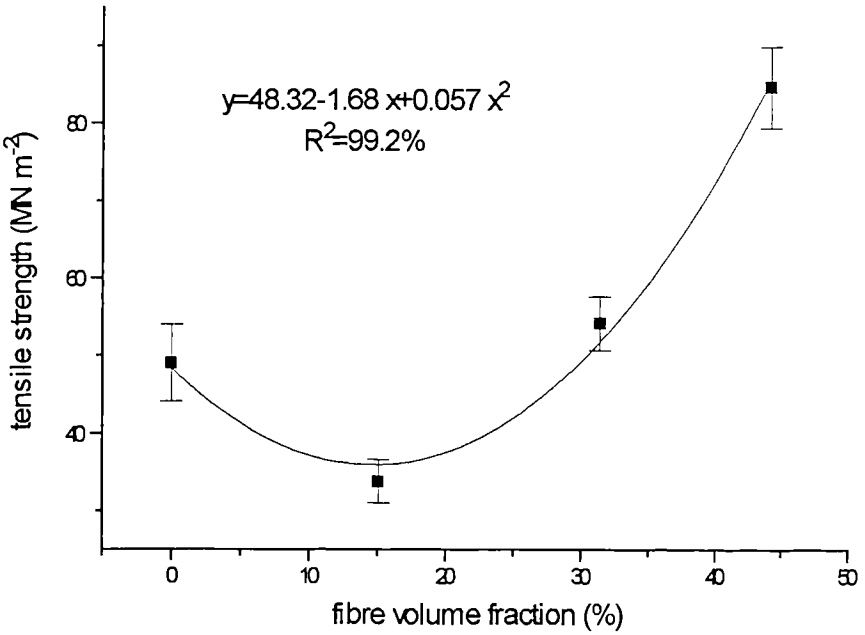

Figure 3.13 Tensile stress at break versus fibre volume fraction. Hemp reinforcement.

It is clear that unlike E, σ_{uc} did not follow a linear relationship with V_f. Indeed, it may be seen that for both fibre types, σ_{uc} appeared to reach a minimum value at a V_f somewhere between 10% to 15%, and only when V_f increased to between 20% and 30% (depending upon reinforcement type) did σ_{uc} equal or exceed the matrix ultimate stress, σ_{mu}.

In the case where very few fibres are added to the matix, the polymer may be weakened rather than strengthened (Piggott, 1980). In these circumstances, a critical fibre volume fraction, $V_{f\min}$, can be identified, below which any fibre added actually weakens the matrix. As noted in Section 3.3.3.1, it seems probable that the strain to failure of bast fibres is probably less than that of the unreinforced polymer. In these circumstances it can be shown that the critical fibre volume fraction may be given by (Piggott, 1980):

$$V_{f\min} = \frac{E_f\sigma_{mu} - E_m\sigma_{fu}}{\left(X_1E_f - E_m\right)\sigma_{fu}} \qquad (3.4)$$

Where:

E_f is the fibre modulus

E_m is the matrix modulus

σ_{fu} is the fibre ultimate strength

σ_{mu} is the matrix ultimate strength

X_1 is a factor less than unity which makes allowance for unaligned fibres (0.38 for planar random reinforcement)

By substituting 'typical' values for the bast fibre properties (tensile modulus ~50 GN m^{-2} and tensile strength ~500 MN m^{-2} - see Table 1.1) and the matrix properties derived in this work (Young's modulus ~3.8 GN m^{-2} and tensile strength ~50 MN m^{-2}) into Equation 3.4, it may be shown that $V_{f\min}$ is theoretically approximately 8%. However, as may be clearly observed from Figures 3.12 and 3.13, the 'break even' fibre volume fractions for both hemp and jute (where the laminate tensile strength

exceeds that of the unreinforced matrix), is considerably higher than this figure. Utilising the regression equations shown in Figures 3.12 and 3.13, it can be shown that the actual minimum fibre volume fractions are 22% and 29 % for jute and hemp respectively. These figures are substantially higher than those predicted from the theory and, even allowing for some error in the estimates of the fibre tensile properties, it seems likely that either the assumptions made regarding the material (fibre failure strain < matrix failure strain) are invalid or some other mechanisms are involved in the weakening of the matrix.

Probable explanations for this behaviour in the plant fibre composites are as follows. At all V_f, the orientation of the reinforcement is 'pseudo-planar random', as a result of which a proportion of the fibres are oriented perpendicular (or at a large angle) to the applied stress; these effectively act in the manner of unidirectional plies under transverse loading. The tensile strength of plies under transverse loading is, however, significantly less than that under axial loading because of a tendency for high local stresses and strains to develop in the matrix; consequently the failure stress of the lamina is less than σ_{mu} (Hull & Clyne, 1996). Nevertheless, it might be argued that this effect would be offset by a significant proportion of the fibres lying along the axis of loading (or nearly so). However, in view of the fibre configuration and other morphological features, which will be discussed in the following chapter, it is likely that these too may create concentrations of stress and strain in the matrix. At low V_f, therefore, when a tensile specimen is strained, stress concentrations are stimulated in the matrix as a result of transversely loaded fibres and other fibre defects. Furthermore, given that the strain to failure of the fibres is less than that of the matrix, it is probable that fibre failure also takes place at low overall strains. This would effectively leave the laminate un-reinforced at relatively low strains, but furthermore, riddled with stress concentrators (added to by the broken fibres). Given the susceptibility of brittle materials to stress concentrators, it is therefore not unreasonable that at low V_f the plant fibre reinforced laminates are weaker than the un-reinforced matrix itself.

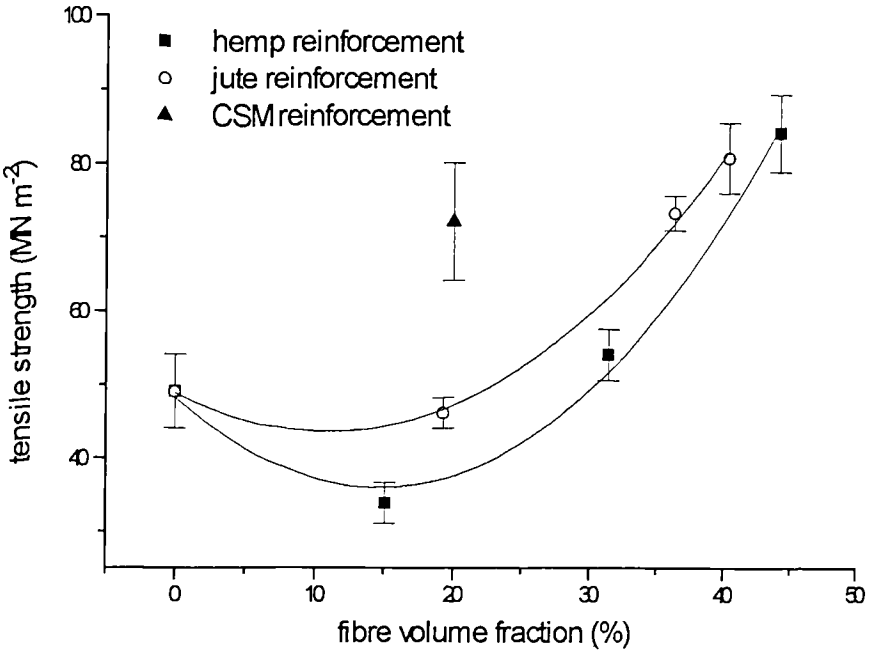

Figure 3.14 Comparison of the tensile strengths of CSM glass fibre, jute and hemp reinforced laminates.

At higher V_f, however, it would seem likely that there might be a proportionately greater number of stress concentrators which could initiate matrix cracking prior to general fibre failure. In these circumstances, a greater proportion of fibres might be considered to give the laminate macroscopic integrity, though irreversible microscopic damage processes may well have already taken place. This explanation could also account for the large 'plastic' region observed, particularly in the hemp reinforced laminate, which at higher volume fractions exhibited extensive transverse micro-cracking.

A comparison with the CSM reinforced polyester (Figure 3.14), revealed that σ_{uc} for this composite was significantly higher than that of either of the two bast fibre reinforced materials at a V_f of 20% (approximately 60% greater than the jute laminate and 100% greater than the hemp laminate at this V_f). Taking into account fibre orientation, the greater strength of the glass fibre reinforced laminates may be

explained by the greater tensile strength of this fibre (approximately 2.5 GN m^{-2} for glass fibre as compared with around 0.5 GN m^{-2} for the bast fibres - see Table 1.1).

3.3.3.4 Yielding

As mentioned above, in order to estimate the amount of 'plastic' behaviour of the laminates the yield stress (0.2% proof stress) was compared with σ_{uc}. Table 3.6 shows a comparison of the yield stress, σ_{ys}, to the ultimate tensile stress of the laminates together with the laminate failure strain, ε_{uc}.

Table 3.6 Ultimate tensile strength, yield stress and failure strain of laminates.

Laminate type	σ_{uc} *(MN* m^{-2}*)*	σ_{ys} *(MN* m^{-2}*)*	σ_{ys}/σ_{uc} *(%)*	ε_{uc} *(%)*
Polymer	49.1	49.1	100	1.66
CSM (V_f ~20%)	73.4	59.6	81	1.74
Hemp (V_f ~15%)	33.8	33.8	100	0.88
Hemp (V_f ~31%)	54.2	44.4	82	1.28
Hemp (V_f ~44%)	84.7	50.8	60	2.06
Jute (V_f ~19%)	46.1	44.2	96	1.09
Jute (V_f ~36%)	73.6	53.7	73	1.46
Jute (V_f ~40%)	81.19	51.0	63	1.67

It is clear that, in the bast reinforced polyester composites, as V_f increased so the ratio of σ_{ys}/σ_{uc} decreased. In other words, it would appear that subsequent to 'yielding' an increasing amount of 'plastic' deformation takes place prior to the attainment of the ultimate tensile strength. This behaviour is readily observed in Figures 3.7 and 3.8. Additionally, the strain to failure, ε_{uc}, increased with V_f. It may be seen that, with the exception of the highest volume fraction laminates, all bast fibre reinforced materials failed at strains below that of the un-reinforced resin. A plot of ε_{uc} versus V_f (Figure 3.15) indicates that with both jute and hemp reinforcement, the strain to failure reached a minimum value at around 20% V_f. It would seem that both

σ_{uc} and ε_{uc} 'bottom out' at a composite V_f of somewhere between 10% and 20%. This, coupled with the observation that little non-linear behaviour was observed in this region, would tend to lend weight to the argument that the inclusion of bast fibres at low V_f actually introduces 'weaknesses' into the laminate structure, most probably in the form of the aforementioned stress concentrations. On a practical note, this would imply that there is little to be gained, in reinforcement terms (other than to increase stiffness), by utilising non-woven bast fibre felts at volume fractions below around 25% V_f. The data from the tensile tests conducted in this work appear in Appendix 4.

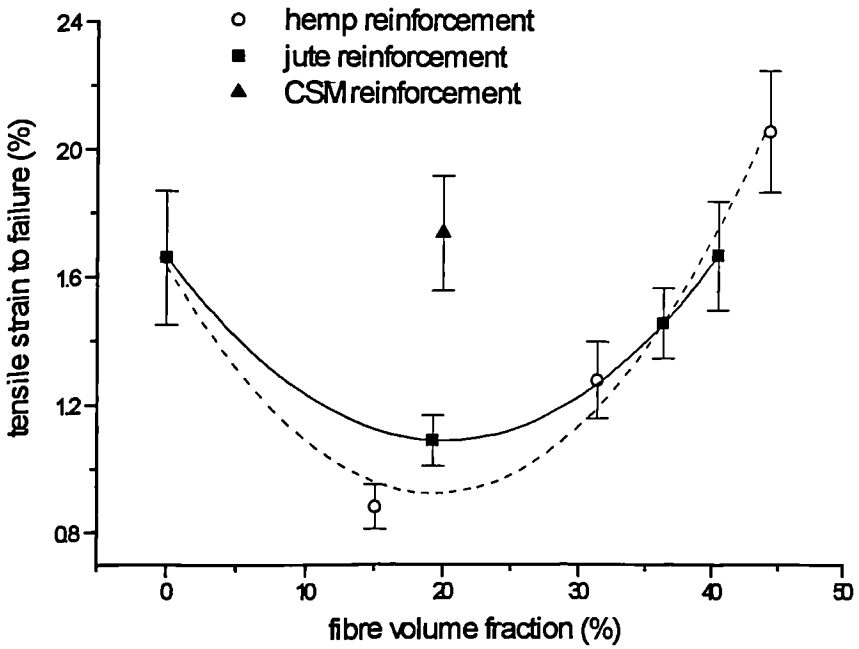

Figure 3.15 Variation of strain to failure with fibre volume fraction. Jute, hemp and CSM reinforced laminates.

3.3.4 Flexural properties

3.3.4.1 Nature of flexural stress-strain records

Typical flexural stress-strain records for jute and hemp fibre reinforced laminates are presented in Figures 3.16 and 3.17 respectively. It may be observed that, as with the tensile tests, the traces show an initially linear portion, followed by a non-linear region

prior to the attainment of maximum flexural stress. Furthermore, with increasing V_f it may be observed that modulus increased, as evidenced by a steeper initial portion of the curve, and that the degree of non-linear behaviour increased (see also below). Once the maximum stress was attained, the recorded stress diminished in a more gradual manner to that observed in the tensile tests. The transformation to this form of post maximum stress behaviour is most probably a result of the shear stresses induced in the specimen during this mode of loading. Failure was observed to invariably initiate on the tension surface and to progress through to the neutral axis of the specimen. At low V_f, failure in both bast fibre reinforced laminate types was noted to be primarily brittle; however, at higher V_f, a certain amount of shear failure was also evident.

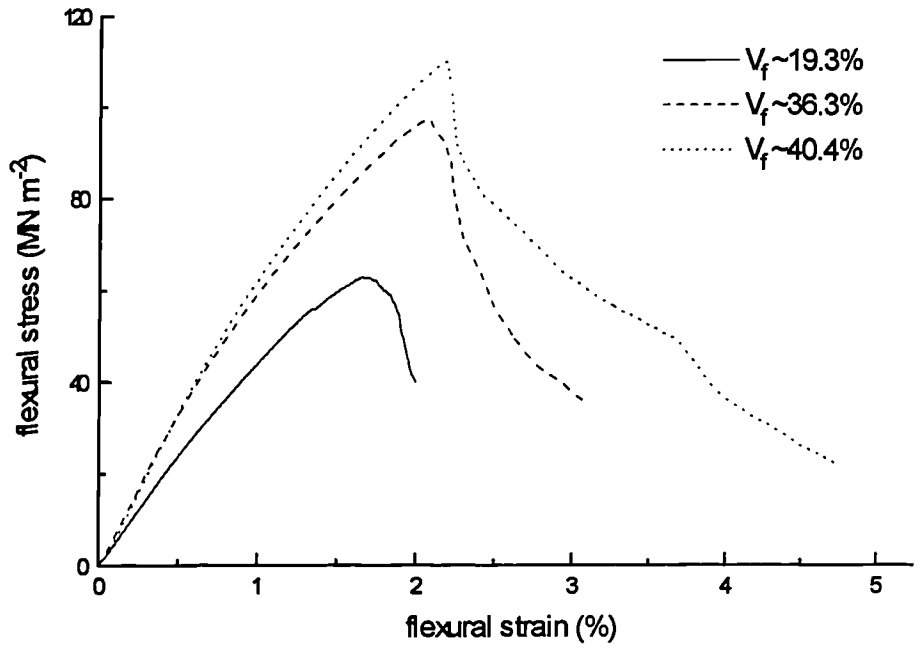

Figure 3.16 Typical flexural stress-strain records for jute reinforced polyester laminate specimens in three point flexure.

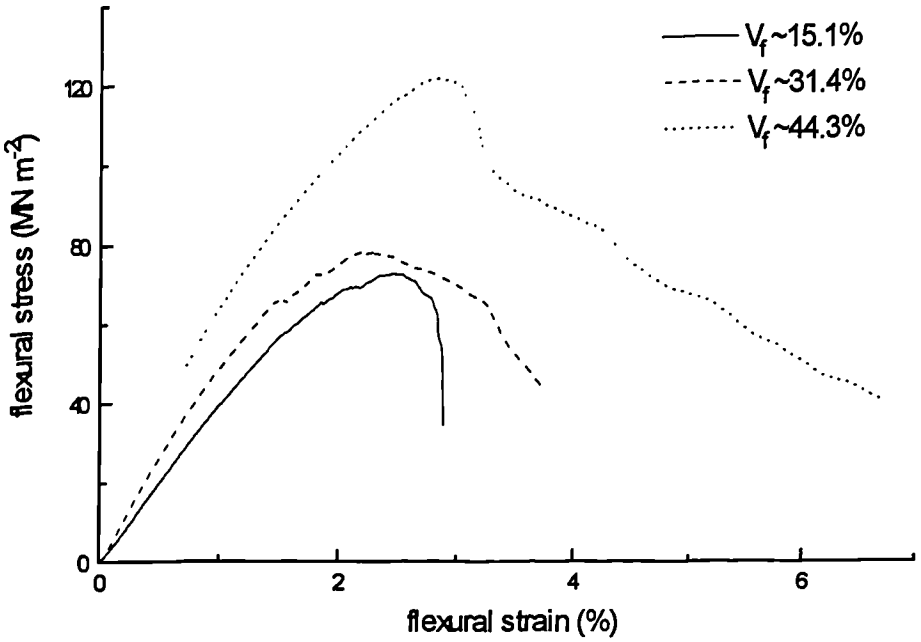

Figure 3.17 Typical flexural stress-strain records for hemp reinforced polyester laminate specimens in three point flexure.

In Figure 3.18, a comparison is presented between typical flexural stress-strain records of the two bast fibre reinforced laminates, CSM reinforced material and the cast polymer. It may be observed that at approximately equivalent reinforcement levels (V_f ~15 to 20%), the flexural stiffness of the synthetic fibre reinforced material exceeded that of either of the two natural fibre reinforced laminates. All reinforcement types, however, seemed to produce an increase in flexural stiffness over that of the neat polymer. Whereas the addition of glass fibre resulted in an improvement in the flexural stress at break, over that of the un-reinforced polymer, at these V_f's bast fibre reinforcement appeared to reduce the strength of the laminates. Flexural strain at break also appeared to be reduced by the addition of all reinforcement types (see below).

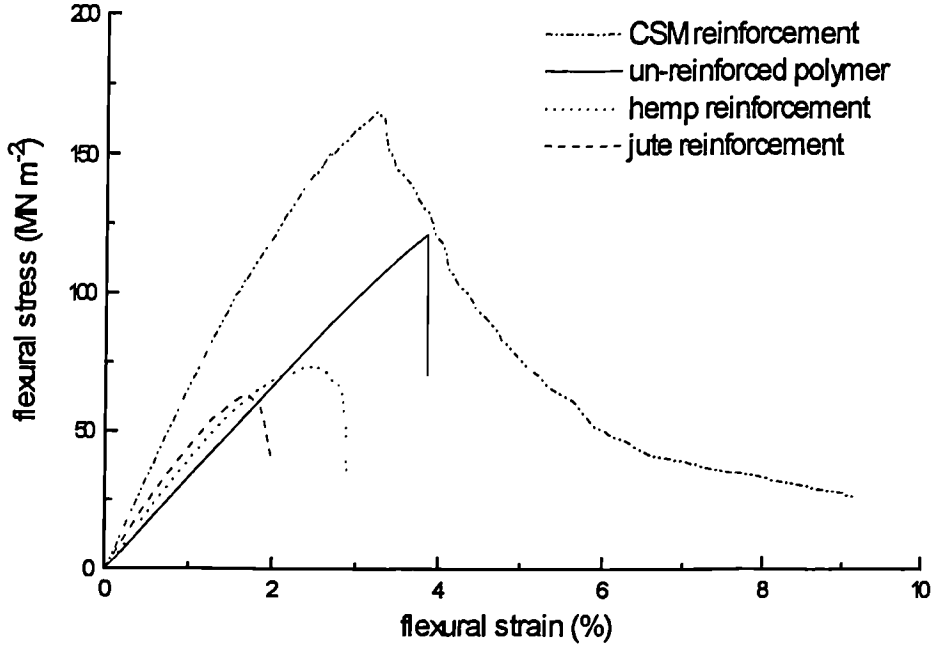

Figure 3.18 Flexural stress-strain records for un-reinforced, jute, hemp and CSM reinforced laminates in three point flexure. The reinforced laminates are at approximately equivalent V_f (15 to 20%).

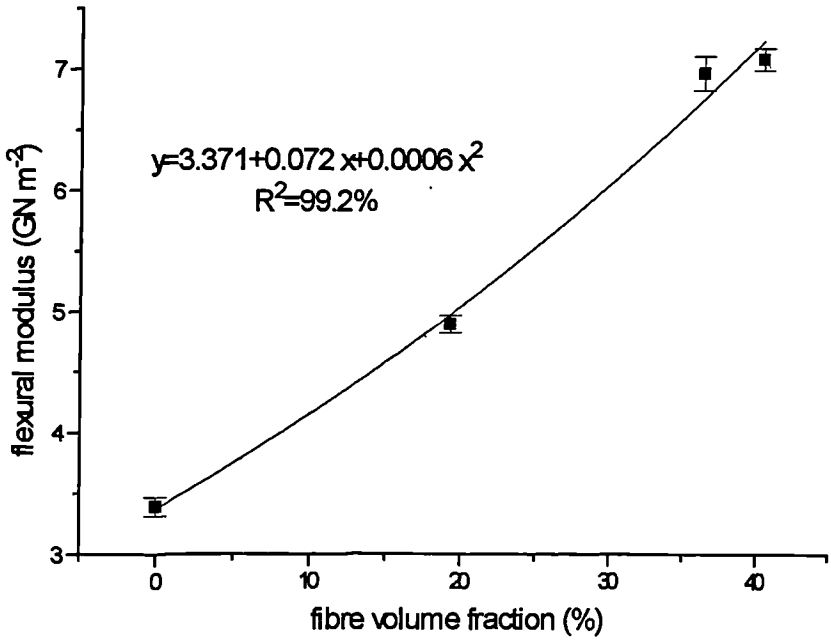

Figure 3.19 The variation of flexural modulus with V_f. Jute reinforcement.

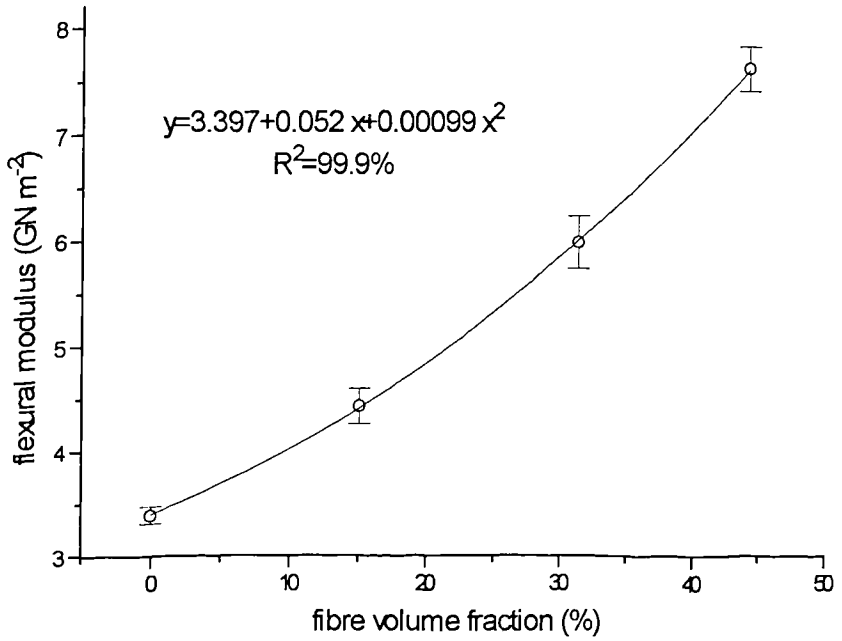

Figure 3.20 The variation of flexural modulus with V_f. Hemp reinforcement.

3.3.4.2 Flexural modulus

Figures 3.19 and 3.20 show the variation of flexural modulus with V_f. These trends are similar to those observed in tensile tests, albeit the relationships do not exhibit the same degree of linearity.

A comparison between the flexural moduli of the various reinforcement types is presented in Figure 3.21. It may be observed that at equivalent V_f, the flexural modulus of the CSM glass fibre reinforced laminate exceeded that of the bast fibre reinforced material. At a fibre volume fraction of 20%, the modulus of the glass fibre reinforced laminate exceeded that of the jute and hemp reinforced material by approximately 32% and 38% respectively. What is of particular interest, however, is to compare these differences with those obtained from the tensile tests. In these, the difference between the glass and the jute and the glass and the hemp laminates was 17% and 19% respectively. Another way of looking at this phenomenon is to compare the differences in the moduli of the laminates at equivalent V_f, obtained

either by tensile or flexural tests. In the case of the CSM laminate, the flexural modulus is around 14% lower than the corresponding tensile modulus. With the un-reinforced polymer, this difference is around 11%. On the other hand, the difference observed in the jute and hemp laminates is around 26% and 28% respectively. Given that some difference in the value of modulus would be expected as a result of the loading configuration, the much larger difference observed in the modulus of the natural fibre reinforced material warrants explanation.

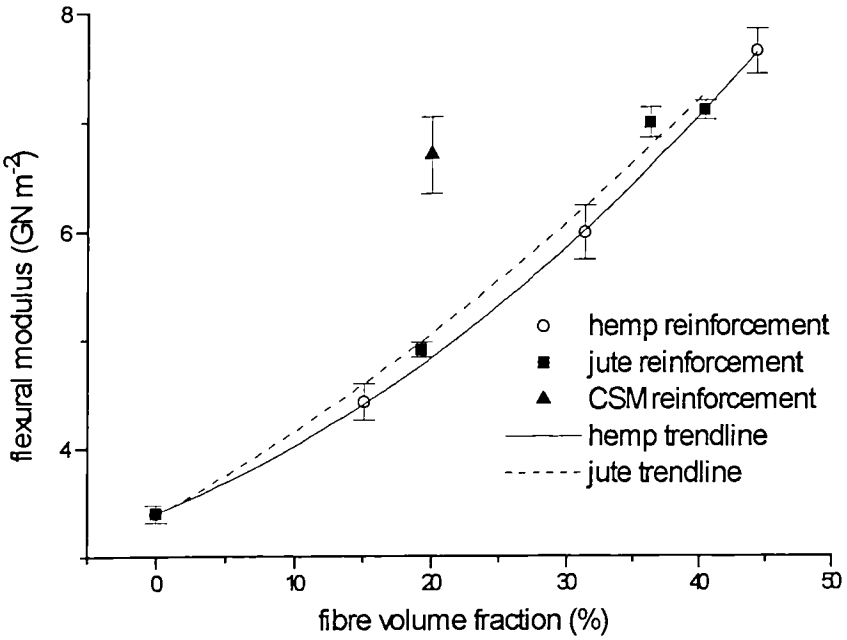

Figure 3.21 Comparison between the flexural moduli of jute, hemp and CSM glass fibre reinforced unsaturated polyester laminates.

In flexural tests, the stress distribution varies through the thickness of the test specimen, from tensile on one face to compression on the opposite face. It should be bourne in mind, however, that the flexural tests undertaken in this work were conducted in three, rather than four point bending; as such there would have been a distribution of shear stresses through the thickness as well as along the specimen. The use of a four point loading configuration would have removed the shearing element in the mid-section and would have provided a more accurate assessment of flexural modulus. Nevertheless, if it were assumed that the material under investigation behaved in the same manner both in tension and in compression (i.e. the same moduli

in both compression and tension), then it might be thought that any difference in the modulus resulted from the test method (either tensile or flexural) employed (in this instance, the lower modulus in flexure may also partly result from the finite compliance of the loading system, making the apparent strain greater and hence the flexural modulus lower). The greater difference observed in the modulus of the bast fibre reinforced laminates between the two tests may be indicative of a certain amount of bimodular behaviour, i.e. they have differing tensile and compressive moduli. As it seems unlikely that this should originate in the polymer itself, it may be that the fibres or the composite structure are the root cause of the behaviour. Bimodular behaviour has, for instance, been noted in solid wood as well as in fibrous composites (Conners & Medvecz, 1992). Since the difference observed was greater in the bast fibre reinforced material than in the CSM glass fibre laminate, this may be indicative that the fibres themselves account for a large proportion of this behaviour. However, since the orientation of the fibres was 'pseudo-planar random' it is impossible to say whether this behaviour occurs during radial or axial loading of the fibres. It should be noted, however, that no compression tests were conducted in this work to confirm or disprove this supposition.

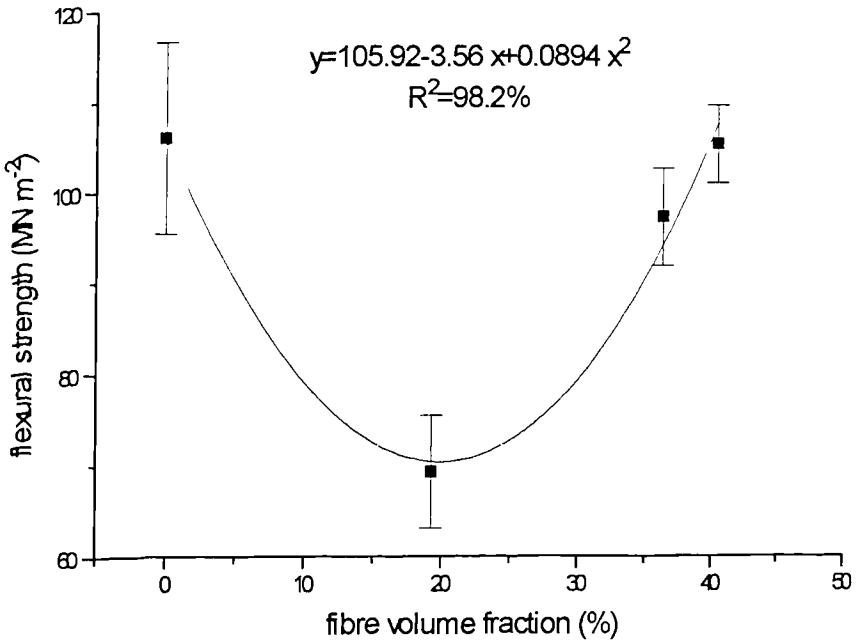

Figure 3.22 Flexural stress at break versus V_f. Jute fibre reinforced unsaturated polyester laminates.

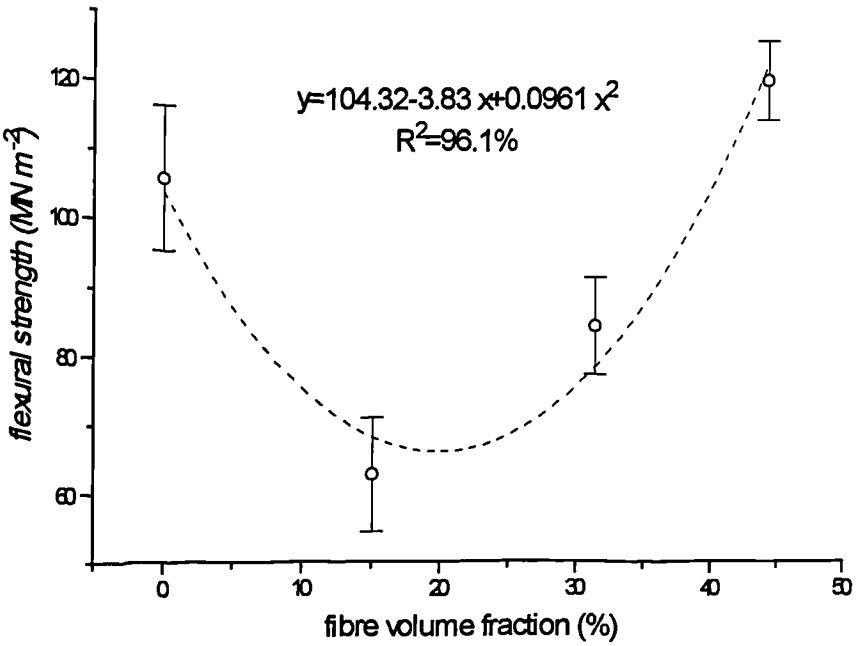

Figure 3.23 Flexural stress at break versus V_f. Hemp fibre reinforced unsaturated polyester laminates.

3.3.4.3 Flexural strength

The flexural strength of jute and hemp fibre reinforced laminates as a function of fibre volume fraction are presented in Figures 3.22 and 3.23 respectively. As with the tensile tests, flexural strength appeared to reach a minimum value at a V_f somewhere in the region of 20%. The reasons for this may again be attributed to the inclusion of a population of stress concentrators at relatively low V_f. The absolute values for the flexural strengths of all laminate types were found to be greater than the corresponding tensile strengths. This, in all probability, is due to the test method (Martin, 1996). As with the tensile tests, the flexural strengths of the CSM reinforced laminate were greater than that of the bast fibre reinforced material at an equivalent V_f, being approximately 135% and 150% greater than the jute and hemp reinforced laminates respectively.

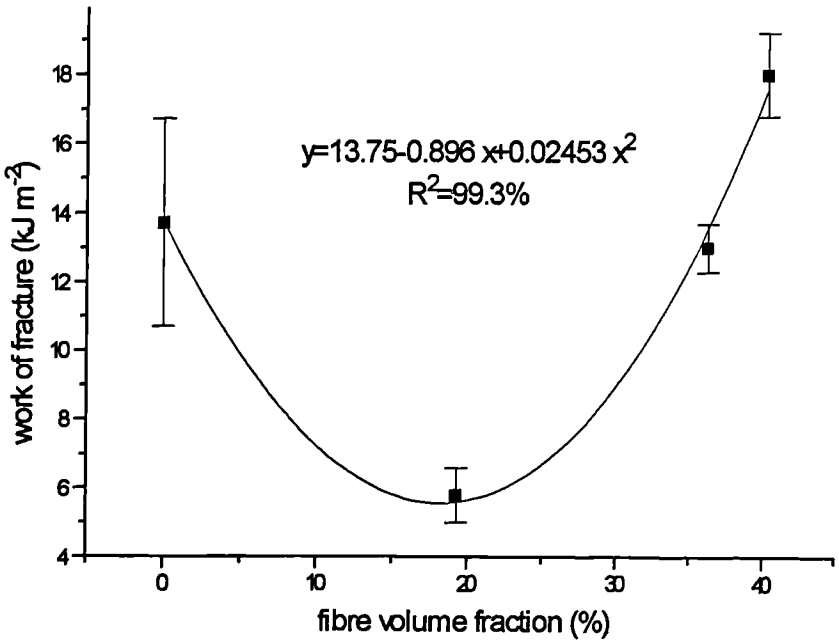

Figure 3.24 Work of fracture in three point flexure versus V_f. Jute reinforcement.

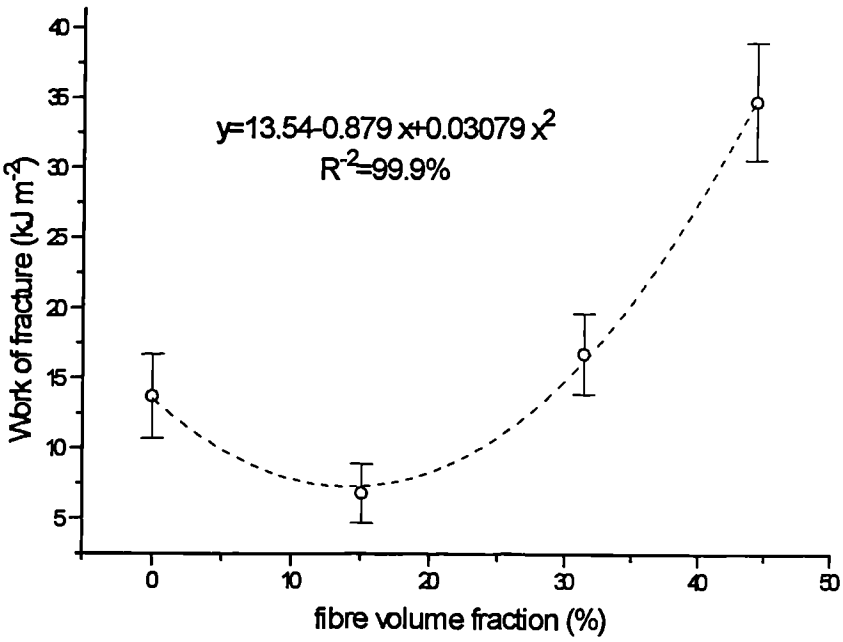

Figure 3.25 Work of fracture in three point flexure versus V_f. Hemp reinforcement.

3.3.4.4 Work of fracture in three point flexure

The work done in a three point flexure test (measured as the area under the load-deformation curve) provides an estimate of the energy absorbed by a material when undergoing fracture. Figures 3.24 and 3.25 show the work of fracture (normalised by dividing the work done by the cross sectional area of the specimen) in three point flexure of the jute and hemp laminates respectively.

It may be observed that, in a similar fashion to tensile and flexural strengths, the works of fracture of the natural fibre reinforced composites reached minimum values somewhere between 15% and 20%. This would indicate that rather than increasing the toughness of the composite, at low V_f, work of fracture is compromised by the addition of plant fibre. As will be discussed more fully in the following section, however, this may be accounted for in part by the test procedure. The un-reinforced polymer underwent considerable flexural strain (3.4%) prior to fracture. In all bast fibre reinforced laminates, the strain to failure was less than that of the resin and only in the CSM reinforced laminates was a greater failure strain observed (3.5%). Upon fracture, the pure resin specimens shattered and flew apart. It is therefore likely that the stored strain energy in the specimen, upon fracture was used to create many fracture surfaces and converted to kinetic energy, thus the work done (area under the load-deformation curve) probably gives a gross overestimate of the true work of fracture (i.e. to propagate a crack in the self same manner through the specimen). At low V_f, the bast fibre reinforced specimens had low strains to failure (1.9% and 2.2% for the jute and hemp reinforced material respectively), and fractured in a quasi-brittle manner with a single macroscopic crack extending through the specimen. It is probable that this is more representative of the actual work of fracture of the material. The apparent reduction in the work of fracture could be brought about by an increase in the incidence of 'critical' defects within the structure of the laminate, resulting in microscopic stress concentrations, instigating failure. As V_f increases beyond around 20%, the apparent work of fracture increases to in excess of that of the un-reinforced resin. This is in all probability accounted for by an improvement in the various toughening mechanisms (e.g. crack blunting, and deflection) which effectively increases the energy absorption capacity of the material. The manner of failure should

be borne in mind, for whilst the un-reinforced polymer fractured with an abrupt, brittle fracture, the addition of fibre at all loading levels resulted in a more 'controlled' failure with what may have been a degree of slow crack advance prior to failure.

A comparison with the CSM glass fibre reinforced laminate (Figure 3.26) revealed a large difference in the works of fracture of the natural and synthetic fibre reinforced materials, the former being between 5.0 and 7.5 times greater than the latter. The reasons for the seemingly large difference in the toughness of the different laminate types will be considered below. A summary of the results obtained during the flexural tests appear in Appendix 5.

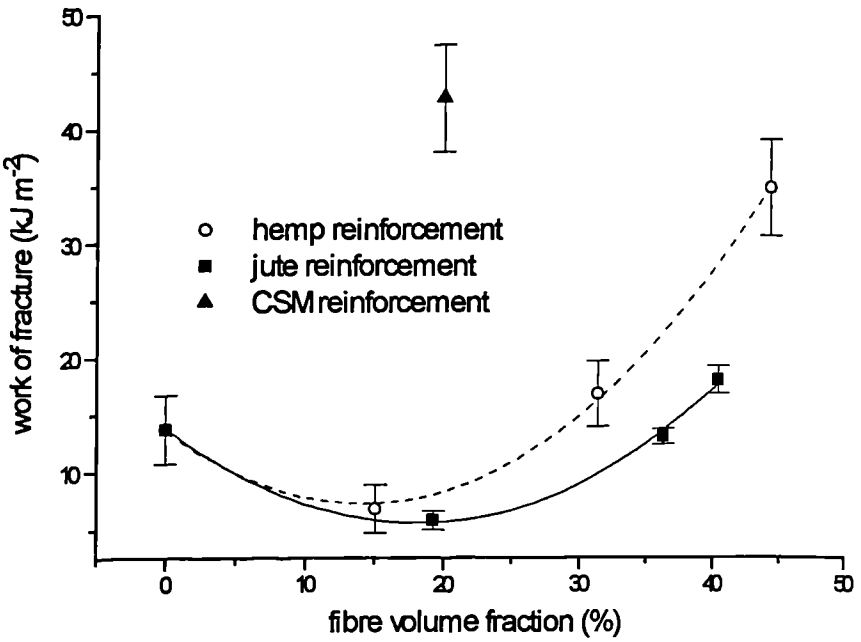

Figure 3.26 Work of fracture in three point flexure. Jute, hemp and CSM glass fibre reinforced laminates.

3.3.5 Impact properties

An assessment of the toughness or work of fracture of the materials was conducted by measuring the Charpy impact strength of the laminates. Figures 3.27 and 3.28 show the Charpy impact strength as a function of V_f, for jute and hemp reinforced laminates respectively. It may be observed that impact strength reached a minimum

value at a V_f of between 10% and 15%, depending upon fibre type. Only when V_f was increased to between 20% and 25%, did the impact strength equal that of the un-reinforced resin. Subsequent increases in V_f resulted in enhanced impact properties.

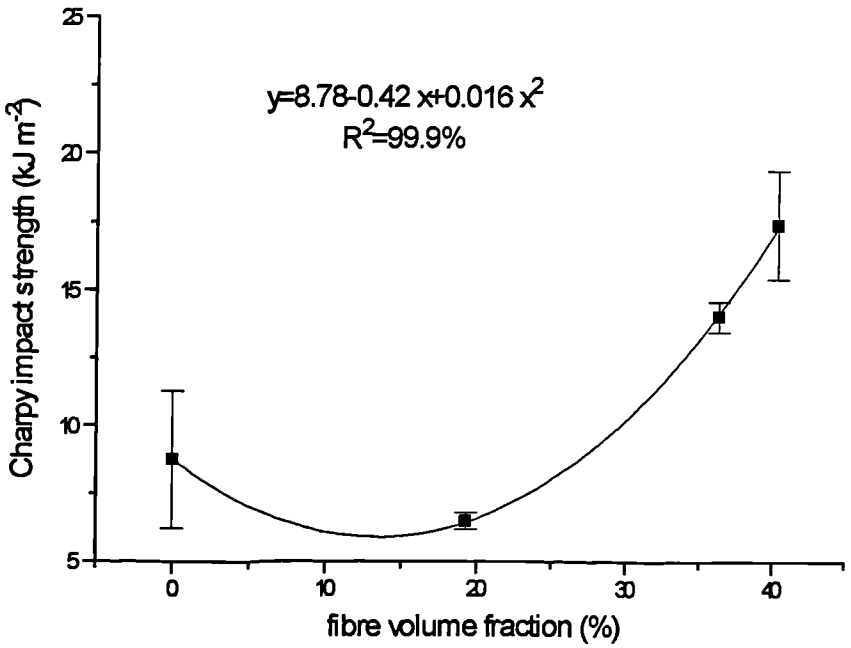

Figure 3.27 Charpy impact strength versus fibre volume fraction. Jute reinforcement.

It should be noted that the tests were, however, conducted using un-notched specimens. It is believed that this may have led to erroneous results for the work of fracture of the specimens; there must therefore be some doubt regarding the validity of the data. Nevertheless, the following observations can be made. Firstly, the Charpy impact strength of the un-reinforced polymer, at around 9 kJ m^{-2}, was almost two orders of magnitude greater than the works of fracture of thermosetting polymers quoted in the literature (e.g. Hull & Clyne, 1996; Williams, 1981). The work of fracture of the polymer used in this work has been calculated by alternative methods (see Section 3.3.6) and found to be in very good agreement with published values. This may be explained by the test methodology; firstly, when the specimens fracture, they do so by shattering into numerous shards and secondly, the shattered specimens are thrown some distance by the apparatus. By shattering, no single crack propagates

in the self-same manner, but numerous additional crack surfaces are created, thereby absorbing energy. This, together with the kinetic energy of the shards (plus any further energy absorbed by the system) may well account for the large work of fracture determined in this manner. Clearly, this might disguise the 'true' trends in composite toughness.

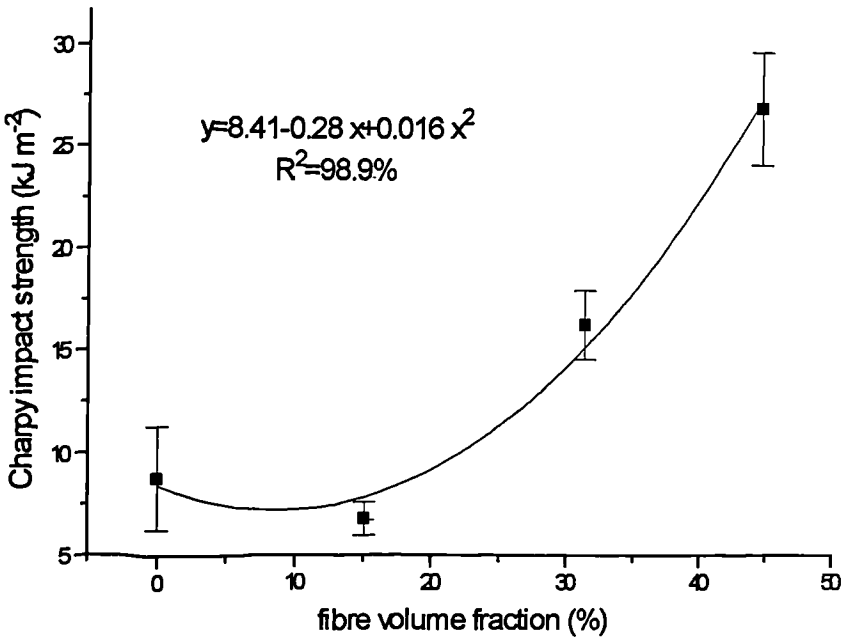

Figure 3.28 Charpy impact strength versus fibre volume fraction. Hemp reinforcement.

The drop in the Charpy impact strength would appear to reflect a reduction in the work of fracture of the laminate. This is consistent with the discussion in Section 3.3.3 regarding the reasons for the drop in tensile strength seen in the plant fibre reinforced laminates at a V_f of around 15-20%. In effect, at these volume fractions, the fibres would seem to introduce a population of defects into the structure of the laminate, without a commensurate increase in mechanisms which serve to improve toughness (such as crack blunting at weak interfaces, energy absorption through the creation of crack surfaces and frictional sliding of the fibres within the matrix). Indeed, it was clearly observed that, at low volume fractions, the bast fibre laminates failed in a brittle manner, with fracture occurring along a single macroscopic crack.

At higher volume fractions, however, toughening mechanisms are introduced which increase the apparent work of fracture to above that of the polymer itself. In these circumstances, although fracture was predominantly macroscopically brittle, there was some evidence of inter-laminar shear failure, which may account for enhanced energy absorption.

The foregoing is, however, probably only partly true since, if the nature of the fracture of the un-reinforced polymer is taken into account, the fibres would serve to improve the work of fracture of the laminate. If it is assumed that the work of fracture of the polymer is in the region of 0.1 kJ m^{-2} (Williams, 1981), for a crack propagating in the self-same manner, then the addition of fibre would be seen to increase the work of fracture at all fibre loadings. The discrepancy between the work of fracture of the polymer itself and those of the bast fibre reinforced laminates, is probably due to the manner in which fracture occurs and also to the test procedure, rather than a reflection of the toughness of the material.

The Charpy test, as used in this work, may well have provided misleading data on the toughness of the composites due to the manner in which the laminates fail. Nevertheless, it may have provided an insight into possible failure mechanisms and may also indeed provide a more representative estimation of the 'brittleness' of the material in service conditions. It could reasonably be claimed that this test, using un-notched specimens, offers a measure of the sensitivity of the material to the initiation and propagation of a pre-existing population of micro-defects. The resistance of the material to the propagation of macroscopic cracks - fracture toughness, may be viewed somewhat differently. A more quantitative approach to toughness, in terms of the sensitivity of the materials to macroscopic cracks, will be presented in the following section.

A comparison of the Charpy impact strength of the bast fibre reinforced material with that of the CSM glass fibre laminate is shown in Figure 3.29. It may be observed that there was a large difference (approximately an order of magnitude) between the Charpy impact strengths of the synthetic and natural fibre reinforced materials.

Similar differences in the impact strengths of vegetable fibre and glass fibre reinforced composites have been reported elsewhere (O'Dell, 1997).

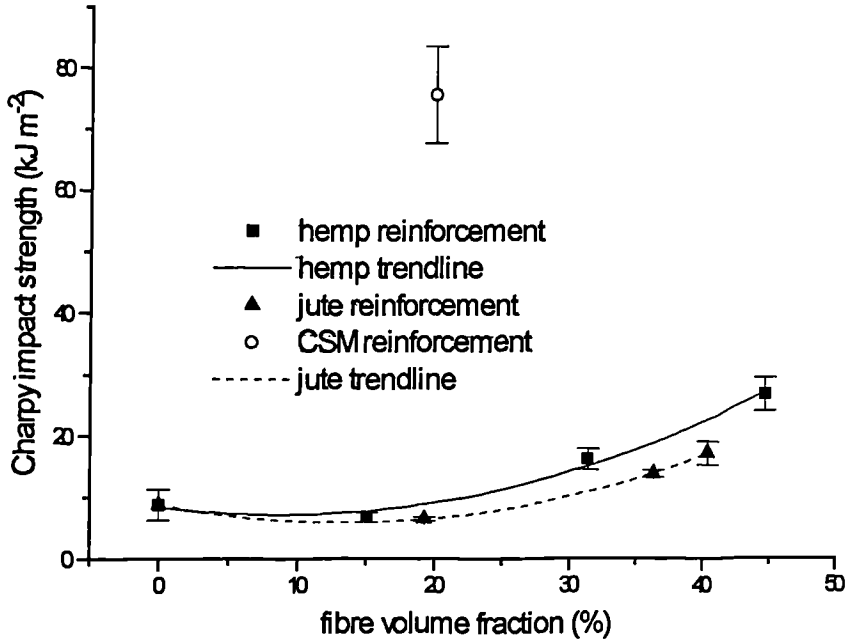

Figure 3.29 Comparison of un-notched Charpy impact strength (un-notched specimens). Jute, hemp and CSM reinforced laminates.

The above findings seem to be in general agreement with those reported by other authors. For example, Roe and Ansell, (1985) found that at a V_f of 20%, the work of fracture of unidirectional jute fibre reinforced polyester was around 4 kJ m^{-2} (obtained using the Charpy test - *notched* samples), rising to around 22 kJ m^{-2} with a V_f of 60%. By way of comparison, for a glass fibre epoxy system at a V_f of 67%, a fracture energy of around 200 kJ m^{-2} has been reported (Harris, 1980). Sanadi *et al.* (1986a), reported a fracture energy of 21.54 kJ m^{-2} using the Izod test for a 24% V_f uniaxial Sunhemp polyester composite. Prasad *et al.* (1983), reported a Charpy impact value of 7.44 kJ m^{-2} for untreated coir-polyester composites of 20% fibre V_f, less than the 8.33 kJ m^{-2} of the un-reinforced resin. White and Ansell (1983), used straw to reinforce polyester resin and found that at a V_f of 70%, fracture energies of around 7 kJ m^{-2} were obtained.

Whilst due account should be taken of the test methods employed to derive works of fracture, it seems evident that for equivalent *volume fractions* of reinforcement the toughness of plant fibre reinforced thermosets is significantly lower (possibly as much as an order of magnitude) than their glass fibre reinforced equivalents. This may well ultimately prove to be a highly significant factor, limiting the potential end uses to which these materials may be applied. Appendix 6 records the full results of the Charpy impact strength tests.

3.3.6 Fracture toughness

In the words of the late Professor J.E. Gordon, (1976): "*The worst sin in a engineering material is not lack of strength or lack of stiffness, desirable as these properties are, but a lack of toughness, that is to say, lack of resistance to the propagation of cracks*". It is a requirement of most engineering materials that they possess adequate toughness or crack stopping ability. One of the attractions of many composite materials is their excellent toughness, especially when viewed on a specific basis (Gordon, 1970). It seems likely, therefore, that if composites based on thermosetting polymers reinforced with vegetable material are to used in structural applications, then it must be ensured that their works of fracture are adequate. The results reported thus far would, however, seem to indicate that bast fibre reinforced polyester composites are considerably less tough (possibly by as much as an order of magnitude) than their glass fibre reinforced counterparts. In view of the importance of this property it was believed that this aspect warranted closer investigation. As a first step, the relative toughnesses of the materials under investigation were quantified.

Pendulum tests such as Charpy and Izod provide a qualitative measure of a material's toughness (Anderson, 1995). However, a more fundamental approach to the study of the toughness is provided by fracture mechanics. Under suitable conditions, fracture mechanics techniques can provide a quantitative measure of toughness. Of particular relevance to this approach, is the way in which the macroscopic toughness of the material can be related to its microstructure, possibly highlighting ways in which toughening mechanisms may be stimulated (Hull & Clyne, 1996). In view of this, it was felt that an evaluation of the fracture toughness of the natural (and synthetic) fibre reinforced composites should be attempted. The applicability of fracture mechanics techniques as applied to these composite materials will be discussed. From the outset it should be pointed out that the results obtained from these tests should be treated with caution since the laminates studied violate many of the material assumptions made in fracture mechanics theory. Nevertheless, it is believed that some insight as to the reasons behind the relatively poor toughness observed in these composites was obtained as a result of this analysis.

3.3.6.1 Fracture mechanics

In essence, fracture mechanics provides a measure of the toughness of a material by considering the conditions under which a pre-existing sharp crack or crack-like defect, which might ultimately lead to failure, begins to propagate (Martin, 1996). Both energy and force based failure criteria have been developed for materials exhibiting brittle or quasi-brittle behaviour (Knott, 1973; Parton, 1992). These are collectively known as linear elastic fracture mechanics (LEFM). Primarily developed for metals (BSI, 1991, ASTM, 1991), LEFM has nonetheless been applied, with varying degrees of success to non-metallic materials including wood and synthetic PMCs (Patton-Mallory & Cramer, 1987; Williams, 1981; Stanzl-Tschegg, *et al.*, 1994, 1995, 1996) as well as to other biological materials (Lucas *et al.*, 1991, 1995, 1997).

3.3.6.2 Linear-Elastic Fracture Mechanics

Fracture mechanics evolved from the early work of Griffith (1920), in which the thermodynamics of the fracture process in a nearly perfectly linear-elastic material (glass) containing a sharp crack, was considered. Griffith derived an expression for fracture stress as a function of crack length and work of fracture (taken to be the work required to create new crack surfaces). It was shown that, for a crack of length $2a$ contained in an infinite body, with a stress applied normal to the plane of the crack, the following relationship exists between fracture stress σ_F, crack length and work of fracture:

$$\sigma_F = \left(\frac{2\gamma_S E}{\pi a}\right)^{1/2} \tag{3.5}$$

Where: E is Young's modulus

$2\gamma_S$ is the work of fracture (γ_S is the surface energy)

This work was later extended to encompass materials which were capable of energy dissipation through plastic flow, as well as the creation of new surfaces. In this approach, the γ_S term is supplemented by other, irreversible, contributions to the energy absorbed in the vicinity of the crack-tip. A new term was subsequently

introduced to replace work of fracture, known as the *energy release rate*, G, defined as (Anderson, 1995):

$$G = -\frac{d\Pi}{d\mathrm{A}} \tag{3.6}$$

Where Π is potential energy

A is crack area

Thus G is a measure of the rate of change of potential energy with respect to crack area. For the example noted above, it can be shown that $G = \sigma^2 \pi a / E$. For fracture to occur, G must exceed a critical value G_C, the *critical energy release rate*, or *fracture toughness*. In the above noted example, it can be shown that the relationship between fracture stress and G_C is (Anderson, 1995):

$$\sigma_F = \left(\frac{G_C E}{\pi a} \right)^{1/2} \tag{3.7}$$

An equivalent, force-based approach, considers the stress field in the vicinity of the crack-tip. It may be shown that a constant K, the *stress intensity factor* (units of MN $m^{-3/2}$) characterises the crack-tip stress-strain conditions. Furthermore, it can be shown that G and K are related as follows (Anderson, 1995):

$$G = K^2 / E \quad \text{(in plane stress)} \tag{3.8}$$

$$G = K^2 (1 - \nu^2) / E \quad \text{(in plane strain)} \tag{3.9}$$

Where: ν is Poisson's ratio

It may be shown that the stress distribution in a material ahead of a crack in a loaded homogeneous, isotropic and ideally linear-elastic body takes the general form (Parton, 1992):

$$\sigma = \frac{K}{(2\pi z)^{1/2}} f(\alpha) + \ldots\ldots \qquad (3.10)$$

Where z is the distance from the crack tip, α, the angular displacement about the plane of the crack. The stress intensity factor characterises the intensity of the stress field ahead of the crack (Knott, 1973). The stress field in the vicinity of the crack-tip therefore differs only by a constant (depending upon the mode of the crack surface displacement), K, which encompasses the external load and geometry of the body. A critical value of $K = K_C$ defines the onset of crack growth and provides a force based fracture criterion. The *critical stress intensity factor* K_C, is also referred to as *fracture toughness*. Under opening mode, plane strain conditions, "plane strain fracture toughness" (K_{IC}) can be regarded as a material parameter, provided stringent validity criteria are met (e.g. BSI, 1991; ASTM, 1991).

For a range of specimen configurations and loading schemes, standard solutions for the determination of the stress intensity factor (K) are available and generally take the form $K = \sigma_{app}\sqrt{(l)}Y$, where σ_{app} is the nominal applied stress, l the crack length and Y is a dimensionless constant, known as the K-calibration. The K-calibration depends upon the ratio of crack length to specimen thickness, b. K-calibrations usually take the form of a polynomial, thus (Parton, 1992):

$$Y(\lambda) = c_0 + c_1\lambda + c_2\lambda^2 + c_3\lambda^3 + \ldots\ldots\ldots \qquad (3.11)$$

Where: $\lambda = l/b$

It is therefore possible to determine the fracture toughness of a material, if the remote stress at crack initiation can be determined, if the global behaviour of the material is linear-elastic, and if the specimen geometry and loading fall within certain bounds. These validity criteria are set out in the standards (BSI, 1991; ASTM, 1991).

The advantage of a LEFM approach to materials' failure lies in the fact that, provided valid figures for fracture toughness can be determined, the strength of real structures containing cracks can be ascertained. As well as providing characterisation of material toughness, this approach, as indicated above, can be used to link material toughness with micro-structure. For instance, the size of the plastic zone ahead of a crack is given by (Hull & Clyne, 1996):

$$r_y \approx \frac{1}{2\pi}\left(\frac{K}{\sigma_{ys}}\right)^2 \qquad (3.12)$$

Where: r_y is the radius of the plastic zone

σ_{ys} is the yield stress of the material

3.3.6.3 Fracture toughness of laminates

An estimate was made of the fracture toughness (K_{IC}) of the natural fibre reinforced polyester composites and compared with that of material reinforced with CSM glass fibre. The procedure adopted to measure K_{IC} was based heavily upon that set out in BS 7448 (1991), employed in the measurement of the fracture toughness of metallic materials.

This standard sets out a procedure for analysing the force versus load-line displacement records, obtained during a fracture toughness test and when certain criteria are met, establishing a value for K_{IC}. The point of interest on the record is the load at which unstable crack extension begins. For linear elastic materials, this load can taken to be the maximum load observed on the load-displacement record. For materials which exhibit a limited amount of non-linear behaviour prior to the attainment of a maximum force or 'pop-in' (a jump in the force-displacement curve corresponding to sudden crack advance) in the load-deformation record, a procedure known as the 'offset procedure' (Knott, 1973; Parton, 1992) is adopted. This involves the construction of a secant with a gradient 5% less than that of a tangent drawn parallel to the initial elastic region. The point of intersection with the record line is taken to be the critical load, P_Q, from which a provisional value of $K = K_Q$ is

computed and which is subsequently tested for validity. If these validity criteria are met, then this is taken to be the plane strain fracture toughness (K_{IC}) of the material (BSI, 1991). The offset procedure estimates the size of the plane strain plastic zone and compares this with the dimensions of the specimen (Knott, 1973; Anderson, 1995). If the plastic zone is large in comparison to other specimen dimensions, then it is likely that any value of K determined by this method will not provide a realistic measure of the fracture toughness of the material. For instance, in a material which undergoes a significant amount of plastic deformation prior to failure, this method would underestimate the toughness of the material. In such cases, yielding fracture criteria may be more appropriate (Williams, 1981).

The offset procedure provides a point on the curve (corresponding to 2% apparent crack growth) at which crack extension is assumed to occur. However, if possible, it is preferable to detect the onset of crack growth by some direct means (Knott, 1973). In this work, an alternative (Kimber, 1999) to the offset procedure, which involved the direct detection of crack initiation was employed. If even small pop-ins can be detected, then it should be possible to define the onset of crack growth in the material. Essentially pop-ins represent changes in compliance of the specimen. Digital data acquisition enables computer numerical techniques, such as differentiation to be easily performed on the force versus load-line displacement record. If the second derivative of the load-deformation record is obtained, then this effectively represents the rate of change in stiffness of the specimen with respect to deformation; large changes in rate thus correspond to pop-ins and can effectively be used to detect the onset of crack growth in the material. This method was used to detect crack initiation in the laminates studied in this work and the values for load thus obtained were utilised in the determination of K_{IC} (it should be noted that the values for critical K determined in this work carry the suffix '$_{IC}$' even though in reality these are not necessarily valid K_{IC} figures (see below). Nevertheless, this convention has been used for convenience to denote the critical value of K determined using this technique). Figure 3.30 shows a typical load-displacement record for a CSM glass fibre SEN test specimen, with the corresponding second derivative curve shown beneath. A small pop-in is observed in the former, whilst the corresponding rate change associated with the pop-in is clearly noted in the latter.

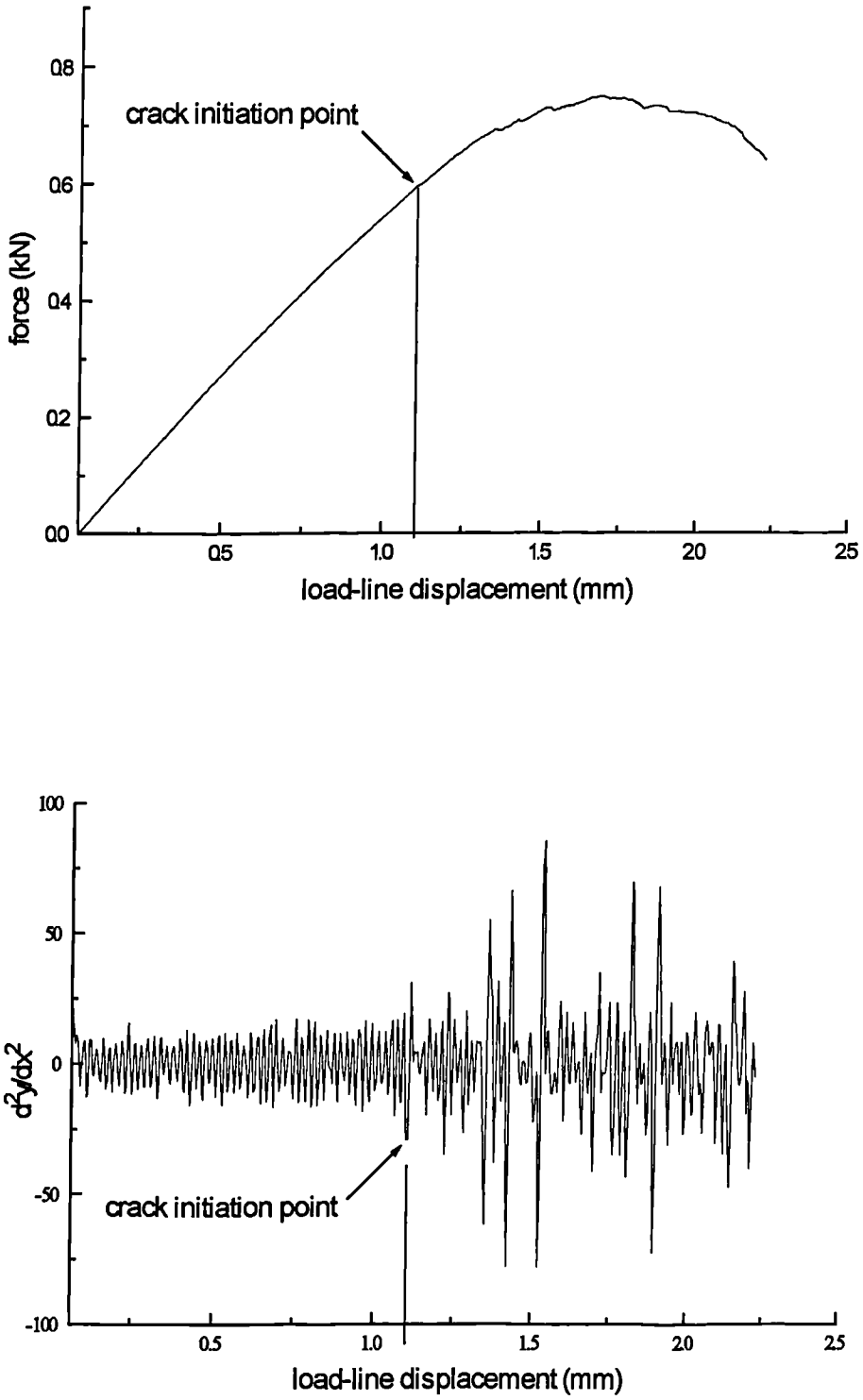

Figure 3.30 Force versus load-line displacement record for a cracked CSM glass fibre laminate in three point flexure (above). Second derivative of the record with respect to displacement (below). The point at which crack initiation is assumed to occur is marked.

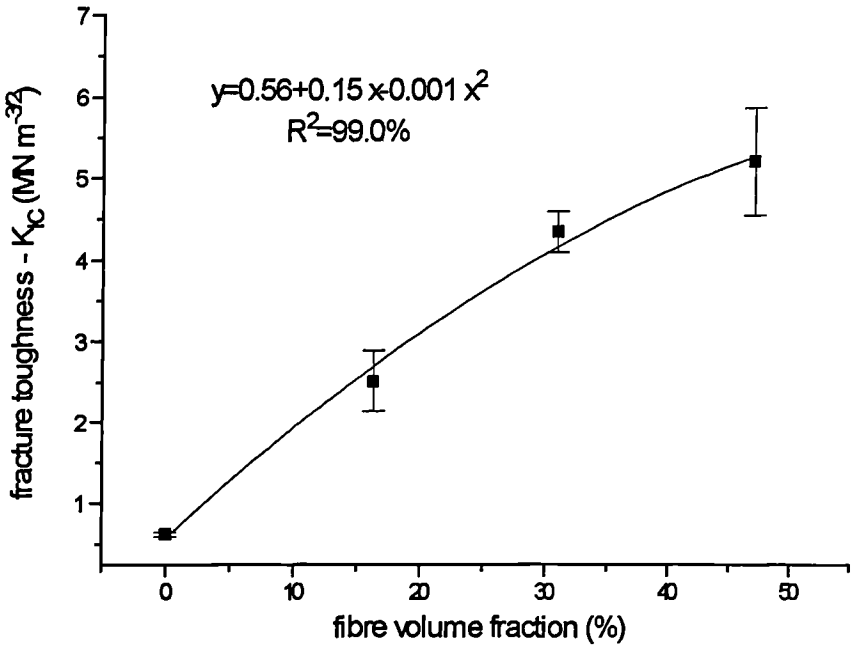

Figure 3.31 Variation of K_{IC} with fibre volume fraction. Jute reinforcement.

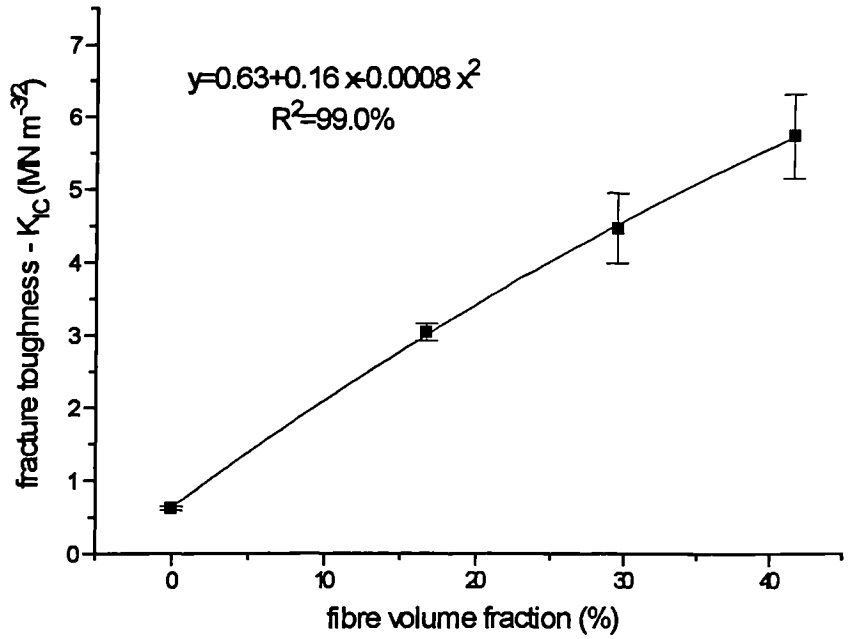

Figure 3.32 Variation of K_{IC} with fibre volume fraction. Hemp reinforcement.

The suitability of the experimental technique used in this work to assess the fracture toughness of these composite materials is demonstrated by considering fracture of the un-reinforced polymer itself. The value for K_{IC} of this material was determined to be 0.62 MN $m^{-3/2}$, which is in excellent agreement with values published in the literature for thermosetting polyesters (Williams, 1981) and is in good agreement with the order of magnitude for other thermosetting resins such as epoxies (Hull & Clyne, 1996). Utilising Equation 3.8 and the value obtained for Young's modulus, a value for the G_{IC} of the polymer was calculated to be 0.09 kJ m^{-2} (assuming ν=0.38 (Hull & Clyne, 1996)). Again, this is in good agreement with reported values for the work of fracture of other organic glasses (Ashby & Jones, 1980). It is worthwhile noting the difference between the work of fracture figures obtained by this method and those determined through the Charpy test, which differ by almost two orders of magnitude.

3.3.6.4 Variation of fracture toughness with V_f

Figures 3.31 and 3.32 show the variation of fracture toughness with fibre volume fraction for jute and hemp reinforced laminates respectively. Both reinforcement types show a strong positive correlation between fracture toughness and fibre volume fraction. The relationship does not appear to be quite linear, which may indicate that at higher volume fractions, at least, the benefit to toughness of adding fibre is somewhat reduced. This relationship could be expected if, say, at a higher fibre loading, difficulty in wetting out the fibres occurred, leading to reduced bonding between fibre and matrix and to a greater number of voids in the microstructure. However, as discussed in Section 3.3.1, up to the fibre volume fractions studied (~45%) little evidence either of poor wetting or void inclusion was observed, indicating that other factors may be important in determining fracture toughness. If it is assumed that there is little effect upon the quality of the interface as V_f increases (in other words that the interfacial shear strength remains constant) and the ratio of fibre modulus to matrix modulus remains the same, then factors such as the relative fibre to fibre spacing may well be of significance. For example, it has been shown that reducing the fibre to fibre spacing (i.e. increasing V_f) results in higher stress concentrations occurring in fibres adjacent to cracked fibres (He & Hutchinson, 1989

cited in Hull & Clyne, 1996). This could undoubtedly contribute to a reduction in composite toughness. This aspect is explored further in Chapter 6.

3.3.6.5 Influence of fibre type

The fracture toughness of the glass fibre reinforced material was evaluated at one fibre volume fraction (~20%) only. In order to make a comparison, therefore, between the fibre types at equivalent V_f, the regression equations shown on Figures 3.31 and 3.32 were invoked. Table 3.7 provides a comparison of the fracture toughness of the reinforced laminate types as well as with the un-reinforced polymer itself. An estimate of the critical energy release rate (G_C) was made utilising Equation 3.8. The effect of ignoring the $(1-\nu^2)$ term under plane strain conditions (Equation 3.9) is negligible, and would not alter the order of magnitude of the differences between the laminate toughness figures appreciably. Young's modulus at the V_f in question was calculated from the regression equations shown in Figures 3.9 and 3.10. It must be noted that this is very much an estimate of the order of magnitude of G_C, since the materials are treated as being isotropic and E is taken to be the experimentally determined values along one axis only. As this was parallel to the preferred fibre direction, E would no doubt be somewhat greater than if the reinforcement was planar random. Clearly, this is a simplification of the situation, but necessary in order to make the comparison.

Table 3.7 Comparison between the fracture toughness of laminates reinforced with jute, hemp and glass fibre and the un-reinforced polymer. (V_f = 20%).

Laminate type	K_{IC} $(MN\,m^{-3/2})$	E $(GN\,m^{-2})$	G_C $(kJ\,m^{-2})$
CSM laminate	9.0	7.97	10.2
Jute laminate	3.1	6.77	1.4
Hemp laminate	3.4	6.74	1.7
Un-reinforced polymer	0.6	3.80	0.1

As discussed above, a value of 0.62 MN $m^{-3/2}$ for K_{IC} for a thermosetting polymer is realistic. Likewise, the value for CSM reinforced material is in good agreement with other published data; a figure of 7.0 MN $m^{-3/2}$ being quoted by Williams (1981) for a similar laminate type, albeit at a higher (33%) fibre loading. A slightly higher value for K_{IC} might well be expected since the method used to determine the load at crack initiation differs from the 'offset procedure', leading to somewhat higher values. This issue is discussed below. No figures could be found in the published literature for the K_{IC} of plant fibre reinforced material. Nevertheless, these figures again do not look unreasonable and are on a par with those quoted for a number of thermoplastic polymers, for example Nylon 6.6 and polypropylene (Ashby & Jones, 1980).

With regard to K_{IC}, the addition of reinforcing fibre to the polymer results in an order of magnitude improvement in fracture toughness, with an approximately three-fold difference between natural and synthetic fibre types being observed. Hemp would seem to provide a marginally greater toughness enhancement than jute. The stress intensity factor, in essence, provides a measure of the severity of the stress field ahead of a sharp crack. Simplistically therefore, K_{IC} can be viewed as providing a measure of the strength of the material in the presence of a notch. The lower fracture toughness observed in the natural fibre reinforced material, may, in part at least, be attributed to the lower tensile strengths reported for these fibres (see Table 1.1).

As may be seen, the addition of both natural fibre types resulted in an order of magnitude improvement in the G_C of the laminates over that of the un-reinforced polymer, hemp possibly providing a somewhat greater improvement. The difference, however, between the G_C of natural fibre reinforced composites and the glass fibre reinforced material was also approximately an order of magnitude. This order of difference is more or less the same as observed between the Charpy impact strengths of the reinforced fibre laminates (although not the same as between the un-reinforced polymer and reinforced material). The implications of this are that the energy dissipative processes involved in the toughness of the bast fibre reinforced composites are not as effective as those seen in their glass fibre reinforced counterparts.

One of the advantages of a fracture mechanics approach to failure is, as mentioned above, its ability to allow a link between macroscopic behaviour to conditions in the region of the crack tip to be made. If it is assumed that the materials under investigation behave elastically, apart from a zone ahead of the crack-tip where limited plastic behaviour occurs, and that the vast amount of the energy absorbing processes occur, within this 'plastic zone', then an estimate of the 'energy absorbing capacity' of the material should be possible if the 'volume' of the 'plastic zone' can be established. Figure 3.33 shows an idealised representation of the 'plastic zone' ahead of the crack tip. Equation 3.12 provides a relationship between the radius of the plastic zone, fracture toughness and the yield stress, σ_{ys}.

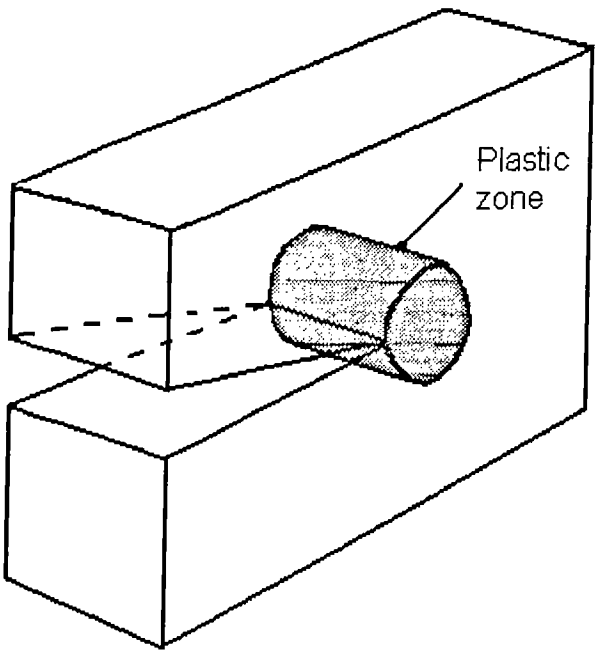

Figure 3.33 Schematic representation of the crack-tip plastic zone.

The composites under investigation were, however, heterogeneous and anisotropic and thus contravened LEFM assumptions. Nevertheless, if the situation is idealised and *it is assumed that the materials were homogeneous, isotropic and that macroscopically they behaved in a linear-elastic fashion and furthermore that they possessed* K_{IC} *and* σ_{ys} *values equal to those determined for the 'real' laminates, then for these 'equivalent' materials* r_y *may be computed.* It is fully appreciated that

this is very much a simplification of reality, but the exercise was conducted in order to try and gain an *estimation* of the relative sizes of the plastic zones of the laminates. From these, it was hoped that some inferences regarding the 'energy absorbing capacity' of the laminates could be made.

In this instance, σ_{ys} is taken to be the 0.2% proof stress (see Table 3.6). The radii of the plastic zones, as calculated from Equation 3.12 are presented in Table 3.8.

Table 3.8 Crack-tip plastic zone radius (V_f = 0.2)

Laminate type	r_y *(mm)*	r_y^2 *(mm²)*
Unreinforced polymer	0.03	9×10^{-4}
Jute reinforced laminate	0.70	0.50
Hemp reinforced laminate	1.30	1.70
CSM reinforced laminate	3.70	13.70

As can be seen, the value of r_y for the un-reinforced polymer is significantly less than that of the reinforced laminates. Its value of ~30μm is probably realistic, denoting a very small region of plastic flow and consistent with other predominantly brittle materials in which the main energy absorbing process is through the creation of new crack surfaces. Of all the laminate types studied, the un-reinforced polymer is nearest to the idealised 'equivalent' material; being essentially elastic, homogeneous and isotropic. Similarly, the r_y values for the 'equivalent' reinforced materials do not appear unreasonable. Visual inspection of the failed bast fibre reinforced specimens revealed that damage extended beyond the apparent crack face into the laminate itself by <1 mm; in other words the advancing crack left a 'wake' of micro-damaged laminate, analogous to the plastic wake left behind an advancing crack in metals (Anderson, 1995). This would seem to be consistent with calculated values for r_y. With increasing V_f the extent of the damage zone appeared to increase. This would again seem to be consistent with the predictions made by Equation 3.12, since the

ratio of K_{IC} to σ_{ys} increased with V_f. In other words, yield strength rose at a disproportionately lower rate with V_f than did K_{IC}, due to an increasing amount of non-linear, plastic, behaviour. The radius of the plastic zone determined for the glass fibre reinforced 'equivalent' laminate was approximately 3 to 4 times that of the natural fibre reinforced 'equivalent' material. Again, this prediction was supported by visual inspection of the ruptured laminate. However, whilst in the bast reinforced material the visible micro-damage was confined to what seemed to be a well defined region along the crack face, in the glass fibre reinforced material, micro-damage appeared to be far more extensive. Micro-damage, associated with fibre breakage, fibre-matrix debonding and matrix cracking, appeared to be a more diffuse and extensive affair in the glass reinforced polymer than the natural fibre reinforced equivalent material.

If, as mentioned above, it is assumed that most energy dissipation occurs in the damage region ahead of the advancing crack-tip, then it is reasonable that the amount of energy absorption is proportional to the volume of the damage zone. Thus, for a crack of unit width, the volume of the damage zone is proportional to r_y^2. Table 3.8 shows a comparison of the computed r_y^2 values. As may be seen, the estimated volume of the damage zone observed in the 'equivalent' natural fibre reinforced composites is approximately an order of magnitude lower that that seen in the 'equivalent' glass fibre reinforced material at equal fibre volume fractions. This would seem to point to a possible explanation for the lower toughness observed in the bast fibre reinforced materials, in that energy dissipative processes are simply not stimulated in the crack-tip region to the same extent as they are in their glass fibre reinforced equivalents. Visual examinations of the fractured specimens seem to bear this out. The order of magnitude difference seen in r_y^2 is also consistent with the measured works of fracture of the natural and synthetic fibre reinforced composites which are also approximatly an order of magnitude in difference.

This analysis has not been presented as a rigorous proof, rather simply to establish orders of magnitude for the relative quantities. Nevertheless, the computed sizes of the plastic zones for the 'equivalent' materials seem to be in broad agreement with the

observed behaviour, as indeed is the increasing size of r_y with V_f. Furthermore, it is not the intention to suggest that the lower toughness of the natural fibre materials is due solely to the relative volumes of the damage zone. Nevertheless, it does provide an indication that this region should be studied more closely, and in particular the micro-structure. This aspect is dealt with in more detail in following chapters.

3.3.6.6 Validity of K_{IC} measurements

Typical force versus load-line displacement records up to the point of maximum load, obtained from the fracture toughness tests, are presented in Figures 3.34 and 3.35. As can be clearly seen, particularly with the hemp reinforced material and at higher volume fractions, non-linear behaviour becomes significant.

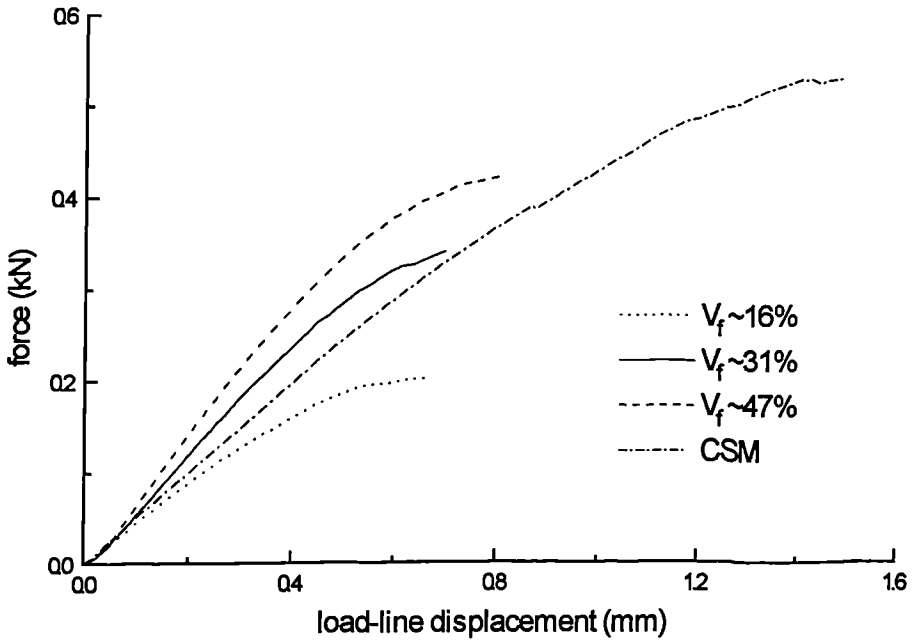

Figure 3.34 Force versus load-line displacement records for SEN jute specimens under three point flexure (quasi-static loading). Various V_f are shown, together with the record obtained for a CSM laminate (~21% V_f).

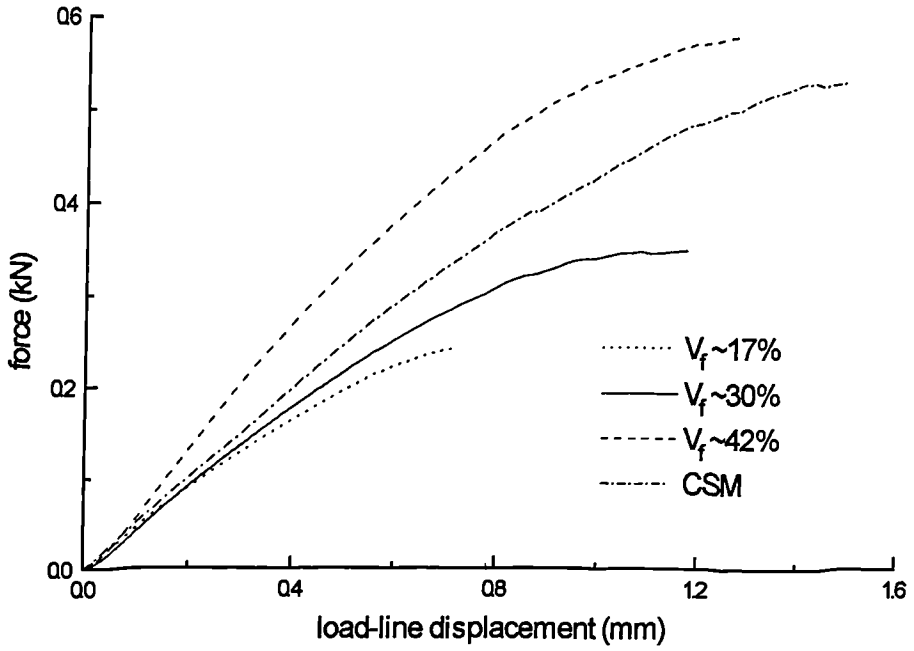

Figure 3.35 Force versus load-line displacement records for SEN hemp specimens under three point flexure (quasi-static loading). Various V_f are shown, together with the record obtained for a CSM laminate (~21% V_f).

If a secant is drawn with a gradient 5% less than that of the initial tangent, the point of intercept, i.e the value P_Q is typically at a much lower load than the value obtained through noting the onset of crack of growth directly from the force versus load-line displacement record, the method employed in this study. Figure 3.36 shows a typical force-displacement curve for a hemp reinforced laminate (30% V_f). As can be clearly seen, the gradient of a secant constructed between the origin and the point of intercept on the curve where crack initiation is taken to occur, is approximately 21% less than the gradient of the initial tangent. When the 5% secant is drawn, the intercept occurs at a markedly lower force. Computed values of K_{IC} would therefore differ considerably if this procedure had been adopted.

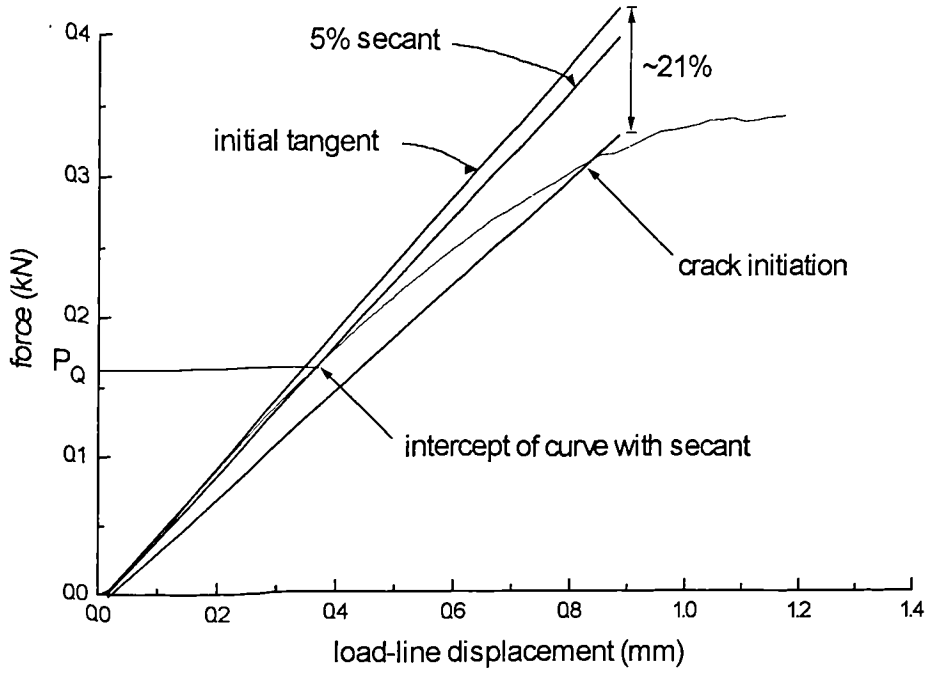

Figure 3.36 A typical force versus load-line displacement record for a hemp reinforced SEN specimen (V_f ~30%), showing secant constructions.

As discussed previously, the construction of the secant in the 'offset procedure' is designed to test whether the degree of plasticity prior to crack advancement is small enough to ensure that LEFM principles are not invalidated. Further, it examines whether any non-linear behaviour can be attributed to slow crack growth or to plasticity effects. In this study, it is believed that the non-linear behaviour prior to the attainment of a pop-in (taken to be the onset of macroscopic crack extension) is attributable to 'plasticity'. It is, however, clearly difficult to differentiate between what might be termed micro-cracking ('plastic' behaviour) and the initiation of macro-crack advance. Nevertheless, it is believed that the technique used here, of detecting small pop-ins, does make the distinction between the two more easily observable. Relying upon the construction of a secant and assuming that cracking initiates at the point of intercept with the force versus load-line displacement may therefore, in this instance at least, bear no relation to the actual behaviour of the material.

The 5% secant line represents the change in compliance that would be associated with a crack extension equal to the maximum allowable size of the plane strain plastic zone, such that LEFM principals are not violated. That is, the size of the plastic zone is small in comparison to the overall specimen dimensions, or in other words, that global behaviour is predominantly linear elastic and the plastic zone is confined to a small region at the crack tip. The purpose of this is to ensure that the asymptotic equations (*cf.* Equation 3.10), which are based upon linear elastic theory, are not invalidated by excessive plastic behaviour.

The purpose of the foregoing is to argue that, rather than using the 'offset procedure' to determine the point of crack advance, direct detection through an analysis of the load-displacement trace provides a better physical meaning to the onset of crack advance. Nevertheless, this cannot necessarily be associated with brittle fracture of the material, simply the onset of macroscopic crack advance. A result of using this method is that, with the specimen dimensions employed, excessive plastic behaviour prior to crack growth was apparent (at least in those laminates with higher V_f), making the results from these tests questionable since LEFM assumptions were in all probability invalidated. Specimens very much larger than those used would be required for valid results to be obtained (BSI, 1991). In view of the foregoing, the data was reanalysed using elastic-plastic fracture mechanics (EPFM) techniques.

3.3.6.7 Critical J fracture toughness

The J contour integral can be used as a fracture characterising parameter for non-linear materials. J, defined as a path independent contour integral, is equal to the energy release rate in a non-linear body containing a crack and is analogous to G in lincar-elastic materials. In linear materials J–G. Further, the J integral can also characterise crack tip stress-strain conditions in non-linear materials (Anderson, 1995).

Elastic-plastic fracture analysis was used to reanalyse the force versus load-line displacement records obtained in the above tests, utilising the procedure set out in BS 7448 (1991). The standard sets out a procedure to evaluate a critical value of J, the experimental equivalent of the J contour integral which can be used as a measure of a

material's fracture toughness. As in the case of the determination of K_{IC} above, the point of interest is that at which macroscopic crack advance initiates. This analysis differs from the K_{IC} determinations, however, in that plastic behaviour preceding crack initiation is taken into account. According to BS 7448 (1991), the procedure for calculating critical J, (J_C), involves determining the amount of plastic work U_P prior to crack initiation. From a knowledge of this, the 'plastic' component of J can be established. When added to the 'elastic' component, an overall value for J can be computed. The experimental value of J for a bend specimen can be given by (Knott & Withey, 1993, Anderson, 1995):

$$J = \frac{K^2}{E}(1-\nu^2) + \frac{2U_P}{B(W-a)} \tag{3.13}$$

As can be seen, the first term on the right hand side of the expression is equivalent to that for G (Equation 3.9), the elastic energy release rate (the $(1-\nu^2)$ term has been ignored in the calculations for the same reasons as discussed previously). The second term is the plastic component of J. For a linear elastic material this latter term would have a zero value and hence J would be equivaent to G.

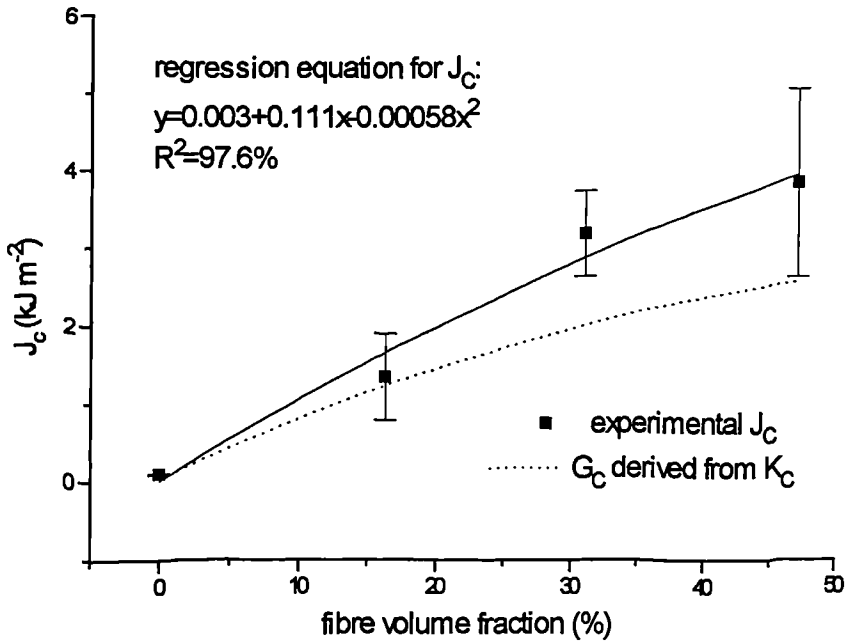

Figure 3.37 Critical J versus V_f for a jute reinforced SEN bend specimen.

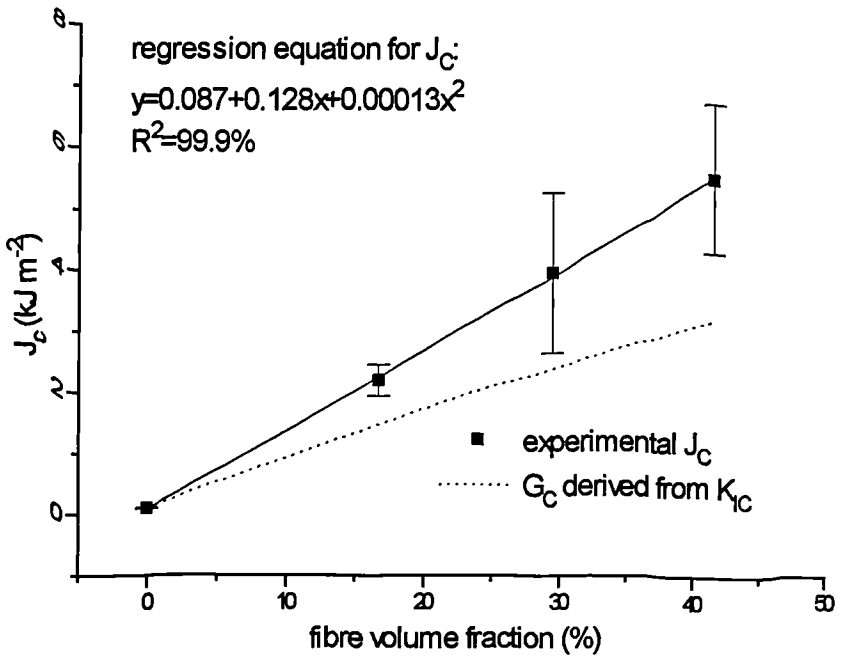

Figure 3.38 Critical J versus V_f for a hemp reinforced SEN bend specimen.

Figures 3.37 and 3.38 show respectively the variation of J_C with V_f for jute and hemp reinforced laminates. It may be observed that with increasing V_f, J_C also increases, in what would appear to be an almost linear fashion. Also shown on these figures is G_C, derived from the values of K_{IC} obtained previously. Effectively, this provides a representation of the relative contributions of the two components of J_C, namely the 'elastic' and 'plastic' parts. What is immediately apparent is that the two curves converge on the unreinforced polymer, which is as expected from the theory. Further, with increasing V_f the two components diverge, such that at higher volume fractions, the contribution from the 'plastic' component becomes significant, further casting doubt upon the validity of LEFM to characterise toughness in fibre reinforced composite materials. The relationship linking K and G is given by Equations 3.8 and 3.9. Analogous relationships between equivalent values for the stress intensity factor, K_J and J are given by (Knott & Withey, 1993):

$$K_J^2 = JE \qquad \text{(in plane stress)} \qquad (3.14)$$

$$K_J^2 = \frac{JE}{(1-\nu^2)} \qquad \text{(in plane strain)} \qquad (3.15)$$

If values for critical K_J (K_{JC}) are calculated utilising Equation 3.14, it is apparent that these will exceed those derived from LEFM, and perhaps provide a more representative assessment of the critical stress intensity factor. Table 3.9. shows a comparison between J, G, K_{IC} and K_{JC} for the three reinforced laminate types along with the un-reinforced polymer.

Table 3.9 Comparison of the fracture toughness of laminates derived by LEFM and EPFM methods.

Laminate type	K_{IC} *(MN m$^{-3/2}$)*	K_{JC} *(MN m$^{-3/2}$)*	*Diff. (%)*	G_C *(kJ m^{-2})*	J_C *(kJ m^{-2})*	*Diff. (%)*
Polymer	0.62	0.62	0.0	0.09	0.10	11.0
CSM	9.01	9.58	6.3	10.35	12.79	23.6
17% hemp	3.08	3.54	16.4	1.53	2.21	44.4
30% hemp	4.47	5.53	23.7	2.47	4.04	63.6
42% hemp	5.73	6.77	18.2	3.37	5.62	66.8
16% jute	2.51	2.76	10.0	1.04	1.35	29.8
31% jute	4.34	4.96	14.3	2.26	3.21	42.0
47% jute	5.21	6.18	18.6	2.56	3.86	50.8

With the unreinforced polymer, it may be observed that the difference between the two toughness characterising parameters is negligible. This would be expected from the theory in that the polymer itself, of all the materials investigated, would be expected to behave most closely to that of an ideally linear-elastic material. With the glass fibre reinforced material the fracture toughness obtained through LEFM and EPFM are similar, whereas at similar V_f (~15-20%) it may be observed that the

difference is somewhat greater in the bast fibre reinforced materials. This would imply that the plant fibre reinforced laminates exhibit greater plastic behaviour than the glass fibre material. This would seem to present an anomaly, in that the 'plastic zone' of the plant fibre reinforced material is smaller than that of the glass fibre material, yet, the former displays greater 'plasticity'. This, however, can be explained by the fact that the yielding takes place at far lower stress levels in the plant fibre reinforced material than it does in the glass fibre reinforced material. The reasons for the early onset of this non-linear behaviour will be explored in the following chapters. A comparison of the two plant fibre reinforced materials reveals that there would appear to be a somewhat greater difference in the toughness, as assessed by the two methods, in the hemp reinforced material than the jute reinforced material.

If the same argument to describe the size of the plastic zone is followed, it would be concluded that the derivation of r_y from K_{IC} rather than K_{JC} and would probably somewhat underestimate its relative size. Results from the K_{IC} and J_C tests appear in Appendix 7.

3.3.7 Fractography

The fracture surfaces of laminates (V_f ~18%) fractured in the Charpy test were examined. At this volume fraction, both the jute and the hemp fibre reinforced materials showed macroscopically brittle failure, with little apparent fibre pull-out. The CSM reinforced laminates rarely failed completely and by comparison, exhibited substantial amounts of shear failure and fibre pull-out.

3.3.7.1 Fracture surfaces

An examination of the fracture surfaces by SEM revealed a number of notable features. Plates 3.3 and 3.4 show typical fractures in jute and hemp reinforced laminates respectively. It is clear that fibre pull-out is limited in both instances, especially when compared with the extensive fibre pull-out exhibited by the CSM glass fibre reinforced laminate shown in Plate 3.5.

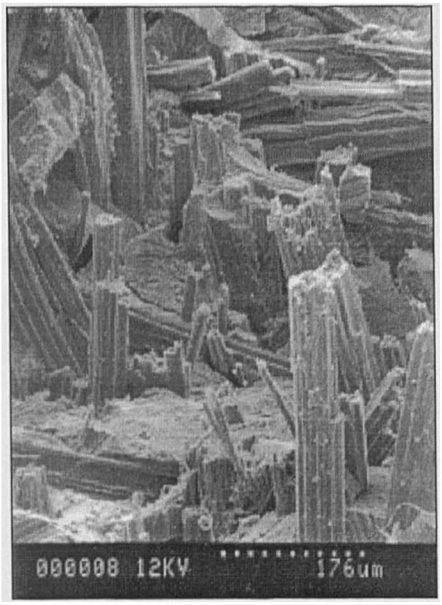

Plate 3.3 Fracture surface of a jute reinforced laminate.

Plate 3.5 Fracture surface of a CSM glass fibre reinforced laminate.

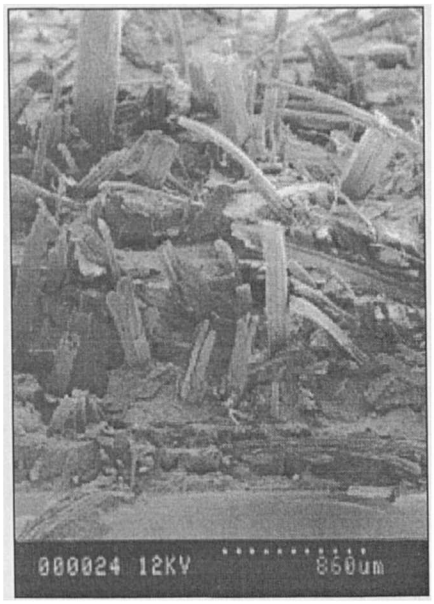

Plate 3.4 Fracture surface of a hemp reinforced laminate.

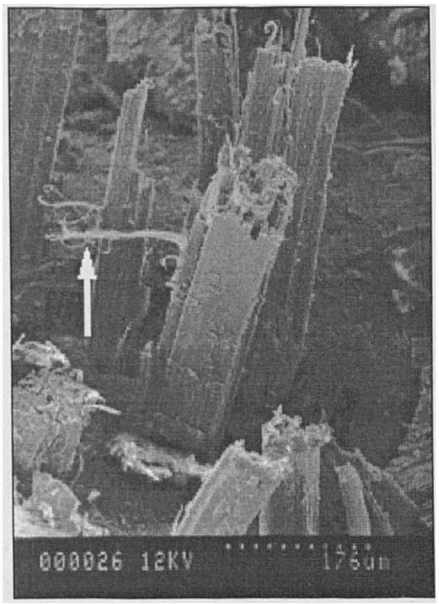

Plate 3.6 Fracture in a hemp laminate, arrow showing fibrillation at the fibre surface.

Although not quantified in any way, in the former, pull-out aspect ratios were perhaps of the order of 10:1, whereas in the latter they were evidently far greater. As mentioned in the previous chapter, fibre pull-out is generally considered to account for a large proportion of the total energy absorbed in fibre composites during fracture (Hull & Clyne, 1996). This supposition would lead to the conclusion that, in the bast

reinforced laminates, significantly less energy is absorbed through frictional sliding than in the glass fibre reinforced matierial. The lack of fibre pull-out may well be a result of the relatively low fibre strength, exacerbated by damage (see Chapter 4) and to good fibre to matrix interaction.

Good mechanical fibre to matrix interaction might be expected considering the rough fibre surface. As may be observed in Plates 3.3 and 3.4, both bast fibre types exhibit quite irregular surface topographies. This, coupled with good wetting, would likely lead to significant mechanical interlocking of the fibre into the matrix and may result in the fibre being too well constrained, having little opportunity to pull-out of the matrix. This may partly explain the low pull-out aspect ratios observed. In addition to this, there may be relatively good adhesion between the phases. As discussed previously, the first requirement for good adhesion, namely intimate contact with the substrate would appear to occur and although this does not necessarily imply good adhesion, there is some evidence to suggest that reasonably good adhesion does take place. Examination of Plate 3.6 reveals fibrillation at the fibre surface, indicating that a portion of the fibre has been torn away from the bulk during fracture. This is likely to have occurred if there had been good adhesion between the two phases.

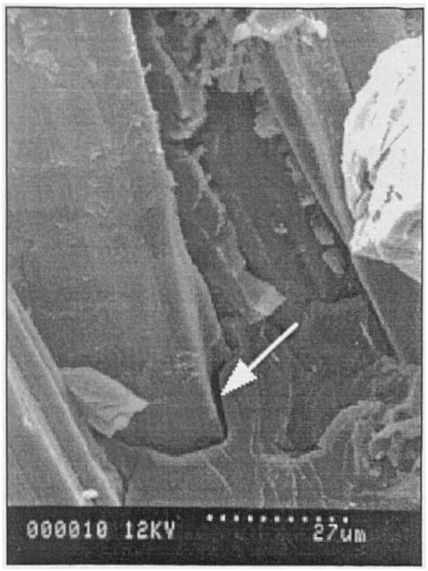

Plate 3.7 Debonding cracks in jute reinforced polyester.

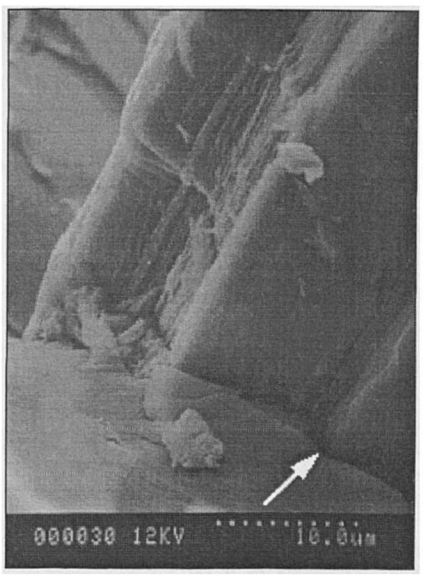

Plate 3.8 Debonding cracks in hemp reinforced polyester.

Nevertheless, it is clear that a degree of fibre-matrix debonding does take place, as evidenced by the cracks seen where the fibres project through the matrix at the fracture surface (Plates 3.7 and 3.8). This, in all probability, allows for a degree of crack-deflection to take place, as well as enabling limited fibre pull-out to occur. It has been clearly demonstrated that the suppression of fibre-matrix debonding in hemp fibre reinforced unsaturated polyester composites, by introducing strong interfacial adhesion, substantially lowers the Charpy impact strength (Sèbe *et al.*, 2000). This is most likely to be due to the suppression of crack blunting and deflection mechanisms.

Plate 3.9 Fracture surface of a hemp fibre bundle.

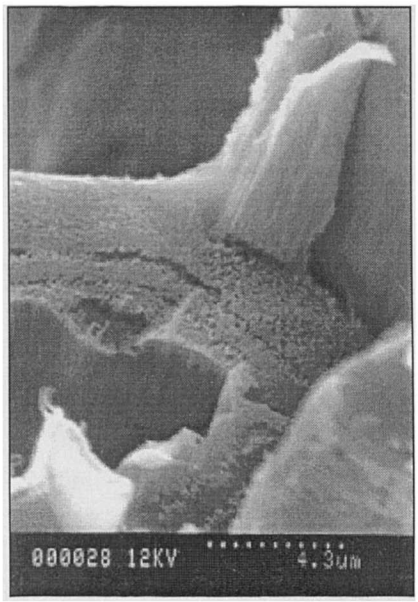

Plate 3.10 Close up of a fractured hemp fibre ultimate showing 'brash' failure of the cell wall.

3.3.7.2 Fibre fracture

Examination of fractured fibres indicates that these fail in a 'brash' manner, evidenced by the 'squared-off' appearance of the fibre ends (Plate 3.9). Closer examination of the fractured fibre bundles revealed that often individual ultimates also failed in a brash or brittle manner (Plate 3.10), with no evidence of the pseudo-plastic tensile buckling mechanism implicated in the high toughness of wood fibres (Gordon & Jeronomidis, 1974). Nevertheless, a certain amount of intra-wall shear failure was observed (Plate 3.11). Interestingly, transverse, intra-wall fibre failure

appeared to take place almost perpendicular to the fibre axis. Longitudinal inter- or intra-cell failure was evident from the 'splintering' of fibre bundles (Plate 3.12).

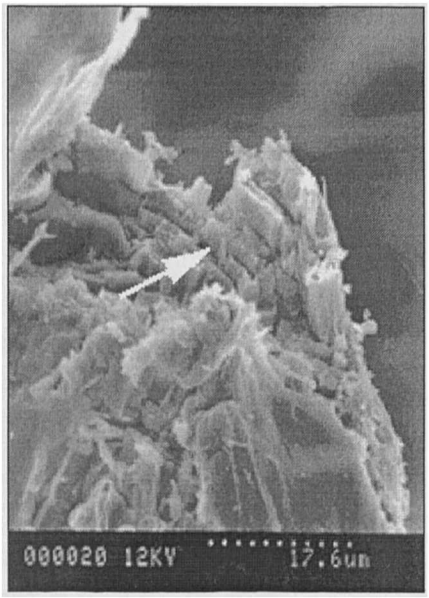

Plate 3.11 Shear failure in the cell all of a hemp fibre ultimate.

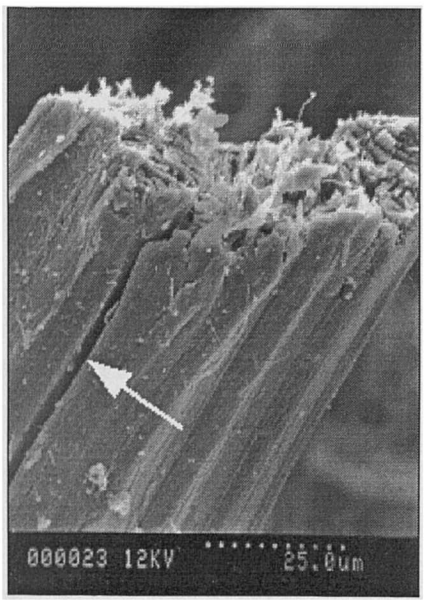

Plate 3.12 Longitudinal splitting in a hemp fibre bundle.

From an examination of the fracture surfaces of the bast fibre reinforced material, it seems likely that fibre pull-out would contribute little to the overall fracture energy of the laminates. Furthermore, the observed fibre fracture indicated that this too was brittle and may be expected to account for little energy absorption. As for the ability of cracks to be repeatedly blunted and deflected at the interface, it is evident that some fibre-matrix debonding does occur during fracture, but to what extent and how this affects the toughness is unknown. However, based upon the observation that improved interfacial adhesion substantially reduces (by more than 50%) the Charpy impact strength of RTM hemp fibre reinforced unsaturated polyester composites (Sèbe, *et al.*, 2000), this is likely to be of some significance.

3.4 Conclusions

Un-saturated polyester laminates reinforced with non-woven, needle punched, jute and hemp fibre felts, exhibited good stiffness, especially on a specific basis, when compared with materials reinforced with equivalent volume fractions of CSM glass fibre. Strength similarly was found to be acceptable. The toughness of the natural fibre reinforced materials were, however, found to be substantially inferior and it is believed that this might be a factor limiting their potential applications.

Analysis of the physical properties and fractography of the plant fibre reinforced material indicated that an intimate bond is formed between the resin and natural fibre (at least up to the volume fractions studied). Adhesion between the two is believed to be intimately linked with mechanical keying rather than true adhesion. Nevertheless, this is an aspect which warrants further investigation.

A potential area of concern from a practical standpoint is the observation that yielding would appear to initiate at low stress levels and although the materials showed substantial plastic deformation prior to fracture, in reality this could be limiting from a design point of view. The initiation of microscopic damage may be the likely cause of this behaviour. This aspect is considered in more detail in Chapter 6.

Work of fracture in three point flexure tests and Charpy impact strength measurements indicated that the toughness of the natural fibre reinforced material was poor, in comparison to their synthetic fibre reinforced counterparts. The use of fracture mechanics to characterise the toughness of these materials has hopefully provided a more quantitative assessment of the relative toughness of the laminates under study. It would appear to have confirmed that initial concerns regarding the toughness of the materials are valid. The applicability of fracture mechanics techniques to characterise toughness in this class of material is perhaps open to some criticism. Nevertheless, it is believed that this approach has provided an insight into the mechanisms involved in the toughness of these materials and highlighted the fact that the microstructure should be investigated more closely. In particular, it is

believed that energy absorbing mechanisms are simply not stimulated to the same extent in the bast fibre reinforced materials as they are in the CSM glass fibre reinforced laminates. These issues are considered in the following two chapters.

4 Fibre Characterisation

4.1 Introduction

4.1.1 Background

In the previous chapter, the mechanical properties and behaviour of unsaturated polyester resin laminates reinforced with either non-woven jute, or non-woven hemp fibre felts, was investigated. The properties of these composites were then compared with those of laminates reinforced with a commercial CSM glass fibre. Broadly speaking, for equivalent fibre loadings (by volume), acceptable values for strength and stiffness were achieved with the bast fibre reinforced materials. However, toughness was substantially inferior to that of the glass fibre reinforced equivalent. The fracture behaviour and low toughness exhibited by the plant fibre reinforced composites were considered to be of particular concern; it is believed that these properties would severely restrict the potential applications for the materials. A fuller understanding of the micro-mechanics of deformation and fracture could, however, highlight ways in which material performance might be improved. The behaviour of the fibres themselves and the micromechanics of the fibre-matrix interface are considered in this and the following chapter.

In this chapter, the mechanical properties of bast fibres are considered. This includes, by way of a literature survey, a discussion of the mechanical properties of fibres in relation to their ultastructure, as well as presenting the results of a study on fibre damage. The latter includes a discussion of the mechanisms, origins and implications of such damage upon fibre properties. The study of fibre damage consisted of a microscopic examination of hemp and jute technical fibres and ultimates. Although not utilised as a reinforcing fibre in this work, flax was included in the study due to its similarity to hemp and potential as a reinforcing fibre.

4.1.2 The influence of fibre ultrastructure on mechanical properties

The structure of flax and other bast fibres is, in general terms, similar to that of other plant fibres in as much as the cell wall follows the same overall ultrastructural organisation of lignocellulosic fibres, outlined in Chapter 2 (Roland *et al.*, 1995). Whilst much work has been undertaken with a view to gaining a fundamental understanding of the mechanics of individual wood fibres in relation to their structure and chemical composition, comparatively little is to be found in the literature on similar studies conducted on bast fibres. This is presumably due to the fact that the latter have, in recent times at least, been used almost exclusively in textile applications and that, compared with other natural fibres (such as cotton and wool), only to a relatively limited extent. On the other hand an understanding of the mechanics of individual wood fibres is extremely important because of the influence of the mechanical properties on not only wood, but also paper and wood-based panel products. Doubtless, however, if bast fibres are to be used as reinforcement in "high performance" PMCs, with structural end uses in mind, a much fuller understanding of the structure-property relationships will be required.

4.1.2.1 Axial tensile properties

A significant volume of experimental work has been published over the years relating to the determination of the Young's modulus and the tensile strength of individual wood pulp fibres (e.g. Jayne, 1960; Dinwoodie, 1965; Page *et al.*, 1971). It has been clearly demonstrated that these properties are controlled by the ultrastructural organisation of the fibre, in particular the winding angle of microfibrils in the dominant S_2 layer. It has been shown, for example, that both tensile strength and stiffness, as well as the mode of deformation and fracture of the fibres, are dependent upon the microfibril angle of the S_2 layer (Mark, 1967; Page *et al.*, 1971; Page *et al.*, 1972). Whereas, the S_2 layer dominates the properties of the fibre in tension, the S_1 layer is thought to be important in controlling fibre stability in compression, by limiting excessive lateral cell expansion (Booker & Sell, 1998). The S_3 layer, on the other hand, is believed to resist hydrostatic pressure within the cell lumen (Booker & Sell, 1998) whilst the combined laminate structure is considered to be of importance in controlling trans- and intra-wall crack propagation (Booker, 1995).

Over the years, many models have been proposed to predict the elastic behaviour of the lignocellulosic fibre cell wall (e.g. Mark, 1967, Cave, 1968, 1969; Tang & Hsu, 1973; Page *et al.*, 1977; Salmén & de Ruvo, 1985; Harrington *et al.*, 1998; Astley, *et al.*, 1998). These models are based on orthotropic elasticity theory, in which the cell wall was considered to be a composite laminate structure composed of balanced plies (Page *et al.*, 1977; Salmén & de Ruvo, 1985). The models have been used to predict the Young's modulus and tensile strength of fibres as a function of the microfibril angle of the S_2 layer (Page *et al.*, 1971; Page *et al.*, 1977). Good agreement between theoretical and experimental values for stiffness and strength have been obtained, discrepancies being attributed to defects and inhomogeneities within the fibre (Page *et al.*, 1971; Kim *et al.*, 1975; Page & El Hosseiny, 1976). Whilst most models have been constructed to predict the behaviour of wood fibres, some work has recently been undertaken with a view to modelling the behaviour of flax and other plant fibres (Davies & Bruce, 1997).

A simple model to predict the tensile modulus of an idealised bast fibre is presented in Section 4.4 and is compared with literature values for the moduli of flax and hemp.

4.1.2.2 The toughness of plant fibres

One of the great attractions of wood as a structural material is its excellent work of fracture, which, on a specific basis is on a par with that of mild steel and higher than that of synthetic PMCs (Jeronomidis, 1980). This too has, in part at least, been attributed to the fibre ultrastructural organisation. As stated by Lucas *et al.* (1997), the overall work of fracture of plant fibre material can be attributed to:

- fracture of the cell wall material itself
- plastic buckling of the cell wall into the lumen as a result of shear stresses
- pull-out of intact cells.

Fracture toughness (K_{IC}) measurements conducted by Lucas *et al.* (1995, 1997) on a range of plant fibre material and wood species, using a method which involved driving a crack through the material using scissors, indicated a figure which was identified as the work of fracture of the cell wall material itself. This figure, which they referred to as the 'intrinsic toughness' of the cell wall (independent of contributions from either

plastic work or cell pull-out) was for a crack traversing a fibre perpendicular to its axis, in other words, 'across the grain'. The results of these investigations pointed to a figure of around 3.45 kJ m^{-2} for the intrinsic toughness of the cell wall. This value is in broad agreement with a figure of 1.65 kJ m^{-2} for the intrinsic toughness of cell wall material reported by Ashby *et al.* (1985), obtained by a different method.

If the cell wall is considered to be an heterogeneous orthotropic material itself, then a certain degree of variation in the intrinsic toughness, or cell wall work of fracture, would be expected. This would depend upon the path followed by a crack propagating through the cell wall. This is supported by the fact that Gibson and Ashby (1988) report a figure for the intrinsic toughness of <0.35 kJ m^{-2} 'along the grain', whilst measurement of the fracture energy of solid wood conducted 'with the grain' indicates values of between 0.2 to 0.3 kJ m^{-2} (Stanzl-Tschegg, 1995). In these tests it might be supposed that crack propagation would be either intra-wall i.e. along the middle lamella or inter-wall, through the cell wall material, along the direction of the microfibrils in the S_2 layer.

Notwithstanding the above, the intrinsic toughness of the cell wall is substantially lower than the measured works of fracture of wood across the grain which fall in the region of 10-30 kJ m^{-2} (Jeronomidis, 1980). The work of fracture attributed to the pull-out of individual cells is, however, believed to contribute little to the overall work of fracture ($\approx$1.6 kJ m^{-2}) of the material (Jeronomidis, 1980). The major contribution is thought to be due to a pseudo-plastic tensile buckling mechanism first proposed by Gordon and Jeronomidis (Gordon & Jeronomidis, 1974; Jeronomidis, 1976). This was based on observations made by Page *et al.* (1971) that some individual wood pulp fibres undergo unstable buckling when loaded in axial tension. Lucas *et al.* (1997) were also able to estimate the amount of 'plastic work' occurring during fracture. They estimated that approximately 90% of the overall work of fracture could be attributed to plastic deformation, the balance being due to the intrinsic toughness of the cell wall. This pseudo-plastic mechanism of energy absorption is due to shear failure occurring within the S_2 layer as the fibre buckles. In the process, considerable amounts of energy are absorbed irreversibly (Jeronomidis, 1980). The

effectiveness of this mechanism in enhancing energy absorption has been subsequently confirmed using synthetic analogues of the wood cell (Gordon & Jeronomidis, 1980).

The above, outlines some of the factors influencing the tensile mechanical properties of plant fibres and plant fibre material. Nevertheless, whilst these properties are of great importance, there is reason to suspect that the properties of plant fibres in compression, particularly the mode of failure in compression, are of particular relevance to plant fibre reinforced composites. As will be discussed in Section 4.4, compression failure in bast fibres is often reminiscent of the failure seen in many unidirectional composites and to that observed in a number of highly oriented synthetic polymeric fibres. This has ramifications for interface behaviour and is discussed more fully in Chapter 5.

4.1.3 Fibre micro-compressive damage

4.1.3.1 Origin of micro-compressive damage in wood and wood fibres

In solid wood, microscopic damage to individual cells caused by mechanical overloading in compression can dramatically affect its mechanical properties (Dinwoodie, 1978). This damage takes the form of small creases in the cell wall known variously as slip planes, kink bands or micro-compressions. These features can be observed by polarised light microscopy and appear in the form of a bright 'X' traversing the double cell wall as shown in Figure 4.1. The appearance of these features under polarised light is due to misalignment of the microfibrils in the cell wall (Dinwoodie, 1968). Frequently, a line of micro-compressions form, due to co-operative micro-buckling of cell walls forming a crease in the structure of wood. Under certain circumstances these creases are visible to the naked eye and are readily observable under a microscope using low angle incident light (Desch & Dinwoodie, 1996). In wood, these micro-compressive defects can arise as a result of growth or mechanical stresses within the tree (Dinwoodie, 1976). Micro-compressions may also result from compressive stresses in the wood induced during harvesting, conversion or whilst in service (Dinwoodie, 1976).

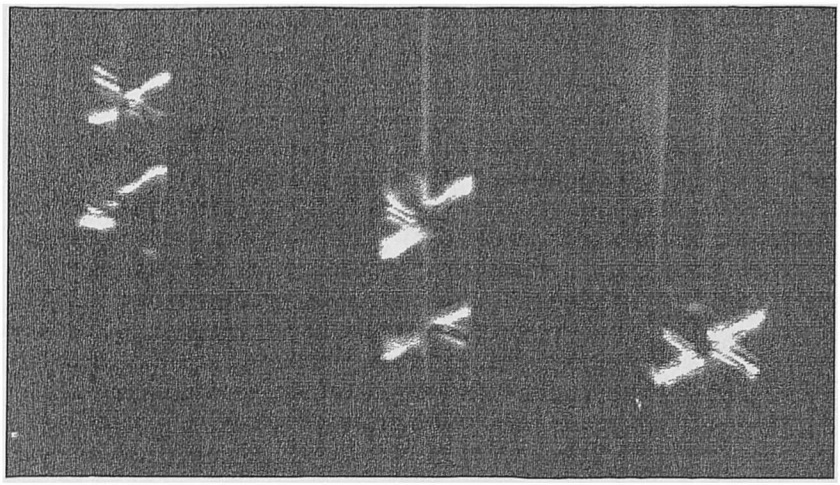

Figure 4.1 Micro-compressive damage in the cell wall of wood (*Source:* Dinwoodie, 1968).

4.1.3.2 Effect of micro-compressions on the mechanical properties of wood and wood fibres

Slightly lower tensile strengths and moduli have been noted in pre-compressed wood. However, the most significant effect observed in pre-compressed wood is the reduction in impact properties (Dinwoodie, 1978). Failure is invariably noted to follow the line of the compression crease (Dinwoodie, 1978). Micro-compressions formed during cyclic loading have been shown to propagate a line of compression creases in wood which can subsequently lead to crack formation and ultimately to failure (Imayama, 1994).

Individual wood fibres carefully isolated from a block of pre-compressed wood, containing micro-compressive defects, have shown failure loads which are reduced by around 46%, as well as decreased stiffness (Dinwoodie, 1978). Micro-compressions in wood pulp fibres, most likely caused by isolation and handling, have been shown to result in lowered fibre tensile strengths and moduli (Page *et al.*, 1971; Page & Seth, 1980). It has also been shown that the elastic modulus of paper is reduced by the presence of fibre micro-compressive defects, crimps and curls (Page *et al.*, 1979; Page & Seth, 1980). By drying fibres under tension, these kinks and micro-compressions may sometimes be straightened out, resulting in improved tensile properties (Kim, *et al.*, 1975).

In addition to reduced tensile strength and stiffness, micro-compressions have been noted to act a critical defects in the fibre structure (Page *et al.*, 1971; Page & Seth, 1980) and fibre fracture has been successfully explained in a probabilistic manner (Page & El-Hosseiny 1976).

Further, it has been shown that micro-compressions (as well as other features such as pit apertures, creases etc.) can affect the surface strain distribution in single wood pulp fibres (Mott *et al.*, 1996).

4.1.3.3 Micro-compressions in bast fibres

A number of features, similar to those seen in wood, have been noted in flax, hemp and jute fibres, and are referred to as nodes or dislocation marks (Catling & Grayson, 1982; Rahman, 1979). These features too can be observed, using a polarising microscope, as bright bands traversing the fibre in the same way as in individual micro-compressed wood fibres (Davies & Bruce, 1998). Such features have been shown to reduce both the tensile strength and modulus of flax and nettle fibre ultimates (Davies & Bruce, 1998).

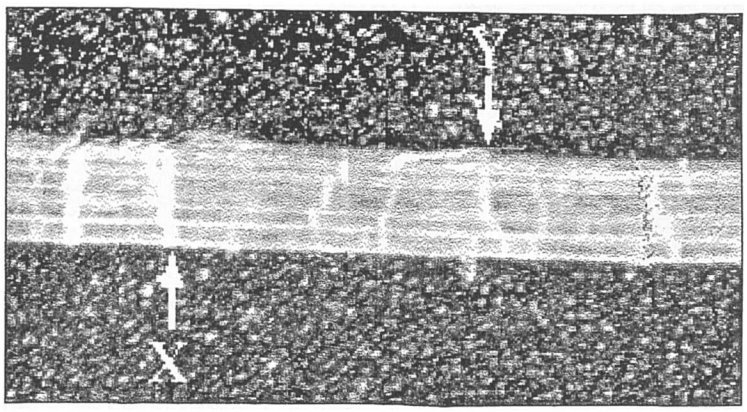

Plate 4.1 Water retted and scutched flax fibre bundle showing compression creases (X & Y) running across the fibre (low angle incident light microscopy - x12 magnification.).

A preliminary examination of bast fibres using low angle incident light microscopy at low magnification (Plate 4.1) revealed what appeared to be creases (X and Y), similar to those observed in compression damaged wood. It was believed that such gross

damage might well influence the properties, not only of the fibres themselves, but also those of the PMCs reinforced with such material. It was considered that this warranted a detailed microscopic study of the structure and morphology of this fibre damage. The study was undertaken with a view to elucidating how the damage was induced and how it might affect the performance of composites reinforced with such a material.

4.2 Materials and method

4.2.1 Introduction

The fibre bundles and fibre ultimates of flax, hemp and jute were examined by optical microscopy, using both polarised and ordinary light. Flax and jute were examined 'as received' i.e. after retting and decortication, but without further processing. Hemp fibre was examined after having undergone differing degrees of mechanical processing.

4.2.2 Sample preparation

Water retted and decorticated flax was supplied by McConvilles Flax Mills of Northern Ireland. Jute fibre (grown in Bangladesh), water retted, decorticated and chopped into approximately 50 mm lengths, was supplied by Sidlaws of Dundee. For examination of the fibre bundles, short lengths of fibre (approximately 10 mm long) were chopped from the long strands with a fresh razor blade. These were then placed in a small (25 ml) beaker containing de-ionised water and allowed to soak for approximately 30 minutes in order to 'wet-up'. Individual fibre bundles were then transferred to a microscope slide, holding the fibres carefully with tweezers at one end only. Temporary slides were prepared by mounting the fibres in de-ionised water only. Semi-permanent slides were prepared by mounting the fibre bundles in glycerol. For studies conducted at high magnification (x100 objective lens), individual ultimates were mounted temporarily in benzyl benzoate because of its higher refractive index,

which provided improved definition when used in conjunction with an oil immersed objective lens.

The preparation of fibre ultimates involved macerating short lengths (~20 mm) of the fibre bundles, in a 1:1 (by volume) mixture of hydrogen peroxide and acetic acid (Catling & Grayson, 1982) for approximately 1 hour. Mechanical agitation was kept to an absolute minimum so as to reduce, if not totally eliminate, further damage to the fibres (Dinwoodie, 1974). After maceration, the fibres were washed thoroughly with de-ionised water and stored in small phials containing the same. When required, a small quantity of the macerated fibres were decanted into a Petri dish containing de-ionised water. This resulted in them being thoroughly dispersed without the need for excessive agitation. Individual cells were carefully retrieved from the dish with tweezers, taking care to hold the fibres at their ends so as to minimise damage, and thence transferred to glass microscope slides. The fibre ultimates were subsequently mounted temporarily or semi-permanently as described above.

Hemp fibres were obtained from several sources:

- From freshly pulled 'green' hemp stem grown at Henfaes farm, University of Wales, Bangor Gwynedd.
- From dew retted (but not decorticated straw), supplied by Hemcore Ltd.
- Fibres extricated from felted mats. These had been manufactured from UK - grown hemp, dew retted and mechanically decorticated (from Hemcore Ltd) and felted by the process described in Chapter 2 (J.B. Plant Fibres Ltd.).

From the 'green' hemp stem, only ultimates were isolated. One stem (selected at random) was cut into short lengths. Each section was labelled so that the position in the plant could be identified (i.e. top or bottom of the stem) and immediately immersed in water to prevent drying. Small rings of stem (approximately 20 mm in length in the longitudinal direction) were cut from each section with a razor blade and slivers of bark carefully removed from the rings, again using a razor blade. The slivers of bark were subsequently macerated in the manner described above. The tissue thus treated, contained not only fibre ultimates but also other, non-structural

elements surrounding the fibres, some of which could still be clearly seen adhering to the ultimates when examined by microscope.

Dew retted but undecorticated hemp straw was soaked in cold tap water for approximately 24 hours. After this period, strips of bark were readily separated from the woody core material. Short sections of bark (~20 mm) containing loosely bound fibre bundles were then transferred to a Petri dish containing deionised water and by gentle manipulation, released from the surrounding tissue. Some of the fibre bundles were mounted as described above, or else macerated and then mounted.

Short lengths of fibre (~20 mm) removed from felted mats were soaked in deionised water contained in a Petri dish. Wetted fibre bundles were mounted, as described, on microscope slides. A quantity of fibre bundles were subsequently macerated in the manner described and thereafter mounted as either permanent, or temporary slides.

4.2.3 Optical microscopy

The slide specimens prepared above were examined using a Leitz Weltzlar microscope, under both polarised and ordinary light. The microscope was equipped with x2.5, x4, x10, x40 and x100 objective lenses. Images could be viewed either directly using a binocular eyepiece (x10 magnification) or indirectly, as a real-time digital image displayed on a PC monitor. To facilitate this, the microscope was equipped with a digital camera ('Pixera Visual Communication System'), with a maximum resolution of 1260 x 960 picture elements ('pixels'). A proprietary software programme ('Pixera studio', 'Pixera album') facilitated image capture, enhancement and storage.

4.3 Results

4.3.1 Occurrence of damage

4.3.1.1 Fibres in 'as received' condition

Plates 4.2-4.4 show respectively flax, hemp and jute fibre ultimates, viewed under polarised light at low (x100) overall magnification. All fibres were in the 'as received' condition, in other words having been retted and decorticated (save the hemp which had not been decorticated) but having undergone no further processing. Micro-compressions were clearly visible as bright bands stretching across the fibres. Although no attempt was made to quantify the frequency of these defects, it appeared that in flax they occurred at less frequent intervals along the fibre than in either hemp or jute. In the latter, defects were often observed at intervals of between only one or two fibre diameters along the length of the fibre. The damage observed in jute did, however, appear to be decidedly less severe than in either of the other two bast fibres (ses Section 4.4.2.2). Micro-compressive damage was not only confined to the fibre ultimates, but was also clearly seen in the intact fibre bundles (Plates 4.5 - 4.7). The severity of the damage appeared to vary, ranging from areas which seemed to affect only individual cells, to complete creases running across the fibre bundle.

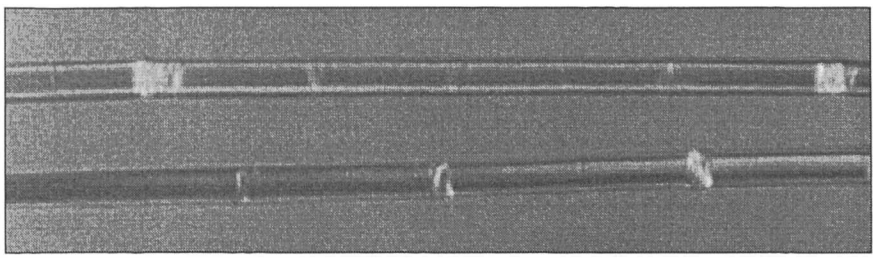

Plate 4.2 Flax ultimate (polarised light x100 magnification).

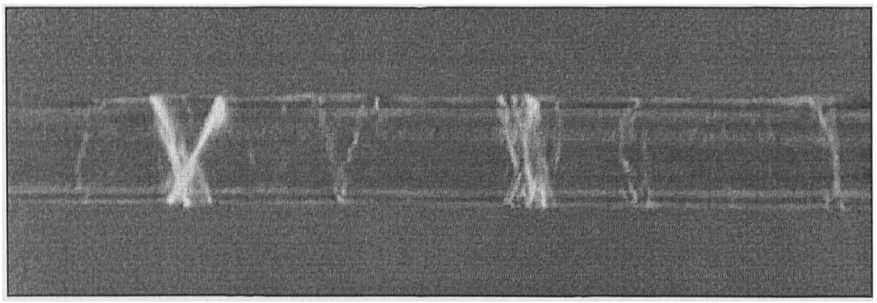

Plate 4.3 Hemp ultimate (polarised light x100 magnification).

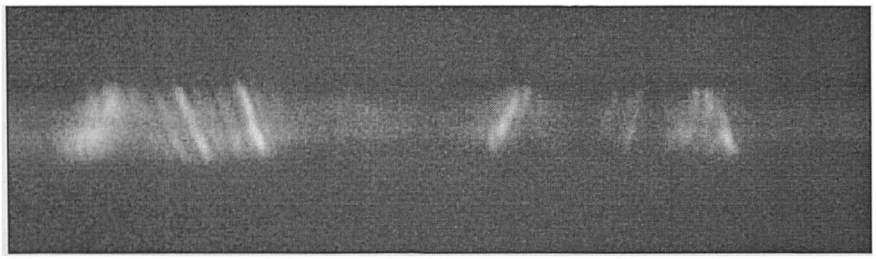

Plate 4.4 Jute ultimate (polarised light x100 magnification).

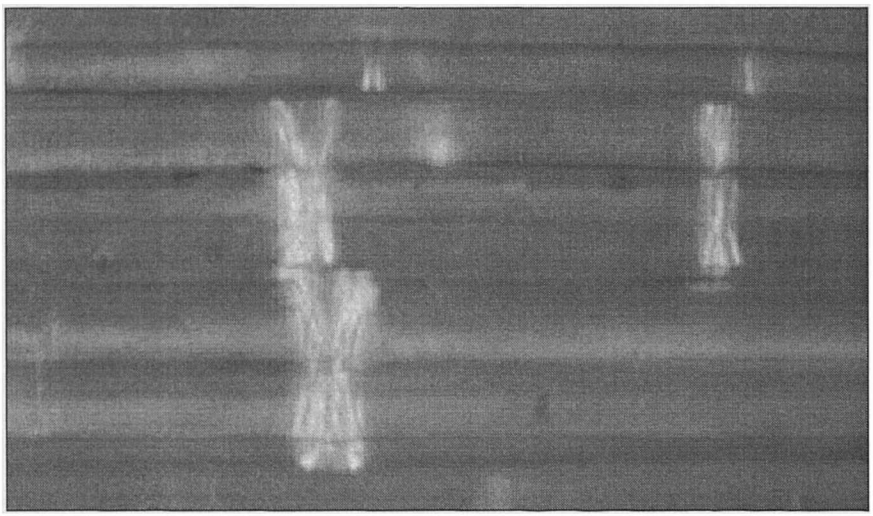

Plate 4.5 Flax fibre bundle (polarised light x100 magnification).

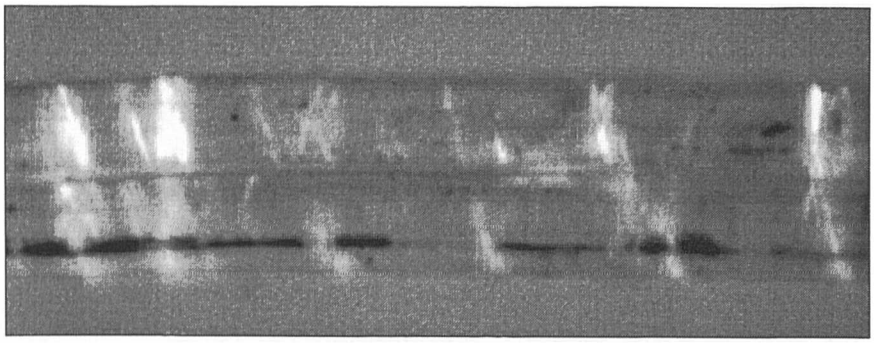

Plate 4.6 Hemp fibre bundle (polarised light x100 magnification).

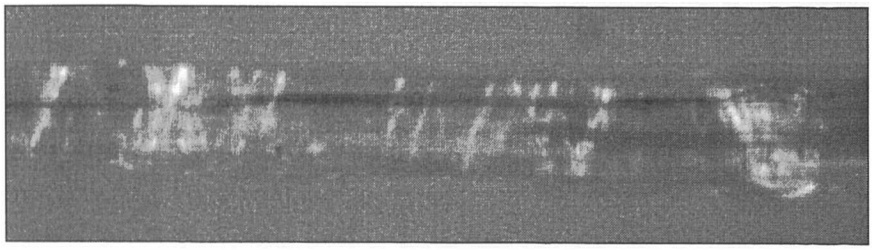

Plate 4.7 Jute fibre bundle (polarised light x100 magnification).

4.3.1.2 Fibre from 'green' hemp stem

Plate 4.8, shows micro-compressive damage in fibres taken from the lower stem of 'green' hemp straw. The damage here again appeared to be extensive, occurring at frequent intervals along the length of the fibre. Whilst it is impossible to be certain that no damage was induced during the isolation process, great care was taken to avoid this. Much of the damage appeared as thin bright lines extending across the cell wall. Interestingly, as can be seen from Plate 4.9, there appeared to be a significant amount of damage in fibre taken from the upper part of the stem also, although this seemed to be far less severe. As will be discussed in the following section, this may give some insight into the cause of the damage.

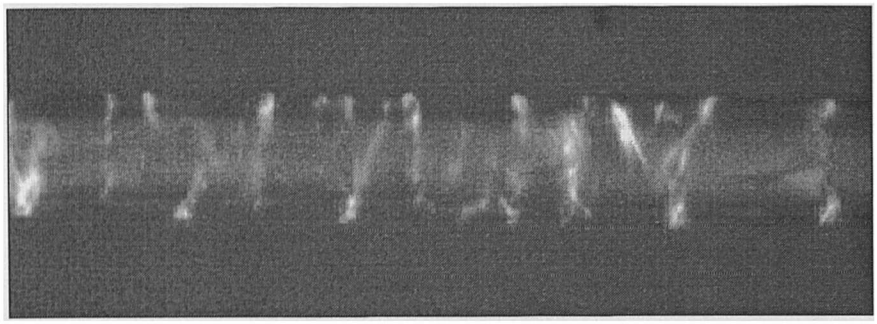

Plate 4.8 Fibre ultimate from the lower stem of 'green' hemp straw (polarised light x100 magnification).

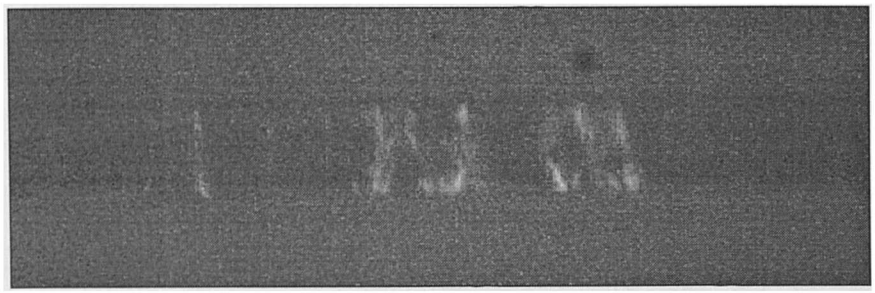

Plate 4.9 Fibre ultimate from the upper stem of 'green' hemp straw (polarised light x100 magnification).

4.3.1.3 Processed hemp fibre

Processed hemp (Plate 4.10) fibre appeared to be significantly more damaged than the 'as received' variety. This is hardly surprising, given the intensive mechanical action to which the fibres are subjected during the felting process. In the fibre shown in Plate 4.11, distinct 'kinks' (A and B) can be observed in its structure.

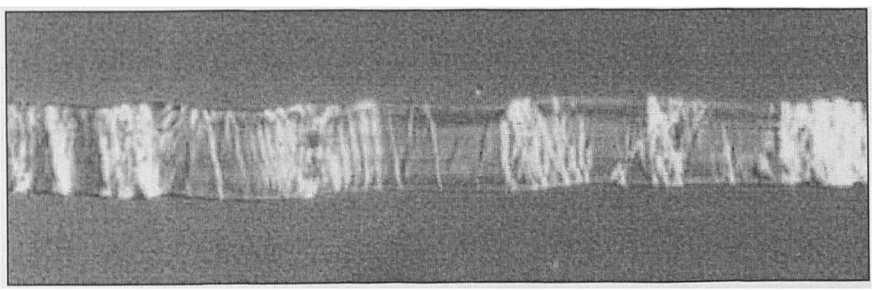

Plate 4.10 Fibre ultimate - processed hemp (polarised light x100 magnification).

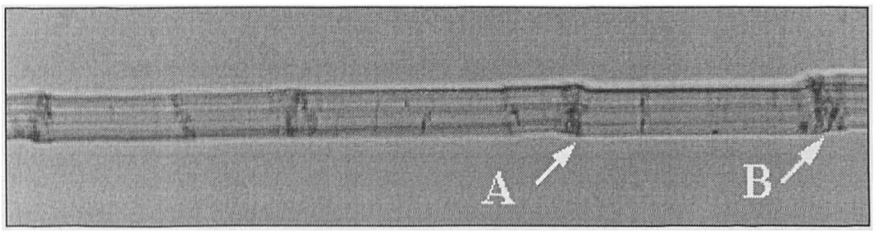

Plate 4.11 Fibre ultimate - processed hemp showing 'kinks' (A & B) in the fibre structure (un-polarised light x100 magnification).

4.3.2 Morphology of micro-compressions

At low magnification (x100) under polarised light, it was difficult to see clearly the morphology of the micro-compressive damage (Plates 4.2-4.4). What did seem to be evident, however, was that the severity or degree of damage varied quite considerably, from almost imperceptible, fine cracks traversing the fibre to gross deformations of the cell wall structure. As shown in Plate 4.12, fine fissure-like features could be observed traversing the cell wall. In some instances, minute disruptions to the fibre wall appeared to be present (Plate 4.13).

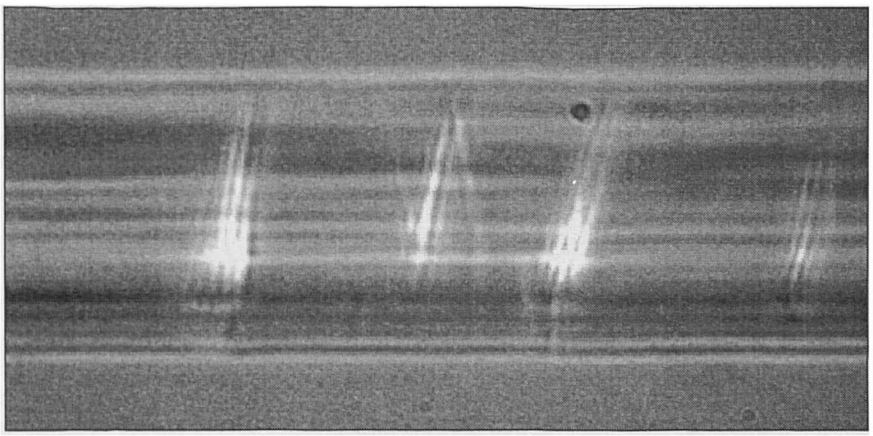

Plate 4.12 Fine, 'fissure-like' defects in hemp fibre ultimate (polarised light x400 magnification).

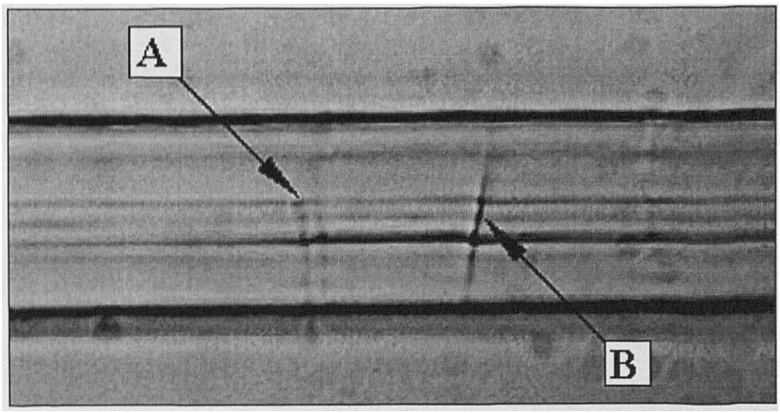

Plate 4.13 Microscopic kinking in an (unprocessed) hemp ultimate showing minute 'fissure-like' compression failures at (A) and (B) (ordinary light x100 magnification).

At high magnification, (ordinary light), two distinct types of gross failure geometry become clearly distinguishable. Plate 4.14 is a photomicrograph (digitally enhanced to highlight the morphology of the damage) of a compression failure in hemp fibre. Two major shear planes can be readily discerned, running across the entire width of the fibre ultimate and converging near the lower fibre surface. The angle made between the longitudinal axis of the fibre and the shear planes is approximately 60^{O}-70^{O}. There appeared to be a distinct lateral displacement of the cell wall microfibrillar structure in the region of the damage. In addition, a number of minor creases were evident in the vicinity of the deformation. As can be seen in Plate 4.15, disruptions to the cell wall were evident, which take the form of a distinct kink (Plate 4.16). What was apparent was that some of these defects were barely perceptible, either under polarised or ordinary light. The morphology of this damage was similar to the compression failure seen in solid wood (Desch & Dinwoodie, 1996). In Plates 4.17 and 4.18 only single shear planes are observable (although in the former, there is some evidence of a second) with the structure of the cell wall being laterally displaced. The angle made between the shear plane and the axis of the fibre was approximately 60^{O}. Although not quantified, the transition between the undisrupted microfibrillar structure and the microfibrils in the kink zone appeared to be very sharp.

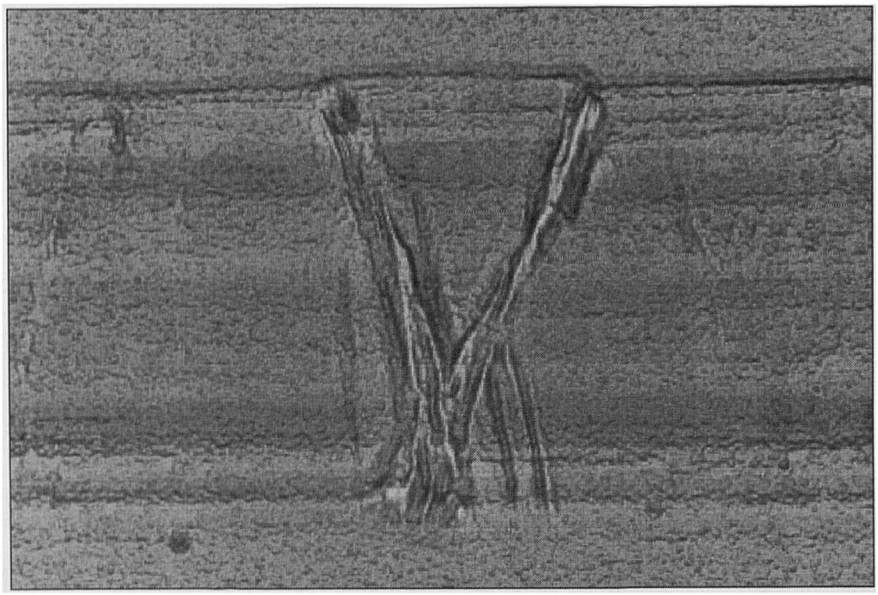

Plate 4.14 Detail of the morphology of microcompressive failure in an unprocessed hemp fibre ultimate showing typical 'minute compression failure' (ordinary light x1000 magnification).

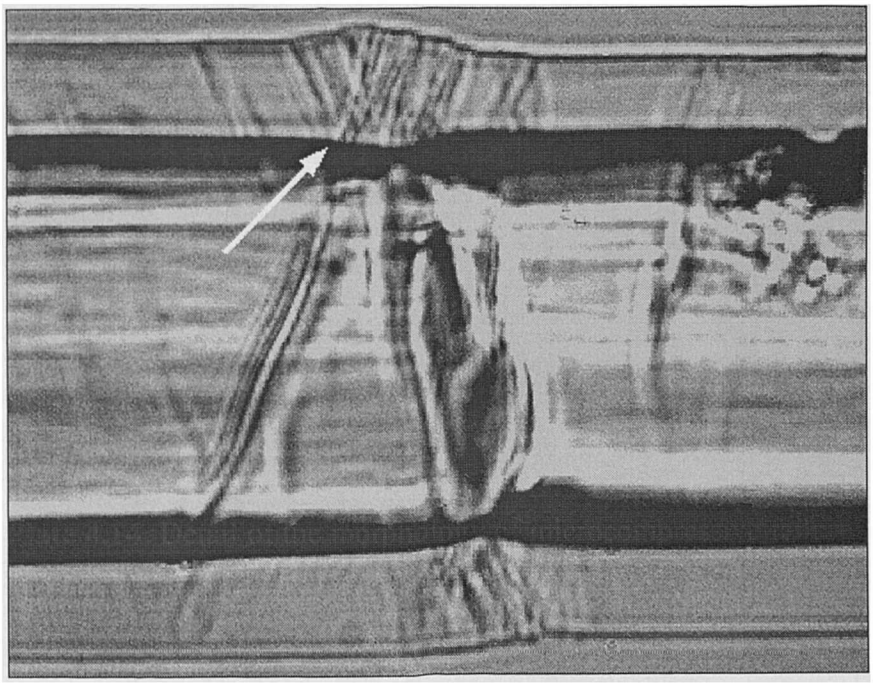

Plate 4.15 Disruptions in the cell wall of an unprocessed hemp ultimate. The gross failure mode of the fibre is also visible (ordinary light x1000 magnification).

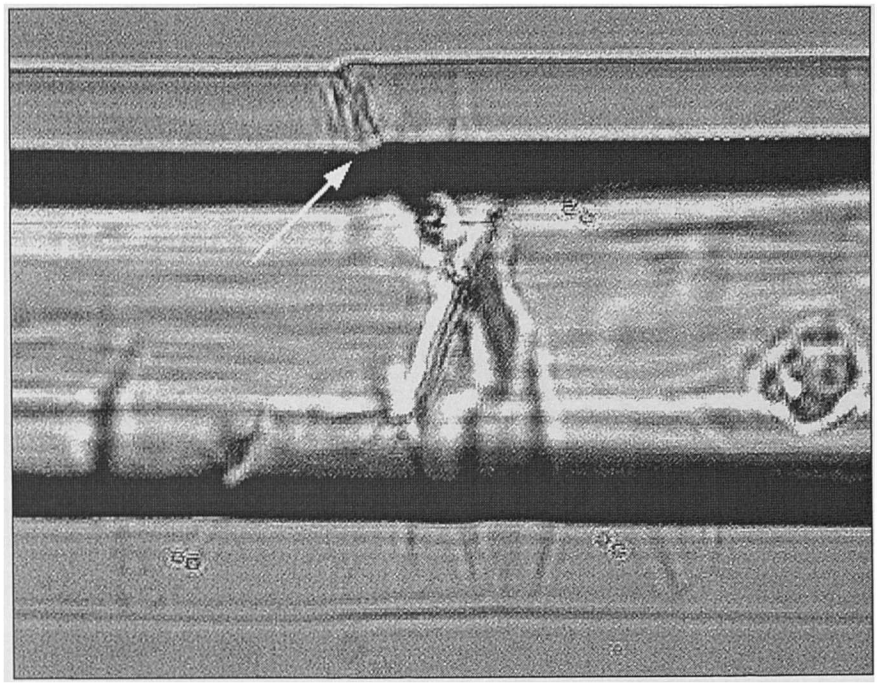

Plate 4.16 Kink observed in the cell wall of a hemp ultimate (ordinary light x1000 magnification).

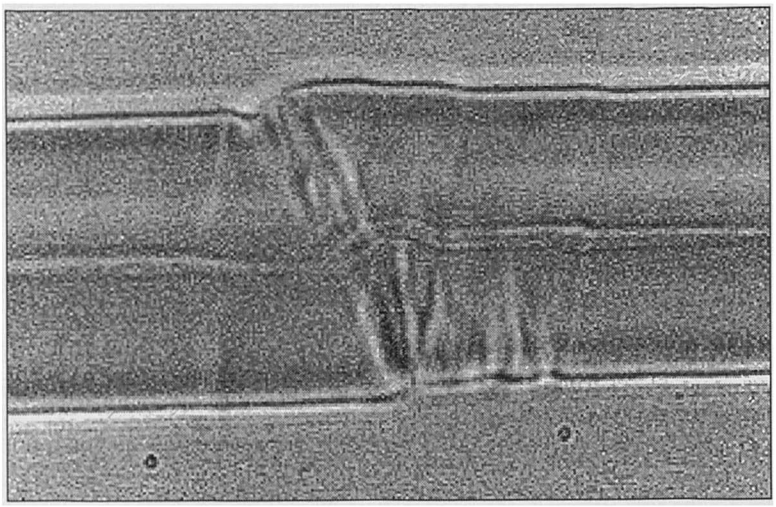

Plate 4.17 Detail of the morphology of micro-compressive failure in a flax fibre ultimate showing typical 'kink band' (ordinary light x1000 magnification).

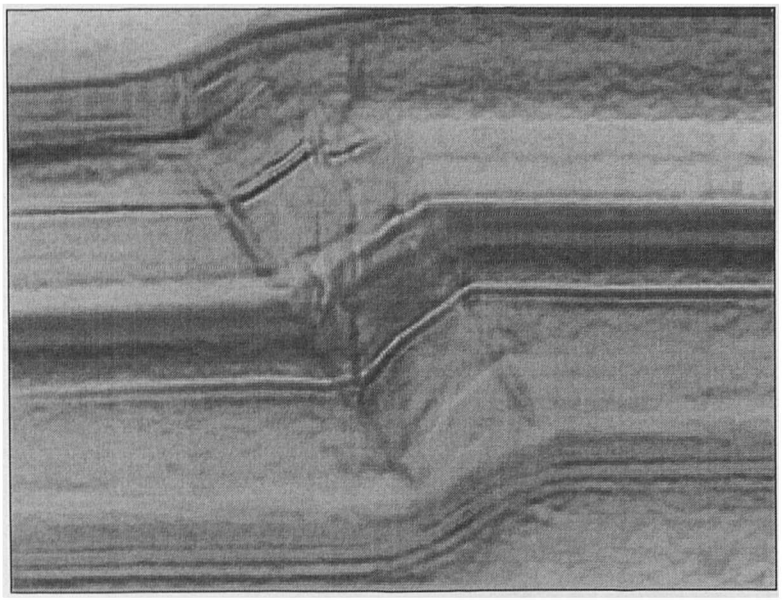

Plate 4.18 Fine detail of a 'kink band' in a flax fibre ultimate (ordinary light x1000 magnification).

Wardop and Dadswell (1947), described two basic types of cell wall deformation, firstly 'slip planes', corresponding to what are now more commonly referred to as 'kink bands' and secondly 'minute compression failures'. The former can be regarded as a wrinkle in the cell wall, with the angle between the plane of the kink and the fibre axis lying somewhere between 50^{O} and 70^{O} (Dinwoodie, 1974). The latter are effectively two kinks oriented at opposing angles, with an included angle of around 40^{O}. Figure 4.2 shows diagrammatically, both kink band and minute compression failure. Both these failure types were observed in the fibres examined in this study. It should, however, be noted that although there is a similarity in the morphology of these deformations, a distinction should be made regarding the location of the damage.

As may be noted from Figure 4.1, in wood, kinks are formed in the double cell wall of adjacent cells (i.e. the combined cell wall of two adjacent fibres with the middle lamella sandwiched in between). In a number of the fibres studied in this work, particularly those with very thick cell walls and practically no lumen, shear failure was observed to traverse the whole cell, as if individual cells were acting as a solid mass with kinking or minute compression failures traversing the whole cell, rather than the than the double cell wall as in the case of solid wood. Figure 4.3 shows schematically the morphology of the compression failures observed in this study.

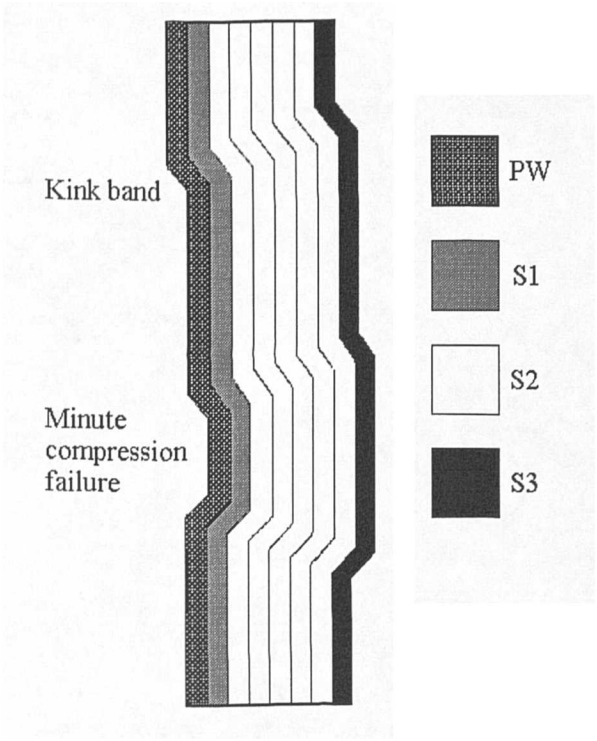

Figure 4.2 Types of cell wall micro-compressive failure in wood fibres.

Key: PW – primary wall; S1, S2 and S3 are respectively the inner, middle and outer layers of the secondary cell wall (*Adapted from:* Wardop & Dadswell, 1947).

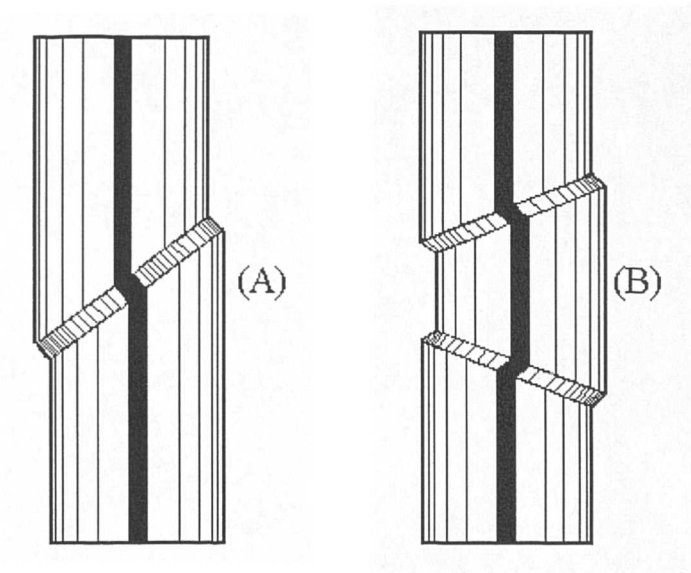

Figure 4.3 Schematic representation of the morphology of micro-compressive failures observed in bast fibres. *a)* 'Kink band' and *b)* 'minute compression failure'.

4.4 Discussion

4.4.1 The structure of bast fibres

In general terms, the ultrastructural organisation of bast fibres is, as discussed in Section 4.1.2, similar to that of wood. Nevertheless, in detail there are a number of significant differences. A summary of the chemical composition of flax, hemp and jute was presented in Table 2.2. Clearly, the cellulose content is significantly higher and its crystallinity greater than in wood, whilst the percentage of other cell wall polysaccharides (hemicelluloses and pectins) and lignin is much lower. Using an analogy with fibre reinforced composites, there is a significantly greater proportion of reinforcement in bast fibres than in wood. This is particularly so in hemp and flax. In addition, in many bast fibres, the microfibrils of the S_2 layer are aligned almost parallel with the axis of the fibre. In hemp, for instance the measured mean microfibril angle is 2.3^{O} (Preston, 1974). The microfibril angle of jute is, however, somewhat higher at around 8^{O} (Preston, 1974). Furthermore, the S_2 layer comprises by far the greatest proportion of the cell wall, accounting for up to 90% of the total bulk (Booker & Sell, 1998).

In Section 4.1.2, it was noted that many models have been constructed to predict the elastic properties of the wood cell wall. It is proposed here, in view of the foregoing, that a simplified model of the cell wall of hemp and flax may be utilised, to give an estimate of the order of magnitude of the tensile modulus of an ideal bast fibre. In this model, the fibre is considered as a unidirectional long fibre composite in which the small microfibrillar angle observed in real fibres is ignored, as too is the contribution made to axial tensile stiffness by the S_1 and S_3 layers. This model is more applicable to flax and hemp, in which the microfibril angle of the S_2 layer is almost parallel with the axis of the fibre, than jute in which the microfibril angle is somewhat greater. In view of this, much of the following discussion is largely relevant to flax and hemp alone.

4.4.2 Formation of micro-compressive defects

4.4.2.1 Kinking

The morphology of much of the micro-compressive damage observed in bast fibres is, as mentioned previously, reminiscent of that seen in highly oriented polymeric fibres such as polyethylene (Grubb & Li, 1994) and rigid rod polymers (Martin & Thomas, 1991). Such fibres exhibit superb tensile strengths, but are often a factor of ten weaker in compression (Martin & Thomas, 1991). These fibres, which consist of fibrils having low interfibrillar bonding strength, are susceptible to kink band formation when loaded in compression (Grubb & Li, 1994).

Kinking is also observed in unidirectional PMCs under compression parallel to the axis of the fibres (Hull & Clyne, 1996). Argon (1972), proposed a model for the initiation of kinks in such materials. At the onset of instability, it was predicted that the compressive stress, σ_{comp} , would be given simply by:

$$\sigma_{comp} = \tau_s / \Delta\Phi \qquad (4.1)$$

Where: τ_s is the plastic shear strength of the matrix

$\Delta\Phi$ is the average misorientation angle of the reinforcing elements (in radians)

4.4.2.2 Kinking in bast fibres

The bulk density of bast fibre, as noted in the previous chapter, can be as high as 1450 kg m^{-3} (Ivens, *et al.*, 1996). If the density of the cell wall material is assumed to be 1500 kg m^{-3}, then certain individual fibres may be thought to consist almost entirely of cell wall material. In other words, the fibres might be considered to be solid composite structures. This supposition has been substantiated through observation in this work; many fibres appearing as though they possessed almost no lumen whatsoever. Nevertheless, as mentioned previously, bulk density can vary considerably (from 600 kg m^{-3} to 1200 kg m^{-3} according to Bolton, 1994). This

would imply that relatively thin walled fibres may also be found (this too was observed).

There is good reason to believe that the relative thickness of the cell wall could affect the macroscopic mode of failure of the fibre. Simplistically, thick and thin walled fibres might be likened to either columns, or thin walled cylinders respectively. The type of compressive failure thus expected might be as shown in Figure 4.4. Here, the thin walled cylinder (A) corresponds to lower density fibres in which macroscopic failure is by gross 'crumpling' of the cell, albeit the wall exhibits kinking within itself (see below). Failure of the column (B), corresponding to high density, thick walled fibres is through shear, such as might be observed in solid wood in pure compression (Desch & Dinwoodie, 1996) and in flax fibre (Rowland *et al.*, 1995). Both failure types were observed in the fibres studied in this work, along with what appeared to be a form of 'hybrid' failure mode.

The fibre failure observed in Plate 4.14 would appear to correspond to a form of macroscopic shear failure ('minute compression failure') such as might be expected from the failure of a solid column in pure compression (*cf.* Figure 4.3B). This form of macroscopic shear failure is, however, more clearly observed in Plate 4.17 in which the whole cell has apparently failed in shear ('kink band'). However, when the cell wall is examined in detail (Plate 4.15), it would appear that this too failed in a shearing mode. This is perhaps more clearly observed in Plate 4.16, in which the macroscopic failure form is indistinct, but in which shear failure within the (relatively thin) cell wall itself was noted. This can be likened to the form of failure expected in a thin walled cylinder (*cf.* Figure 4.3A). The form of failure observed in Plate 4.15 could be considered to correspond to the form of 'hybrid' failure envisaged, in which both the macroscopic failure of the cell is through shear, as is that of the cell wall itself.

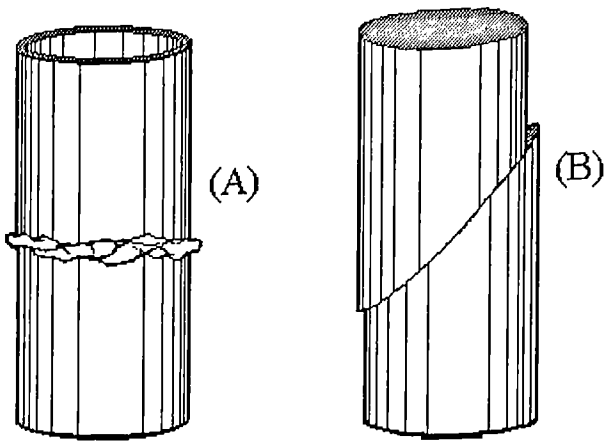

Figure 4.4 Schematic representation of compression failure by *a)* localised crumpling in a thin walled cylinder and *b)* shear failure in a solid column.

From the relationship in Equation 4.1, it has been shown that a misalignment angle of 3^{O} is sufficient to cause the onset of kinking in unidirectional composites (Jelf & Fleck, 1992). However, it is unclear what proportion of the fibres need to be misaligned in order to initiate kinking (Hull & Clyne, 1996). In wood fibres, kinking of the cell wall occurs, as pointed out by Dinwoodie (1974), in a plane normal to that in which the microfibrils lie. This is perhaps more clearly expressed diagramatically (Figure 4.5). As can be seen, in the plane of kinking, the microfibrils, or rather lamellae, are aligned parallel with the fibre axis. It is perhaps not difficult, however, to imagine regions in which the microfibrils are misaligned by greater than 3^{O} which might be sufficient to initiate local instability leading to kinking. The possible loci of micro-compressive failure could well be misaligned microfibrils lying at the surface of the cell wall layer (S_2/S_3 interface) or, alternatively amorphous domains within the fibrillar structure, nucleating kink band formation. Dinwoodie (1968), for instance, noted that "stress lines" appeared to be precursors of kinking in the cell wall. These had the appearance of fine lines which were almost imperceptible under a polarising microscope. The deformation of the microfibrils was thought to be very small. This type of failure could lead to the type of macroscopic fibre failure envisioned by considering the fibre to be a thin walled cylinder (Fig. 4.4A) and was observed in hemp fibre examined in this study (Plate 4.16).

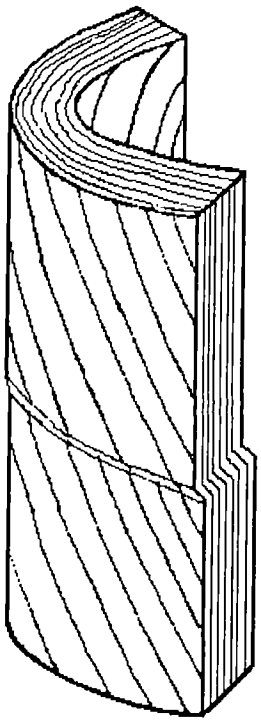

Figure 4.5 Schematic representation of kinking in the S_2 layer of the wood cell wall (*Adapted from:* Dinwoodie, 1974).

By considering flax and hemp to be solid (or near solid) columns in which the winding angle of the microfibrils in the S_2 layer is all but parallel to the fibre axis, the whole fibre rather than just the cell wall may kink (macroscopically in a similar fashion to synthetic polymer fibres) in the manner depicted in Figure 4.4B. Plates 4.17 and 4.18 clearly show that this type of failure also occurs in bast fibres. In this instance, the microfibrillar angle may itself be sufficient to act as the instigator of instability. In X-ray diffraction studies of softwood tracheids, the microfibril angle of the S_2 layer is seen as a distribution, rather than a discrete and constant value (Cave & Robinson, 1998). In hemp for example, in which the mean microfibrillar angle is reported to be in the region $2\text{-}3^{O}$ (Preston, 1974), only a slight perturbation would be required in order to create a region of misalignment greater than 3^{O}, resulting in localised instability. Using a similar argument, if the compressive loading on the fibre was even slightly off-axis, then this might be sufficient to cause instability, thereby initiating kinking. Such a scenario is perhaps not too difficult to imagine occurring in the plant (see below).

In addition to the above, the amount and type of 'matrix' material (other polysaccharides and lignin), as well as the way in which it is bonded to the cellulosic components (lignin-polysaccharide complex), would undoubtedly play a part in the lateral constraint of the microfibrils. In bast fibres, this 'matrix' likely consists of a higher proportion of pectin which, being more flexible than lignin (which is highly cross-linked), would probably provide less lateral support to the microfbrils than in wood, which contains not only a higher proportion of 'matrix', but also this is mainly lignin. This might also explain why jute appears to be somewhat less susceptible to micro-compressive damage than either flax or hemp. Furthermore, it is worthwhile noting, that the microfibrillar angle of the S_2 layer in compression wood is higher than in normal wood (up to 45^{O} - Desch & Dinwoodie, 1981). This would presumably also confer greater stability in compression (although to the detriment of tensile strength).

Bast fibres might be thought to be analogous to the reaction (tension wood) tissue found in hardwoods, wherein the lignin content of the gelatinous layer is lower than in normal wood (whilst the microfibril angle is zero). Tension wood is noted to be somewhat stronger in tension than normal wood, but "exceptionally weak in compression parallel to the grain" (Desch & Dinwoodie, 1981).

As stated in Section 4.3, no attempt was made in this study to quantify the extent of the micro-compressions, but nevertheless, this type of damage appeared to be rife in the bast fibres examined and was even evident in (hemp) fibres carefully extracted from the plant. This would indicate that these fibre types are particularly prone to damage by kinking.

4.4.2.3 Compressive strength of bast fibres

Based on the foregoing, it would seem reasonable to expect that the strength of bast fibres is lower in compression than in tension. Whether this difference is as great as that observed in synthetic fibres, which similarly fail through kink band formation, is a matter for conjecture. It would seem likely, however, that the difference should be less, since in the conventional model of the cell wall, cellulose chains ('reinforcement') are supported with a 'matrix'. If, as proposed by Argon (1972), compressive strength

is governed by the plastic yield strength of the matrix, it would seem reasonable that the 'matrix' of the bast fibres would confer greater stability and resistance to kinking than in synthetic polymeric fibres. It is worth noting that these synthetic fibres do not possess 'matrix', but rely instead on weak Van der Waal's forces for interfibrillar bonding (Mathur & Netravali, 1996). Indeed, it has been found that in synthetic polymeric fibres, improved fibre compressive properties can be achieved by artificially introducing a 'matrix' through polymer infiltration (Mathur & Netravali, 1996). Lee and Santhosh (1993), consider that hoop constraint around the fibre may be an effective method of improving compressive strength. Bast fibres effectively possess such constraint in the form of the primary wall and S_1 layer which, as was discussed in Section 4.1.2, is considered to be of importance in stabilising the fibre in just this manner (Booker & Sell, 1998).

It would seem plausible, therefore, that bast fibres should be significantly stronger in compression than synthetic fibres. This contention has, indeed, been borne out by recent work carried out on flax ultimates (Bos *et al.*, 1997). It was found that these fibres displayed axial tensile strengths of around 1500 MN m^{-2}, whilst in compression the strength was found to be around 1200 MN m^{-2}. In other words, the compressive strength of flax fibres is around 80% of the tensile strength, which compares with around 20% for Kevlar (Mathur & Netravali, 1996).

Nevertheless, it remains likely that bast fibres will be susceptible to compressive damage and this could well impact upon the compressive properties of laminates. This would be particularly so in uniaxially aligned fibre composites loaded parallel to the fibre direction. Unfortunately, no such compression tests were performed during the course of this work and thus this supposition cannot be validated.

4.4.3 Origin of micro-compressive defects

4.4.3.1 Formation of kink bands in the plant

The examination of fibres taken from the 'green' stem of hemp revealed the existence of numerous micro-compressive defects. It is interesting to note that the occurrence of damaged fibres appeared to be very extensive within the plant. Why this should be

so and the mechanisms by which this occurs requires explanation. In trees, it is thought that compression damage occurs as a result of both externally applied loads (gravity and wind induced mechanical loads) or internal growth stresses (Dinwoodie, 1976). It is likely that these factors operate in annual plants too. Plants such as flax and hemp are likely to sway significantly during their life-time. This would in all probability lead to the fibres being stressed cyclically in axial tension and compression. Such fatigue loading has been shown to lead to compression creases in wood, ultimately resulting in crack formation and failure (Imayama, 1994). It might be thought, however, that if this were the only mechanism involved, damage would be prevalent in the lower part of the stem (which would have undergone more fatigue cycles and the fibres would also, in all probability, undergo greater compressive strain). Whilst a greater level of damage appears to be present in fibres isolated from the lower stem, there is still a significant amount visible in fibres taken from the upper stem. Micro-compressions may also arise from growth stresses induced by the surrounding plant tissue. This has been cited as a possible explanation for the appearance of these features in flax (Focher *et al.*, 1992).

4.4.3.2 The influence of decortication and processing

The processes involved in the decortication and refining of the fibres would in all probability result in further micro-compressive damage being introduced. In any process in which the fibres are bent into sharp radii, the compressive stresses induced in the fibre could well result in localised kinking. This failure mechanism has been observed in flax fibres in loop tests conducted in an environmental scanning electron microscope (Bos & Donald, 1999). The fibres used as reinforcement in this study were, as stated previously, formed into non-woven felted mats. This process involves an intensive mechanical process (carding) in which the fibres are separated by 'combing' the fibres between pins moving in opposite directions. This process would undoubtedly induce a significant amount of bending in the fibres which may well account for the extensive damage observed.

4.4.4 Implications of micro-compressive defects

If bast fibres are to be used as reinforcement in PMCs, then it is essential to gain a full understanding of their behaviour. This study has highlighted the fact that these fibres are susceptible to damage through kinking. It is of prime importance, therefore, to understand the influence that these defects have on the fibres themselves, since this will have a direct bearing upon the mechanical properties of composites reinforced with such fibres. It should be noted that in this work, no separate study was conducted to determine the mechanical properties of the fibres (bundles or ultimates). Thus, the following discussion is based upon data obtained from the literature.

4.4.4.1 Influence of micro-compressive defects on tensile (Young's) modulus

It is reasonable to suppose that when a damaged fibre is strained, individual micro-compressive defects or kinks will have a tendency to 'straighten out'. Furthermore, as individual kinks straighten, the relative strain which each kink undergoes will reduce as it straightens out. As more and more kinks straighten, the resistance of the fibre to straining should increase. Thus, intuitively, the fibre should become stiffer as it is strained and a non-linear stress-strain response would be expected. There is some evidence to support this supposition. Hornsby *et al.* (1997), for instance, observed such non-linear behaviour in pulped flax fibres. The fibres used in that investigation were noted to contain a significant number of "dislocations" (kinks), some of which no doubt resulted from the pulping process.

With regard to the direct effect of micro-compressive damage on the tensile modulus of individual fibres, Page *et al.* (1977), who investigated the influence of the microfibril angle on the elastic modulus of single wood pulp fibres, found that there was significant scatter in the results for fibres with nominally the same fibril angles. They were able to confirm through ciné photography that this was attributable to micro-compressions and other inhomogeneities in the fibre cell wall, with defects and micro-compressions resulting in a reduced tensile modulus. Davies and Bruce (1998) found that as the level of micro-compressive damage increased, fibre modulus decreased. This again might be expected; a greater number of micro-compressions leading to a greater overall fibre strain for a given level of stress.

If flax or hemp fibres are indeed considered as unidirectional fibre reinforced composites, then a simple 'Voight' model (Hull & Clyne, 1996) to predict the tensile modulus might be instructive. In this, the overall tensile modulus of the fibre is considered to be the volume weighted average of the moduli of the individual components. The data presented in Table 4.1 were derived from the literature and represents a 'best guess' at material properties and relative proportions (see Section 2.3.2) of constituents for an 'ideal' bast fibre.

Table 4.1 Material properties of an 'ideal' bast fibre.

Constituent	V_f *(%)*	*Axial modulus, E* $(GN\,m^{-2})$	*Reference*
Cellulose	85*	134.0	Sakurada *et al.*, 1962
Other polysaccharides	10*	8.0	Cousins, 1978
Lignin	5*	4.0	Cousins, 1976

* Estimated volumetric proportions (see Section 2.3.2).

The tensile modulus E_{fibre} of the fibre is given by:

$$E_{fibre} = V_{cel.}E_{cel.} + V_{pol.}E_{pol.} + V_{lig.}E_{lig.} \qquad (4.2)$$

Where:

$V_{cel.}$ is the volume fraction of cellulose

$V_{pol.}$ is the volume fraction of other polysaccharides

$V_{lig.}$ is the volume fraction of lignin

$E_{cel.}$ is the axial modulus of cellulose

$E_{pol.}$ is the axial modulus of other polysaccharides

$E_{lig.}$ is the axial modulus of lignin

Substitution of the material data and relative proportions of each constituent given in Table 4.1 into the Equation 4.2, yields a theoretical tensile modulus of ~115 GN m^{-2}. To give an effective fibre modulus, the fact than no contribution to the overall stiffness from either the S_1 or S_3 layers is assumed, must be taken into account.

Similarly, it is assumed that in measuring the cross section of real fibres, no account is taken of the lumen space; allowance should be made for this too. Assuming the density of a mature fibre to be 1400 kg m^{-3} and 90% of the cell wall is comprised of the S_2 layer, then the effective stiffness would be ~97 GN m^{-2}. This figure compares with ~70 GN m^{-2} for glass fibre (Ivens *et al.*, 1997). In the only known study of the influence of fibre damage on the tensile modulus of flax fibres, Davies and Bruce (1998) observed a static tensile modulus of around 93 GN m^{-2} for undamaged fibre. As can be seen, this figure compares well with the predicted value.

4.4.4.2 The influence of micro-compressions on the tensile strength of fibres

In the same study, Davies and Bruce (1998) found that not only do micro-compressions affect the tensile modulus of the fibres, but also their strength, with increasing damage levels resulting in lower tensile strengths. Further, failure in flax fibre has been observed to initiate at micro-compressions (Focher *et al.*, 1992; Rahman, 1979). Page *et al.* (1971) using ciné photography noted that in single wood pulp fibres, failure was initiated at the defects. Also, they attributed the large variation in tensile strengths, for a given microfibril angle, to the influence of these defects on fracture. Kim *et al.* (1975), investigating the effect of drying stress on the tensile strength of pulp fibres, found that micro-compressions could, in some instances, be removed by drying under tension, resulting in an improvement in tensile strength. Later, Page and El-Hosseiny (1976), successfully fitted Pierce's weak link theory to the failure of Black spruce fibres and concluded that, for fibres of similar microfibril angle, tensile strength is controlled by a randomly distributed population of defects in the fibre. Furthermore, Dinwoodie (1978) found that artificially induced micro-compressions reduced the failing load of individual Norway spruce fibres by nearly 50%, although the effect in solid wood was far less, with a reduction in tensile strength of around 10% being observed.

From the foregoing, it is evident that the presence of micro-compressions in the fibre reduces tensile strength and, as noted by various authors, failure is observed to initiate at these features. What is of interest is the mechanisms by which the strength reduction takes place. Evidently, micro-compressive defects, particularly those which

are observed in thick walled bast fibres, change the geometry of the cell wall, introducing a step into the structure and effectively creating a stress concentrator.

Using the Griffith criterion (Equation 3.7) a critical crack length can be deduced (by making the assumption that the cell wall behaves as an elastic, isotropic continuum - this is an over-simplification but is believed to be valid in order to establish orders of magnitude for critical crack lengths) from the cell wall material constants and an estimate of failure stress. If the fracture toughness of the cell wall material, normal to the microfibrillar direction is taken to be 3.45 kJ m^{-2} (Lucas *et al.*, 1997) and the modulus of elasticity is assumed to be 100 GN m^{-2}, then for an applied tensile stress of 500 MN m^{-2}, the critical crack length would be of the order ~450 μm. If the tensile stress is raised to 2000 MN m^{-2}, then the critical crack length reduces to ~28 μm. Given that the diameter of flax or hemp ultimates is often around 25 μm, it seems unlikely that the morphological change to the fibre could alone constitute a critical length crack.

Dinwoodie (1978), postulated that the decrease in tensile strength is a manifestation of damage to the cellulose molecule. In the zone of the micro-compression, microfibrils are bent in the form of a sharp 'Z' or kink. It is believed that this results in a loosening of the structure, with the severance of cross-bonds in the unit cell and possibly a limited amount of breakage of the longitudinal covalent bonds (Dinwoodie, 1978). It would certainly seem as though structural alterations take place in the kinked zone, since it has been reported that increased chemical reactivity, uptake of dyes etc. occurs in these regions (Keith & Cote, 1968). It seems feasible that in addition to lateral, interfibrillar bond scission, damage to the longitudinal covalent bonds, as postulated by Dinwoodie (1978), may also take place. Although not directly applicable to micro-compressed bast fibres, a recent study on kink band formation in rigid-rod polymers, using low-dose high resolution electron microscopy, has shown that at the juncture between undisturbed fibrils and those lying in the kinked zone, very large angle changes in molecular orientation (40^{O}) at very sharp (0.5 nm) tilt boundaries are observed (Martin & Thomas, 1991). It has been calculated that a radius of curvature of ~9 nm is sufficient to cause damage to the cellulose microfibril (Mühlethaler, 1965). If similar kink conformations were to occur

in micro-compressed bast fibres, it is perhaps reasonable to suppose that localised axial damage to the cellulose molecules may occur. This, coupled with the stress concentrating effect of the gross morphological changes to the fibre cell wall, may account for the loss in tensile strength of the fibres.

Whilst it is interesting to speculate upon the theoretical strength which might be achieved from in 'ideal' undamaged fibre, the prediction of this is complicated because of uncertainty regarding fracture mechanisms involved and the properties of the fibre constituents. Nevertheless, if it is assumed that the model fibre behaves perfectly elastically to (brittle) fracture, which is not unreasonable, bearing in mind experimental observations (e.g. Davies & Bruce, 1998), then it should be possible to estimate a value for tensile strength. Assuming a strain to failure of around 2% for cellulose (Mühlethaler, 1965), this would, if the effective fibre modulus is taken to be 100 GN m^{-2}, lead to a tensile strength of 2000 MN m^{-2}. This figure does not look too unreasonable, given that the tensile strength of some individual flax fibres can approach this value (Davies & Bruce, 1998).

4.4.4.3 The toughness of bast fibres

As mentioned above, the stress-strain relationship for bast fibres under axial tension is essentially linear, culminating in brittle fracture of the fibres. As was seen in the SEM micrographs in the previous chapter, (Plate 3.10) the fracture surfaces of individual fibres had the brash 'carroty' appearance of brittle failure. This type of failure is perhaps not unexpected given the fibre ultrastructure. As mentioned in Section 4.1.2, much of the high work of fracture observed in wood can be attributed (possibly up to 90% of the overall work of fracture) to the pseudo-plastic buckling mechanism proposed by Gordon and Jeronomidis (1974). A prerequisite for this mechanism to operate, however, is a non-zero value for the microfibrillar angle of the S_2 layer (15^0 was determined to be optimal in Gordon and Jeronomidis' work). Since the microfibril angle in flax and hemp is at most only a couple of degrees little, if any, contribution to the overall work of fracture could be expected from this form of plastic deformation. The work of fracture of flax and hemp fibres is, at best, probably akin to the intrinsic toughness of the plant cell wall determined by Lucas *et al.* (1997), with a value of around 3.45 kJ m^{-2}. This value is probably an overestimate if there is

a severe disruption to the ultrastructure, or even longitudinal bond severance in the region of micro-compressions.

4.5 Conclusions

Bast fibres, particularly flax and hemp which are potentially the most valuable in terms of composite reinforcement, would appear to be very sensitive to the formation of kink bands or micro-compressive defects. This is most probably due to their ultrastructure, which perhaps makes them more susceptible to this form of damage than wood. There are a number of implications for this behaviour.

Firstly, the tensile properties are affected. Young's modulus and strength are reduced whilst the defects act as loci for fibre failure. This will undoubtedly have ramifications as far as the properties of composites reinforced with these fibres are concerned. Secondly, the fibres themselves would appear to be brittle, with little work of fracture. No significant contribution to the overall work of fracture of composites reinforced with these fibres could therefore be expected from fibre fracture alone. Further, this may affect the manner in which cracks propagate through the composite material. In addition, a factor, not extensively discussed above, is the potentially poor properties of composites in compression. In this work, no separate study of the compression behaviour of laminates was undertaken. This is an area which should be investigated. Poor properties in compression have limited the use of certain synthetic polymeric fibres (Grubb & Li, 1994). Finally, and thought to be potentially extremely important, is the effect that these micro-compressions have on the heterogeneity of strain within the fibre.

In the region of the micro-compression, it is to be expected that for a given load, the fibre will undergo greater strain. In other words there will be a strain concentration at the micro-compressive defect. This supposition is supported by recent work undertaken using the technique of digital image correlation to map strain in single wood pulp fibres, where it was found that strain concentrations existed in the vicinity

of fibre defects and inhomogeneities, including micro-compressions (Mott *et al.*, 1996). The fibre could thus be thought of as having different moduli in different regions. This, coupled with the distinct morphology of some of the more extreme examples of these defects, would undoubtedly impact upon the micromechanics of deformation and fracture, occurring at the interface when the fibres are used to reinforce what is essentially a homogeneous, isotropic medium. This issue is considered in the following chapter.

5 Interface Micromechanics

5.1 Introduction

5.1.1 General background

In the previous chapter, the effect of fibre micro-compressive defects and processing damage was discussed in relation to the mechanical properties of the fibres themselves. From the standpoint of composite manufacture, however, the important questions which arise are: in what way and to what extent do these defects influence the mechanical properties of the laminates themselves? Evidently, the mechanical properties of the composite will be affected by the tensile and compressive moduli and strengths of the fibres, which in turn have been shown to be influenced by fibre damage (Davies & Bruce, 1998). However, another factor which needs to be considered is the effect that these damage features have on the interaction between fibre and matrix; in particular how they influence the deformation and fracture processes occurring at the fibre/matrix interface.

Recently, it has been shown that a variety of cell wall defects including pit apertures, processing induced creases and micro-compressions can affect the cell wall strain distribution in single wood fibres, leading to localised strain concentrations (Mott *et al.*, 1996). It is plausible, therefore, that a similar fibre strain heterogeneity occurs in hemp, flax and jute fibres, with the region of the fibre in the vicinity of the micro-compression undergoing greater strain relative to undamaged portions of fibre. Such behaviour is likely, since when a fibre is subject to a tensile load, the 'kinks' would tend to straighten out. This can be observed as the so called 'strain hardening' observed in individual fibre tensile tests (Hornsby *et al.*, 1997). An heterogeneous fibre strain distribution, coupled with the distinct geometry of the micro-compressive features, could well lead to stress concentrations occurring in the matrix (which is essentially homogeneous and isotropic) when the fibres are used as reinforcement. In turn, these stress concentrations could promote crack formation at the interface, leading to fibre-matrix debonding and to localised rupture of the matrix. This

hypothesis is supported by work carried out on the effects of residual thermal stresses in high-modulus polyethylene fibre composites. In these composites, it was found that kink bands formed in the fibres as a result of axial curing stresses. These, as well as pre-existing damage had the effect of creating stress concentrations in the matrix in the vicinity of the kinks which were thought to act as sites of potential crack initiation and fibre-matrix debonding (Grubb & Li, 1994). It is feasible too, that residual stresses may exacerbate the effect of the microcompressive features found in bast fibres. In view of the importance of the interface in controlling the performance of composite materials (Hull & Clyne, 1996), it was believed that an investigation into the nature of the interface would lead to a fuller understanding of the material behaviour as a whole. In particular, it was thought that an examination of the stress field in the matrix adjacent to the micro-compressions would be of particular relevance.

Photoelasticity offers a potentially convenient method for the analysis of stresses in polymeric matrices, such as epoxies and polyesters, which exhibit artificial birefringence when stressed (Dally & Riley, 1965; Burger, 1993). Photoelasticity is an experimental method for analysing stress or strain fields in mechanics, inferring stresses in certain transparent materials from their optical effects (Burger, 1993). The optical effects in photoelasticity appear as a form of interference pattern, with the number of fringes generated (fringe order), or the density of the spacing, being a function of the stress response (Burger, 1988).

5.1.2 Experimental technique

In this chapter, the matrix stress-field in the vicinity of micro-compressive defects is examined in a model system. This system consisted of single filament composites (SFCs) reinforced with either individual bast fibre (hemp) ultimates and bundles or E-glass fibres. These composites were loaded in tension, parallel to the axis of the fibre in a miniature tensile frame and the state of stress in the matrix inferred from the photoelastic response of the matrix utilising a technique known as half fringe photoelasticity (HFP). Essentially HFP combines classical photoelasticity with modern digital image analysis using computers, enabling the rapid, whole-field stress analysis of a photoelastic sample to be undertaken (Burger, 1993).

5.1.3 Photoelasticity theory - behaviour of light

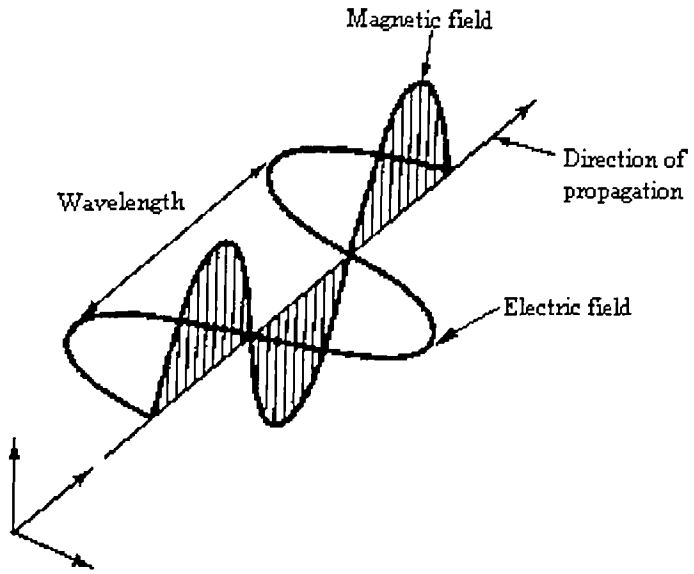

Figure 5.1 Instantaneous field pattern of a linearly polarised ray (*Source:* Burger, 1993).

For the purposes of describing the photoelastic effect observed in birefringent materials, the electromagnetic theory due to Maxwell is often used (Dally & Riley, 1965). In this, light propagates as a transverse electromagnetic wave as shown in Figure 5.1. The disturbance producing the light can be considered as wave motion, where, the instantaneous magnitude E, of the electric field vector, observed at a fixed point along the direction of propagation is (Burger, 1993):

$$E = a\sin\frac{2\pi}{\lambda}ct \qquad = a\sin 2\pi f t \quad = a\sin\omega t \tag{5.1}$$

Where:

a	is amplitude
λ	is wavelength
c	is the velocity of propagation (3×10^8 ms^{-1})
t	is time
ω	is angular frequency
f	is frequency

The above relationship describes the situation for a *linearly* polarised ray. However, photons emitted in any direction from a light source will have electric fields randomly oriented and will produce an un-polarised beam of light. In a beam of light which is made up of photons with their electric fields preferentially aligned, the light is said to be polarised. For instance, when the E fields are parallel to one another, the light is linearly, or *plane*, polarised. Linear polarisation is a special case of the general state of polarisation - *elliptical* polarisation. Another special case of polarisation is *circular* polarisation in which the electric field vector describes a circle of constant magnitude rotating about the direction of propagation. These states of polarisation are depicted schematically in Figure 5.2.

Plane polarised light may be obtained by a number of methods, one of the most convenient of which is to use 'polaroid' sheet. As will be discussed in more detail in Section 5.1.6, circular polarised light is often employed in photoelastic studies. Circular polarised light may be obtained by 'conditioning' plane polarised monochromatic light using an optical element known as a quarter-wave retarder or quarter-wave plate ($\lambda/4$ retarder/plate).

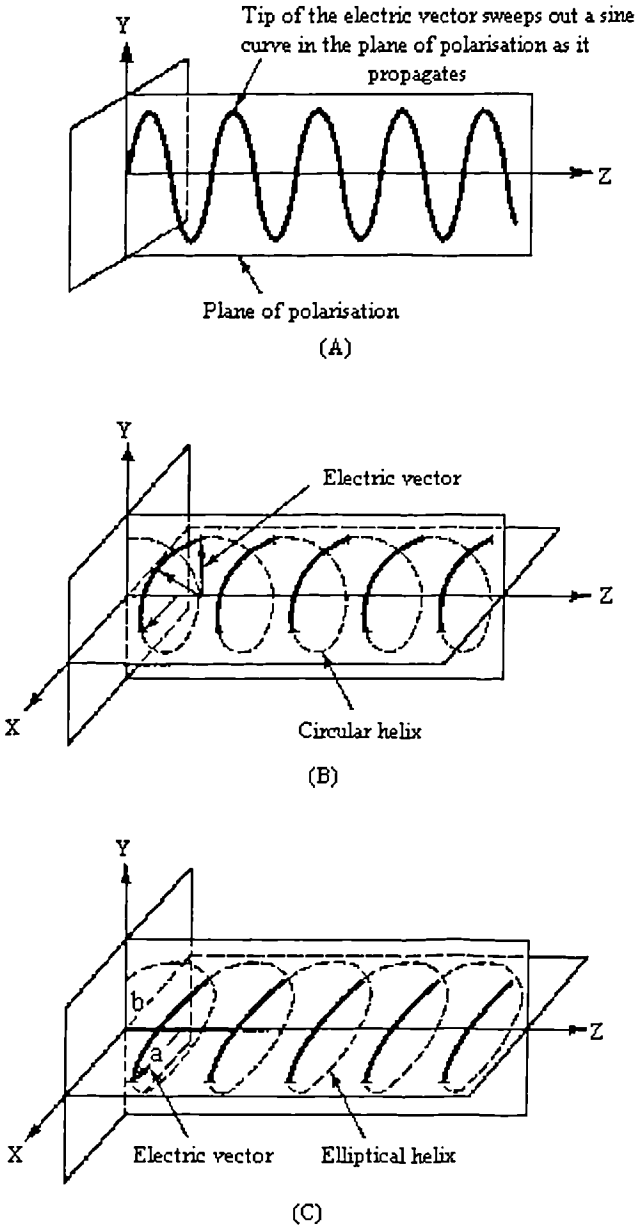

Figure 5.2 Motion of the electric vector for *a)* plane, *b)* circular and *c)* elliptically polarised light (*Source:* Burger, 1993).

5.1.4 Wave retarders or wave plates

A number of materials possess the ability to resolve a linearly polarised light vector into two orthogonal components and moreover, to transmit each component through the material at different velocities. These include various crystalline materials such as mica and quartz, as well as many polymers which exhibit artificial anisotropy as a result of residual stresses induced during the manufacturing process. These materials

are said to be doubly refracting or *birefringent.* An optical element made from a birefringent material is known as a wave plate or wave retarder.

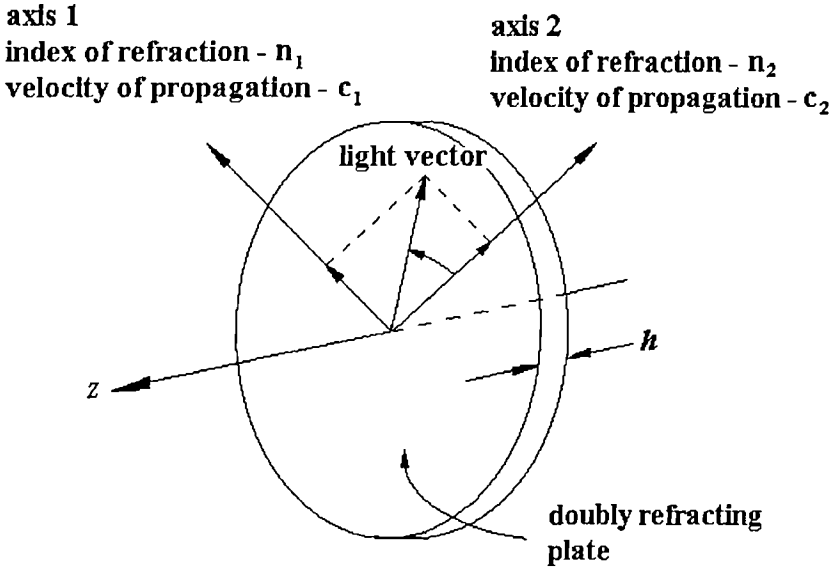

Figure 5.3 Schematic representation of a wave plate or wave retarder.

A wave retarder can be considered as having two principal axes (Figure 5.3) 1 and 2 along which the light vectors propagate at velocities c_1 and c_2. Where $c_1 > c_2$, axis 1 is known as the 'fast axis' and axis 2, the 'slow axis'. Furthermore, the axes possess different indices of refraction n_1 and n_2 respectively. It can be shown that the angular phase shift, Δ, between the two components when they emerge from the wave retarder is (Dally & Riley, 1965):

$$\Delta = \frac{2\pi h}{\lambda}(n_1 - n_2) \qquad (5.2)$$

Where: h is the thickness of the wave retarder

The angular shift is thus determined by the plate thickness, the wavelength of light used and by the optical properties of the retarder. A plate designed to give an angular retardation of $\pi/2$ is known as a quarter wave retarder or quarter wave plate.

Circular polarised light may be obtained by aligning the axis of the $\lambda/4$ retarder axis so that it forms an angle of $\pi/4$ with the axis of the linearly polarised light (Figure 5.4).

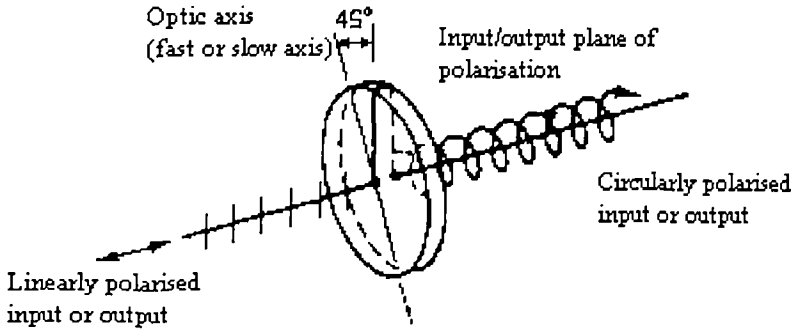

Figure 5.4 'Conditioning' of linearly polarised light to obtain circularly polarised light and *vice versa* (*Source:* Burger, 1993).

5.1.5 Stress-optic law

Certain amorphous polymeric materials such as epoxies, polyesters and urethane rubbers are normally optically isotropic. However, when stressed, they become doubly refracting (Dally & Riley, 1965). The indices of refraction for such temporarily birefringent materials are linearly proportional to the stresses therein. For the general three dimensional case, the relationships between the three principal stresses σ_1, σ_2 and σ_3 and the principal indices of refraction n_1, n_2 and n_3, for waves vibrating parallel to the principal stresses are given by (Burger, 1993):

$$n_1 - n = c_1\sigma_1 + c_2(\sigma_2 + \sigma_3)$$
$$n_2 - n = c_1\sigma_2 + c_2(\sigma_3 + \sigma_1)$$
$$n_3 - n = c_1\sigma_3 + c_2(\sigma_1 + \sigma_2)$$

Where: n is the index of refraction of the unstressed material in its optically isotropic state

c_1, c_2 are varying constants (depending upon the material), termed the 'stress-optic coefficients' for a specific material

On subtraction to eliminate n, the following relationship is obtained:

$$n_1 - n_2 = (c_1 - c_2)(\sigma_1 - \sigma_2)$$
$$= C(\sigma_1 - \sigma_2) \qquad (5.3)$$

Where: $C = (c_1 - c_2)$ is the relative stress-optic coefficient

$(\sigma_1 - \sigma_2)$ is the principal stress difference

Similarly it can be shown that:

$$n_1 - n_3 = C(\sigma_1 - \sigma_3)$$
$$n_2 - n_3 = C(\sigma_2 - \sigma_3)$$

If the photoelastic sample is a plate and the stress normal to the plate is zero, i.e. conditions of plane stress, and further, the in-plane stresses do not vary through the thickness, then the stressed plate can be regarded as a temporary wave plate with the optical fast and slow axes coinciding with the axes of the principal stresses.

However, as shown previously, for a wave plate, the difference in the indices of refraction (n_1 - n_2) are given by:

$$n_1 - n_2 = \frac{\lambda \Delta}{2\pi h} \tag{5.4}$$

Substituting Equation 5.3 into Equation 5.4 and re-arranging yields:

$$\Delta = \frac{2\pi hC}{\lambda}(\sigma_1 - \sigma_2) \tag{5.5}$$

Equation 5.5 is the classical description of the 'stress-optic law' in two dimensions at normal incidence. Nevertheless it is more convenient in photoelasticity work to re-write this expression and re-define a number of units as follows:

$$(\sigma_1 - \sigma_2) = \frac{Nf_\sigma}{h} \tag{5.6}$$

Where:

$N = \Delta / 2\pi$	is the relative retardation known as 'fringe order' and is wavelength dependent (dimensionless)
$f_\sigma = \frac{\lambda}{C}$	is the material fringe value (N m^{-1})
h	is the specimen thickness

Thus, if the fringe order, N can be measured, the principal stress difference may be determined, provided the material fringe value f_σ can be established by means of calibration. A polariscope is a means of determining N at each point in a stressed photoelastic specimen.

5.1.6 Behaviour of a stressed photoelastic specimen in a polariscope

If a photoelastic sample is loaded in a plane polariscope, such that the principal stress direction makes an arbitrary angle α with the axis of polarisation, as depicted in Figure 5.5, then it can be shown that the intensity of the light emerging from the polariscope at this point in the sample is (Dally & Riley, 1965):

$$I = K \sin^2 2\alpha \sin^2 \frac{\Delta}{2} \tag{5.7}$$

Where: I is the intensity of light emerging from the polariscope

K is a constant.

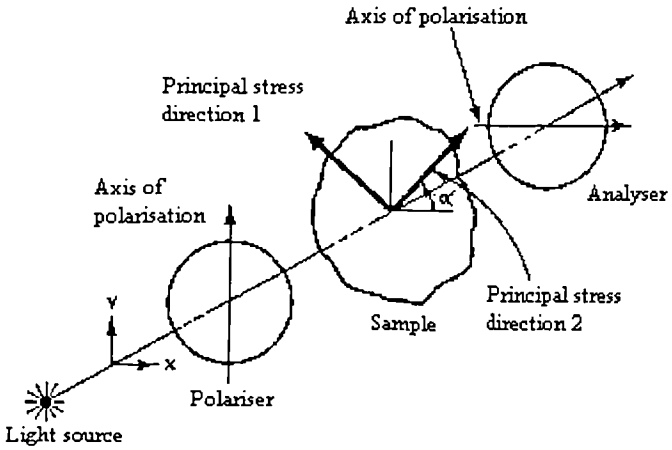

Figure 5.5 Stressed photoelastic model in a plane polariscope (*Source:* Burger, 1993).

As can be seen, the intensity goes to zero, i.e. extinction occurs, when either the $\sin^2 2\alpha$ or $\sin^2 \Delta/2$ terms are zero. Strictly, the above relationship includes a $\cos^2 \omega t$ term. However, since the angular frequency is so great, the conditions under which extinction occurs as a result of this may be ignored for practical purposes (Dally & Riley, 1965). Considering first the $\sin^2 2\alpha$ term, this goes to zero when $2\alpha = n\pi$, where n = 0,1,2,3, etc., in other words, $\alpha = 0, \pi/2$ or an exact multiple

thereof. This implies that extinction will occur if either of the principal stress directions σ_1 or σ_2 coincide with the axis of polarisation. This results in a fringe pattern appearing over the whole sample, where the fringes are the loci of points where either of the principal stress directions coincide with the axis of the polariser (Dally & Riley, 1965). This fringe pattern is known as the *isoclinic* fringe pattern.

The second condition of extinction occurs when $\Delta/2 = n\pi$, where n = 0,1,2,3, etc. In other words when $\Delta/2\pi = n$, the intensity goes to zero. From the above and from Equation 5.6, it can be shown that (Dally & Riley, 1965):

$$n = \frac{\Delta}{2\pi} = N = \frac{h}{f_\sigma}\left(\sigma_1 - \sigma_2\right) \tag{5.8}$$

Thus the intensity of light emerging form the polariscope at a point in the sample goes to zero when the principal stress difference is such that:

$$\frac{h}{f_\sigma}\left(\sigma_1 - \sigma_2\right) = 0,1,2,3, \text{ etc.}$$

The order of extinction or 'fringe order' (i.e. N = 0,1,2,3, etc.) is thus a function of the magnitude of the principal stress difference $\left(\sigma_1 - \sigma_2\right)$ and is dependent upon the sample thickness and the material fringe value (a measure of the stress-optical sensitivity of the photoelastic material). When the sample is viewed in whole-field, a second set of extinction lines, being the loci of points of equal principal stress difference (where $\left(\sigma_1 - \sigma_2\right) = Nf_\sigma/h$), are observed. The fringe pattern thus formed is known as the *isochromatic* fringe pattern.

Therefore, in a plane polariscope two fringe patterns, one dependent upon the directions of the principal stresses - the isoclinics and the other - the isochromatics, dependent upon the magnitude of the principal stress difference, are observed, superimposed upon one another.

A polariscope employing circular polarised light is commonly used in photoelastic studies, as it has the effect of eliminating the isoclinics, leaving only the isochromatic fringe pattern which may then be used to determine the principal stress differences. It may be shown that for a model loaded in a circular polariscope in dark-field (linear polariser and analyer crossed) set up such that the principal stress direction makes an arbitrary angle α with the axis of the polariser, as depicted in Figure 5.6 then the intensity of light emerging from the polariscope is given by (Dally & Riley, 1965):

$$I = K \sin^2 \frac{\Delta}{2} \tag{5.9}$$

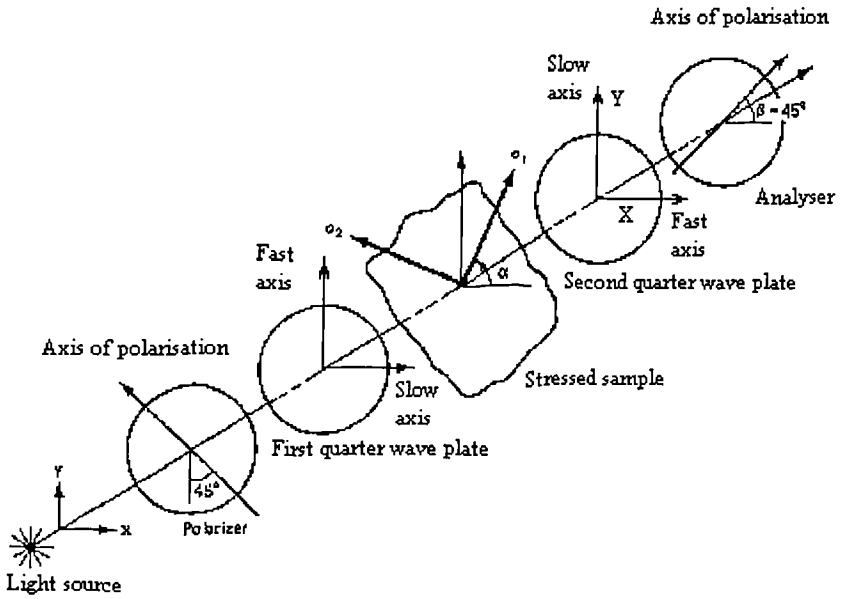

Figure 5.6 Stressed photoelastic sample in a circular polariscope in 'dark-field' set up (*Source:* Burger, 1993).

This expression contains an additional term $[\cos(\alpha + \omega t) - \sin(\alpha - \omega t)]^2$. However, for practical purposes this may be ignored since the angular frequency is so high. Further, since α is combined with the ωt term in the sine and cosine functions, it is effectively eliminated from the expression. In other words, no isoclinic fringe pattern is superimposed upon the isochromatic fringe pattern.

5.1.7 Half fringe photoelsticity

The determination of the state of stress in a photoelastic model in a circular polariscope is a matter of counting and locating the fringes. As such, the method is discrete. Nevertheless, the relationship between light intensity and relative retardation (Equation 5.9 for dark-field set up), is a continuous function. Half fringe photoelasticity is a technique, developed in the early 1980's by Burger and Voloshin, which utilises the continuous nature of this function (Burger & Voloshin, 1982; Voloshin & Burger, 1983; Burger, 1988). The name derives from the fact that the system operates within the first 'half fringe' of relative retardation (Figure 5.7). Half fringe photoelasticity has been used to determine stress intensity factors in cracked isotropic bodies (Burger & Voloshin, 1983; Miskioglu, *et al.*, 1987) and to study the stress field around single wood pulp fibres embedded in a polyurethane matrix (Mercado, 1992).

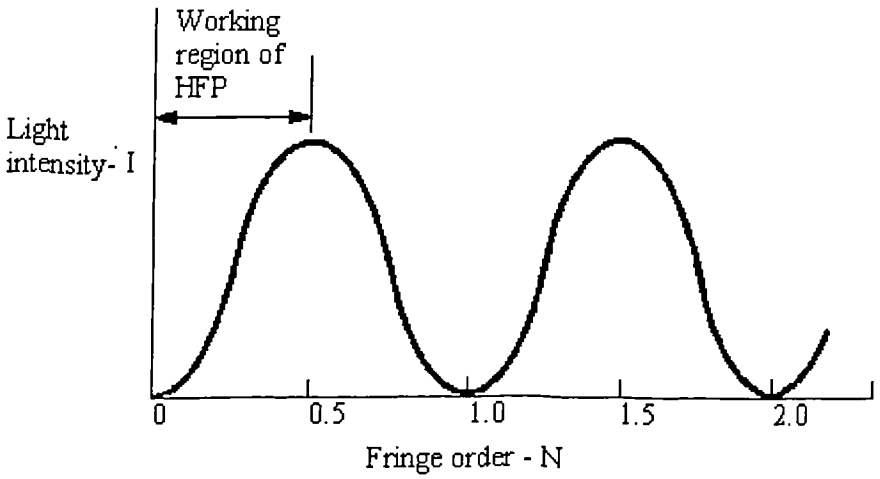

Figure 5.7 Working range of Half Fringe Photoelasticity
(*Source:* Burger, 1993).

The principal stress difference in a photoelastic model may be calculated from Equation 5.6, provided the material fringe value, f_σ is known and the fringe order, N at a particular point in the sample can be determined. In half fringe photoelasticity, rather than counting discrete fringes, the intensity of light between

fringes (or rather, within the first half fringe) is measured by means of a video camera able to record light intensity with a high degree of accuracy. This is then used to determine the 'partial fringe order' within the working range of HFP (i.e. between $N = 0$ and $N = 0.5$). Consequently, the principal stress difference at a given point in the photoelastic model can be determined from the measured intensity once suitable calibration has been established to convert intensity to 'partial fringe order'. The theoretical basis for HFP is an extension of the discussion above.

By substituting $N\pi$ for $\frac{\Delta}{2}$, Equation 5.9 can be rewritten as:

$$I = K \sin^2 N\pi \tag{5.10}$$

Introducing a reference intensity, I_{max}, to replace K (Burger, 1988), Equation 5.10 may be rewritten:

$$\frac{I}{I_{max}} = \sin^2 N\pi \tag{5.11}$$

The video response Z is not, however, linearly related to light intensity, but in the following manner (Voloshin & Burger, 1983):

$$Z = \psi I^{\gamma} \tag{5.12}$$

Where: ψ is a constant

γ is the log linear sensitivity curve of the video camera on a log Z versus log I plot

Nevertheless, the light intensity emerging from the polariscope must have its maximum when the Z value is a maximum (Miskioglu, 1987). Thus:

$$Z_{max} = \psi I_{max}^{\gamma} \tag{5.13}$$

By taking ratios:

$$\frac{Z}{Z_{\max}} = \left(\frac{I}{I_{\max}}\right)^{\gamma} \tag{5.14}$$

Substitution of Equation 5.11 into Equation 5.14 and taking logs, yields the following relationship:

$$\log\left(\frac{Z}{Z_{\max}}\right) = \gamma \log\left(\sin^2 N\pi\right) \tag{5.15}$$

Thus a plot of $\log\left(Z/Z_{\max}\right)$ versus $\log\left(\sin^2 N\pi\right)$, yields a straight line of slope γ, enabling evaluation of the camera sensitivity to be undertaken.

However, Equation 5.14 may also be expressed in the form:

$$\frac{I}{I_{\max}} = \left(\frac{Z}{Z_{\max}}\right)^{\frac{1}{\gamma}} \tag{5.16}$$

Substitution of Equation 5.16 into Equation 5.11 and rearranging gives:

$$N = \frac{1}{\pi}\sin^{-1}\left(\frac{Z}{Z_{\max}}\right)^{\frac{1}{2\gamma}} \tag{5.17}$$

Thus, it is possible to determine the fringe order, N, if the ratio of $\left(Z/Z_{\max}\right)$ is known and if γ can be established. Further, if the material fringe value, f_{σ}, is determined by calibration, the principal stress difference may be evaluated for any point in a photoelastic model from Equation 5.6.

5.2 Materials and method

5.2.1 Specimen preparation

Epoxy, rather than polyester, resin was chosen for the matrix material because of its good stress-optic properties (Dally & Riley, 1965; Burger, 1993). Epoxy resin (Epiglass HT9000 - International) was cured by the addition of catalyst (Epiglass HT9000 standard hardener - International) in the ratio 4:1 (by volume) resin:catalyst. Care was taken during mixing to minimise the inclusion of air bubbles and any extraneous matter. Prior to use, the catalysed resin was degassed under vacuum for 5 minutes.

Reinforcing fibres were prepared from dew retted but undecorticated hemp. Sections of stem were soaked in deionised water for approximately 24 hours at ambient temperature. Strips of bark were then easily separated from the woody core material. Individual fibre bundles were carefully teased from the bast using tweezers. Fibre ultimates were prepared from the bundles by maceration in a mixture of 50/50 (by volume) hydrogen peroxide/acetic acid as described more fully in Chapter 4. Throughout, great care was taken in handling to minimise fibre damage. Once separated, the fibres were carefully washed and stored in deionised water.

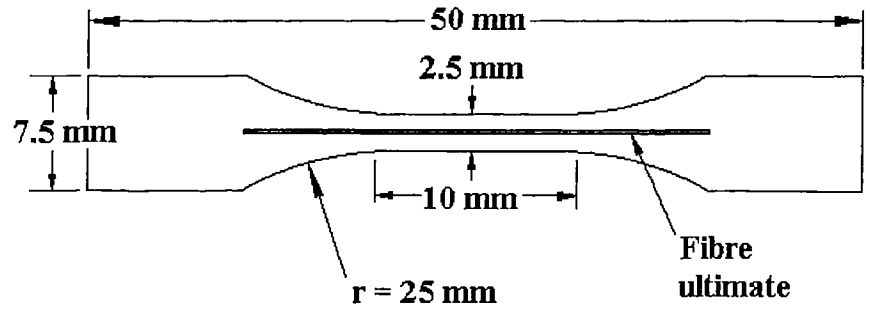

Figure 5.8 Schematic diagram of a single filament composite (*dimensions are approximate*).

Individual fibre ultimates were dried on microscope slides under ambient conditions. Single filament composites (SFCs) were prepared by casting catalysed resin, containing a single hemp fibre ultimate (or bundle), between glass plates. For comparative studies, SFCs reinforced with a single E-glass filament were also prepared. For calibration purposes, un-reinforced polymer specimens were fabricated. The resin was cured for two hours at 50^{O}C. Waisted tensile specimens (Figure 5.8) were cut from the resin film with a fresh razor blade. In this way it proved possible to produce specimens, approximately 150 μm in thickness and 2.5 mm in width, at the necked down portion. The specimens were conditioned at 65% RH and 20^{O}C for at least one month, prior to testing.

5.2.2 Half fringe photoelasticity system

A schematic representation of the HFP system used in this work is shown in Figure 5.9. Plate 5.1 shows the working system (further photographs showing details of the system may be found in Appendix 8). Essentially, the system consisted of a standard circular polariscope, in 'dark-field' set up, operated through an optical microscope (Leitz, 'Laborlux'). The optical response of the photoelastic model was viewed with a monochrome video camera (Sony CCD unit). The video signal was digitised and recorded, using a capture card and associated software (Prolab 'Videoworks' and 'Image folio') and subsequently stored for analysis on PC. The digitised image was composed of 480 by 360 picture elements ('pixels'), each divided into 256 levels of grey (Z values), ranging from 0 (black) to 255 (white). This represents 8-bit resolution. Image analysis was performed using a number of software programmes including 'Optimas' (Bioscan), 'Idrisi for Windows' (Clark Labs for Cartographic Technology and Geographic Analysis, IDRISI Project, at Clark University, USA) and 'Unimap 2000'. The SFCs and clear resin specimens were strained in a miniature tensile rig (PL Thermal Systems 'Minimat'), clamped onto the microscope stage. Control of the tensile frame and data acquisition were by a separate PC.

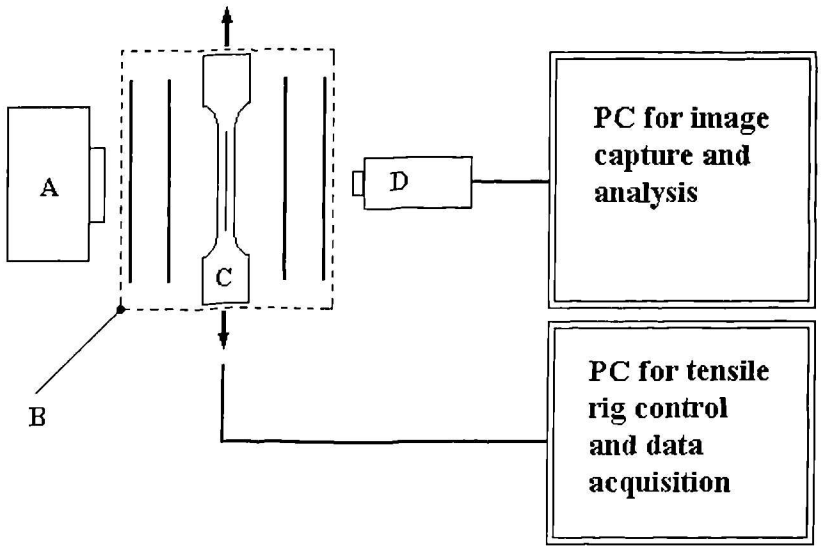

Figure 5.9 Schematic representation of the HFP operating system.

Key: *a)* Monochromatic light source. *b)* Circular polariscope operated through microscope. *c)* Tensile specimens strained in a miniature tensile rig clamped to the microscope stage. *d)* CCD camera.

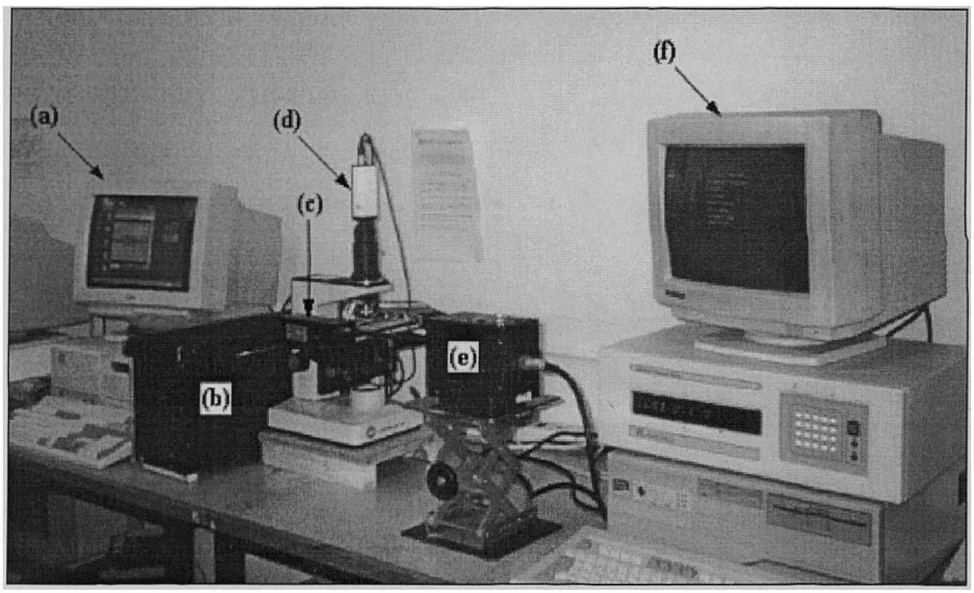

Plate 5.1 Half fringe photoelasticity apparatus.

Key: *a)* PC for image capture and analysis. *b)* Monochromatic light source. *c)* Miniature tensile rig clamped to microscope stage. *d)* CCD unit. *e)* Stepper motor. *f)* PC for tensile rig control and data acquisition.

The monochromatic light source for the circular polariscope consisted of a 55 watt low pressure sodium lamp (standard street lamp) with associated control equipment. This was sited in a purpose built lamp house, painted a flat white on the interior. This lamp replaced the existing white light source of the microscope. The polariser

and first quarter wave plate were sited below the condenser assembly of the microscope, in a specially fabricated mount. The second quarter wave plate and analyser were again provided with a purpose built mount and sited above the objective lens. The polariser, quarter wave plates and analyser were carefully aligned for 'dark-field' set up before final mounting. This was necessary as no means were available to accurately rotate the wave plates and polarisers relative to one another, once mounted in the microscope. Indirectly, this led to an alternative calibration procedure, to the ones described in the HFP literature, being adopted (see Section 5.3.2). Both polariser and analyser were obtained in the form of 'polaroid' sheet (Polaroid corporation). Quarter wave plates were fabricated from 'retarder' sheet (International Polarizers, Inc.). To obtain circular polarised light, it is necessary to ensure $\lambda/4$ retardation with a wave plate suitable for the particular wavelength of the monochromatic light being used (the use of white light results in elliptically polarised light due to the different wavelengths constituting white light). Since sodium light ($\lambda = 589.6$ nm) was used, it was necessary to obtain retarder sheet giving $\lambda/4$ retardation at the same wavelength. The retarder sheet used nominally gave $\lambda/4$ retardation at 560 nm, but nonetheless, this was deemed satisfactory since there was a range of wavelengths over which the retarder sheet gave the required retardation (International polarizers Inc., 1998). The assembly, comprising, light source, polariser, two quarter wave plates and analyser constituted the standard arrangement for a circular polariscope (see Figure 5.6).

Due to the relatively low light intensity of the sodium light source, it was found that it was not possible to use the polariscope at high magnification. However, this did not prove problematic since at higher magnifications it proved difficult to satisfactorily focus on the desired region of the specimen. In the event, the system was calibrated and set up to operate using a x4 objective lens, giving good results.

The photoelastic sample under consideration, as indicated, was loaded using a miniature tensile testing frame, located on the microscope viewing stage in such a way that adjustment in the X, Y and Z planes was possible. The 'Minimat' was equipped with a 20 N load cell (beam). Load data were acquired by PC. Cross-head movement was achieved using a stepper motor, again controlled from the PC. Cross-

head displacement was measured from the stepper motor increments. The tensile specimens used were gripped in specially fabricated clamps.

5.2.3 Testing

5.2.3.1 Calibration specimens

The thickness of clear resin specimens at the necked down portion was measured to 0.01 mm with a dial micrometer. The width of the specimens in the necked down region was measured optically, under a microscope (Letiz Wetzlar), by means of calibrated graduations.

The specimens were located in the 'Minimat' in such a way that the imaged area was sited in the centre of the sample. This was to ensure that the imaged region (using a x4 objective lens) did not include, and was remote from, the edges of the specimen, thereby rendering it free from any residual birefingence imparted to the specimen during preparation (cutting), which might otherwise have affected image quality. Furthermore, it was ensured, as far as possible, that the imaged area was free from any debris which would adversely affect image quality and consequently the intensity of the transmitted light emerging from the polariscope. These procedures were adopted with a view to reducing possible calibration errors.

The specimens were then loaded incrementally in tension and the grey level ('Z') value recorded for each increment. Loading was continued until it became apparent that the first half-fringe had been exceeded (i.e. the recorded light intensity had reached a maximum and was beginning to fall-off). At least four clear resin specimens from each batch were tested in order to calibrate the system.

5.2.3.2 Single filament composites

The dimensions of the SFC's were measured in the manner described above. Each specimen was loaded incrementally on the tensile stage. Once a target load had been reached, the photoelastic image was captured and the specimen immediately unloaded. This was done to reduce, as far as possible, any visco-elastic effects. The nominal stress in the specimens was kept as low as possible (<15 MN m^{-2}) so as to reduce, if not totally eliminate, non-linear behaviour of the matrix. Only one image

for each level of loading was captured; averaging of multiple images to eliminate random optical and electrical noise was not undertaken.

5.3 Results and discussion

5.3.1 Photoelastic material selection

The stress-optic law in two dimensions, for a linearly elastic material at normal incidence, provides that relative retardation (Δ) is linearly proportional to the principal stress difference ($\sigma_1 - \sigma_2$). Further, from Equation 5.5 it is observed that Δ is linearly proportional to the sample thickness h and the relative stress-optic coefficient C (a material constant) and is inversely proportional to the wavelength (λ) of monochromatic light used in the polariscope. An ideal photoelastic material would be one in which its stress-optic, strain-optic and stress-strain behaviour were linear, in addition to which, the material should be free from mechanical and optical creep over the time-scale of the photoelastic investigation and be isotropic and homogeneous (Dally & Riley, 1965). Furthermore, the material should be stress-optically sensitive and possess good stiffness to prevent excessive deformation under load. A figure of merit can be associated with each photoelastic material, being the ratio of elastic modulus E to the material fringe value f_σ. Table 5.1 shows a comparison of the approximate properties of typical epoxy and polyester resins (Burger, 1993). Whilst the Young's modulus, limit of proportionality and Poisson's ratio of the two polymers are similar, the material fringe value of epoxy is about half that of polyester, giving epoxies a figure of merit around twice that of polyesters.

Table 5.1 Comparison of mechanical and stress-optical properties of typical thermosetting polyester and epoxy resins (*Source:* Burger, 1993).

Material	*Material fringe value - f_σ (green light, λ =546 nm) ($N\,m^{-1}$)*	*Young's modulus, E ($GN\,m^{-2}$)*	*Proportional limit ($MN\,m^{-2}$)*	*Poisson's ratio*	*Figure of merit (E/f_σ)*
Polyester	24,000	3.9	48	0.35	4000
Epoxy	11,000	3.3	55	0.37	8000

Most polymeric photoelastic materials, including epoxies and polyesters, exhibit linear stress-strain and stress-fringe order behaviour up to a point, but deviate from linearity at higher stresses (Burger, 1993; Dally & Riley, 1965). When these materials are prepared for photoelastic studies, they are usually cast from liquid resin and are generally homogeneous and isotropic (Dally & Riley, 1965). At room temperature, epoxy resins have little tendency to creep; polyester resins, on the other hand, do exhibit some visco-elastic behaviour (Burger, 1993).

For reasons of handling and cutting and the wish to destructively test the specimens, a specimen thickness of around 150 μm was adopted. For calibration purposes, however, it proved necessary to load the specimens to a point at which the first half fringe appeared. Utilising the material properties listed in Table 5.1, substituting in Equation 5.6 and solving for $(\sigma_1 - \sigma_2)$, yields a principal stress difference of around 37 MN m^{-2} at the first half fringe for epoxy resin, whilst for polyester this figure is around 80 MN m^{-2}. Thus with epoxies, the stress difference at the first half fringe is likely to be within the elastic limit of the material (~55 MN m^{-2}) whilst for polyesters it is in all probability beyond the limit of proportionality (~48 MN m^{-2}). This effectively precluded the use of polyesters due to the inability to calibrate the system by the method envisioned. Further, in applications in which the photoelastic model contains cracks or discontinuities with attendant stress concentrations, there is a likelihood of localised non-linear behaviour which must be guarded against. By definition, HFP operates at low levels of birefringence and when used in conjunction with stress-optically sensitive materials, low loads and hence small deformations may be expected with a decreased risk of non-linear behaviour.

Some initial trials were, nevertheless, performed on SFC utilising a polyester matrix. Whilst these showed what appeared to be stress concentrations in the matrix in the vicinity of micro-compressive defects, it became clear that if the stress concentrations were to be quantified successfully, it would be necessary to use an epoxy matrix. In view of its optical sensitivity, and in other respects similarity in mechanical properties to polyesters, it was decided to utilise an epoxy matrix for the remaining photoelastic studies.

5.3.2 Calibration

Essentially, the calibration procedure adopted in this work involved loading a tensile specimen in the HFP apparatus and recording $(\sigma_1 - \sigma_2)$ at known values of N. This procedure is similar to that adopted in classical photoelasticity, wherein the fringe order is noted for various values of applied load. A plot of load against fringe order is then constructed with the slope of the resultant linear plot providing a value for the material fringe value (Dally & Riley, 1965). Due to the aforesaid limitations imposed by specimen dimensions and geometry it was not possible, however, to obtain fringe orders substantially greater than $N = 0.5$. Effectively, this meant that it was impossible to directly construct a plot of N against load. An alternative method would have been to interpolate between $N = 0$ and $N = 0.5$, obtaining values of N by the method of Tardy compensation (Dally & Riley, 1965). Noting the applied tensile stress at different values of 'partial fringe order' thus obtained, would have facilitated the construction of a curve, similar to that derived by the classical method. This would then have enabled the material fringe value to be evaluated. Methods based on this approach have been used in previous HFP studies (e.g. Burger & Voloshin, 1983; Mercado, 1992). In order to operate the method of Tardy compensation, however, it is necessary to accurately align the axes of the optical elements relative to one another. Unfortunately, due to certain limitations of the HFP apparatus used in this work, this was not possible and is considered to be one of the drawbacks of the system in its present form (see also Section 5.4). The method of calibration adopted in this work relied upon locating the first 'half fringe' and measuring, accurately, the principal stress difference at this point (i.e. determining $(\sigma_1 - \sigma_2)$ at $N = 0.5$). Substituting for $(\sigma_1 - \sigma_2)$ and N in Equation 5.6 and solving, enabled the

material fringe value f_σ to be obtained. By repeating this procedure with several specimens it was believed that this yielded a reliable figure for the material fringe value.

As detailed in Section 5.2.3, calibration of the HFP system involved incrementally loading clear resin tensile specimens and noting the grey level value recorded by the video camera for each increment. The theoretical two dimensional principal stress difference $(\sigma_1 - \sigma_2)$ in a tensile specimen is given by the tensile stress (σ_1) alone (assuming the normal components of stress are zero). Thus:

$$\sigma_1 = \frac{P}{wt} \qquad \text{and} \qquad \sigma_2 = 0 \qquad \text{gives:} \quad (\sigma_1 - \sigma_2) = \frac{P}{wt}$$

In practice, however, obtaining perfect alignment of the specimen in the grips was difficult to achieve. This, in all probability, led to the incorporation of some bending moment resulting in a non zero value for σ_2. To reduce, if not eliminate the effects of this problem, the tensile specimens were very carefully loaded onto the tensile stage. Furthermore, each specimen was positioned in the polariscope such that the image was recorded as near to the midspan of the necked down portion and as near to the centreline as possible, thereby reducing edge effects and any influence from the 'shoulders' of the specimen. A plot of light intensity recorded along a line perpendicular to the applied load, traversing a typical image recorded for calibration purposes is shown in Figure 5.10. It can be observed that there is some fluctuation in the light intensity from one side of the image to the other (indicating the application of a bending moment). However, as the image intensity (grey level) is taken as the mean value for the whole image (480 x 360 pixels) rather than discrete points, it was believed that such discrepancies would be averaged out. In addition to the method of loading causing variations in the amount of birefringence, other factors may well have influenced the overall image intensity. For instance, it cannot be ruled out that there may have been variations in the thickness of the specimens. Furthermore, uneven lighting and imperfect optical elements (microscope optics, polarisers and wave plates) may all have contributed to variations in image intensity. Nevertheless, the recorded grey level versus applied stress plots (see below) gave excellent correlations between the two variables.

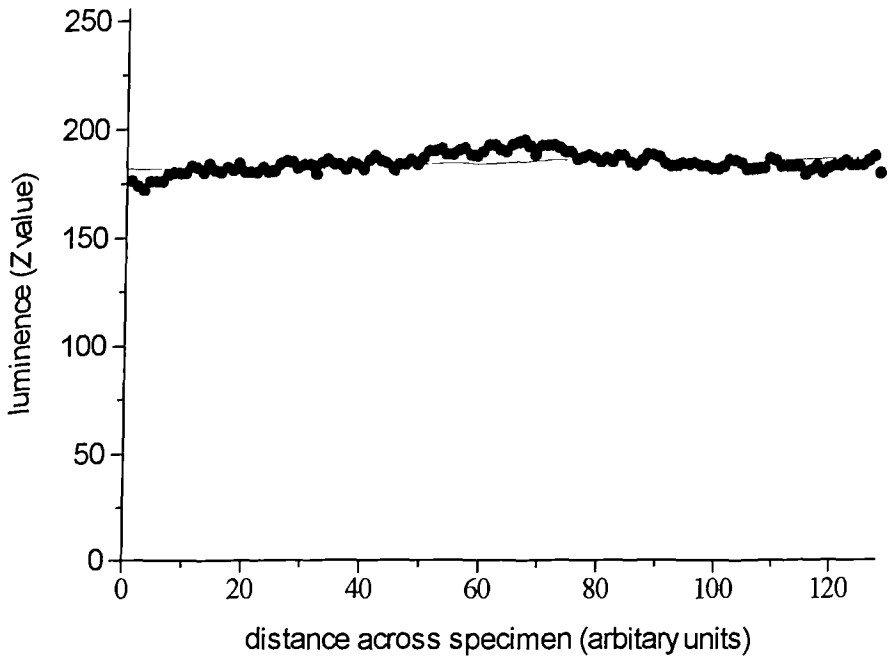

Figure 5.10 The recorded light intensity traversing loaded, unreinforced polymer tensile specimen.

A typical stress-strain curve for a clear epoxy micro-tensile specimen used in this work is presented in Figure 5.11. As can be seen, the initial portion of the curve is essentially linear. However, once a tensile stress of approximately 25 MN m^{-2} was reached, the behaviour appeared to depart from linearity. It is believed that in this instance, the limit of proportionality was in the region of 25 MN m^{-2}. In subsequent testing of reinforced specimens, efforts were taken to ensure that stress levels in the photoelastic model did not exceed this value.

Nevertheless, the principal stress difference versus optical response (grey level value - *Z*) plot, shown in Figure 5.12, indicated that the maximum light intensity transmitted through the polariscope occurred, in this particular specimen, at a stress of around 32 MN m^{-2}. Due to the variation in the thickness between specimens (with a consequent variation in relative retardation), the peak value of *Z* generally occurred at values of between 30 MN m^{-2} and 40 MN m^{-2}. It might therefore be expected that at higher stresses, a certain degree of departure from linearity may have occurred (see below).

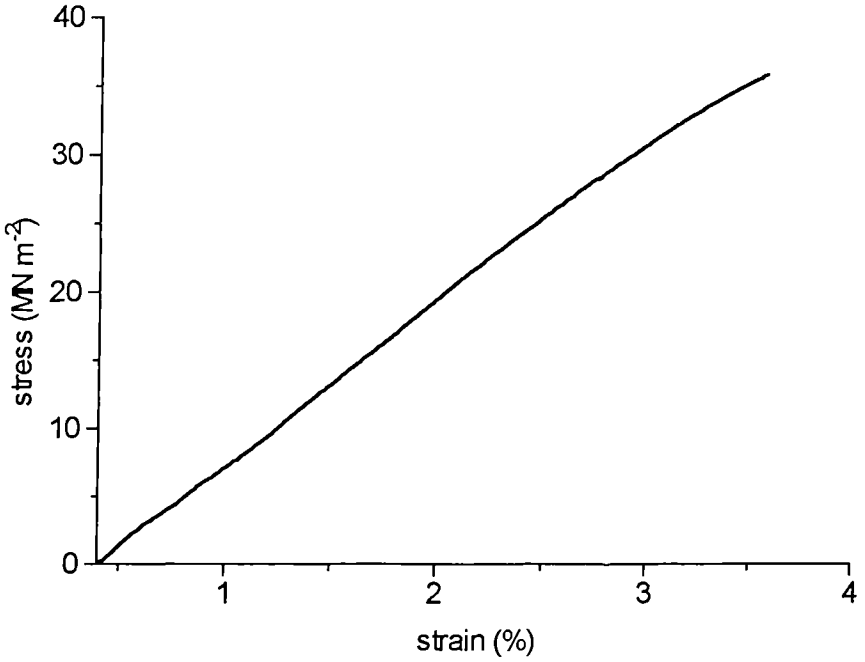

Figure 5.11 A typical stress-strain curve for an unreinforced epoxy micro-tensile specimen.

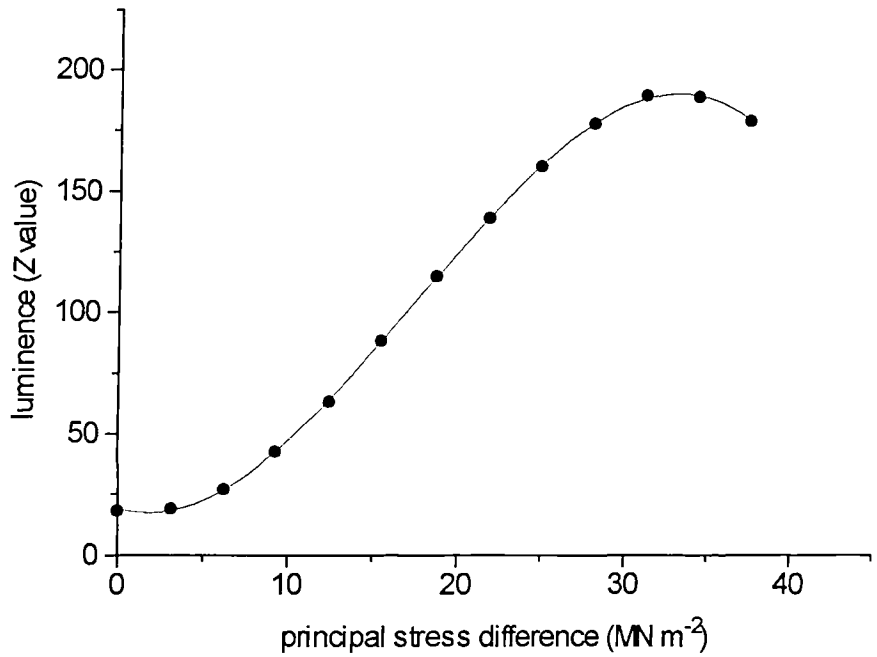

Figure 5.12 A typical stress-optical response of a micro-tensile specimen.

As stated, calibration of the system relied upon determining the principal stress difference at $N = 0.5$. This was achieved by plotting $(\sigma_1 - \sigma_2)$ versus Z values and fitting a suitable function to this data (see Appendix 9). From the theory, a sine square relationship would be expected. However, it was found that a third order polynomial could be applied with some accuracy to the data and R^2 values better than 99.9% were always achieved. The form of the applied function was, to a large extent, unimportant since the main purpose of this curve fitting exercise was simply to determine $(\sigma_1 - \sigma_2)$ at the peak value of Z (i.e. at $N = 0.5$) and to derive maximum and minimum values for Z. Differentiation of Z (y variable) with respect to principal stress difference (x variable) and solving $dy/dx = 0$, provides values for x at the maximum and minimum values of Z. Substitution for x gives numerical values for Z. These values were used later in the calibration process to correct measured Z, since there was a finite, rather than zero, intensity of transmitted light emerging from the polariscope with the specimen under zero load. It is believed that this phenomenon was due to flaws in the optical elements and imperfect alignment, rather than birefringence of the photoelastic model itself, since the same phenomenon was observed without the specimen installed in the apparatus. Substitution in Equation 5.6 for $(\sigma_1 - \sigma_2)$ at the maximum value of Z and solving, provides a value for f_σ. The material fringe value was determined for each batch of specimens at the time of conducting the investigations, as this material property can vary according to resin composition, curing conditions etc. (Burger, 1993). Typically, for epoxy cured at $50^{\circ}C$ for two hours and tested a month or so after casting, a value of around 11 KN m^{-1} was obtained. An example of the calculation of material fringe value f_σ is provided in Appendix 9. The values obtained for f_σ were in good agreement with those reported in the literature (Burger, 1993). Examples of the calculations adopted in order to determine f_σ and γ appear in Appendix 9.

To complete the calibration procedure, it was necessary to determine a value for the camera sensitivity (γ). Rearrangement of Equation 5.6 and substitution for $N\pi$ in Equation 5.15 yields the following relationship:

$$\log\left(\frac{Z}{Z_{max}}\right) = \gamma \log\left\{\sin^2\left[\frac{h(\sigma_1 - \sigma_2)\pi}{f_\sigma}\right]\right\} \qquad (5.18)$$

Utilising Equation 5.18, γ was determined from the slope of a $\log\left(\frac{Z}{Z_{max}}\right)$ versus $\log\left\{\sin^2\left[\frac{h(\sigma_1 - \sigma_2)\pi}{f_\sigma}\right]\right\}$ plot. It should be noted that the values of Z and Z_{max} were corrected by the subtraction of the minimum value of Z. Excellent linear relationships were obtained (see Appendix 9) with R^2 values better than 99% being normal. A value of 1.12 was derived for the camera sensitivity.

Once f_σ and γ were obtained, it was possible to determine the fringe order, N, directly from the 'Z' value utilising the relationship given by Equation 5.17. Further, by substitution of the acquired value for N, together with f_σ and the specimen thickness, into Equation 5.6, the principal stress difference could be obtained. If average values of f_σ and γ are used to predict N from the recorded Z values, and a plot of derived partial fringe order versus calculated stress (Figure 5.13.) is drawn, then an excellent linear relationship is obtained. It should be noted from Figure 5.13 that data points with fringe orders in excess of 0.5 have been plotted. These were obtained for stress differences greater than that at N = 0.5, by adding the difference between the derived fringe order and the half order fringe to the latter. This required manipulation of data beyond the half order fringe and was done purely to investigate whether the relationship between $(\sigma_1 - \sigma_2)$ and N remained linear at stresses beyond N = 0.5. It can be observed that this was so, indicating that the stress-optic relationship was linear, at least within the operating range of HFP.

A comparison between the principal stress difference derived from the image intensity (Z value) and that calculated directly from the applied load and specimen dimensions is shown in figure 5.14. A good correlation was apparent between the two variables, suggesting that good repeatability might be expected. It may be noted that there was not an exact match between the derived stress and tensile stress (since

the slope of the curve is less than unity). However, this may well be within the range of experimental error.

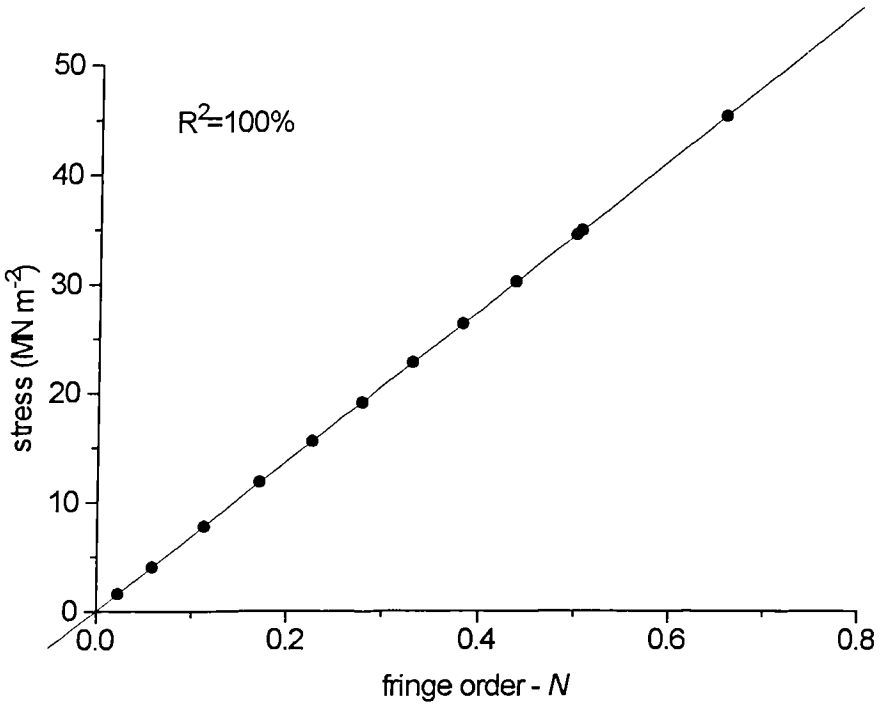

Figure 5.13 Variation of derived fringe order with applied stress.

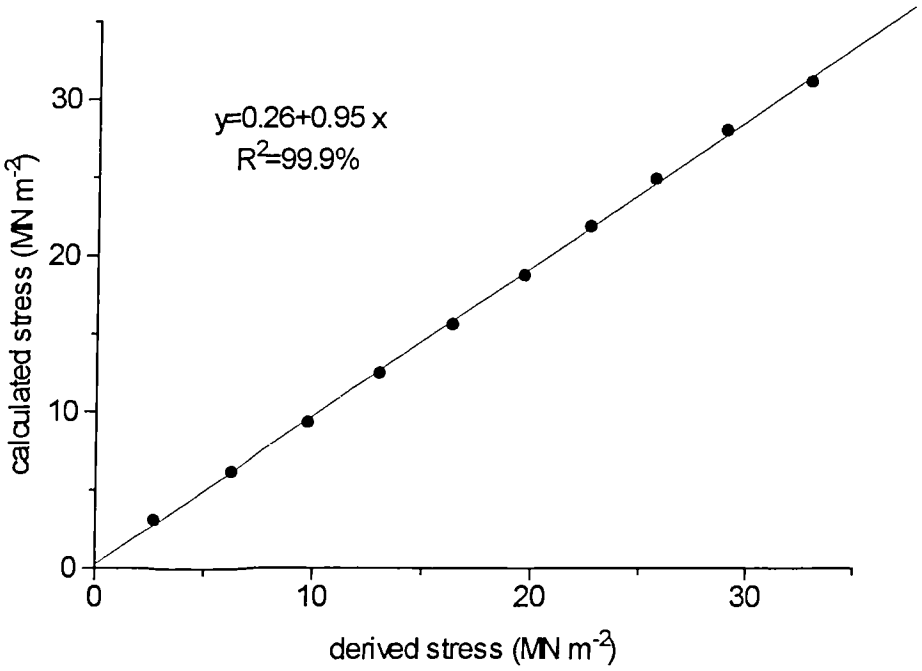

Figure 5.14 Relationship between $(\sigma_1 - \sigma_2)$ derived from Z and calculated (tensile) stress.

With f_σ and γ determined, N and consequently $(\sigma_1 - \sigma_2)$ were derived for each pixel in the image by applying Equation 5.17 to the Z value of each pixel by the use of a mathematical operator incorporated in the image analysis software. For the purpose of performing this operation, 'Idrisi for Windows' software was utilised. In practice, regions of interest were selected and the function applied to these areas only. A further programme, 'UNIMAP 2000', was used to map N and $(\sigma_1 - \sigma_2)$ over the entire region of interest of the image.

5.3.3. Demonstration of technique

By way of demonstration, Plate 5.2 shows a grey-scale image of the photoelastic response around a circular hole in an epoxy resin film (resulting from an included bubble in the liquid resin) when viewed through the circular polariscope. The film was under uniaxial tension acting in the plane of the image, normal to the line A--B, to a nominal far field stress of around 8 MPa. Since the resin film was thin (~150 μm) in comparison to other specimen dimensions, conditions of plane stress were believed to prevail. Figure 5.15 represents the principal stress difference $(\sigma_1 - \sigma_2)$ derived from the acquired Z value along the line A--B.

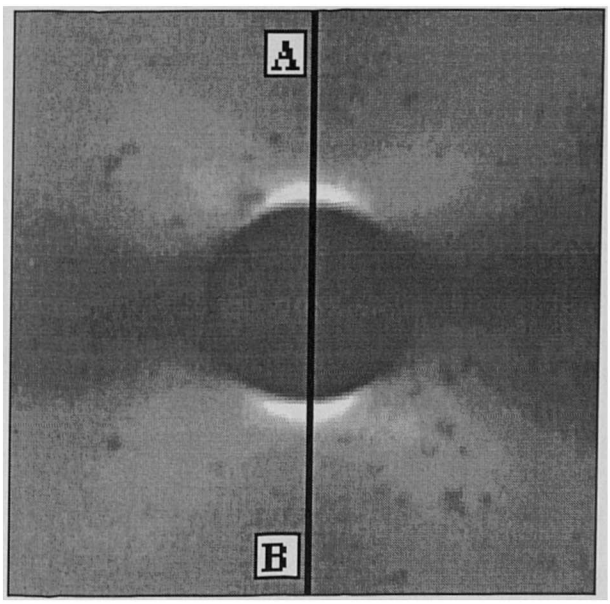

Plate 5.2 Birefringence in an epoxy resin film around a circular hole (*circular polarised light*).

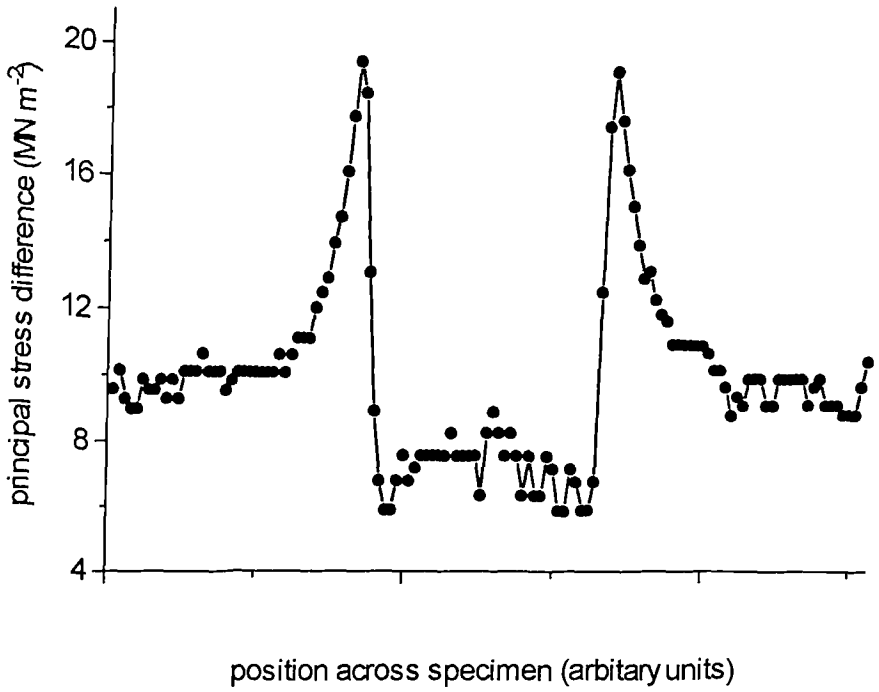

Figure 5.15 Principal stress difference along a line (A--B) perpendicular to the applied tensile load, traversing the hole at the maximum diameter.

It can be observed that the principal stress difference reached a maximum at a point close to where the line A--B intersects the hole contour. Here, $(\sigma_1 - \sigma_2)$ rises dramatically. A stress concentration factor K, can be identified, defined as follows:

$$K = \frac{(\sigma_1 - \sigma_2)_{max}}{(\sigma_1 - \sigma_2)_{min}} \qquad (5.19)$$

The maximum principal stress difference referred to in Equation 5.19, corresponds to the maximum stress difference obtained through birefringence analysis whilst the minimum value is the 'far-field' matrix stress (again derived through birefringence analysis). In this instance, the experimentally derived value for K was around 2.3. This compares with a theoretical K of 3.0 for a circular hole ('Kirsch solution') in an infinite elastic plate subject to uniaxial tension (Parton, 1992). The observation of a reduced K value is consistent with the findings of previous workers using photoelastic techniques to investigate stress concentrations and may be explained by

the fact that, in this case, the diameter of the hole was relatively large in comparison to the width of the specimen (Boresi *et al*, 1993). Figure 5.16 shows a contour map of the derived partial fringes around the hole.

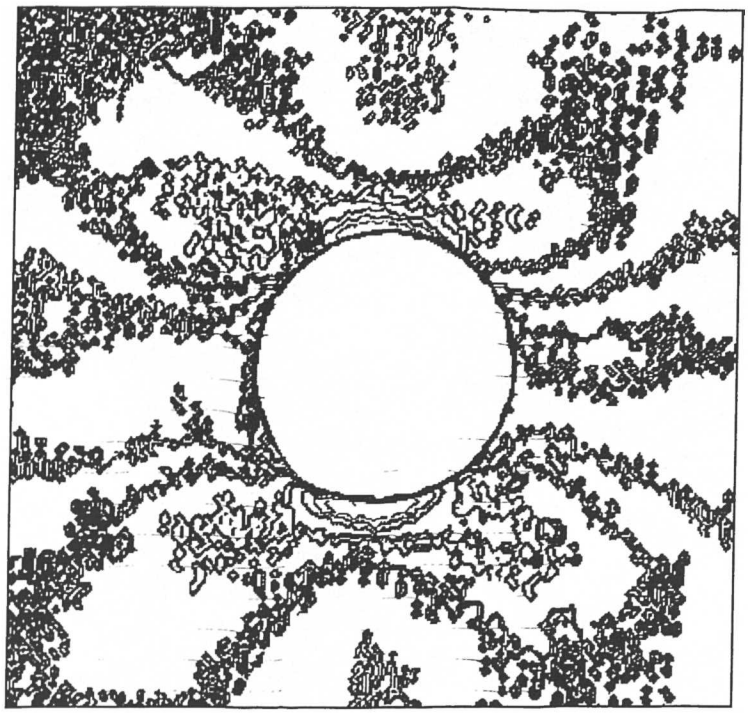

Figure 5.16 Contour map of partial fringe orders around a circular hole in a polymer film obtained with half fringe photoelasticity.

The original images were captured in a 480 by 360 pixel format. The optical magnification (x4 objective) was kept relatively low, in order to ensure good focus on the fibre-matrix interface. Furthermore, it was necessary to keep the magnification fairly low because of the relatively poor intensity of the light source. Consequently, 'zooming' in on a particular feature was achieved by selecting the region of interest in the acquired image and enlarging this area. As a result, if high magnifications were required, the image became 'blocky' in appearance due to the pixel dimensions becoming significant. Nevertheless, for most purposes, when operated in this manner the system was found to be satisfactory.

These results demonstrated the ability of HFP to experimentally measure $(\sigma_1 - \sigma_2)$ in a polymeric matrix, provided that the relative retardation remained within the bounds $0 > N > 0.5$ and that due account was taken of any non-linear behaviour.

5.3.4 Matrix stress field in the vicinity of micro-compressive defects

In previous chapters, the lack of toughness exhibited by vegetable fibre reinforced composites was highlighted as being potentially one of the factors severely limiting their use in structural or semi-structural applications. In Chapter 4, the influence of micro-compressive defects found in these fibres was discussed in relation to the mechanical properties of the fibres themselves. The primary aim of the work presented in this chapter, was to investigate the influence that these micro-compressive defects have upon the deformation and fracture behaviour of bast fibre reinforced polymer matrix composites. This was achieved by looking specifically at the interaction between fibre defect and the matrix, in a model composite system. It was believed that the simplest model would be a single fibre composite (SFC) loaded in tension parallel to the axis of the fibre. It was hypothesised that a change in the morphology of the fibre at the micro-compressions, together with an heterogeneous strain distribution at the surface and within the fibre at these points, could lead to concentrations of stress in the matrix in the vicinity of the defects. It was believed that such stress concentrations could initiate localised rupture of the matrix and might possibly contribute to the overall failure of the composite.

Plate 5.3. shows a typical micro-compressive defect in a single hemp fibre ultimate embedded in an epoxy resin matrix (SFC). When the SFC was strained, the recorded photoelastic response was used to examine the stress field surrounding the micro-compressive feature. The simplest manner in which the stress field (principal stress difference) could be visualised was to view the photoelastic effect observed in the matrix. Plate 5.4 shows the birefringence pattern observed in the epoxy matrix surrounding the micro-compressive defect shown in the Plate 5.3, when the SFC was loaded to a nominal tensile stress in the laminate of around 15 MN m^{-2}. To assist in visualisation, the image has been enhanced by applying 'pseudo-colour' (which was subsequently converted to grey scale).

What is discernible is a distinct pattern of stress in the matrix surrounding the micro-compressive defect when the SFC was strained. This looks somewhat akin to the pattern observed previously in the vicinity of a circular hole in a resin film under uniaxial tension. Nevertheless, whilst this method does show that concentrations of

stress appear in the matrix around micro-defects, what is not evident is the magnitude of the stress concentration, nor the severity of the stress gradient.

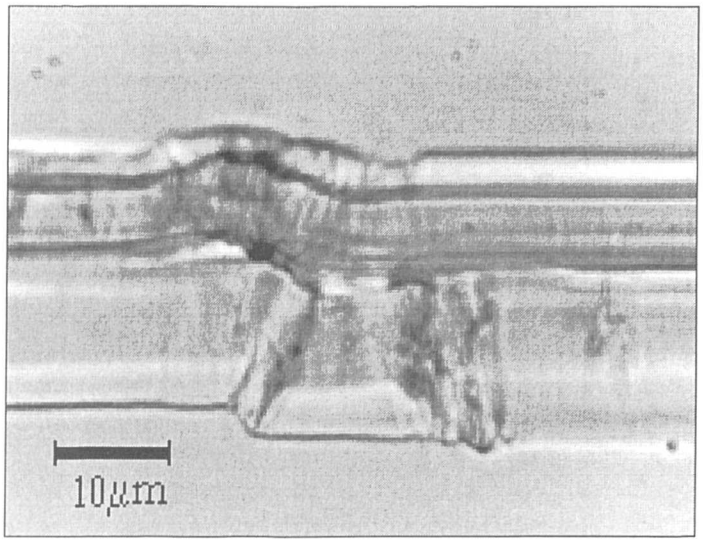

Plate 5.3 Micro-compressive defect in a hemp fibre ultimate embedded in an epoxy matrix. (ordinary white light x400 magnification).

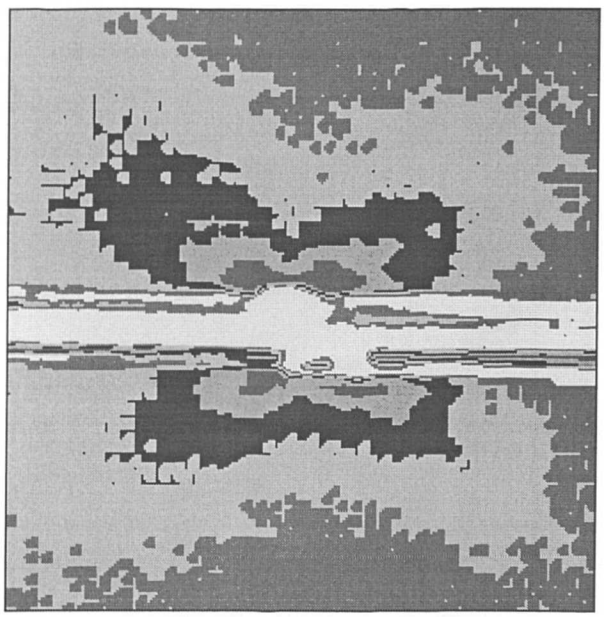

Plate 5.4 Grey-scale adjusted 'pseudo-colour' image showing the birefringence pattern in an epoxy matrix in the vicinity of a micro-compressive defect.

By utilising the calibration procedure described in Section 5.3.2, a pixel by pixel conversion of the luminance (grey level) value to 'partial fringe order' (or principal stress difference) was conducted. Figure 5.17 provides an illustration of the stress

field in the matrix surrounding the micro-compressive defect shown in Plate 5.3. The contours are loci of equal partial fringe order (isochromatic fringes). In this figure, the fibre ultimate runs from left to right across the image, with the micro-compressive defect situated at the centre. As may be seen, the values of these partial fringe orders ranged from $N \cong 0.23$ remote from the interface, to $N = 0.31$ in close proximity to the defect. This would indicate that a K value of at least 1.4 exists in the matrix in the vicinity of this particular micro-compressive defect.

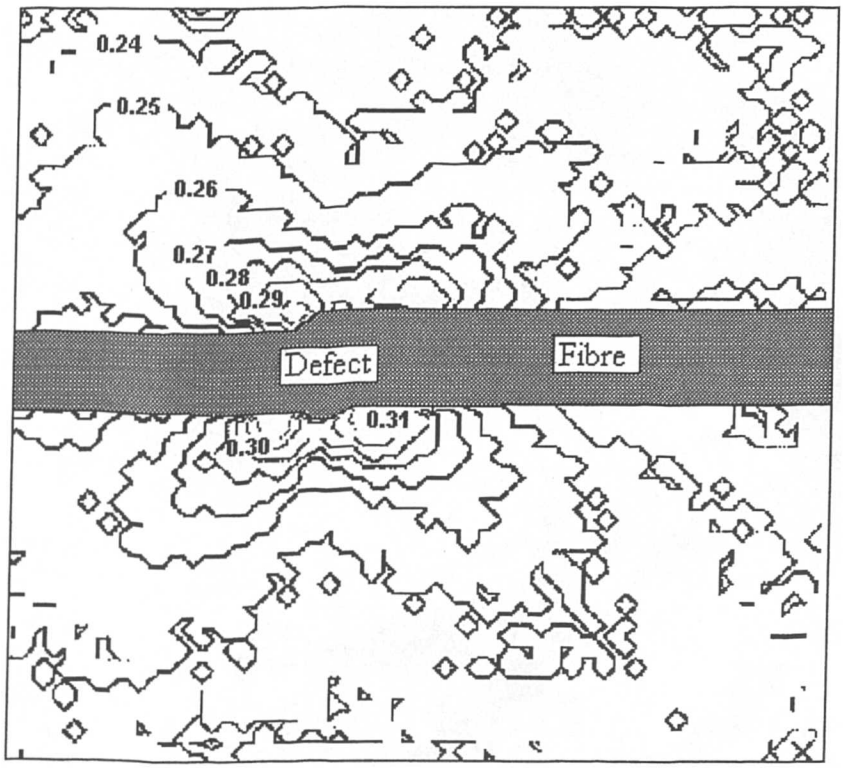

Figure 5.17 Contour map of partial fringe orders around a single micro-compressive defect.

Of particular note is the distribution of the principal stress differences. It may be seen that there is a distinct pattern to the stress distribution, taking the form of an 'X' (similar to the distribution around the hole shown in Plate 5.16). The 'arms' of the 'X' form angles of approximately $\pm 45^{O}$ with the axis of the applied tensile load (parallel to the fibre axis).

As noted previously, a circular polariscope is employed in photoelasticity work since it eliminates the isoclinic fringe pattern leaving only the isochromatics which are

related to the *magnitude* of the principal stress difference $(\sigma_1 - \sigma_2)$. Elimination of the isoclinic fringe pattern means that the effect of the directions in which the principal stresses act are neglected.

It may be shown that in the general case for a planar stressed state, a rectangular element of a plate under the action of normal stresses σ_x and σ_y along the x and y axes and shear stresses τ_{xy} and τ_{yx}, the principal stress difference $(\sigma_1 - \sigma_2)$ is related to shear stress as follows (Parton, 1992):

$$\tau_{xy} = \frac{(\sigma_1 - \sigma_2)}{2} \sin 2\alpha \qquad (5.20)$$

Where: α is the angle of inclination to the normal stresses of the principal stresses.

From Equation 5.20, it may be observed that τ_{xy} will be maximal when α is 45^O. In the case of a bar or plate under uni-axial tension, the axis of one principal stress will coincide with that of the tensile stress (the principal stress normal to this would be zero). Thus the maximum shear stress would act along a plane inclined at $\pm 45^O$ to the principal stress. Ideally, the micro-tensile specimens under investigation in this work may be viewed as being loaded in uni-axial tension. In a pure polymer specimen, therefore, the principal stress difference $(\sigma_1 - \sigma_2)$ may be taken as the tensile stress of the specimen. The maximum shear stress, τ, would therefore be expected to lie at an angle of $\pm 45^O$ to the specimen axis.

In a clear resin tensile specimen, since the shear stresses are equal (theoretically) at all points in the specimen, no optical evidence of an uneven shear stress distribution would be expected. In tensile specimens reinforced with a single hemp ultimate, however, it may be observed that a concentration of stress occurs in the matrix in the vicinity of micro-compressive defects. The distinct pattern of the principal stress difference distribution noted above may therefore be attributed to the observation that the maximum shear stresses occur at $\pm 45^O$ to the specimen axis. The reason for their being observed in the reinforced SFC rather than in the pure resin specimens is

due to the stress gradient in the matrix. This is highlighted in the partial fringe pattern since this is effectively a contour map of equal principal stress differences.

It is interesting to speculate (but not possible to ascertain using this particular analysis) upon the directions in which the principal stresses act in close proximity to the interface. It would seem plausible, based on the above argument, that remote from the interface, σ_1 acts parallel to the direction of the tensile load whilst σ_2 remains zero. However, in close proximity to the interface, particularly in the vicinity of the micro-compression, it is feasible that this is not so. Regrettably, due to limitations of the system in its present form, it was not possible to analyse the isoclinic fringe pattern and so only the magnitude of the principal stress difference may be commented upon with any degree of certainty. Nevertheless, it would be an interesting exercise to develop the system to allow an analysis of stress trajectories to be undertaken.

Another interesting feature of the principal stress difference contour map is the similarity to the theoretical predictions made by the 'Kirsh solution' (Parton, 1992). According to this, the maximum shear stress distribution lies along axes inclined at $\pm 45^{O}$ to a uni-axially applied load. A comparison of Figures 5.16 and 5.17 show a distinct similarity between the two principal stress difference distributions.

Further contour maps of partial fringe order (although the actual fringe orders are not noted on the diagrams) are shown in Appendix 9. Whilst the maps are not as well defined as that shown in Figure 5.17, the distinct patterns appearing in the matrix as described above are readily observed.

Micro-compressive defects can occur frequently (sometimes at intervals of only one fibre diameter along the fibre length) in many bast fibres (see previous chapter) and this has implications for the stress distribution along the length of the fibre. Figure 5.18 shows a contour map of the principal stress difference in the matrix in the vicinity of two relatively closely spaced micro-compressive features in a hemp fibre ultimate.

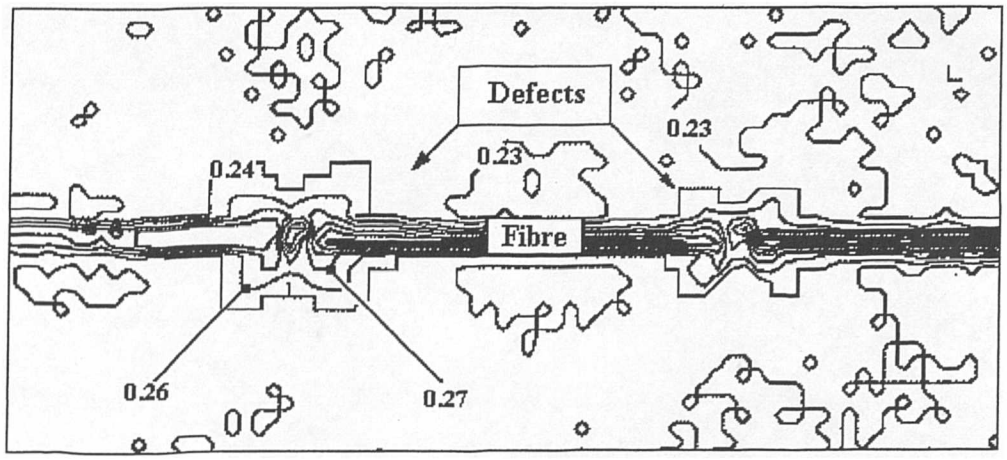

Figure 5.18 Contour map of partial fringes surrounding two micro-compressive features in close proximity to one another.

5.3.5 Principal stress difference distribution

Another way in which the optical data may be interpreted, is by evaluating the principal stress difference along the interface, or rather the principal stress difference in the matrix in close proximity to the true interface. This concept is shown schematically in Figure 5.19. In addition to recording the matrix principal stress difference along this 'interface' (the 'interface' in this instance refers to the line A-B, within the matrix but in close proximity to the true fibre-matrix interface), in a number of the examples shown below, the principal stress difference is also recorded along lines parallel to the true interface, but at a discrete distance remote from it (Figure 5.19). It is worthwhile noting that the abscissa scale is in 'fibre diameters' rather than absolute values. In this way it is possible to immediately view the figure in terms of aspect ratio. Furthermore, the principal stress differences at discrete distances from the interface have also been obtained at multiples of the fibre diameter (0.25, 0.5, 1.0) and are thus more readily visualised. Since principal stress difference is related to shear stress (Equation 5.20), this interpretation should provide a measure of the shear stress distribution along this 'interface'. It was hoped that this approach would allow some inference regarding the true interfacial shear stress distribution to be made, in the expectation of providing some insight into the stress transfer mechanisms operative in such systems.

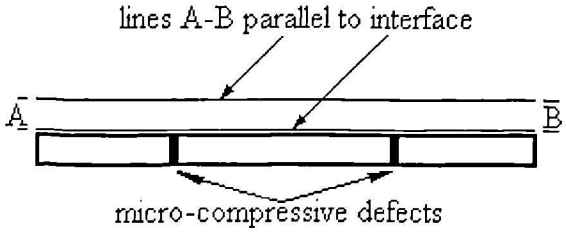

Figure 5.19 Schematic representation of position of data acquisition along fibre length.

Plate 5.5 shows a hemp fibre bundle (technical fibre) embedded in an epoxy matrix. As noted in the previous chapter, both fibre ultimates (single cells) and bundles exhibit micro-compressive damage. Since the latter are generally used as reinforcing media, it was felt appropriate to investigate both fibre forms. In this plate, three micro-compressive defects are readily observed as dark bands traversing the fibre. The defect to the right of the image in fact appears to be a 'minute compression failure', as described in the previous chapter. The SFC has been loaded to a nominal tensile stress of approximately 16.5 MN m^{-2} and a distinct pattern of birefringence may be observed. It should be noted that this and a number of the following images were digitally enhanced to make the pattern more distinct. However, the stress analyses were based upon the original unaltered optical data. Figure 5.20 depicts the principal stress difference in the matrix along the 'interface'.

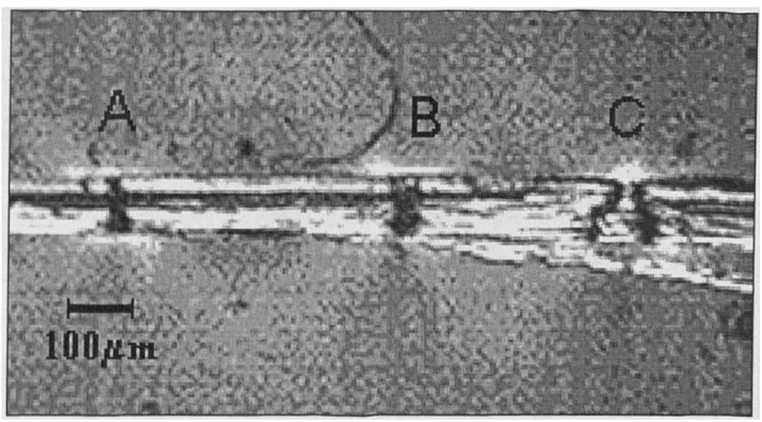

Plate 5.5 Grey-scale representation of the birefringence pattern in an epoxy matrix surrounding three micro-compressive defects in a hemp fibre bundle. Nominal tensile stress 16.5 MN m^{-2} (*circular polarised light*).

It is readily apparent from Figure 5.20 that the distribution of stress along the 'interface' was extremely uneven, peaking in the vicinity of the defects. In the region of the defect on the right hand side of the image, the maximum stress is recorded, resulting in a stress concentration factor of approximately 1.64 (where the nominal stress is taken to be the far-field stress derived through optical means rather than the tensile stress obtained by considering the load on the specimen and its geometry - see below). This value for K is somewhat higher than that recorded in Figure 5.17. Higher values for K would be expected using this method since the optical data is taken along a line parallel with the true fibre-matrix interface and in very close proximity to it. As such, this method would undoubtedly include optical data from the more highly stressed regions adjacent to the interface, rather than at a discrete distance remote from it. As such, this method may well provide a more realistic estimate of K. Nevertheless, the system is limited by the resolution of the camera and by the optical magnification possible. At this juncture, however, a word of caution should be introduced, in that possible non-linear behaviour may occur very close to the interface and also the condition that $0>N>\pi/2$ may be violated. These would undoubtedly have introduced errors into the analysis.

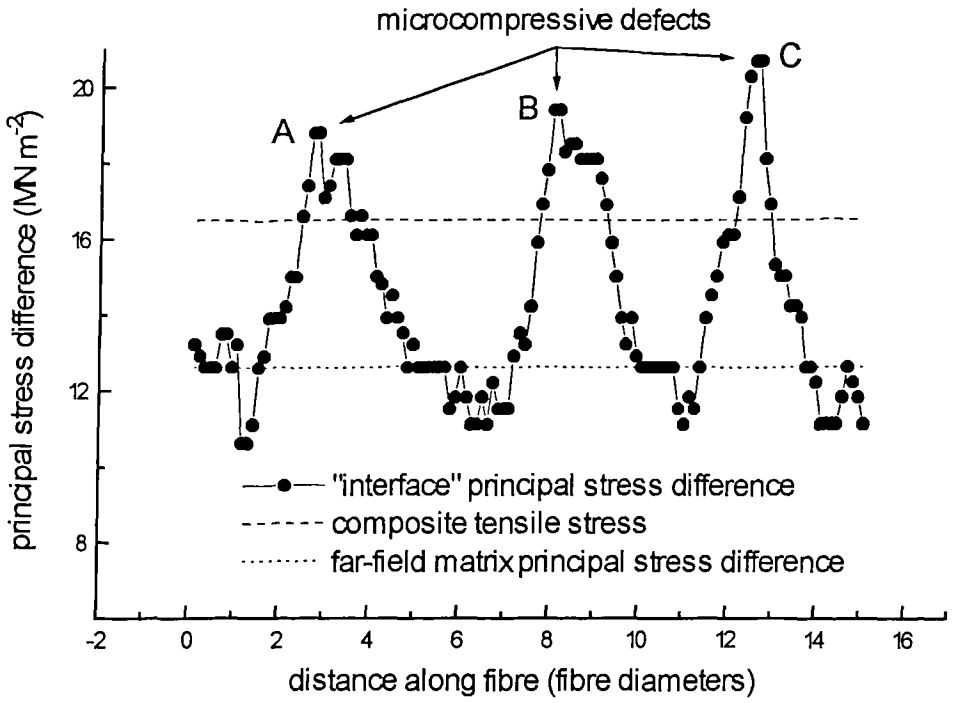

Figure 5.20 Plot of principal stress difference as a function of the distance along the fibre (*measured in fibre diameters*).

It may be noted from Figure 5.20 that the regions where the matrix principal stress difference rises above that of the nominal stress in the matrix appears to be a fairly localised phenomenon. It may be observed that the maximum stress diminishes to the nominal stress in a little over one fibre diameter. Furthermore, it may be noted that the 'interface' stress, as calculated in this manner, drops below the nominal far-field stress. This aspect is discussed further below.

One point of note is that the plot of stress difference has a decidedly 'jagged' profile, with a number of minor peaks and troughs evident. This proved to be a common feature in practically all the plots obtained through this method. It is believed that the principal reason for this was optical 'noise' caused by dust and other detritus, either encapsulated in the resin during fabrication of the SFCs, or trapped on the optical elements of the system. Additional factors contributing to this 'noise' were thought to be unevenness of the illumination system and optical elements. Extreme care during manufacture of the SFCs in a 'clean' environment would in all probability assist in limiting this effect, as would regular and thorough cleaning of all the optical elements of the polariscope and microscope system. Likewise, operating the system in a sterile environment would also probably be beneficial. As for the illumination system and polarising elements themselves, these were of a fairly rudimentary construction and no doubt improvements made here would be of benefit. Another aspect which should be taken into account is possible random electrical 'noise'. This too could affect image quality and subsequent stress analysis. By averaging several images this could be alleviated (Voloshin & Burger, 1983). It is believed that by utilising higher optical magnification, far more detailed stress analysis could be undertaken and the effects of optical 'noise' reduced. However, for this to be achieved, the illumination system would have to be improved.

It should be possible, using suitable digital image analysis software, to remove some of the optical 'noise'. However, this method would need to be used with a degree of caution, as it could lead to erroneous stress analysis. Nevertheless, it is felt that from the experimental data obtained, it is possible to discern the broad pattern of principal stress difference in the matrix and to make certain predictions about the micro-mechanical behaviour of SFCs.

Plate 5.6 shows two micro-compressive defects in a hemp fibre bundle reinforcing an epoxy matrix (once again this image has been enhanced for the sake of clarity). The SFC was loaded to a nominal stress of approximately 24.7 MN m^{-2}. Figure 5.21 is a plot of the principal stress difference between the micro-compressive defects, not only adjacent to the interface as shown in the previous example, but also along lines parallel to the interface situated 0.25 and 0.5 fibre diameters remote from the fibre-matrix interface.

The plot of principal stress difference along the 'interface' shows that a maximum stress concentration factor of approximately 1.6 occurs in the matrix in the vicinity of the micro-compressive defects. As in the previous example, the stress rapidly reduces from the maximum value to that of the nominal matrix stress, within around one fibre diameter of the micro-compressive defect.

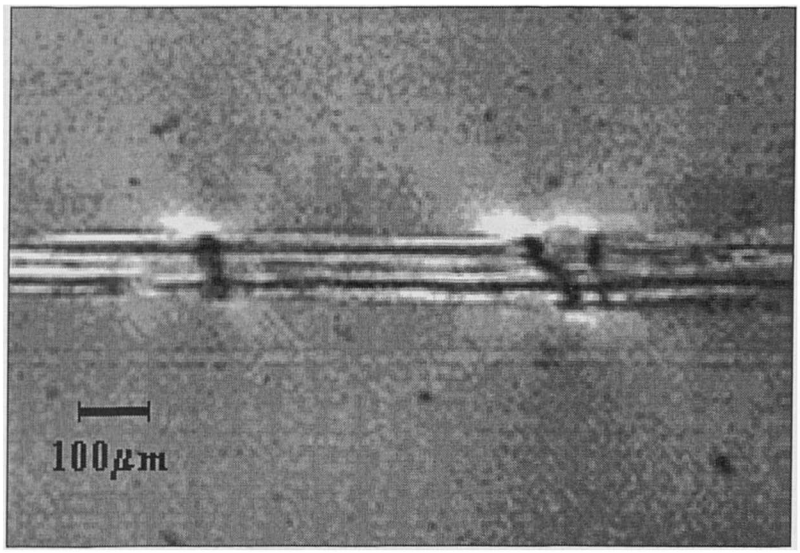

Plate 5.6 Two micro-compressive defects situated in a hemp fibre bundle embedded in an epoxy matrix. Nominal tensile stress 24.7 MN m^{-2} (*circular polarised light*).

If the defect on the right hand side of the image only is considered, then it may be observed that at 0.25 fibre diameters away from the interface, K has reduced to 1.32, whilst at 0.5 fibre diameters this has reduced still further to 1.14. This would indicate that the stress concentrating effects of the micro-compressive defects are quite localised and rapidly diminish with distance; in other words there is a large stress gradient in the matrix in the vicinity of the micro-compressive defect. A plot

of the variation of K with radial distance from the interface is presented in Figure 5.22.

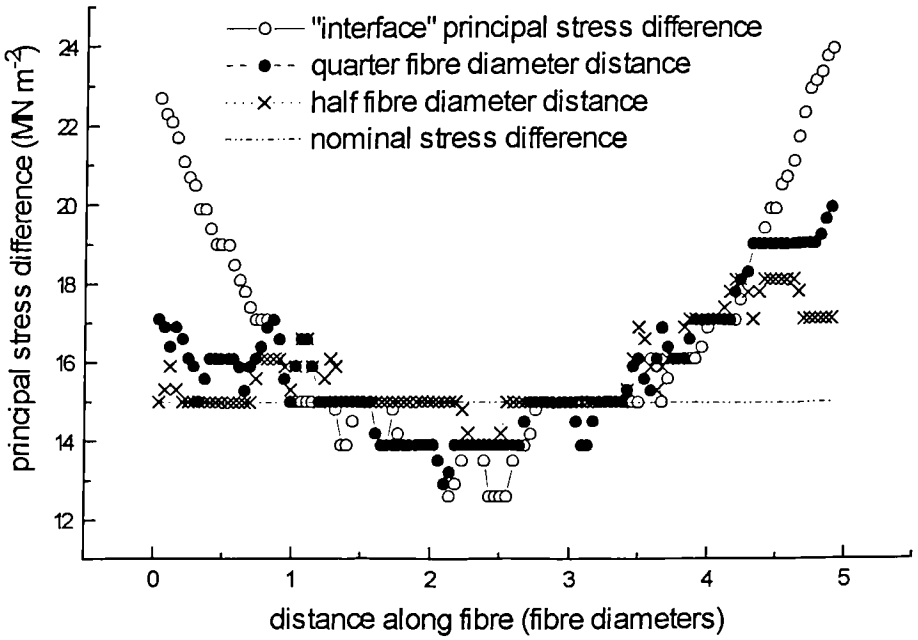

Figure 5.21 Plot of principal stress differences along lines between the two micro-compressive features shown in Plate 5.6, *a)* along the 'interface', *b)* at one quarter fibre diameter from the interface and *c)* at one half fibre diameter from the interface.

From Figure 5.22, it would appear that at only around 0.3 fibre diameters removed from the interface, the matrix stress concentration has reduced to half the maximum and that at one fibre diameter from the interface, this has reduced still further and is barely greater than the nominal far-field stress.

It would again appear as though midway between the two defects, the 'interface' principal stress difference drops to below that of the nominal (far-field) stress. It is, however, uncertain whether this is in fact truly the case or if it is the result of optical noise. Nevertheless, such a behaviour might not be unexpected and may be rationalised in the following manner. If it is assumed that the fibre has a certain 'effective' modulus, E_{eff}, relating to the 'overall' stiffness response of the fibre, but that straining is heterogeneous, then it may be postulated that in certain localised

areas (such as at micro-compressive defects) the modulus is reduced to E_{defect} (where $E_{eff} > E_{defect}$). However, to give the resultant overall stiffness E_{eff}, the undamaged section of the fibre would need to have a stiffness, $E_{undamaged}$, higher than that of the effective fibre modulus. Thus, the condition $E_{undamaged} > E_{eff} > E_{defect}$ would exist. It might be expected that remote from the fibre-matrix interface, the straining characteristics of the SFC would be dominated by the overall elastic response of the fibre (since, as has been discussed above, the stress concentrating effects of micro-compressive defects appear to be a localised phenomenon). Therefore, the matrix might be expected to undergo greater strain remote from the interface than it would in close proximity to sections of undamaged fibre where the greater stiffness of the fibre might be expected to dominate straining behaviour. This may, indirectly, provide confirmation that the straining characteristics of the fibre are, truly, heterogeneous. The above hypothesis assumes that the behaviour of the composite remains elastic and that there is no slippage at the interface.

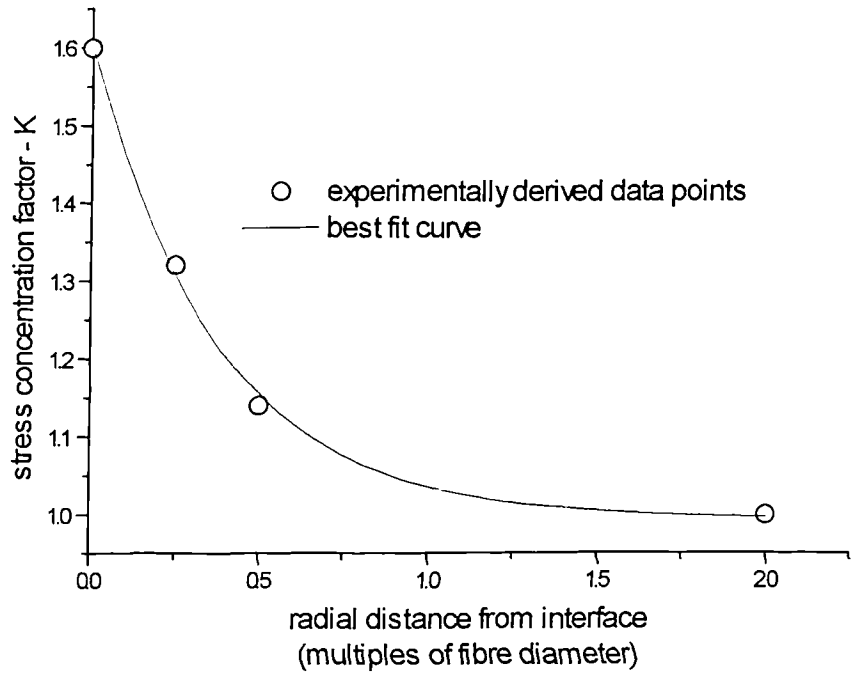

Figure 5.22 Variation of stress concentration factor - K, with radial distance from the fibre-matrix interface for the micro-compressive defect shown on the right hand side of Plate 5.6.

As a means of confirming the above, the stress distribution along a fibre having a homogeneous modulus (E-glass) was evaluated (Figure 5.23). A photomicrograph (once again digitally enhanced) of a single glass fibre, approximately 15 μm in diameter, embedded in an epoxy matrix and loaded to a nominal composite (SFC) tensile stress of approximately 25.8 MN m^{-2} is shown in Plate 5.7.

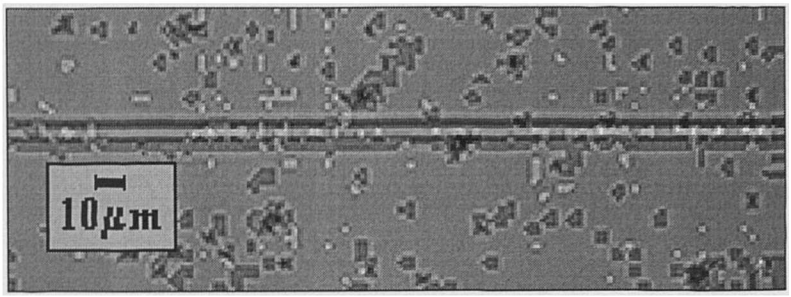

Plate 5.7 Photomicrograph of an E-glass fibre reinforced SFC loaded to approximately 25.8 MN m^{-2} (*circular polarised light*).

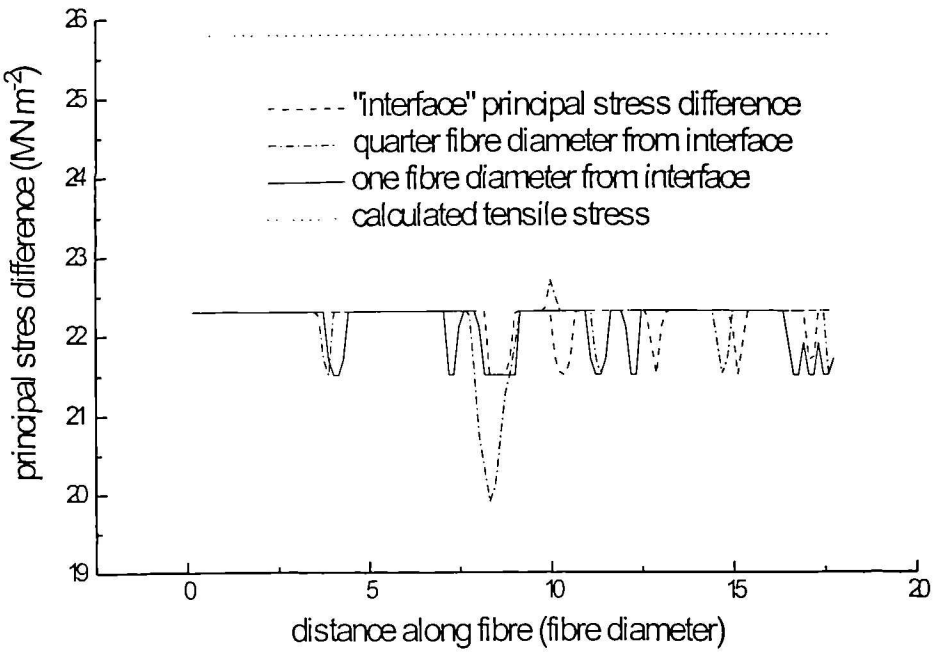

Figure 5.23 Plot of the principal stress differences along the E-glass fibre shown in Plate 5.7, *a)* along the 'interface', *b)* at one quarter fibre diameter from the interface and *c)* at one fibre diameter from the interface.

Firstly, it may be noted from Figure 5.23 that there is no obvious variation in the principal stress difference along the length of the fibre, other than a number of small 'jagged' peaks and troughs, attributable to the aforementioned optical 'noise'. Secondly, it may be observed that the stress difference taken along lines at the 'interface' and parallel to it but remote by 0.25 and 1.0 fibre diameters essentially coincide. This implies that the principal stress difference in the matrix remains constant, regardless of the distance from the interface. It should be remembered that the fibres under investigation all possess high aspect ratios and that the stress analyses were conducted remote from the ends of the fibre. The high matrix shear stresses associated with stress transfer at the fibre ends would not, therefore, be expected to be present and thus (assuming the system behaves elastically and that there is no slippage at the interface) fibre and matrix strain would be equal (Hull & Clyne, 1996). Any perturbations in the stress distribution along the fibre should, therefore, be the result of fibre inhomogeneity. It is therefore consistent that in the E-glass fibre reinforced SFC, in which the stiffness of the reinforcement phase is homogeneous, the stress in the matrix should remain constant, regardless of position relative to the fibre-matrix interface.

The behaviour observed in the E-glass reinforced SFC would seem to lend weight to the argument that the apparently lower matrix principal stress difference observed near the interface, adjacent to undamaged portions of the bast fibre, are the result of inhomogenous straining characteristics, brought about by the presence of micro-compressive defects in the fibre.

Another feature of note is the difference observed between the tensile stress of the SFC (calculated from the applied tensile load and the cross-sectional area of the composite) and the nominal principal stress difference derived through a consideration of the optical response of the matrix. As may be observed, the latter is significantly less than the former. This may be explained by load sharing between the two phases. If it is assumed that in these regions both phases undergo equal strain, then since the fibre modulus is much larger than that of the matrix (~70 GN m^{-2} for the fibre, ~3.3 GN m^{-2} for the matrix), the former will be subject to a much higher tensile stress (assuming both phases behave as linear-elastic materials). Thus, although V_f is very small (generally < 1% for the SFC studied), each fibre may carry

an appreciable proportion of the load. By considering a force balance, the matrix would carry a proportionately lower load and hence the matrix stress would be lower (direct calculation of tensile stress assumes the SFC to be homogeneous and takes no account of the heterogeneous micro-structure). A matrix stress lower than that of the tensile stress was noted in all the specimens investigated. It is believed that this phenomenon could be utilised to ascertain an 'effective' modulus for the fibre without the need to measure fibre strain directly.

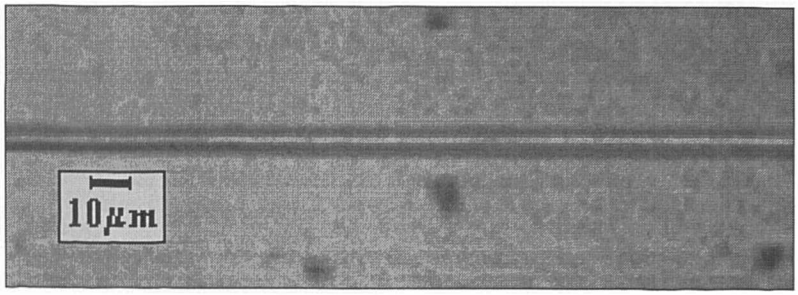

Plate 5.8 Photomicrograph of a hemp ultimate reinforced SFC loaded to approximately 23.4 MN m^{-2} (*circular polarised light*).

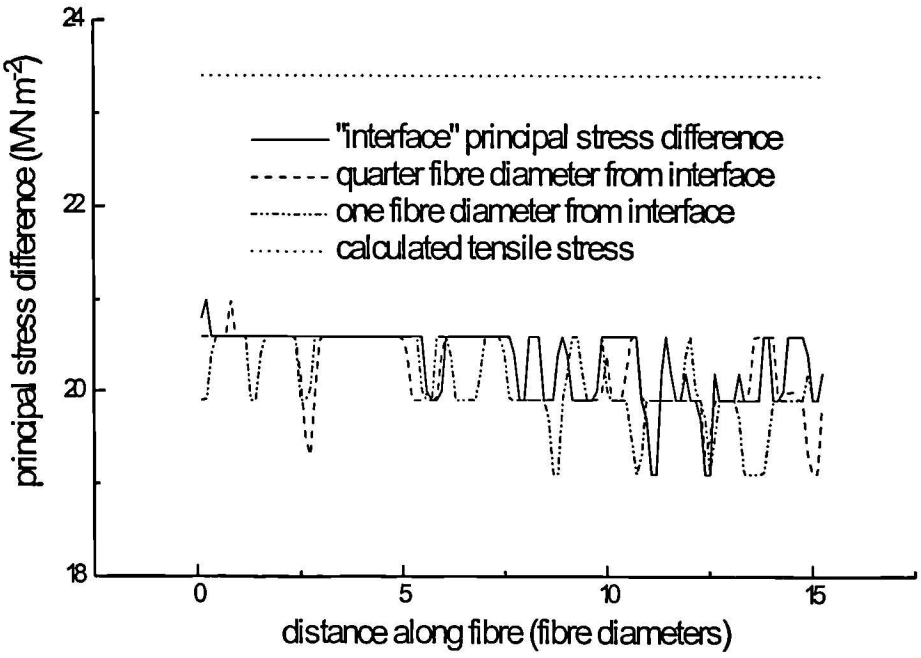

Figure 5.24 Plot of the principal stress differences along the hemp fibre ultimate shown in Plate 5.8, *a)* along the 'interface', *b)* at one quarter fibre diameter from the interface and *c)* at one fibre diameter from the interface.

Not all (but nearly so!) fibres contain micro-compressive defects. Plate 5.8 shows an example of a relatively undamaged hemp fibre ultimate in an epoxy matrix. As may be observed, no micro-compressive defects are visible (although there was some evidence of minor defects when the SFC was examined under a normal polarising microscope). The SFC was loaded to a tensile stress of around 23.4 MN m^{-2}. The corresponding principal stress differences along lines parallel with the interface are shown in Figure 5.24. Once again, if optical 'noise' is taken into consideration, then there would seem to be little fluctuation in the principal stress difference along the fibre length. The only anomaly appears to the right of the plot after around 7 fibre diameters when the stress difference is observed to drop. This is most likely to be an artefact rather than a true drop in principal stress difference, especially considering that similar trends are observed at all distances from the interface. In similar fashion to the E-glass fibre reinforced SFC, the principal stress difference in the matrix has essentially the same value regardless of the distance from the interface.

It is probably a realistic assumption that a less micro-compressed hemp fibre would have a more even strain distribution than a more highly micro-compressed sample. If it is assumed, therefore, that the fibre shown in Plate 5.8 has more even straining characteristics than those presented in either Plates 5.5 or 5.6, then the variation in the distribution of principal stress observed in the corresponding figures would in all probability be the result of an heterogeneous fibre modulus (together with the fibre morphology, as discussed below). As discussed above, this would in all probability, account for the principal stress distribution along the fibre length and in particular why this appears to drop below the nominal far-field matrix stress in regions adjacent to undamaged fibre.

In terms of their elastic properties, it may thus be possible to view micro-compressed bast fibres as having zones of lowered modulus corresponding to defected regions, in series with higher modulus zones as depicted schematically in Figure 5.25. In this model, the overall modulus of the fibre E1 is the series weighted average of E2 and E3, the latter thus being the moduli of the fibre in the defect free and micro-compressed regions respectively.

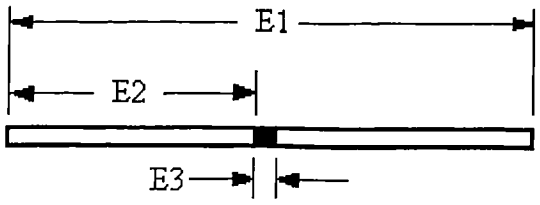

Figure 5.25 Schematic representation of the 'composite' modulus of a micro-compressed fibre.

The variation of the principal stress difference observed in the matrix, along the length of the fibre, adjacent to the interface (the 'interface' principal stress difference) may be explained in terms of the heterogeneity of the fibre modulus. In a long fibre composite, the fibres can be effectively viewed as being infinitely long. In other words, an individual fibre may be viewed as having an infinite aspect ratio. In a SFC reinforced with a fibre having an homogeneous modulus, it may be thought (providing the system behaves elastically and that there is no slippage at the interface) that remote from the fibre ends, both fibre and matrix undergo equal strain when the composite is subjected to a tensile load parallel to the fibre axis. In this situation, a condition of load sharing equilibrium would exist between the fibre and matrix. If, however, it is now assumed that a section in the fibre has a different and lower modulus than the remainder, then since strain was originally equal in both fibre and matrix, the stress in the portion of the fibre with the lower modulus would necessarily be reduced (Hooke's Law). If it is assumed that the fibre is of constant cross-sectional area, the fibre load would be reduced. Since this would alter the state of equilibrium in the composite, the load would be redistributed through the matrix. The matrix would thus undergo relatively greater strain (and hence would be more highly stressed), whilst the fibre too would undergo greater strain until a condition of equilibrium was re-established. Since the matrix would be subjected to higher loads in the vicinity of micro-compressive defects, concentrations of stress and strain would be expected to appear in the matrix.

As has already been mentioned above, the principal stress difference along the 'interface' adjacent to regions of the fibre between defects (which may be assumed to be relatively less damaged) is observed to fall below that of the nominal far-field

matrix stress level. It has already been discussed that this may be attributable to the difference between the modulus of the undamaged fibre and its 'effective' modulus, taking into account the micro-compressed regions. The differential between the matrix stresses lying adjacent to damaged and undamaged portions of the fibre gives rise to the stress gradients observed in Figures 5.20 and 5.21. A schematic representation of the probable relationship between the matrix principal stress difference and fibre modulus is presented in Figure 5.26.

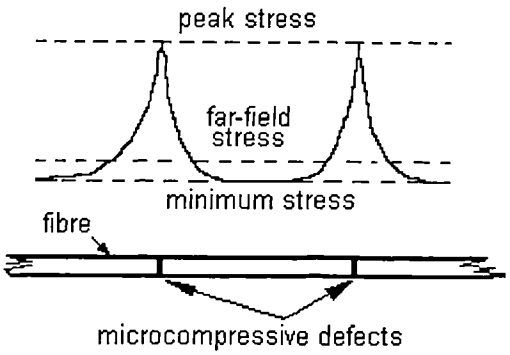

Figure 5.26 Schematic representation of the matrix principal stress difference along the interface' and the influence of micro-compressive defects.

What is evident from the experimental data (shown schematically above) is that from the micro-compressed region to the undamaged section of fibre, a steep stress gradient exists in the matrix adjacent to the true interface. This would imply that there could be a corresponding variation in the true interfacial shear stress distribution along the interface between micro-compressive features. This type of behaviour could be reasoned from shear-lag theory (Hull & Clyne, 1996). According to this approach, relatively higher shear stresses act on the interface at the fibre ends, reducing to zero at some finite distance from the ends (depending upon the elastic properties of the constituents) when the fibre and matrix strain are equal and the fibre axial stress has reached a plateau. The axial stress in the fibre would, however, under equilibrium conditions, be expected to be lower at the micro-compressive defects (since a greater proportion of the load is taken by the matrix at these points). Making an analogy with the shear-lag model, the fibre ends would correspond to the regions of the fibre directly adjacent to micro-compressive defects. The shear stresses (inferred from the distribution of matrix principal stress difference in close

proximity to the interface) are then observed to reduce with increasing distance from the micro-compressions, in accordance with shear-lag theory. The implications of this are that in a highly damaged fibre, where the distance (or aspect ratio) between successive micro-compressions is small, there may be insufficient fibre length over which loads can be transferred in order to develop a maximal axial stress in the fibre. In other words, the length between defects may well be below the critical stress transfer aspect ratio. This may indicate that the transference of stress from one phase to another is compromised, leading to reduced reinforcement efficiency by micro-damaged fibres.

Thus far, only the heterogeneity of the straining behaviour has been considered in connection with the occurrence of stress concentrations in the matrix. However, the morphology of these features may also be of significance. Many of the defects appear as sharp kinks in the structure of the fibre. When such a distinct change in section is introduced into the matrix, it might well be expected that this too could constitute a stress raiser, exacerbating the effects of the straining behaviour of the fibre.

5.3.6 Effect of micro-compressive defects on the fracture behaviour of SFC

Of particular interest as far as the macro-mechanical properties of the composite are concerned is the influence that micro-compressions have on fracture. As discussed above, the maximum values for $(\sigma_1 - \sigma_2)$ were recorded in close proximity to the fibre-matrix interface, adjacent to the micro-compressive defects. As a result, it has been inferred that high interfacial shear stresses exist in these regions, the consequences of which are that debonding between fibre and matrix may be stimulated. This behaviour has been observed in composite systems reinforced with micro-compressed synthetic (high modulus polyethylene) organic fibres (Grubb & Li, 1994). This prediction seems to be validated by observations of a failed SFC, in which debonding in the region of the fibre fracture is observed (Plate 5.9.).

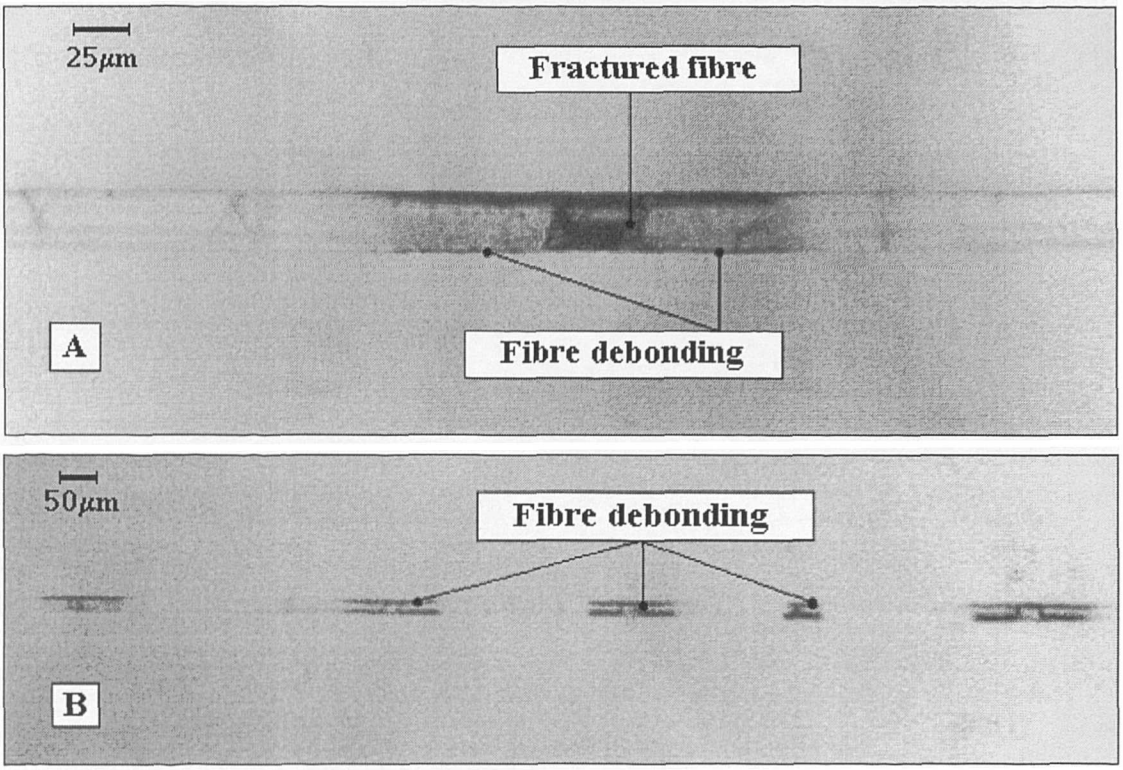

Plate 5.9 Fibre-matrix debonding at the point of fibre fracture (*ordinary light x100 magnification*).

It is believed that fibre fracture occurs first at the micro-compressive defect; failure in flax fibre having been observed to initiate at these locations (Focher *et al*, 1992). This does not seem unlikely, given that this region of the SFC would undoubtedly strain to a greater extent than elsewhere in the composite and that the fibre may also be in a 'weakened' state. Following fibre fracture, it seems reasonable to assume that debonding cracks may well propagate along the interface as a result of the release of stored strain energy as the fibre unloads.

In addition to the stimulation of fibre-matrix debonding, the concentrations of stress in the vicinity of the defect may well lead to crack initiation within the matrix due to localised rupture of the matrix, resulting from highly localised regions of the polymer undergoing strain in excess of that required to cause failure (it would certainly seem probable that some plastic behaviour could well take place here). This behaviour may well be exacerbated by the morphological changes in the matrix, brought about by the micro-compressive kink structure. Evidence for micro-compressions initiating matrix failure was provided by the small visible transverse cracks seen in Plate 5.10, located in the regions formerly occupied by the fibre (also cracks in the

matrix were observed to initiate and propagate when SFC's were tested to destruction). It is thought that such cracks could, in turn, lead to macroscopic fracture of the composite.

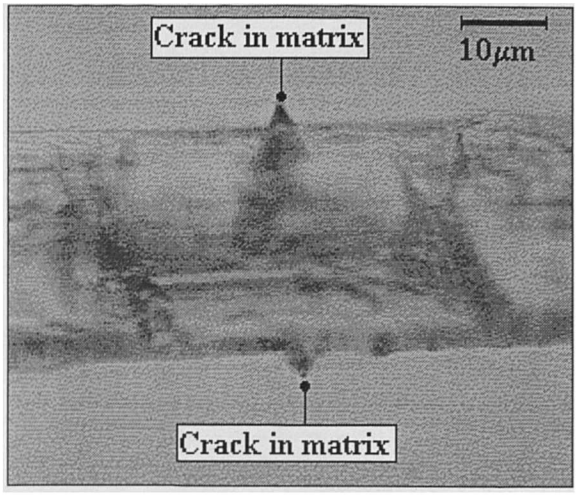

Plate 5.10 The formation of cracks in the matrix at the location of fibre fracture (*ordinary light x 400 magnification*).

5.4 Conclusions

Half fringe photoelasticity has proved to be a useful technique for detailed examination of the stress field in an epoxy matrix. With some minor refinements, it is believed that the system could be adapted to analyse other matrix materials which exhibit artificial birefringence, most notably polyesters. Furthermore, the system could be extended to the recording and analysis of the isoclinic fringes, enabling stress trajectories to be computed. Nevertheless, in its present form, the system has proved to be useful in identifying and quantifying stress concentrations in epoxy matrix SFCs in the vicinity of micro-compressive defects.

The findings presented in this chapter indicate that it is likely that micro-compressed fibres undergo heterogeneous straining. When combined with the distinct morphology of the micro-defects, stress concentrations in the matrix result. Furthermore, it would seem probable that the stress transfer mechanism between fibre and matrix is impeded, resulting in lowered reinforcement efficiency. The

presence of micro-compressive defects could therefore be viewed in a two-fold manner. Firstly, they are responsible for the creation of stress concentrations in the matrix, which it seems might lead directly to matrix cracking and to fibre-matrix debonding. As such they may be likened to a series of small cracks or holes in the matrix. Secondly, micro-compressed fibres may be thought of as a succession of short fibres, less than the critical length, in series with one another with loads being transferred from matrix to fibre via a form of 'shear-lag type' mechanism. However they are viewed, it seems very likely that micro-compressive defects contribute to the macroscopic behaviour of bast fibre reinforced PMCs. This aspect is discussed more fully in Chapter 6.

6 General Discussion

6.1 Introduction

6.1.1 Summary of work

In Chapter 3, the findings of a study into the macroscopic, physical and mechanical properties of an unsturated polyester reinforced with two unmodified, non-woven, bast fibre types were presented and discussed. The properties of these laminates were compared with those of a composite material reinforced with CSM glass fibre. The general findings of this part of the study indicated that, on a volume for volume basis of reinforcement, the stiffness of the non-woven plant fibre reinforced laminates was on a par with that of the CSM glass fibre reinforced material, particularly on a specific basis. The results of the strength tests, though not as encouraging as stiffness, nevertheless indicated that acceptable properties could be obtained. It is believed that both strength and stiffness can be be explained in terms of fibre properties. Toughness, on the other hand, was found to be substantially inferior (possibly by as much as an order of magnitude) to that of the inorganic fibre reinforced polymer. In view of the importance of this property in an engineering material (Gordon, 1976), it was felt that this aspect warranted more detailed investigation. In addition to displaying a lack of toughness, the materials also exhibited behaviour which, it was believed, might well impact upon their potential end uses. It was felt that this too required explanation. The behaviour referred to is primarily concerned with the deformation properties of these laminates.

Firstly, it was noted that during loading (both in tension and flexure) a departure from linearity occurred at seemingly very low stress levels. It was unclear from the tests, however, up to what point the behaviour remained elastic (and how far beyond the proportional limit this extended). Nevertheless, the onset of irreversible (plastic) behaviour at low stress levels would undoubtedly have practical implications concerning the design of structures utilising such materials. In addition to this, it was

believed that the bast fibre reinforced PMCs exhibited a degree of bimodular behaviour, which again might have ramifications in practical terms. In view of the dependence of composite macroscopic properties on microstructure, it was believed that a thorough investigation of this, particularly with regard to the micromechanics of deformation and fracture, was required.

The character of the reinforcing fibres themselves was considered in Chapter 4. A number of investigators (e.g. Bolton, 1994; Ivens, *et al.*, 1997; Robson *et al.*, 1993; Snell, *et al.*, 1997) have reported on the mechanical properties of bast fibres. However, as far as is known, only one report exists in the literature on the effect of micro-compressive damage ('kinks') on the tensile properties of these fibres (Davies & Bruce, 1998). It is, nevertheless, known that in wood fibres, kink bands or minute compression failures are responsible for a loss in properties (Dinwoodie, 1978) and it has been postulated that these could influence the quality of the interface between fibre and matrix in a wood fibre reinforced polymer composite system (Mott *et al.*, 1996). In view of the foregoing, it was believed that a detailed microscopical study of the fibres would be of benefit, hopefully elucidating potential areas of concern.

Microscopy revealed that all of the bast fibre types examined exhibited varying degrees of micro-compressive damage. It was thought that this initiated during plant growth and was exacerbated during the subsequent decortication and felting processes. It was speculated that these fibres were particularly sensitive to micro-compressive damage due to their structure. This, it was believed, indicated that the compressive strength of these fibre types might well be lower than their tensile strength (*cf.* synthetic polymer fibres). It was postulated that the morphology of this damage might well result in heterogeneous fibre straining characteristics. This (coupled with the change in section of the fibre at the defect), it was hypothesised, could give rise to the formation of stress concentrations in the matrix in the vicinity of the interface when such fibres were embedded in an essentially homogeneous, isotropic matrix. To investigate this hypothesis, an idealised situation was considered.

It was shown using photoelastic techniques (Chapter 5), that concentrations of stress did indeed appear in the matrix in the vicinity of micro-compressive defects when

single filament composites (SFCs) were strained in tension parallel to the fibre axis. Stress concentration factors (K) of up to 1.65 were recorded in close proximity to the interface in the vicinity of the 'kinks'. Furthermore, it was observed that the severity of the damage appeared to affect the value of K.

When compared with (relatively) undamaged fibres (and also with glass fibre - considered to posses homogeneous straining characteristics) it was found that the matrix principal stress difference distribution in close proximity to the 'true' interface was decidedly irregular in the SFCs reinforced with micro-compressed fibres. As a result, it was postulated that this could lead to an inefficient transfer of stress from the matrix to the fibre, with some form of 'Cox-type' shear-lag mechanism probably being operative in such systems. In many instances, fibres had been found (Chapter 4) to possess micro-compressive defects at intervals of only few fibre diameters along their length. In consequence, it was believed that in these regions the build-up of axial stresses in the fibre would be impeded, which might well result in poor reinforcing efficiency. Furthermore, it was believed that in the vicinity of the micro-compressive defects, localised debonding could occur as a result of high interfacial shear stress. Analysis of failed specimens (as well as unrecorded visual observations during testing) indicated that the fracture of both fibre and matrix initiated in these regions of high local stress.

The purpose of this chapter is to discuss the separate findings of the previous three in relation to the overall mechanical behaviour of natural fibre reinforced PMCs. The discussion concentrates primarily on the two macroscopic properties which are perceived to be of greatest concern, namely non-linear behaviour and toughness. These macroscopic properties are considered in relation to microstructural behaviour. Additionally, bimodular behaviour is also considered.

6.2. Bimodular behaviour

In Section 3.3.4, it was noted that bast fibre reinforced PMCs appeared to exhibit bimodular behaviour. Whilst this was not tested directly (rather, it was inferred from the difference between tensile and flexural moduli), it is not unreasonable to suppose that this might be so, since such behaviour has been recorded in other fibre composite materials and is also thought to occur in wood (Conners & Medvecz, 1992).

If, firstly, fibre architecture is considered. The laminates studied in this work were reinforced with what might best be described as a 'pseudo planar-random' array of bast fibres. As a result, the fibres within the structure of the laminate would have been oriented at various angles between 0^{O} and 90^{O} to the axis of the applied load. It is, in fact, unlikely that any one fibre would be aligned at any particular angle along its length, due to the 'curliness' of individual fibres. However, it may be envisioned that the fibres (or segments thereof) were distributed, in some manner, at angles between 0^{O} and 90^{O} to the laminate axis. The axis of any individual fibre within the composite structure would therefore be oriented at an angle θ to that of the applied compressive or tensile load as shown schematically in Figure 6.1.

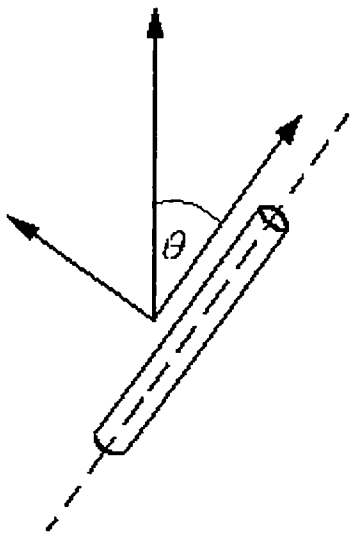

Figure 6.1 Schematic representation of the resultant forces acting on an individual fibre inclined at an arbitary angle θ to the loading axis.

Simplistically, the applied load acting across the interface on the fibre, may be resolved into two components, one parallel and the other normal to the fibre axis. The question then arises; do individual fibres exhibit bimodular behaviour, either along the fibre length or perpendicular to it, or both? It would seem likely, from the discussion on fibre structure in Chapter 4, that individual bast fibres could be thought of as uniaxially aligned fibre composites themselves. It has been recorded that a number of synthetic composites show differences between their tensile and compressive moduli (Conners & Medvecz, 1992). Conners and Medvecz (1992), speculated upon the possibility of bimodular behaviour occurring in individual wood fibres and concluded that this was plausible, particularly if the 'encrusting matrix' was absent. It seems probable, therefore, that this type of behaviour might also occur in bast fibres loaded uniaxially, particularly since the amount of matrix (hemicelluloses and lignin) surrounding individual microfibrils would appear to be significantly less in bast fibres than in wood (see Table 1.1). It seems reasonable too, from a consideration of the ultrastructure, that bast fibres might also exhibit bimodular behaviour when loaded perpendicular to the fibre axis, although this is purely conjecture.

It would not seem too unlikely, that, if individual bast fibres behave in a bimodular manner, then (coupled with the fibrous structure of the composite itself) the laminates might also be expected to exhibit similar behaviour.

6.3 Failure mechanisms

In the bast fibre reinforced material studied, macroscopic laminate fracture appeared to occur primarily through axial tensile failure. At higher volume fractions there was, nevertheless, some evidence of laminate failure through shear, but this seemed to be limited.

6.3.1 Effect of fibre architecture upon fracture

As noted in the previous section, the orientation of the bast fibre reinforcement may be described as 'pseudo planar-random'. As such the fibres would be oriented at various angles to the applied load. In addition to this, a factor which may be of potential relevance is the 'curliness' of the fibres. This would no doubt affect not only the mechanism and efficacy of stress transfer, but could also play a part in the fracture process itself.

In Section 2.1.6, it was noted that a unidirectional lamina, subject to an arbitrary state of stress, may fail as a result of critical values of axial tensile, transverse tensile or shear stresses being exceeded. The failure of laminae is related to the loading angle, with the maximum strength of a unidirectional ply being observed when the fibres are aligned parallel to the applied stress and the minimum when the applied stress acts perpendicular to the fibre direction (Hull & Clyne, 1996). As noted previously, the strain to failure of laminae loaded perpendicular to the fibre direction is generally significantly lower than when loaded parallel to the fibre direction. Furthermore, both the stress and strain to failure of the transversely loaded lamina are generally less than that of the unreinforced matrix itself. As a result, in a crossply laminate (0/90) the transverse plies crack before the parallel plies, leading to a distinctive 'knee' in the stress-strain record for such materials, the 'knee' occurring at strains comparable to the failure strain of the transverse ply and corresponding to the onset of irreversible damage (Chou, 1994; Hull & Clyne, 1996).

At intermediate angles (i.e. between 0^{O} and 90^{O}) lamina failure may occur as a result of critical values of either axial tensile, transverse tensile or shear stresses (or a combination thereof) being exceeded. A theoretical prediction for the dependence of lamina failure stress on loading angle is provided by the 'Tsai-Hill Criterion' (Equation 2.15).

6.3.2 Transverse tensile failure

If, firstly, these hypothetical laminae, subject to essentially transverse tensile loading (i.e. high values of ϕ) are considered, then it is likely that concentrations of stress would occur in the matrix due to constriction by the fibres. This would in all probability be more severe at higher V_f. These stress concentrations could possibly stimulate matrix failure. However, it cannot be ruled out that fibres aligned perpendicular to the applied load (or nearly so) may fail, rather than the matrix itself. Plate 3.12 clearly showed either inter- or intra- wall splitting to have taken place during fracture. It does not seem too unlikely then that such behaviour might occur, given that in such circumstances the fibre itself might be likened to a ply under transverse loading and would, therefore, be loaded in its weakest orientation. Since the longitudinal ('along the grain') fracture toughness of plant fibre material has been reported to be in the region of 0.3 kJ m^{-2} (Gibson & Ashby, 1988; Stanzl-Tschegg, 1994), this might indicate that cracks would propagate relatively freely in this plane (*c.f.* log splitting). Of course, it cannot be ruled out that fibre splitting may have occurred as a result of shear (mode II) rather than opening (mode I) mode loading.

It is also possible that fibre-matrix dedonding occurs when the applied load acts normal to the interface. Fibre-matrix debonding clearly occurred during fracture as shown in Plates 3.7 and 3.8, whilst in SFC tests (Plate 5.9) debonding also appeared to have taken place. This raises the question; how strong is the fibre-matrix bond? If, as was discussed in Section 3.3.1, wetting is good, but adhesion is primarily the result of mechanical interlocking, rather than any true 'adhesion', then it would seem probable that debonding could occur relatively easily. This would be particularly so if the applied stresses were acting normal to the interface, such as might be considered to occur in transversely loaded laminae. In these circumstances, the purely mechanical 'lock and key' effect of the fibre surface might well be less effective than under shear loading. The conditions under which debonding takes place are discussed further in a later section.

The above serves to illustrate that, in a transversely stressed hypothetical lamina, failure could take place either in the matrix (as a result of stress concentrations), the

fibre itself or at the fibre-matrix interface. It is probably reasonable to expect, therefore, that failure could occur at relatively small overall strains, if low intra-fibre cohesion exists together with (arguably) low fibre-matrix adhesion. If these suppositions are correct, then it seems reasonable to assume that at relatively low overall stresses in the 'real' laminates, irreversible micro-structural damage might take place, as a result of transverse loading on fibres (the hypothetical laminae) oriented at large angles to the applied tensile stress.

6.3.3 Axial tensile and shear failure

In reality, it might reasonably be expected that the vast majority of fibres in the non-woven material would be inclined at some lower value of ϕ. Indeed, it might well be expected that the fibres should lie preferentially in the direction of the applied load as a result of the felt manufacturing process (see Section 3.3.2). If the situation is idealised and hypothetical laminae, inclined at some intermediate angle are considered, then these would in all probability fail by some combination of axial tension, transverse tension and shear. At higher ϕ, shear and transverse tension might be expected to prevail, whilst at lower ϕ, shear and axial tension could well be dominant.

Failure through transverse tension has already been considered. Shear failure may occur either in the matrix, at the interface or in the fibre itself. It would seem likely, based on photomicrographic evidence, that interfacial shear failure does occur. In Plate 5.9, debonding is clearly visible in the vicinity of the fibre breaks as darker regions (due to scattering of light at the interface - Grubb & Li, 1994) extending some way from the fibre break along the fibre. There would also appear to be some evidence of shear failure in the fibres themselves. Plate 3.12 clearly shows a longitudinal fracture which might be indicative of fibre shear failure.

Axial tensile failure in unidirectional laminae is largely governed by the failure strains of the constituents (Hull & Clyne, 1996). As discussed in Section 3.3.3, in the case of bast fibre reinforcement it seems probable that their failure strain is less than that of the matrix. Simplistically, it may therefore be envisaged that, as the laminate is

progressively strained, fibre fracture would occur first of all leading to the axial load on the laminate being progressively transferred to the matrix. As strain increases, fibre fragmentation would reach a saturation condition depending upon the strength of the fibre and the efficacy of stress transfer from matrix to fibre. Laminate fracture would then occur when the matrix reaches its failure strain (Hull & Clyne, 1996). This view of uniaxial laminate failure is, however, likely to be complicated by other miromechanical events, such as stress concentrations associated with micro-compressive defects and fractured fibre ends. These probably result in the initiation of matrix cracking and fibre-matrix debonding and might well result in macroscopic laminate fracture at strains below that of the matrix failure strain. These issues are addressed in the following section.

6.4 The influence of fibre micro-compressive defects on microstructural damage

6.4.1 Influence of defects on the state of stress in a laminate

It has been clearly shown that flax, hemp and jute fibres all contain numerous micro-compressive defects. When embedded in a polymeric matrix and strained parallel to the fibre axis, it has been demonstrated that stress concentrations arise in the matrix in the vicinity of these defects. Prior to discussing how these might influence fracture behaviour, it is appropriate to consider the state of stress, not only in the micro-compressed fibre itself and the immediate surrounding matrix, but also in neighbouring fibres, prior to the onset of damage.

Consider a lamina under uniaxial tension applied parallel to the fibre direction. As the overall strain increases, so too will the strain on individual fibres. However, as discussed in the previous chapter, the straining behaviour of bast fibres is thought to be heterogeneous. In regions of higher fibre strain (i.e. in the vicinity of micro-compressive defects), therefore, the proportion of load supported by the fibre will probably diminish. The balance of force must then be transferred to the surrounding

matrix and to neighbouring fibres. As such, it seems probable that a rise in the axial stress in these fibres would be observed in a position adjacent to the micro-compressed fibre. This hypothesis is supported by the observation that concentrations of axial stress are formed in fibres adjacent to one which contains a break. By using Raman spectroscopy, it has been clearly demonstrated that in synthetic polymeric or carbon fibre-epoxy systems, stress concentrations occur in neighbouring fibres and that these diminish with increasing radial distance from the broken fibre (Grubb *et al.*, 1995; Chohan & Galiotis, 1997; Van den Heuvel *et al.*, 1997). If a similar situation arises in bast fibre reinforced composites (where the microcompressions can be regarded as a fibre 'break'), it seems reasonable that the influence of fibre straining heterogeneity will depend upon the relative inter-fibre spacing, which in turn is governed by the fibre volume fraction.

Whilst it is difficult to know precisely the inter-fibre spacing in the 'real' laminates, it is not too difficult to envisage that this is less than one fibre diameter. In the case of a uniaxially aligned composite (assuming either square or hexagonal packing array) of volume fraction around 30%, the inter-fibre spacing is less than one fibre diameter (Hull & Clyne, 1996). In the composites studied in this work, it is very probable (especially at higher V_f) that the interfibre spacing between some fibres was considerably less, due to the uneven packing arrangement and heterogeneity of fibre morphology. The photomicrographs in Chapter 3 would certainly seem to support this.

The exact mechanism(s) responsible for the load sharing operation described above is/are probably difficult to predict. Nevertheless, it seems plausible that whilst some of the redistributed axial stress is taken by the matrix, a proportion would be transmitted by matrix shear to the neighbouring fibre. In addition to this, a direct transfer of axial load to intact fibres could account for some of the re-distributed load.

6.4.2 Fracture in neighbouring fibres

If a neighbouring fibre were to contain a defect, in an approximately adjacent position (which is not an unreasonable assumption, given the frequency with which micro-

compressive defects can sometimes occur) then it is plausible that the axial stress in the neighbouring fibre might be raised sufficiently to cause failure. As reported by Van den Heuvel *et al.* (1997) and Chohan and Galiotis (1997) stress concentrations in neighbouring fibres caused by a single fibre break can lead to co-operative fibre failure, resulting in composite fracture. If such a system were to exist in the 'real' bast fibre composites, it is not unreasonable to consider that at relatively low overall composite stresses, fibre failure could be initiated in neighbouring fibres as a result of the fibre strain heterogeneity. Based on the foregoing argument, high volume fractions (i.e. low interfibre spacing) and highly micro-compressed fibres would encourage this behaviour. A schematic representation of this process is presented in Figure 6.2.

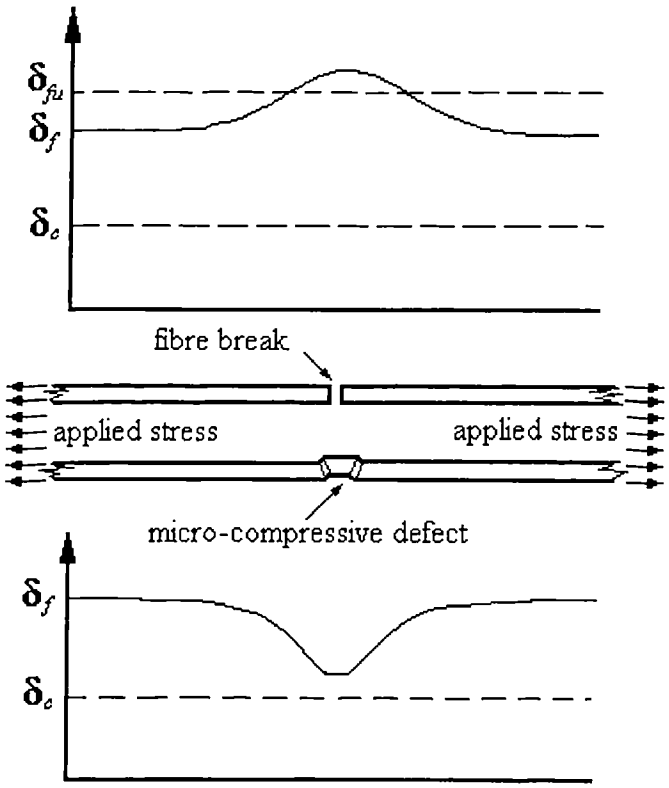

Figure 6.2 Fracture in a neighbouring fibre adjacent to a micro-compressive defect.

6.4.3 Matrix rupture

As discussed in the previous chapter, it is believed that matrix stress concentrations caused by the presence of micro-compressive defects can result in matrix fracture at

these locations. If neighbouring fibres are considered, then there is the possibility that adjacent micro-compressive features exist in these. Given that the affected zone of the matrix (in which a stress concentration exists) extends by up to say 0.5 fibre diameters from the interface, the combined 'interaction' zone could be quite appreciable (up to one fibre diameter). Therefore, at the interfibre spacing envisaged in 'real' laminates, it seems quite likely that appreciable stress concentrations could be stimulated in the matrix between fibres. These, it is believed, could result in plastic deformation or fracture of the matrix. This scenario is depicted schematically in Figure 6.3. It should, however, be remembered that if the surrounding fibres were undamaged, again using a load sharing argument, it is probable that the matrix stress concentration would reduce rather than increase.

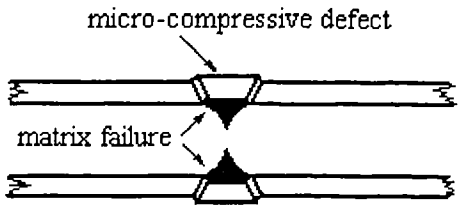

Figure 6.3 Representation of matrix failure between two adjacent micro-compressive defects.

6.4.4 Interfacial debonding

As noted in Chapter 5, interfacial debonding in SFCs was observed as part of the composite failure process. It was considered that this resulted from high interfacial shear stresses induced at the micro-compressive defects. Following fibre fracture, it is likely that the released strain energy would propagate the crack along the interface, particularly if the fracture toughness of the interface was low. This would, in all likelihood, account for the debonded zones observed in the failed SCFs. Strong evidence for interfacial debonding in 'real' laminates was provided by the occurrence of cracks formed between the matrix and fibre at the fracture surface, as shown in Plates 3.7 and 3.8. This situation may be compared with interfacial debonding arising from the high interfacial shear stresses observed in model carbon fibre-epoxy

systems (Melanitis *et al.*, 1992). Whilst debonding along individual micro-compressed fibres as a result of stress concentrations would seem likely, it is possible too that micro-compressions could stimulate fibre-matrix debonding in neighbouring fibres. Two potential mechanisms can be identified.

Firstly, shear stresses in the matrix surrounding micro-compressive defects could, if the inter-fibre spacing was sufficiently small, induce interfacial shear stresses in neighbouring fibres (as part of the load transfer mechanism). If the interface associated with the neighbouring fibre was particularly poor, then it would seem possible that interfacial shear failure could be stimulated in this manner.

Secondly, whether any significant tensile stresses are stimulated which act in a plane normal to the interface, in a fibre adjacent to one containing a micro-compressive defect, is open to conjecture. If this were so, however, the stress concentrations caused by micro-compressive defects may also stimulate debonding (and act in co-operation with the interfacial shear failure described above) in a manner analogous to the 'Cook-Gordon' mechanism of crack-blunting. As noted in the previous chapter, the effect of micro-compressive defects on the matrix might be likened to the presence of a hole in the matrix. Theoretically, it may be shown (using the 'Kirsch solution' - Parton, 1992) that, around a circular hole in an infinite elastic plate, a perpendicular stress equal in value to 3/8 of the nominal uniaxial tensile stress exists, which acts in a sense so as to produce a tensile stress normal to the interface (i.e. to pull it apart). The maximum stress would occur at a location approximately 0.2 fibre diameters from the interface. If, as has been previously considered, interfacial bonding is primarily due to mechanical interlocking, which would be inhibited if stresses acted perpendicular to it, then it seems plausible that debonding could be stimulated. It would, therefore, seem feasible that debonding might be stimulated in neighbouring fibres, either through matrix shear stresses, or as result of normal stresses acting on the interface (or a combination of the two). A schematic representation of these possible mechanisms is presented in Figure 6.4.

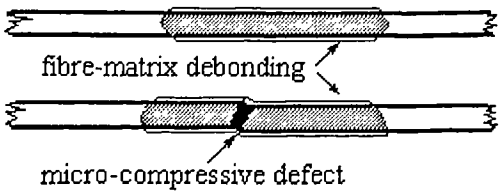

Figure 6.4 Debonding stimulated in a neighbouring fibre as a result of an adjacent micro-compressive defect.

Although the possible effects of the micro-compressive defects on 'real' laminates is mainly conjecture, the arguments appear reasonable. It would be of benefit to actually study the interaction between neighbouring fibres, to ascertain the true effects and to confirm or disprove these hypotheses. It is proposed that multi-filament micro-composites (containing 3, 5, or more fibres aligned parallel to each other) should be used to investigate this phenomenon.

In summary, a picture emerges of a composite microstructure riddled with stress concentrations, leading to numerous potential mechanisms by which microstructural failure may take place. These include; fibre failure, interfacial debonding and matrix plastic deformation and fracture. It is interesting now to consider how these various mechanisms might affect the macroscopic behaviour of the composites.

6.5 Plastic deformation of laminates

6.5.1 Macroscopic behaviour

The nature of the tensile stress-strain relationship was discussed in Section 3.3.3. Particularly at higher V_f and more especially in the hemp fibre reinforced laminates, it was noted that a departure from linearity occurred at comparatively low stress levels. In the case of hemp, at a volume fraction of around 44%, analysis of the stress-strain

record revealed that departure from linearity initiated at a composite tensile stress possibly as low as 10 to 15 MN m^{-2}. In the CSM laminate at a V_f of only 20%, this departure from linearity did not occur until a tensile stress of around 25 MN m^{-2}. It is believed that such behaviour could impact upon the potential end uses to which these materials might be put and therefore requires consideration. As stated previously, no tests were undertaken to verify whether stresses beyond these limits resulted in irreversible deformation (i.e. beyond the elastic limit) nor whether the behaviour remained elastic up to some point beyond the proportional limit. Nevertheless, visual (and audible) observations of the straining specimens did indicate that irreversible processes were taking place, as evidenced by the appearance of extensive transverse cracking in the matrix. However, in the medium volume fraction hemp reinforced laminates (~31%), considerably fewer matrix cracks were visible; whilst in the low volume fraction samples (~15%), no cracking whatsoever was noted. This behaviour seemed to be reflected in the nature of the stress-strain behaviour; in the lower volume fraction specimens there was a far greater degree of linearity in the stress-strain curves than at higher volume fractions. A similar trend was observed in the jute fibre reinforced material, however, non-linear behaviour (at all volume fractions) did not appear to be so pronounced. The degree of plastic behaviour was also assessed by establishing the yield point (0.2% proof stress) and comparing this with the ultimate tensile strength. It was found that non-linear behaviour seemingly increased with volume fraction. Whilst it is impossible to state clearly the point at which elastic behaviour ceased, it was apparent that the degree of plastic deformation displayed by the laminates increased with V_f. Since this must be related to irreversible damage occurring within the micro-structure of the composite, it is relevant to look to this for an explanation of the behaviour.

6.5.2 Mechanisms of plastic deformation

As discussed above, there are potentially many different mechanisms by which damage at the microstructural level could take place. If, firstly, it is assumed that a departure from linearity is indicative of irreversible micro-structural damage ('plastic' behaviour), then it is reasonable to argue that in the bast fibre reinforced PMCs, incipient microstructural damage may occur at relatively low nominal stress levels.

This could take place through the action of stress concentrators initiating failure by any, or all of the aforementioned mechanisms.

It is interesting to note that in the lower volume fraction materials there was little deviation from linearity preceding fracture. This may be explained by the larger interfibre spacing and, as a result of fewer fibres, a lower total number of stress concentrations. As has been discussed above, higher volume fractions would favour more fibre-fibre interaction resulting from, in particular, micro-compressive defects. At low volume fractions, therefore, fewer stress concentrations (either in neighbouring fibres of the matrix) would presumably result in less micro-structural damage. However, because of the far greater proportion of matrix material at these low V_f, once initiated, fracture could be expected to occur rapidly, since there would be relatively less fibre with which to create crack stopping/blunting and energy dissipating mechanisms. Simplistically, fracture at these V_f would be dominated by the behaviour of the matrix, the fibres offering little reinforcement or resistance to brittle fracture. Indeed, at low V_f, the fibres may indeed act as a population of critical defects which, as discussed in Chapter 3, may actually initiate failure at low stresses (and strains). This might well account for the fact that at low V_f, the strength (and failure strain) of the laminates is observed to fall to below that of the unreinforced resin itself. It should also be noted that the failure strain of the fibres is probably less than that of the matrix. In these circumstances, it is likely that some fibre fracture could well precede matrix failure, thereby exacerbating the effects of the stress concentrators.

However, as V_f increases, so too will the proportion of stress concentrators. In addition to this, because of the smaller interfibre spacing, their effect would become more and more exaggerated. Nevertheless, there would be a 'trade-off', for whilst the effects of the stress concentrations would be increased, the greater proportion of fibre would tend to give enhanced reinforcement and toughness. The result might be that as stress levels are increased, matrix fracture (plus no doubt other damage mechanisms) would occur and load would be progressively transferred to the fibres

(since a single macroscopic crack would be prevented from causing failure of the composite at low stress levels). This is consistent with the observed behaviour.

At higher volume fractions, therefore, it could well be expected that as the load on the specimen is increased, matrix fracture first occurs in those regions most susceptible to the effects of the stress concentrators (or where limited fibre failure occurs). Once matrix fracture has occurred, the load would then be taken by the fibres. As the load is progressively increased, further regions of matrix cracking occur, resulting in a greater and greater proportion of the load being transferred to the fibres. Nevertheless, with the occurrence of matrix cracking and the transference of load to the fibres, strain would necessarily increase, thereby resulting in a reduction in the slope of the stress-strain curve (i.e. modulus decreases). It is interesting to note that at the highest V_f studied (44%), the hemp reinforced laminate exhibited substantial 'plastic' deformation, prior to failure. Indeed ε_{uc} exceeded that of either the fibre or matrix. It is likely that this behaviour resulted from localised microcracking of the matrix away from the fibre, with the latter subsequently 'realigning' in the direction of the applied stress. This would effectively increase the laminate strain dramatically in these regions, resulting in high overall composite failure strains.

A comparison of the deformation behaviour of the two bast fibre reinforced PMCs revealed what appeared to be very different responses (this was particularly noticeable during testing). At the highest V_f studied, the hemp reinforced material exhibited what appeared to be a far greater degree of plastic behaviour than the jute reinforced material at a similar V_f. This appeared to be reflected in the frequency of matrix micro-cracking, being significantly greater in the hemp reinforced laminates than in jute. This might indicate that a greater degree of micro-structural damage takes place in the former laminate type. The reasons for this are open to conjecture. Nevertheless, one possible explanation would be that such damage is related to a difference in the relative frequency and severity of the micro-compressions in the two fibre types. Again, however, there is a slight anomaly in that the tensile strengths quoted for jute (see Table 1.1) are generally lower than those of hemp and yet the tensile strength of the jute laminates were on the whole greater. This could be

indicative of the occurrence of micro-structural damage taking precedence over fibre strength - leading to overall composite failure. On the other hand, the toughness of the jute fibre reinforced composites was observed to be poorer than that of the hemp reinforced material, particularly under impact loading (Charpy test). It is believed that under these circumstances, it is the strength of the fibres, rather than the occurrence of micro-structural damage, which dominates the laminate behaviour. This would seem to be confirmed when a comparison is made with the CSM reinforced laminate in this test.

It seems plausible, therefore, that microstructural damage arising from stress concentrations caused by, in particular, fibre damage can contribute to the type of irreversible non-linear behaviour seen in bast fibre reinforced PMCs.

6.6 Toughness

6.6.1 Introduction

As noted in Section 6.1.1, one of the greatest concerns, with respect to the mechanical properties of bast fibre reinforced PMCs, is their lack of toughness; that is to say their lack of resistance to the propagation of cracks. In this context, it is the lack of resistance to macroscopic cracks, which may ultimately result in component or structural failure, which is of most concern.

Work of fracture under three point flexure (quasi-static and dynamic loading conditions) measurements both indicated that, on a volume for volume basis, the toughness of the natural fibre reinforced composites was considerably less than that of the inorganic fibre reinforced PMC. Subsequent fracture toughness calculations confirmed that the difference in works of fracture could be as much as an order of magnitude. Clearly, this could be of potential concern if the bast fibre reinforced materials were to be used in any structural or semi-structural applications.

As noted in Section 3.3.6, a fracture mechanics approach to the toughness of materials allows for scaling effects to be taken into consideration. If suitable toughness characterising parameters can be established (K_{IC} or J_C) then a link between the macroscopic toughness of a material and the microstructure can be established. As discussed previously, values of both K_{IC} and J_C were evaluated, the latter being thought to be a more representative measure of the material toughness in this instance. It was hypothesised that the relative 'volume' of the plastic, or damage zone region ahead of the crack-tip was of importance in relation to the macroscopic toughness of the material, since it is here that most energy absorption processes are likely to occur. From a visual examination of failed laminates containing initially sharp notches, it was considered that this was physically reasonable, since the relative sizes of the observed damage regions approximated to those predicted from the theory. The findings indicated that the 'volume' of the damage zone could be significantly smaller (by more than an order of magnitude) in the vegetable fibre reinforced PMCs than in the glass fibre reinforced material at equivalent V_f. This suggested that in the former, the lack of toughness may be attributable to a reduced 'energy absorbing' capacity. That is to say, toughening mechanisms were simply not stimulated to the same extent in the bast fibre reinforced material. The following discussion attempts to relate the macroscopic toughness of the laminates to the micro-structural observations made in this work.

6.6.2 Nature of crack propagation in laminates

One of the problems associated with the application of fracture mechanics to composite materials is that of ensuring macroscopic crack propagation in the desired direction. This is due to cracks being blunted and deflected at interfaces (Piggott, 1980). In other words, rather than a single macroscopic crack propagating in a self-same manner through the material, there is a tendency for a crack to 'dissipate' and meander, forming numerous micro-cracks within the structure of the laminate. It is precisely this ability for cracks to be repeatedly deflected and blunted that, in part, accounts for the high toughness of composite materials (Gordon, 1970; Hull & Clyne, 1996). No doubt however, if the material specimen was sufficiently large, micro-cracking would be confined to a relatively small zone at the crack-tip and an

identifiable macroscopic crack would propagate through the material. The results of this work indicated that for this to occur a very large specimen size would be required.

It was believed that much of the deformation behaviour observed with the laminate specimens tested could, therefore, be associated with microscopic crack growth (together with other damage processes such as fibre and matrix fracture) taking place within the laminate in the vicinity of the crack-tip rather than with macroscopic crack advance. These processes would all, nevertheless, account for the absorption of released strain energy and this probably explains why the fracture process (at higher V_f) in the reinforced materials was a rather gradual affair.

During the fracture toughness tests conducted in this work an attempt was made to distinguish between macroscopic and microscopic crack growth. This issue was resolved by assuming that macroscopic crack advance was accompanied by a 'significant' change in specimen compliance (a 'pop-in' in the force versus load-line displacement record). It was assumed that the gradual change in the slope of the force versus load-line displacement record was attributable to 'plasticity', or irreversible damage events taking place within the laminate, as described in the previous paragraph. It is the nature of this microscopic damage which is of interest in terms of material toughness, since it is through these that energy absorption takes place.

6.6.3 Crack-tip stresses

In an ideal elastic material, the state of stress ahead of the tip of a sharp crack may be described by asymptotic equations, the general form of which were given in Equation 3.6. These predict that at the crack-tip infinitely high stresses will be observed, reducing in magnitude with increasing distance from the crack-tip. Whilst the materials under scrutiny in this study were far from elastic, homogeneous or isotropic, it is probably fair to assume that macroscopically, the crack-tip stress conditions follow some form of 'asymptotic type' relationship. Assuming this to be so, then

there could be a region ahead of the crack-tip in which high local stresses would prevail, albeit the far-field stress (and strain) in the laminate might be quite low.

Against this background of high stress (and strain), it is reasonable to envisage localised microstructural rupture of the laminate occurring, by any or all of the mechanisms described previously in Section 6.4. In this situation, the macroscopic stress concentration created by the crack-tip may be thought to act as a stimulator for microscopic damage. Stored strain energy released during crack (either microscopic and diffuse or a single macroscopic crack) growth would then be absorbed within the laminate micro-structure through various mechanisms.

Microstructural damage accumulation in the crack-tip region would undoubtedly have the effect of 'blunting' the stress concentration ahead of the macroscopic crack, leading to lower crack-tip stresses. This may be thought to be analogous to the yielding at the crack-tip observed in ductile metals.

6.6.4 Energy absorbing processes

The processes thought to account for energy absorption in composite materials were noted in Chapter 2. To reiterate, these include:

- energy absorbed during fibre-matrix debonding
- energy absorbed through frictional sliding of the fibre pulling-out of the matrix
- energy absorbed during plastic deformation and fracture of the matrix
- energy absorbed in fibre fracture.

6.6.4.1 Fibre-matrix debonding

Although fibre debonding itself is thought to account for a relatively small proportion of the total energy absorption in composite materials (Hull & Clyne, 1996), the conditions under which debonding occurs are of importance since the fractured fibre, once debonded it is able to pull-out from the matrix, thereby absorbing energy through frictional sliding. This latter mechanism is thought to absorb a significant amount of fracture energy (Piggott, 1980; Hull & Clyne, 1996).

Since the macroscopic toughness of composites is closely linked with interfacial effects (Hull & Clyne, 1996), it appropriate to consider here, briefly, the conditions under which fibre-matrix debonding and other interfacial failure events occur. Various tests involving pulling a single fibre from a block of neat resin have been employed to simulate debonding and interface processes. An extensive review of the fibre pull-out test has been conducted by DiFrancia *et al.*, (1996). The following notes the salient points of their conclusions regarding the interpretation of the pull-out test. Depending upon the length of the embedded fibre, distinct regions of the load-extension trace of a fibre pull-out test can be identified with physical events.

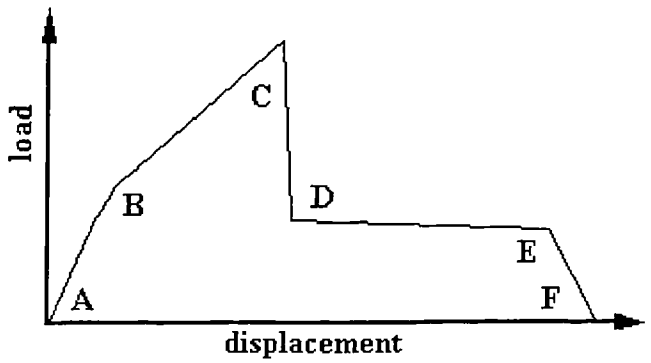

Figure 6.5 Schematic representation of the load-displacement trace in a model fibre pull-out test (*Adapted from:* DiFrancia, *et al*, 1996 and Hampe & Marotzke, 1997).

Figure 6.5 (adapted from DiFrancia, *et al*, 1996 and Hampe & Marotzke, 1997) depicts a model pull-out trace. The first point of interest on the curve occurs at point B, crack initiation. This is the point at which fibre-matrix debonding initiates, and is believed to be the result of normal forces acting across the interface due to Poisson contraction of the fibre (i.e. mode I loading). If the fibre embedded length is now below a critical value to support further, stable, crack growth, catastrophic interfacial failure will result and the debonded fibre will pull-out with friction (as per the tail of the trace D-E). The region B-C represents a region of stable crack growth with increasing frictional resistance. Frictional resistance occurs behind the propagating crack and increases with advancing crack growth, hence the increase in load. At point C, crack growth becomes unstable and the region C-D represents unstable crack

propagation, culminating in total interfacial debonding. The tail of the curve, D-E represents frictional pull-out.

From the foregoing, it follows that the value of the interfacial shear strength (ISS) can be determined at three different experimental times. These correspond to (a) the onset of crack propagation - crack initiation or catastrophic failure, (b) propagation with friction and (c) when debonding is complete, during the pull-out phase (DiFrancia *et al,*. 1996).

It is clear from the above, that if the frictional ISS (region D-E in Figure. 6.5) is very low, then there is little likelihood of any significant energy absorption through frictional sliding. Also, as will be discussed in further detail, high ISS during debonding could result in fibre fragmentation. Since no pull-out tests were conducted in this work, the following is mostly a matter of conjecture. It is, nevertheless, considered that the conditions under which interfacial failure takes place are of prime importance in terms of understanding the behaviour of bast fibre reinforced composites.

The debonding process may, therefore, be thought to be either catastrophic, if the embedded length is small enough, or the result of some stable crack growth accompanied by friction, occurring prior to unstable propagation. It is impossible to say whether the fibre lengths in the hemp-epoxy/polyester systems were long enough to support stable, as well as unstable crack propagation (particularly since it seems probable that the fibre may fragment prior to debonding - see below). However, it is interesting to speculate upon the factors which might affect the initiation and propagation of interfacial cracks in bast fibre reinforced thermosetting polymer systems. Nevertheless, whether the fibre embedded lengths are sufficiently long and the fibres sufficiently strong to support stable crack propagation with frictional resistance could well be important, since energy absorption would accompany this process (DiFrancia *et al.*, 1996).

Qualitative observations conducted in this work indicated that in the bast fibre composite systems, although intimate fibre-matrix contact was achieved during the

fabrication process, adhesion between the two phases is likely to be the result of good mechanical interlocking, rather than any chemical bonding. This would indicate that under suitable circumstances the two might be easily separated. Evidence to support this supposition is provided by the debonding cracks observed in failed SFCs as well as macroscopic laminates, debonding in the former being observed to propagate some way from the fibre break.

According to Hull and Clyne (1996), interfacial debonding often occurs under mixed mode loading (opening and forward shear modes) conditions. Mode I (opening) would presumably be more likely to be associated with crack initiation than propagation, which would probably occur primarily under mode II conditions (DiFrancia *et al.*, 1996). If, as speculated, interfacial adhesion is mainly the result of mechanical interlocking, it seems plausible that debonding would occur far more readily under mode I loading than under mode II conditions. This is likely since, under mode I conditions the interface would tend to separate under the action of normal tensile stresses and this would probably occur relatively easily if there was little 'true' adhesion. Under mode II conditions, however, mechanical interlocking would presumably inhibit debonding.

If these suppositions are correct, it would indicate that whilst crack initiation might be relatively easily achieved, crack propagation would be more difficult. Furthermore, it might imply that those fibres with the most uniform surface topographies would debond most readily. It also raises the possibility that the interfacial fracture toughness may vary along the length of the fibre as a result of differing degrees of surface roughness. This would no doubt impact upon the potential efficacy of any 'Cook-Gordon' type crack blunting/deflection mechanisms.

As discussed previously, it has been demonstrated that the introduction of strong fibre-matrix adhesion has the effect of markedly lowering the Charpy impact strength of hemp reinforced polyester laminates (Sèbe *et al*, 2000). Increased interfacial adhesion would presumably affect crack initiation more strongly (mainly under mode I), than propagation (predominantly mode II). If initiation is suppressed, the debonding process as a whole would be inhibited, resulting in a propagating matrix

crack travelling in a direction normal to the interface passing through the fibre rather than being deflected or blunted at the interface. If debonding under mode I loading is more easily achieved than mode II, it might be implied that crack-deflection and blunting through a 'Cook-Gordon' type mechanism would be inhibited by the introduction of strong interfacial adhesion. The findings of Sèbe *et al.* (2000), would seem to bear this out. If the propagation of a crack along the fibre-matrix interface is, relatively, more difficult to achieve then this could affect the debonding length and consequently the maximum possible pull-out length. This would, of course, affect the maximum energy that could be absorbed through interfacial frictional sliding during pull-out.

Other factors which may influence the conditions under which debonding takes place include any residual stresses acting across the interface, due for example, to a mismatch in thermal expansivities (Grubb & Li, 1994) or volumetric cure shrinkage of the matrix (Hull & Clyne, 1996). An aspect which has thus far been ignored in this discussion on debonding, is the environmental behaviour of the fibre. As noted in Chapter 2, lignocullulosic material is subject to swelling/shrinkage as a result of adsorption/desorption of moisture. It might therefore be envisaged that if any desorption (or cycling) were to have taken place subsequent to manufacture, then the interface would be subject to normal tensile stresses acting across it. It would seem probable that in these circumstances the integrity of the fibre-matrix bond may be compromised, making debonding more likely.

Visual examination of failed SEN specimens as well as the theoretical predictions made using fracture mechanics indicated that fibre-matrix debonding is far less extensive in the bast fibre reinforced material than in the glass fibre reinforced laminates. In other words, the size of the damage zone is small in the bast fibre reinforced PMC. This may be explained in terms of fibre damage and its effect upon the tensile properties of the fibre.

Consider a fibre undergoing debonding, such as might be found bridging a propagating matrix crack. As the macroscopic crack opens, the load on the fibre will increase and the interfacial debond crack will progressively propagate along the

interface. Consequently, the stress in the fibre will build-up along the debonded length (due to the effect of friction) to a maximum, once the fibre is clear of the matrix. If the axial fibre stress at any point exceeds the strength of the fibre, then fracture will occur. Bast fibres, as discussed in Chapter 4, contain a significant number of micro-compressive defects, many of which are very closely spaced and which have been shown to reduce the tensile strength of (flax) fibre ultimates (Davies & Bruce, 1998). It would seem likely, therefore, that a critical defect could well be met after relatively little debonding had occurred. This might well result in short pull-out lengths with consequently little energy absorption.

One of the major differences observed between the fracture surfaces of the bast fibre and glass fibre reinforced polymer systems was fibre pull-out. As noted in Section 3.3.7, the pull-out aspect ratios seen in the bast fibre reinforced laminates were significantly less than in the CSM reinforced material. This may be explained in terms of the relative strengths of the fibres and the stress transfer from matrix to fibre. As composite strain is increased, the axial stress in the fibre also increases, due to a rise in the ISS. If the axial stress in the fibre rises to above that of the fibre strength, it will fracture. Assuming that ISS becomes uniform at the interfacial shear strength, τ_{max}, of the system, it follows that there is a minimum value of fibre aspect ratio below which the build-up of stress in the fibre cannot reach the ultimate strength of the fibre. This introduces the concept of the critical aspect ratio, S_{crit} (aspect ratio in this instance is defined as the length of the fibre divided by its radius). This corresponds to the peak fibre stress just attaining its ultimate strength, σ_{fu}, under the influence of the interfacial shear stress. It may be shown that the following condition exists (Hull & Clyne, 1996):

$$S_{crit} = \frac{\sigma_{fu}}{2\tau_{max}} \qquad (6.2)$$

From Equation 6.2, it may be inferred that the fibre pull-out length (related to critical aspect ratio) is proportional to the strength of the fibre and inversely proportional to the stress transfer from matrix to fibre. If it is taken into consideration that in bast fibres, fracture is likely to be dominated by the presence of micro-compressive defects

and that, based on the forgoing discussion, stress transfer (either elastic or inelastic processes) is probably fairly effective (due to mechanical interlocking), this may provide a likely explanation for the low fibre pull-out lengths observed.

6.6.4.2 Frictional sliding and fibre pull-out

Once the fibre is totally debonded from the surrounding matrix, it is able to slide in the resultant socket. During the process of withdrawal, fracture energy may be dissipated through friction. Depending upon the surface roughness, contact pressure and sliding distance, this mechanism can account for a great deal of energy absorption in composite materials (Hull & Clyne, 1996).

Using a shear-lag analysis, it may be shown that the contribution to the overall work of fracture made by fibre pull-out is given by (Piggott, 1980; Hull & Clyne, 1996):

$$G_{fp} = \frac{V_f \, d \, \tau_{sif} \, S^2}{6} \qquad (6.3)$$

Where:

	G_{fp}	is the work of fibre pull-out
	d	is the diameter of the fibre
	τ_{sif}	is the sliding interfacial shear stress (due to friction)
	S	is the fibre aspect ratio

This relationship predicts that the work of fibre pull-out will increase as the square of the fibre aspect ratio, as well as increasing with volume fraction, fibre diameter, and sliding frictional ISS.

As discussed previously, the morphology of bast fibres is quite irregular, in addition to which the fibre surface has the appearance of being relatively rough. It is probable, therefore, that this would affect the manner in which the fibre withdraws from the matrix socket. In the bast fibre composite systems studied, it seems likely that the frictional ISS would be far from constant, varying as a result of undulations in the fibre cross-section and changes in surface topography. Sanadi *et al.* (1986b), noted that such variations in frictional ISS as might occur during pull-out, could influence

the toughness of Sunn hemp-polyester composites. Variations in the fibre cross-sectional area might lead to fluctuations in the normal forces acting on the fibre surface, as a result of elastic (with possibly inelastic) deformation of the cell wall. Since frictional ISS is the product of the coefficient of friction and the normal pressure acting upon the fibre surface (DiFrancia, *et al.*, 1996), any rise in the normal pressure would be accompanied by a commensurate increase in ISS (if, for the time being it is assumed the coefficient of friction is constant). Not only is it likely that undulations in the fibre surface would result in varying frictional ISS, but it is also possible that mechanical 'keying' of the fibre in the socket may take place, where major changes in fibre section (for instance micro-compressive defects) 'lock' into adjacent regions of the matrix socket. Indeed, it is plausible that this might physically prevent fibre pull-out occurring in the first instance and may actually result in fibre fracture if the axial fibre stress in raised sufficiently (see below). Further, due to apparent variations in surface roughness, it is possible that the coefficient of friction varies along the length of the fibre. This, presumably, would also impact upon the frictional ISS. Based upon the forgoing, it would seem likely that there would be a certain amount of 'stick-slip' activity as a fibre pulls through the matrix. Nevertheless, there are further factors which might affect the normal force acting upon the fibre and which, consequently, could affect ISS and hence the work of fibre pull-out.

It would seem probable that relatively thin walled fibres would undergo deformation more readily as they travel through the matrix socket, than thicker walled individuals. This radial deformation of the fibre would presumably lead to lower contact pressure, lower frictional ISS and hence lower energy absorption. In addition to this, Poisson contraction of the fibre would presumably affect the 'stick-slip' behaviour. As the axial load on the fibre increases during the 'stick' phase (due to the mechanical hold of the matrix on the fibre (DiFrancia *et al.*, 1996)), the fibre would undoubtedly contract to some extent. In doing so, the normal clamping pressure would reduce to a point at which friction is overcome and the fibre undergoes slip. Since the axial load would then reduce, the fibre would expand (assuming that the contraction process was fully reversible) and 'sticking' would be re-established. This behaviour could

well compound the effects of the mechanical 'lock and key' phenomenon described above.

It has, thus far, been considered that the fibres deform elastically up to fracture and whilst the evidence supports this in bast fibres (Davies & Bruce, 1998), 'pseudo-plastic' behaviour is observed in individual wood fibres (Gordon & Jeronimidis, 1974). It is just possible that, during either debonding or pull-out, the fibres deform inelastically to some extent. It might be expected, therefore, that such behaviour would be accompanied by a permanent reduction in the cross-section of the fibre, which if sufficient to prevent contact with the matrix, would result in zero frictional resistance and hence no energy absorption. This same conclusion was reached by Sanadi *et al.* (1986b) in their work on Sunn hemp-polyester composites.

As noted above, 'movement' of the lignocellulosic fibres may alter the normal forces acting across the interface. This could, presumably, also affect the normal pressure acting upon the fibre and consequently energy absorption through frictional sliding.

The relationship given in Equation 6.3 predicts that (assuming all other terms are equal) the work of fibre pull-out is proportional to the square of the aspect ratio of the pulled-out fibre. This may partly explain the reasons for the lack of toughness observed in the bast fibre reinforced materials. As discussed above and in Section 3.3.7 (Plates 3.3-3.5), the fibre pull-out aspect ratios in the bast fibre reinforced laminates are perhaps at best of the order of 10:1, but in any event are significantly less than those observed in the glass fibre reinforced material. Even taking into account the larger 'diameter' of bast fibres and the possibly good frictional ISS, it is difficult to envisage how any significant amounts of energy can be dissipated through frictional sliding, when the pull-out aspect ratios are so low.

The reasons for the low fibre pull-out aspect ratios were partly discussed above, in terms of fibre damage. However, it is appropriate to elaborate upon this at this juncture. During micro-mechanical tests with SFCs (see Section 5.3.6), the reinforcing fibres were noted to fragment, with fracture believed to occur at micro-compressive defects. Since the strain to failure of bast fibres is less than that of

typical epoxy resins, it is not surprising that this behaviour should be observed. Although no statistical records of fragment length were kept, it may be clearly observed from Plate 5.9, that the aspect ratios of the fragments were quite low, being of the order of 40:1 (L/r). It would seem plausible, therefore, that in regions of the laminate subject to relatively higher matrix strains (such as may be found in the vicinity of a stress concentrator), fragmentation (accompanied by limited fibre-matrix debonding) should occur. Consider now a macroscopic crack propagating in a direction normal to a single fragment. On the assumption that no further fragmentation takes place, the maximum aspect ratio available to pull-out (assuming that at best one half of the fragment pulled-out) would be 20:1, or a length to diameter ratio of 10:1. These orders of fibre pull-out aspect ratio were observed in the 'real' laminates.

In this scenario, it seems possible that fragmentation of the fibre prior to macroscopic cracking could occur, severely limiting the fibre pull-out aspect ratio. This type of 'pre-fragmentation' would be dependent upon the relative composite strain, the efficacy of stress transfer from matrix to fibre and may well be dominated by the frequency and severity of micro-compressive (or other) fibre defects. The fibres used in the preparation of SFC, although micro-compressed, were relatively undamaged. It is possible to envisage that in fibres which have undergone any significant processing, additional damage may exacerbate fibre fragmentation, to the detriment of laminate toughness.

If, in the above example, the matrix crack-tip passes the fragmented fibre and debonding proceeds along the fibre-matrix interface to the end of the fragment, then the aspect ratio of the withdrawn fibre would be dependent upon the remaining embedded length. However, to facilitate debonding and fibre pull-out, the faces of the macroscopic crack must continue to separate. As a result, the load on the fibre will continue to increase, supplying the requisite strain energy for the debond crack to propagate and to overcome the frictional resistance following debonding. However, as discussed above, during the debonding process it is possible that the fibre stress may exceed some critical value, either resulting in fracture in the plane of the crack, or

at some point along the debonding region (Hull & Clyne, 1996). This may well have the effect of lowering, still further, the pull-out aspect ratio.

Assuming the fibre, up to a certain aspect ratio, has completely debonded, then pull-out may commence. If, however, the fibre is mechanically constrained due to physical 'keying' within the matrix, then it is feasible that the fibre stress will again rise, possibly resulting in fibre fracture. Similarly, as the fibre withdraws, it is likely to experience stick-slip behaviour. During the 'stick' phase, it is again plausible that the fibre axial stress may exceed some critical value, thereby causing it to fracture. With all these possible mechanisms, micro-compressive defects could play a vital role in the debonding and pull-out of the fibres and may well be, at least partly, responsible for the low toughness of bast fibre reinforced composites.

It can be shown that work of fibre pull-out ($G_{fp_{MAX}}$) reaches a maximum when S is equal to the critical fibre aspect ratio (Equation 6.2) and that in this instance:

$$G_{fp_{MAX}} = \frac{V_f d \sigma_{fu}^2}{24 \tau_{max}} \qquad (6.4)$$

The interesting aspect of this prediction is that the maximum work of fibre pull-out is proportional to the tensile strength of the fibre and is inversely related to the interfacial shear strength. If, following the foregoing discussion, it is assumed that the ultimate strength of micro-compressed fibres is significantly less than that of glass fibre and that the interfacial shear strength is not insignificant, then even allowing for the greater diameter of bast fibres, it is not difficult to envisage a significant difference in the works of fibre pull-out.

6.6.4.3 Plastic deformation and fracture of matrix

The work of fracture of the unreinforced polyester resin determined in this study was about 0.09 kJ m^{-2}. It would seem unlikely that matrix deformation and fracture would account for any significant amount of energy absorption in the bast fibre reinforced composite systems.

6.6.4 Work of fibre fracture

As noted in Chapter 4, the work of fibre fracture in bast fibres is likely to be quite small since any pseudo-plastic deformation of the fibre would seem improbable. The work of fracture in bast fibres is, therefore, likely to be akin to the 'intrinsic toughness' of the cell wall material, determined by Lucas *et al.*, (1996, 1997) to be in the region of 3.45 kJ m^{-2}. Although this figure is significantly greater than glass (a few tens of Joules per square metre - Hull & Clyne, 1996), it seems unlikely that this mechanism could account for large amounts of energy absorption in these composites.

In bast fibre reinforced thermosetting PMCs, it seems probable that the main reason for the low toughness exhibited by these materials, is the lack of energy absorption through fibre pull-out, the mechanism thought to account for substantial amounts of energy dissipation in composite materials (Hull & Clyne, 1996). Simplistically, this is probably the result of relatively low fibre strength (particularly when exacerbated by micro-compressive damage) coupled with good fibre-matrix interaction. The remaining energy absorption mechanisms namely, debonding and fibre and matrix fracture would seem unlikely to contribute significantly to this process. The high works of fracture observed in wood fibres would not appear to be shared by their bast fibre cousins.

6.7 Conclusions

Whilst much of the discussion in this chapter has been based on conjecture, it was believed that some attempt should be made to explain the observed macroscopic properties in terms of the laminate micro-structural organisation. On the basis of the findings of this work it seems very probable that both non-linear behaviour and toughness (or lack of it) can be explained in terms of the fibre properties and the interaction between fibre and matrix.

It seems plausible that micro-compressive defects in the cell wall of bast fibres result in heterogeneous straining characteristics, which lead to microstructural laminate

damage at possibly very low stress levels. This, coupled with fibre architecture and seemingly poor fibre-matrix bonding (adhesion), could account for the onset of non-linear behaviour at low nominal stress levels.

With regard to composite toughness, it would appear that the relative lack of toughness when compared to the CSM glass fibre, can be attributed to poor energy absorption. This is probably due to limited energy dissipation through frictional sliding and pull-out. The likely reasons for this seem to be that, in reality, the fibre strength is quite poor in comparison to glass fibre. Furthermore, good fibre-matrix interaction through mechanical interlocking probably exists, limiting debonding, with consequently shorter pull-out lengths. Coupled with fragmentation of the fibre at low composite strains, it seems likely that the debonded fibre length available for pull-out is relatively low. This is reflected in the short pull-out lengths observed. It would seem unlikely that any significant further contribution to the composite work of fracture is afforded by either debonding, matrix deformation and fracture or fibre fracture.

The apparent bimodular behaviour of bast fibre reinforced polyester laminates may be ascribed to potentially differing tensile and compressive moduli under axial and radial loading.

As noted above, much of this chapter has been based on conjecture. Nevertheless, the discussion has raised a number of issues which should be considered if a deeper understanding of the mechanisms controlling the mechanical behaviour of bast fibre composites is to be achieved. These are outlined in the final chapter.

7 Conclusions and Recommendations for Further Work

7.1 Introduction

The purpose of this, the final chapter, is to review the work presented in the thesis, to summarise the main conclusions drawn and to suggest the direction in which it is believed further research should be pursued, at least as far as the mechanical properties of natural fibre reinforced composites are concerned. Now, with the benefit of hindsight, it is fair to say that a number of issues which arose during the course of this work would have been better approached in a somewhat different manner. Thus, this chapter also aims to highlight what are perceived to be some of the main limitations of this work in the hope that any further work conducted in this area of research can avoid some of these pitfalls.

7.2 Summary of main conclusions

The work undertaken and presented in Chapter 3 was concerned with the macromechanical properties of needle-punched, non-woven bast fibre reinforced unsaturated polyester laminates. The properties of these materials were compared with those of laminates reinforced with CSM glass fibre utilising the same matrix polymer. The main findings were, that whilst the initial stiffness of the bast fibre laminates was on a par with that of the synthetic material, their strength and particularly toughness were substantially inferior, on the basis of equivalent (by volume) fibre loadings. Coupled with this, it was found that the bast fibre reinforced material, particularly the hemp, displayed incipient non-linear behaviour, at low levels of applied stress.

In view of the interest (and concern) regarding the failure of these materials, fracture mechanics techniques were applied in order to quantify the toughness of the laminates. Although the applicability of fracture mechanics (particularly LEFM) in this instance is open to criticism, it is believed that the results were of value in that they seemed to indicate that in the bast fibre reinforced material, toughening mechanisms were simply not stimulated to the same extent as in their glass fibre reinforced equivalents. This led to the conclusion that the microstructure was crucial and should be examined in closer detail. Fracture mechanics provided what is believed to have been a more quantitative assessment of the toughness of these composite systems. It appeared to confirm earlier suspicions that, for equivalent fibre loadings, the difference between the works of fracture of the synthetic and natural fibre reinforcements was almost an order of magnitude. In view of the amount of plasticity exhibited by the natural fibre reinforced materials, EPFM would seem to provide a more representative value of material toughness.

Fractography revealed that, at low fibre loadings, failure in the bast fibre laminates was predominantly brittle, but that at higher V_f, fracture included some evidence of shearing. SEM studies showed that little fibre pull-out occurred (especially when compared with the extensive pull-out observed in the glass fibre reinforced material). This, coupled with brittle fracture of the fibres themselves and seemingly good fibre-matrix interaction, were thought to contribute to the low toughness of the plant fibre reinforced material. The good fibre-matrix interaction was evidenced, not only by the appearance of cured resin within the lumen, but also by the low void content of the laminates. Nevertheless, the degree of true 'adhesion' between the fibre and polymer is open to question and is an aspect which, it is believed, should be explored more thoroughly.

Although the mechanical properties of the fibres themselves were not investigated during the course of this work, it is believed that the lower strength and toughness of the bast fibre reinforced PMCs can, in part at least, be attributed to the significantly lower strength of the natural fibres. In reality (after processing etc.) this might well be as much a factor of 5 difference. In addition to the foregoing, it was believed that fibre damage exacerbated the effects of low fibre strength, by affecting the interface

between fibre and matrix, possibly leading to formation of stress concentrations. This contention was supported too by the onset, in the bast fibre reinforced material, of plastic behaviour at low stress levels. This was attributed, not only to the fibre architecture, but also to fibre damage, resulting in a population of stress concentrators, which it was believed caused microstructural damage at low applied loads.

In general, the findings of Chapter 3 indicated that the microstructure of the bast fibre laminates should be investigated in more detail.

As noted in Chapter 1, the initial concept of this project was that of 'product development' rather than a 'fundamental' study. It is because of this that the laminates investigated in this aspect of the work were reinforced with a non-woven felted material. It is believed, however, that the use of such a reinforcement configuration led to difficulties in the interpretation of test data. It is considered that it would have been preferable to utilise unidirectional laminae, since this would have facilitated simpler analysis and interpretation of the test data. It would be desirable, in future work, to utilise such laminates.

On a practical note, whilst needle-punched non-wovens are relatively easy to produce, they would appear to be of limited use as reinforcement. Firstly, the intensive mechanical action of 'carding', introduces significant damage to the fibres (see below) which no doubt compromises the laminate properties. In addition to this, non-woven felts are inherently bulky, requiring large external pressures to consolidate the mat. In this work, the maximum V_f's achieved were less than 50% and even these were only obtained by pre-pressing the felted fibres. Without pre-pressing, the maximum V_f's attained were generally of the order 15-20%. During this work, however, it was established that the 'break-even' volume fraction was of the order of 25%. This 'break-even' was the mimimum value of fibre addition required, so as to attain the same strength as the unreinforced resin. Thus without pre-pressing, the addition of felts effectively weakens the laminates. In view of this, it is doubtful whether useful composites could be manufactured from non-woven felted material and it would be preferable to consider other reinforcement architectures.

As intimated above, it was believed that fibre damage might well influence the mechanical properties of the laminates. In view of this, a detailed micoscopical study of the fibres was presented in Chapter 4. It was found that all the bast fibres studied exhibited micro-compressive damage to a greater or lesser degree. It was not entirely clear at what stage the fibres became damaged, but it seemed likely that whilst some damage probably occurred within the plant, subsequent processing exacerbated not only the extent, but also the degree of 'kinking'. It was thought that the ultrastructural organisation of bast fibres probably makes them particularly vulnerable to the formation of this type of damage. In studies by other workers, it has been shown that these defects lead to a reduction in both the tensile strength and modulus of the fibres (Davies & Bruce, 1998). A simple model presented herein showed good agreement with other published experimental results for the fibre tensile properties. In this work, it was postulated that the presence of 'kink bands' or 'minute compression creases' led to uneven fibre straining characteristics, which it was believed might well influence the characteristics of the interface.

It has been postulated that fibre fracture might contribute substantially to the overall work of fracture of lignocellulosic based composites. Unfortunately, it would appear that these bast fibres, although amongst the strongest of all vegetable fibres, are brittle, displaying none of the 'pseudo-plastic' behaviour associated with the high toughness of wood fibres. This may, again, be attributed to their ultrastructural organisation.

As will be discussed further, it seems clear that micro-compressive defects do influence the behaviour of bast fibre reinforced PMCs. In view of this, it would seem appropriate to conduct further work into the nature and origin of these features, in the hope that it might elucidate the mechanisms behind 'kinking' in bast fibres and whether means might be sought to reduce their occurrence and/or influence upon fibre properties. It would be very interesting to ascertain whether these features are common to all varieties of the plants producing the fibres (flax and hemp), or whether varieties exist which are not so susceptible. Furthermore, if as is suspected, these features strongly influence composite properties, benign means of separating the fibres

from the plant should be sought as well as more 'fibre friendly' methods of producing reinforcement preforms.

Verification of the supposition that heterogeneous fibre straining characteristics lead to compromised interfacial properties was explored in Chapter 5. The technique of half fringe photoelasticity (HFP) was used to examine the nature of the stress distribution in the vicinity of individual micro-compressive defects. In addition to this, the system was used to make certain inferences regarding the nature and efficacy of the stress transfer mechanisms operative in plant fibre-polymer systems. The influence of micro-compressive defects on fracture behaviour in single filament composites was also investigated.

The applicability of HFP to determine the stress-field in a birefringent polymer was demonstrated by considering the stress distribution around a circular hole in a polymer film, and comparing this with theoretical solutions for such configurations. It was found that good agreement could be obtained. There were, however, a number of drawbacks with the system in its present form. If these were addressed, it is believed that HFP could provide a powerful tool for the analysis of matrix stresses and strains in the interphase region of plant (and other) fibre reinforced PMCs. It is felt that a worthwhile exercise would be to develop the system more fully in this respect.

Ultimately, the quality of the stress analysis which can be performed by digital image analysis (DIA) is dependent upon the quality of the original image. In this respect, attention should be paid to the manner in which the specimens are prepared (avoidance of air bubbles or debris) or any other factors which might ultimately affect image quality. In addition to this, the manner in which the specimens are illuminated should be carefully considered - a greater 'evenness' of lighting would undoubtedly help reduce errors. In particular, it is felt that the HFP system would benefit from a more powerful monochromatic light source. This would, it is believed, make it possible to use higher optical magnification, enabling finer resolution of the stress distribution. In addition to this, electronic averaging of multiple images would, no doubt, help eliminate random electrical 'noise'. An aspect which was considered to be a major drawback, was the inability to accurately rotate the optical elements of the

circular polariscope arrangement relative to one another. If this could be achieved, the calibration procedure would be much simplified. In addition to this, the system could be extended to enable the directions of the principal stresses to be computed from the isoclinic fringe pattern.

It is believed, nevertheless, that HFP has certain limitations. Firstly, the system is bound to operate within the first 'half fringe' of relative retardation. As such, in highly stressed regions with steep stress gradients, not only is it possible that the 'half fringe' might be exceeded, but also non-linear behaviour may become significant. In view of the interest in the fracture behaviour of these systems (which, almost by definition, includes large stresses and non-linearity), it would certainly be of benefit to have the facility to analyse fringe orders > 0.5. This could also be achieved through DIA techniques. It is worthwhile noting that in this work the SFCs were regarded as two dimensional systems. This is undoubtedly a simplification and might lead to errors in analysis if higher resolution were required. Due account should be taken of the three dimensional nature of the systems under investigation.

The analysis of SFC specimens using HFP revealed that concentrations of stress arose in close proximity to the 'kink bands' or 'minute compression failures'. Stress concentration factors of up to around 1.65 were recorded. When the principal stress difference in the matrix adjacent to the fibre surface was considered, it was inferred that the interfacial shear stress distribution varied along the fibre-matrix interface. The principal stress difference (related to shear stress) along the length of the fibre appeared to follow what might be termed a 'shear-lag' type distribution between adjacent micro-compressive defects. From this, it was concluded that the efficacy of stress transfer between fibre and matrix was compromised by the presence of the micro-compressions. This, it was believed, might ultimately affect the macroscopic performance of the composite. The variation in the matrix principal stress difference in close proximity to the true fibre-matrix interface was attributed to un-even fibre straining characteristics and it was concluded that the fibre may be regarded as having an overall or 'composite' tensile modulus. It was postulated that the micro-compressive defects could be likened to a series of small 'cracks' or 'holes' in the matrix, resulting in stress concentrations. Alternatively, micro-compressed fibres

might be thought similar to a number of short fibres in series. In whatever way these features are considered, it seems highly likely that they compromise the performance of the composites.

Analysis of fractured specimens showed that failure occurred at the defects and that fibre-matrix debonding and transverse matrix cracking were also present. It was concluded that fibre-matrix debonding was probably the result of high interfacial shear stresses present in the vicinity to the micro-compressive defects. Coupled with the improvements to the system described above, it would be of great interest to monitor the matrix stress-strain field during the fracture process in SFCs.

In Chapter 6, an attempt was made to pull together the various aspects discussed in the preceding three chapters with the aim of relating the observed phenomena. One issue which was considered in some detail was the possible influence that an individual micro-compressed fibre might have upon its neighbours. Several scenarios were considered, though all were 'hypothetical'. It would, therefore, be of great benefit to investigate this possible behaviour in 'real' systems, in other words in micro-tensile specimens containing more than one fibre. This would, hopefully, provide some insight into whether these failure mechanisms actually occur or not.

The nature of fibre-matrix bonding was considered throughout the text, although no work was actually conducted to measure this. It is believed that this is an aspect which should be addressed. Of particular relevance would be the manner in which the fibres pull-out from the matrix, since this will have a bearing upon the toughness of the material. Techniques should be developed to accurately record the pull-out phenomenon in bast fibre-thermosetting polymer systems (with due regard taken with interpretation of the data).

The findings of this study have indicated that the properties of bast fibres are different in compression and tension. No compression tests were performed during the course of this work, but it is considered that it would be a worthwhile exercise to investigate possible bimodular behaviour and also to assess the compressive strength of laminates parallel to the fibre axis, since this could be another limiting factor.

Overall, it is believed that the work conducted and presented herein accomplished what it set out to achieve, namely, to provide a thorough assessment of the short-term mechanical properties of bast fibre reinforced thermosetting PMCs. It is hoped that some further insight into the mechanisms controlling the mechanical behaviour of these materials has been gained. Whilst it seems improbable that bast fibres will ever directly replace glass fibre as a reinforcement, it is to be hoped that useful applications can be found for bast fibre based PMCs, in which the benefits of light weight and biodegradability might be exploited. Specifically, it is believed that certain aspects should be considered further in the hope that performance might be enhanced. These can be summarised as follows:

- Research into the origin of fibre defects and methods by which their occurrence might be limited.
- New technologies for the preparation of fibres into useful reinforcement pre-forms.
- Processing technologies to fabricate composite structures containing high volume fractions of fibre.
- Further fundamental research into the nature of the fibre-matrix interface, with possible 'interface engineering' to help alleviate some of the worst effects of micro-compressive damage.

The issues of environmental performance have not been considered here, or other aspects such as acoustic properties, creep, fatigue etc. which will all be relevant in practical terms. These too require further consideration. It is firmly believed, however, that new and exciting applications can yet be found for these materials in which their particular properties might be fully exploited.

References

Aero Research Limited, (1945). *A Fighter Fuselage in Synthetic Material.* Aero Research Technical Notes.

Akin, D.E., Gamble, G.R., Morrison III, W.H. and Rigsby, L.L. (1996). Chemical and Structural Analysis of Fibre and Core Tissues from Flax. *J. Sci. Food Agric.*, **72**: 155-165.

Anderson, T.L., (1995). *Fracture Mechanics: Fundamentals and Applications. Second Edition.* CRC Press Inc, Boca Raton.

Argon, A.S. (1972). *Fracture of Composites.* Academic: New York.

Ashby, M.F. and Jones, D.R.H. (1980). *Engineering Materials : An Introduction to their Properties and Applications.* Pergamon Press, Oxford; New York.

Ashby, M.F., Easterling, K.E., Harrysson, R. and Maiti, S.K. (1985). The Fracture Toughness of Woods. *Proc. R. Soc. Lond. A*, **398**: 261-280.

Aspinall, G.O. (1980). *Chemistry of Cell Wall Polysaccharides. In: The Biochemistry of Plants: A Comprehensive Treatise, Vol. 3: Carbohydrates: Structure and Function. Ed. Preiss, J.* Academic Press, New York. pp. 480-486.

Astley, R.J., Stol, K.A. and Harrington, J.J. (1998). Modelling the Elastic Properties of Softwood. Part II: The Cellular Microstructure. *Holz als Roh- Und Werkstoff*, **56**: 43-50.

ASTM. Designation: E 399-90. (1991). *Standard Test Method for Plane-Strain Fracture Toughness of Metallic Materials.* ASTM, Philadelphia, USA.

Bisanda, E.T.N. and Ansell, M.P. (1991). The Effect of Silane Treatment on the Mechanical and Physical Properties of Sisal-Epoxy Composites. *Comp. Sci. and Technol.*, **41**: 165-178.

Bishopp, J.A. (1997). The History of Redux® and the Redux Bonding Process. *Int. J. Adhesion and Adhesives*, **17**: 287-301.

Bledzki, A.K., Reihmane, S. and Gassan, J. (1996). Properties and Modification Methods for Vegetable Fibers for Natural Fiber Composites. *J. App. Polym. Sci.*, **59**: 1329-1336.

Bolton, A.J. (1994). Natural Fibres for Plastic Reinforcement. *Mat. Tech.*, **9**(1/2): 12-20.

Bolton, A.J. (1995). The Potential of Plant Fibres as Crops for Industrial Use. *Outlook on Agriculture*, **24**(2): 85-89.

Bonfield, W. (1994). Artificial Bone. *In: Concise Encyclopaedia of Composite Materials. Ed. Kelly, A.* Pergamon, Oxford, UK. pp. 15-17.

Booker, R.E. (1995). The Reason for the Microfibril Orientations in the Cell Wall of Trees. *In: Recent Advances in Wood Anatomy. Eds. L.A. Donaldson, A.P. Singh, B.G. Butterfield, J. Whitehouse.* NZ Forest Research Institute Ltd. pp. 273-282.

Booker, R.E. and Sell, J. (1998). The Nanostructure of the Cell Wall of Softwood and Its Functions in a Living Tree. *Holz als Roh- und Werkstoff*, **56**: 1-8.

Boresi, A.P., Schmidt, R.J. and Sidebottom, O.M. (1993). *Advanced Mechanics of Materials, Fifth Edition.* John Wiley and Sons, Inc., New York.

Bos, H.L., Van den Oever, M.J.A. and Peters, O.C.J.J. (1997). *In: Proceedings of the 4th International Conference on Deformation and Fracture of Composites.* March, 1997. Manchester, UK.

Bos, H.L. and Donald, A.M. (1999) *In Situ* ESEM Study of the Deformation of Elementary Flax Fibres. *J. Mat. Sci.*, **34**: 3029-3034.

Bos, H.L. and Van den Oever, M.J.A. (1999) The Large Influence of Flax Fiber Structure on Composite Strength. *In: Proceedings of the 5th International Conference on Woodfiber-Plastic Composites, May 26-27, 1999, Madison, WI, USA.* Forest Products Society, Madison, WI, USA. pp. 79-85.

Bos, H.L. (1999). Personal Communication.

Brown, W.J. (1947). *Fabric Reinforced Plastics.* Cleaver-Hume Press Ltd., London.

BS 2782: Part 10: Method 1003: (1977) EN 61. *Determination of Tensile Properties.* British Standards Institution, London.

BS 2782: Part 10: Method 1005: (1977) EN 63. *Determination of Flexural Properties. Three Point Method.* British Standards Institution, London.

BS 7448: Part 1. (1991). *Determination of Plane Strain Fracture Toughness (K_{Ic}), Critical Crack Tip Opening Displacement (CTOD) and Critical J Fracture Toughness Values for Metallic Materials under Displacement Controlled Monotonic Loading at Quasi Static Rates.* British Standards Institution, London.

BS EN ISO 179: (1977). Plastics – Determination of Charpy Impact Strength. European Committee for Standardization, Brussels.

Burger, C.P. (1988). New Approaches to Optical Methods in Experimental Solid Mechanics Through Digital Image Analysis. *In: Proceedings of the VI International Congress on Experimental Mechanics, 1988.* 655-660.

Burger, C.P. (1993). Photoelasticity. *Chapter 5 in: Handbook on Experimental Mechanics. Ed. Kobayashi, A.S.* Society for Experimental Mechanics, Bethel, USA/VCH Publishers, Inc., New York.

Burger, C.P. and Voloshin, A.S. (1982). Half-Fringe Photoelasticity: A New Lease of Life for an Old Method. *In: Proceedings of the 1982 Joint Conference on Experimental Mechanics, Honolulu, Hawaii, May 23-30, 1982.* 972-977.

Burger, C.P. and Voloshin, A.S. (1983). Stress Intensity Factors in Glass and Polycarbonate by Half Fringe Photoelasticity. *In: Proceedings of the Ninth Canadian Congress of Applied Mechanics, University of Saskatchewan, Saskatoon, May 30-June3, 1983.* 915-916.

Carruthers, S.P. (1994). Crops for Industry and Energy. *In: CAS Report 15. Eds. Carruthers, S.P., Miller, F.A. and Vaughan, C.M.A.* pp.92-108.

Catling, D. and Grayson, J. (1982). *Identification of Vegetable Fibres.* Chapman and Hall, London.

Cave, I.D. (1968). The Anisotropic Elasticity of the Plant Cell Wall. *Wood Sci. Technol.*, **2**: 268-278.

Cave, I.D. (1969). The Longitudinal Young's Modulus of Pinus Radiata. *Wood Sci. Technol.*, **3**: 40-48.

Cave, I.D. and Robinson, W. (1998). Measuring Microfibril Angle Distribution in the Cell Wall by Means of X-Ray Diffraction. *In: Microfibril Angle in Wood. The Proceedings of the IAWA/IUFRO International Workshop on the Significance of Microfibril Angle in Wood Quality, Westport, New Zealand, November, 1997. Ed. Butterfield, B.G.* International Association of Wood Anatomists (IAWA)/International Union of Forestry Research Organisations (IUFRO). Westport, New Zealand. pp. 94-107.

Chanzy, H. (1990). Aspects of Cellulose Structure. *In: Cellulose Sources and Exploitation: Industrial Utilization, Biotechnology and Physico-Chemical Properties. Eds. Kennedy, J.F., Phillips, G.O. and Williams, P.A.* Ellis Horwood, New York; London. pp. 3-12.

Chesson, A. (1978). The Maceration of Linen Flax under Anaerobic Conditions. *J. Applied Bacteriology*, **45**, 219-230.

Chesson, A. (1980). A Review: Maceration in Relation to the Post-Harvest Handling and Processing of Plant Material. *J. Applied Bacteriology*, **48**, 1-45.

Chohan, V. and Galiotis, C. (1997). Effects of Interface, Volume Fraction and Geometry on Stress Redistribution in Polymer Composites Under Tension. *Comp. Sci. Technol.*, **57**: 1089-1101.

Chou, T-W. (1994). Laminates: Elastic Properties. *In: Concise Encyclopaedia of Composite Materials. Ed. Kelly, A.* Pergamon, Oxford, UK. pp. 159-165.

Chum, H.L. and Power, A.J. (1992). Opportunities for the Cost-Effective Production of Biobased Materials. *Chapter 3, in: Materials and Chemicals from Biomass, American Chemical Society*, 1992. pp. 28-41.

Conners, T.E. and Medvecz, P.J. (1992). Wood as a Bimodular Material. *Wood and Fiber Science*, **24**(4): 413-423.

Cook, J. and Gordon, J.E. (1964). A Mechanism for the Control of Crack Propagation in All-Brittle Systems. *Proc. Roy. Soc. Lond. A*, **282**: 508-520.

Cousins, W.J. (1976). Elastic Modulus of Lignin as Related to Moisture Content. *Wood Sci. Technol.*, **10**: 9-17.

Cousins, W.J. (1978). Young's Modulus of Hemicellulose as Related to Moisture Content. *Wood Sci. Technol.*, **12**: 161-167.

Cox, H.L. (1952). The Elasticity and Strength of Paper and Other Fibrous Materials. *Brit. J. Appl. Phys.*, **3**: 72-79. (*Cited in:* Hull & Clyne, 1996).

Currey, J. (1984). *The Mechanical Adaptations of Bone*. Princeton University Press, Princeton, N.J., USA.

Dally, J.W. and Riley, W.F. (1965). *Experimental Stress Analysis*. McGraw-Hill. New York.

Davies, G.C. and Bruce, D.M. (1997). A Stress Analysis Model for Composite Coaxial Cylinders. *J. Mat. Sci.*, **32**: 5425-5437.

Davies, G.C. and Bruce, D.M. (1998). Effect of Environmental Relative Humidity and Damage on the Tensile Properties of Flax and Nettle Fibers. *Textile Res. J.*, **68**(9): 623-629.

De Bruyne, N.A. (1937). *Plastic Materials for Aircraft Construction*. The 615th Lecture read before the Royal Aeronautical Society Lecture, 28th January, 1937, Royal Society of Arts, John Street, Adelphi, London.

Dempsey, J.M. (1975). *Fiber Crops*. University Press of Florida, Gainsville, USA.

Desch, H.E. and Dinwoodie, J.M. (1981). *Timber: Its Structure, Properties, and Utilisation, Sixth edition*. Macmillan, London; New York.

Desch, H.E. and Dinwoodie, J.M. (1996). *Timber: Structure, Properties, Conversion, and Use, Seventh edition*. Food Products Press, New York.

DiFrancia, C., Ward, T.C. and Claus, R.O. (1996). The Single-Fibre Pull-Out Test. 1: Review and Interpretation. *Composites: Part A*, **27A**: 597-612.

Dinwoodie, J.M. (1965). Tensile Strength of Individual Compression Wood Fibres and its Influence on Properties of Paper. *Nature*, **205**: 763-764.

Dinwoodie, J.M. (1968). Failure in Timber. Part 1. Microscopic Changes in Cell-Wall Structure Associated with Compression Failure. *J. Inst. Wood Sci.*, **21**: 37-53.

Dinwoodie, J.M. (1974). Failure in Timber. Part 2: The Angle of Shear Through the Cell Wall During Longitudinal Compression Stressing. *Wood Sci. and Technol.*, **8**: 56-67.

Dinwoodie, J.M. (1976). Causes of Brashness in Timber. *In: Wood Structure in Biological and Technological Research. Eds. Baas, P., Bolton, A.J. and Catling, D.* Leiden Botanical Series No. 3, 1976. pp. 238-252.

Dinwoodie, J.M. (1978). Failure in Timber Part 3: The Effect of Longitudinal Compression on Some Mechanical Properties. *Wood Sci. Technol.*, **12**: 271-285.

Fengel, D. and Wegener, G. (1984). *Wood: Chemistry, Ultrastructure, Reactions.* Walter de Gruyter, Berlin.

Focher, (1992). Physical Characteristics of Flax Fibre. *In: The Biology and Processing of Flax. Eds. Sharma, H.S.S. and Van Sumere, C.F.* Belfast, M Publications. pp. 11-32.

Franck, R.R. (1992). The History and Present Position of Linen. *In: The Biology and Processing of Flax. Eds. Sharma, H.S.S. and Van Sumere, C.F.* Belfast, M Publications. pp. 1-9.

Gassan, J. and Bledzki, A.K. (1996). Modification Methods on Nature Fibers and Their Influence on the Properties of the Composites. *54th Annual Technical Conference, Society of Plastics Engineers*, 2553-2557.

Gibson, L.J. and Ashby M.F. (1988). *Cellular Solids: Structure and Properties.* Pergamon Press. Oxford; New York.

Gordon, J.E. (1970). The Design of Materials. *Proc. Roy. Soc. Lond.* A, **319**: 137-143.

Gordon, J.E. (1976). *The New Science of Strong Materials.* Penguin Books, London.

Gordon, J.E. and Jeronimidis, G. (1974). Work of Fracture of Natural Cellulose. *Nature*, **252**(November 8, 1974): 116.

Gordon, J.E. and Jeronomidis, G.J. (1980). Composites With High Work of Fracture. *Phil. Trans. R. Soc. Lond.* A, **294**: 545-550.

Griffith, A.A. (1920). The Phenomenon of Rupture and Flow in Solids. *Phil. Trans. R. Soc. Lond. A*, **221**: 163-198.

Grubb, D.T. and Li, Z-F. (1994). Single Fibre Polymer Composites. Part II: Residual Stresses and their Effects in High-Modulus Polyethylene Fibre Composites. *J. Mat. Sci.*, **29**: 203-212.

Grubb, D.T., Li, Z-F. and Phoenix, S.L. (1995). Measurement of Stress Concentration in a Fiber Adjacent to a Fiber Break in a Model Composite. *Comp. Sci. Technol.*, **54**: 237-249.

Halpin, J.C. and Tsai, S.W. (1967). Environmental Factors in Composite Design. *Air Force Materials Laboratory Technical Report*, AFML-TR-67-423. (*Cited in*: Hull & Clyne, 1996).

Hampe, A. and Marotzke, C. (1997). The Energy Release Rate of the Fiber/Polymer Matrix Interface: Measurement and Theoretical Analysis. *J. Reinforced Plastics and Composites*, **16**(4): 341-351.

Hare, C.H. (1996). Polyester Resins. *Paintindia*, **March 1996**, 41-48.

Harrington, J.J., Booker, R. and Astley, R.J. (1998). Modelling the Elastic Properties of Softwood. Part 1: The Cell-Wall Lamellae. *Holz als Roh- Und Werkstoff*, **56**: 37-41.

Harris, B. (1980). *Engineering Composite Materials*. Inst. of Metals, London.

He, M.Y. and Hutchinson, J.W. (1989). Crack Deflection at an Interface Between Dissimilar and Elastic Material. *Int. J. Solid Structures*, **25**: 1053-67. (*Cited in*: Hull & Clyne, 1996).

Hill, C.A.S. and Cetin, N.S. (2000). Surface Activation of Wood for Graft Polymerisation. *Int. J. of Adhesion and Adhesives*, **20**: 71-76.

Hill, S. (1997). Cars that Grow on Trees. *New Scientist*, **153**(2067): 36-39.

Hornsby, P.R., Hinrichsen, E. and Tarverdi, K. (1997). Preparation and Properties of Polypropylene Composites Reinforced With Wheat and Flax Straw Fibres. Part 1: Fibre Characterization. *J. Mat. Sci.*, **32**: 443-449.

Hua, L., Zadorecki, P. and Flondin, P. (1987). Cellulose Fiber-Polyester Composites With Reduced Water Sensitivity (1) - Chemical Treatment and Mechanical Properties. *Polymer Composites*, **8**(3): 199-202.

Hull, D. and Clyne, T.W. (1996). *An Introduction to Composite Materials*. Cambridge University Press, Cambridge, UK.

Imayama, N. (1994). Relation on Microscopic Compression Creases and Crack of Wood Under Static Cyclic Bending Load. *Holz als Roh-und Werkstoff*, **52**: 49-56.

International Polarizer, Inc. (1998). *Corporate Literature*.

Ivens, J., Bos, H. and Verpoest, I. (1997). The Applicability of Natural Fibres as Reinforcement for Polymer Composites. *In: Renewable Biproducts: Industrial Outlets and Research for the 21st Century*. June 24-25, 1997, EC-symposium at the International Agricultural Center (IAC), Wageningen, The Netherlands.

Jain, S., Kumar, R. and Jindal, U.C. (1992). Mechanical Behaviour of Bamboo and Bamboo Composites. *J. Mat. Sci.*, **27**: 4598-4604.

Jarvis, M.C. (1984). Structure and Properties of Pectin Gels in Plant Cell Walls. *Plant, Cell and Environment*, **7**: 153-164.

Jayne, B.A. (1960). Some Mechanical Properties of Wood Fibres in Tension. *Forest Products Journal*, **June, 1960**: 316-322.

Jelf, P.M. and Fleck, N.A. (1992). Compression Failure Mechanisms in Unidirectional Composites. *J. Comp. Mat.*, **26**(18): 2706-2726.

Jeronimidis, G. (1976). The Fracture of Wood in Relation to its Structure. *In: Wood Structure in Biological and Technological Research. Eds. Baas, P., Bolton, A.J. and Catling, D.* Leiden Botanical Series No. 3, 1976. pp. 253-265.

Jeronimidis, G., (1980). The Fracture Behaviour of Wood and the Relations Between Toughness and Morphology. *Proc. R. Soc. Lond. B*, **208**: 447-460.

Keith, C.T. and Cote, W.A. (1968). Microscopic Characterisation of Slip Line and Compression Failures In Wood Cell Walls. *Forest Products Journal*, **15**(3): 67-74.

Kendall, K. (1975). Transition Between Cohesive and Interfacial Failure in a Laminate. *Proc. Roy. Soc.*, **344A**: 287-302.

Kerestz, Z.I. (1951). *The Pectic Substances*. New York, Interscience Publishers.

Kessler, R.W. and Kohler, R. (1996). New Strategies for Exploiting Flax and Hemp. *Chemtech*, **Dec. 1996**: 34-42.

Kim, C.Y., Page, D.H., El-Hosseiny, F. and Lancaster, A.P.S. (1975). The Mechanical Properties of Single Wood Pulp Fibers. III. The Effect of Drying Stress on Strength. *J. App. Polym. Sci.*, **19**: 1549-1561.

Kimber, P. (1999). Personal Communication.

Kinloch, A.J. (1987). *Adhesion and Adhesives: Science and Technology*. Chapman and Hall, London; New York.

Knott, J.F. (1973). *Fundamentals of Fracture Mechanics*. Butterworths, London.

Knott, J.F. and Withey, P. (1993). *Fracture Mechanics: Worked Examples*. Inst. of Materials, London.

Kohler, R. And Kessler, R.W. (1999). Designing Natural Fibers for Advanced Composites. *In: Proceedings of the 5th International Conference on Woodfiber-Plastic Composites, May, 26-27, 1999, Madison, WI, USA*. Forest Products Society, Madison, WI, USA. pp. 29-42.

Kolosick, P.C., Scott, C.T., Koutsky, J.A. and Myers, G.E. (1990). Effects of Azidosilane Treatments of Wood and Cellulose Fiber Surfaces on Adhesion to Polypropylene. *In Materials Interactions Relevant to the Pulp, and Wood Industries: Proceedings, Materials Research Society Symposium. Eds. Caulfield, D.F., Passaretti, J.D. and Sobczynski, S.F., 1990 April 18-20; San Francisco, CA. Pittsburgh, PA: Materials Research Society*; 119-124. Vol. 197.

Kumar, P. (1986). Mechanical Behaviour of Jute Fibres and their Composites. *Indian Journal of Technology*, **24**: 29-32.

Lee, C.Y.-C. and Santhosh, U. (1993). The Role of the Fibrillar Structures in the Compressive Behaviour of Rigid-Rod Polymeric Fibres. *Polym. Eng. Sci.*, **33**(14): 907-912.

Liang, B-H., Mott, L., Shaler, S.M. and Caneba, G.T. (1994). Properties of Transfer-Moulded Wood-Fiber/Polystyrene Composites. *Wood and Fiber Science*, **26**(3): 382-389.

Lilholt, H. and Bjerre, A.B. (1997). Composites Based on Jute-Fibres and Polypropylene Matrix, their Fabrication and Characterisation. *Proceedings of the 18th Risø International Symposium on Materials Science: Polymeric Composites - Expanding the Limits. Risø National Laboratory, Roskilde, Denmark, 1997, 411-423.*

Liptáková, E. and Kúdela, J. (1994). Analysis of the Wood-Wetting Process. *Holzforschung*, **48**(2): 139-144.

Livingstone Smith, S. (1945). A Survey of Plastics from the Viewpoint of the Mechanical Engineer. *Inst. Mech. Eng.*, 29-43.

Lucas, P.W., Choong, M.F., Tan, H.T., Turner, I.M. and Berrick, A.J. (1991). The Fracture Toughness of the Leaf of the Dicotyledon *Calophyllum inophyllum* L. (Guttiferae). *Phil. Trans. R. Soc. Lond. B*, **334**: 95-106.

Lucas, P.W., Darvell, B.W., Lee, K.D., Yuen, T.D.B. and Choong, M.F. (1995). The Toughness of Plant Cell Walls. *Phil. Trans. R. Soc. Lond. B*, **348**: 363-372.

Lucas, P.W., Tan, H.T.W. and Cheng, P.Y., (1997). The Toughness of Secondary Cell Wall and Woody Tissue. *Phil. Trans. R. Soc. Lond. B*, 342-352.

Mackie, G. (1992). Linen-A Commercial Review. *In: The Biology and Processing of Flax. Eds. Sharma, H.S.S. and Van Sumere, C.F.* Belfast, M Publications. pp. 545-572.

Majumdar, S., Kundu, A.B., Dey, S. and Ghosh, B.L. (1990). Enzymatic Retting of Jute Ribbons. *International Biodeterioration*, **27**: 223-235.

Maldas, D. and Kokta, B.V. (1991a). Performance of Treated Hybrid Fiber-reinforced Thermoplastic Composites under Extreme Conditions. *Holzforschung*, **45**(2): 131-135.

Maldas, D. and Kokta, B.V. (1991b). Performance of Treated Hybrid Fiber Reinforced-Thermoplastic Composites under Extreme Conditions. V. Use of Glass Fiber and Sawdust as Hybrid Fiber. *J. App. Polym. Sci.*, **42**: 1443-1450.

Mark, R.E. (1967). *Cell Wall Mechanics of Tracheids.* New Haven, Yale University Press.

Martin, D.C. and Thomas, E.L. (1991). Micromechanics of Kinking in Rigid-Rod Polymer Fibres. *J. Mat. Sci.*, **26**: 5171-5183.

Martin, J. (1996). *Materials for Engineering*. Inst. of Materials, London.

Mathur, A. and Netravali, A.N. (1996). Modification of Mechanical Properties of Kevlar Fibre by Polymer Infiltration. *J. Mat. Sci.*, **31**: 1265-1274.

Matthews, F.L. and Rawlings, R.D. (1994). *Composite Materials: Engineering and Science*. Chapman and Hall, London.

McMullen, P. (1984). Fibre/Resin Composites for Aircraft Primary Structures: A Short History, 1936-1984. *Composites*, **15**(3): 222-230.

Melantis, N., Galiotis, C., Tetlow, P.L. and Davies, C.K.L. (1992). Interfacial Shear Stress Distribution in Model Composites Part 2: Fragmentation Studies on Carbon Fibre/Epoxy Systems. *J. Comp. Mat.*, **26**(4): 574-610.

Mercado, J.S. (1992). *Using Digital Image Analysis to determine the Reinforcement of Wood Fiber Polyurethane Composites*. MSc Thesis, Michigan Technological University.

Miskioglu, I., Mehdi-Soozani, A., Burger, C.P. and Voloshin, A.S. (1987). Stress Intensity Factors for Near Edge Cracks by Digital Image Analysis. *Engineering Fracture Mechanics*, **27**(3): 329-343.

Mott, L., Shaler, S.M. and Groom, L.H. (1996). A Technique to Measure Strain Distributions in Single Wood Pulp Fibers. *Wood and Fiber Science*, **28**(4): 429-437.

Munikenche Gowda, T., Naidu, A.C.B. and Chhaya, R. (1999). Some Properties of Untreated Jute Fabric-Reinforced Polyester Composites. *Composites: Part A*, **30**: 277-284.

Mühlethaler, K. (1965). The Fine Structure of the Cellulose Microfibril. *In: Cellular Ultrastructure of Woody Plants. Ed. Cote, W.A.* Syracuse University Press, Syracuse, New York. pp. 191-198.

Myers, G.E., Kolosick, P.C., Chahyadi, I.S., Coberly, C.A., Koutsky, J.A. and Ermer, D.S. (1990). Extruded Wood-Flour Polypropylene Composites: Effect of a Maleated Polypropylene Coupling Agent on Fiber-Matrix Bonding and Properties. *In: Materials Interactions Relevant to the Pulp, and Wood Industries: Proceedings, Materials Research Society Symposium. Eds. Caulfield, D.F., Passaretti, J.D. and Sobczynski, S.F., 1990 April 18-20; San Francisco, CA. Pittsburgh, PA: Materials Research Society*; 67-76. Vol. 197.

Newman, G. (1999). Personal Communication.

Norwood, L.S. (1994). Fibre Reinforced Polymers *In: Handbook of Polymer Composites for Engineers. Ed. Hollaway, L.* England, Woodhead Publishing Ltd.

O'Dell, J.L. (1997). Natural Fibers in Resin Transfer Moulded Composites. *In: Proceedings of the 4th International Conference on Woodfiber-Plastic Composites, May 12-14, 1997, Madison, WI, USA.* Forest Products Society, Madison, WI, USA. p. 280.

Oksman, K. (1999). Mechanical Properties of Resin Transfer Moulded Natural Fiber Composites. *In: Proceedings of the 5th International Conference on Woodfiber-Plastic Composites, May, 26-27, 1999, Madison, WI, USA.* Forest Products Society, Madison, WI, USA. p. 97.

Olesen P.O. and Plackett, D.V. (1999). Perspectives on the Performance of Natural Plant Fibres. *In: Natural Fibres Performance Forum Plant Fibre Products - Essentials for the Future*, 27-28 May 1999, Copenhagen Denmark.

Owens Corning (1996). *Corporate literature (1996 Fact Book).* Owens Corning, World Headquarters, Fiberglas Tower, Toledo, Ohio, USA.

Page, D.H., El-Hosseiny, F. and Winkler, K. (1971). Behaviour of Single Wood Fibres under Axial Tensile Strain. *Nature*, **229**(January, 22, 1971): 252-253.

Page, D.H., El-Hosseiny, F., Winkler, K. and Bain, R. (1972). The Mechanical Properties of Single Wood-Pulp Fibres. Part 1: A New Approach. *Pulp and Paper Magazine of Canada,* **73**(8): 72-77.

Page, D.H. and El-Hosseiny, F. (1976). The Mechanical Properties of Single Wood Pulp Fibers. Part 4. The Influence of Defects. *Svensk Papperstidning,* **14**: 471-474.

Page, D.H., El-Hosseiny, F., Winkler, K. and Lancaster, A.P.S. (1977). Elastic Modulus of Single Wood Pulp Fibers. *Tappi,* **60**(4): 114-117.

Page, D.H., Seth, R.S. and De Grace, J.H. (1979). The Elastic Modulus of Paper. I. The Controlling Mechanisms. *Tappi,* **62**(9): 99-102.

Page, D.H. and Seth, R.S. (1980). The Elastic Modulus of Paper. III. The Effect of Dislocations, Microcompressions, Curls, Crimps, and Kinks. *Tappi,* **63**(10): 99-102.

Paramasivam, T. and Abdul Kalam, P.J. (1974). On the Study of Indigenous Natural-Fibre Composites. *Fibre Science and Technology*, **7**: 85-88.

Parton, V.Z. (1992). *Fracture Mechanics: From Theory to Practice.* Gordon and Breach, Philadelphia.

Patent Office (1936). Patent Specification: *'Improvements Relating to the Manufacture of Material and Articles from Resinous Substances'.* (No. 3040/36. 470,331).

Patton-Mallory, M. and Cramer, S.M. (1987). Fracture Mechanics: A Tool For Predicting Wood Component Strength. *Forest Products Journal,* **37**(7/8): 39-47.

Pegoretti, A., Accorsi, M.L. and Dibenedtto, A.T. (1996). Fracture Toughness of the Fibre-Matrix Interface in Glass-Epoxy Composites. *J. Mat. Sci.,* **31**: 6145-6153.

Piggott, M.R. (1980). *Load-Bearing Fibre Composites*. Pergamon, Oxford.

Prasad, S.V., Pavithran, C. and Rohatgi, P.K. (1983). Alkali Treatment of Coir Fibres for Coir-Polyester Composites. *J. Mat. Sci.*, **18**: 1443-1454.

Preston, R.D. (1974). *The Physical Biology of Plant Cell Walls*. Chapman and Hall, London.

Rahaman, M.M.M. (1979). Morphology of the Fibres of Jute, Flax and Hemp as seen under a Scanning Electron Microscope. *Indian J. Agric. Sci.*, **49**(6): 483-487.

Reidel, U. (1999). Natural Fibre-Reinforced Biopolymers as Construction Materials-New Discoveries. *In: Proceedings 2nd International Wood and Natural Fibre Composites Symposium*, 28-29 June, 1999, Kassel, Germany.

Reidel, U., Nickel, J. and Hermann, A.S. (1999). High Performance Applications of Plant Fibres in Aerospace and Related Industries. *In: Natural Fibres Performance Forum Plant Fibre Products - Essentials for the Future*, 27-28 May 1999, Copenhagen Denmark.

Restaino, A.J. and James, D.B. (1994). Thermosetting Resin Matrices. *In: Concise Encyclopaedia of Composite Materials. Ed. Kelly, A.* pp. 289-297.

Robson, D., Hague, J., Newman, G., Jeronomidis, G. and Ansell, M.P. (1993). *Survey of Natural Materials for Use in Structural Composites as Reinforcement and Matrices*. The BioComposites Centre, University of Wales, Bangor, Gwynedd, U.K. (1993).

Roe, P.J. and Ansell, M.P. (1985). Jute-Reinforced Polyester Composites. *J. Mat. Sci.*, **20**: 4015-4020.

Roland, J-C., Mosiniak, M. and Roland, D. (1995). Dynamique du Positionnement de la Cellulose dans le Parois des Fibres Textiles du Lin (*Linum usitatissimum*). *Acta Bot. Gallica*, **142**(5): 463-484.

Rowell, R.M. (1992). Opportunities for Lignocellulosic Materials and Composites. *Chapter 2, in: Materials and Chemicals from Biomass, American Chemical Society*, 1992. pp. 12-27.

Sakurada, I., Nukushina, Y. and Taisuke, I. (1962). Experimental Determination of the Elastic Modulus of Crystalline Regions in Oriented Polymers. *J. Polym. Sci.*, **57**: 651-660.

Sanadi, A.R., Prasad, S.V. and Rohatgi, P.K. (1985). Natural Fibres and Agro-Wastes as Fillers and Reinforcement in Polymer Composites. *Journal of Scientific and Industrial Research*, **44**: 437-442.

Sanadi, A.R., Prasad, S.V. and Rohatgi, P.K. (1986a). SEM Observations on the Origins of Toughness of Natural Fibre-Polyester Composites. *J. Mat. Sci. Letters*, **5**: 395-396.

Sanadi, A.R., Prasad, S.V. and Rohatgi, P.K. (1986b). Sunhemp Fibre-Reinforced Polyester; Part 1: Analysis of Tensile and Impact Properties. *J. Mat. Sci.*, **21**: 4299-4304.

Salmén, L. and de Ruvo, A. (1985). A Model for the Prediction of Fiber Elasticity. *Wood and Fiber Science*, **17**(3): 336-350.

Schuh, T.G. (1999). Renewable Materials for Automotive Applications. *In: Natural Fibres Performance Forum Plant Fibre Products - Essentials for the Future*, 27-28 May 1999, Copenhagen Denmark.

Searle, A.G. and Tuck, J.W. (undated). *The King's Flax and the Queen's Linen.* The Larks Press, Dereham, UK.

Sèbe, G., Cetin, N.S., Hill, C.A.S. (1999). Resin Transfer Moulding of Hemp Fiber-Reinforced Polyester Composites. *In: Proceedings of the 5th International Conference on Woodfiber-Plastic Composites, May 26-27, 1999, Madison, WI, USA.* Forest Products Society, Madison, WI, USA. pp. 131-136.

Sèbe, G., Cetin, N.S., Hill, C.A.S. and Hughes, M. (2000). RTM Hemp Fibre-Reinforced Polyester Composites. *Applied Composite Materials (in press).*

Sharma, H.S.S. (1987a). Screening of Polysaccharide-degrading Enzymes for Retting Flax Stems. *International Biodeteriortation*, **23**: 181-186.

Sharma, H.S.S., (1987b). Studies on Chemical and Enzyme Retting of Flax on a Semi-Industrial Scale and Analysis of the Effluents for their Physico-Chemical Components. *International Biodeterioration*, **23**: 329-342.

Sharma, H.S.S. (1987c). *'Treatment of Flax'.* Brit. Pat. No. GB2186002.

Sharma, H.S.S., Mercer, P.C. and Brown, A.E. (1989). A Review of Recent Research on the Retting of Flax in Northern Ireland. *International Biodeterioration*, **25**: 327-342.

Sharma, H.S.S. (1999). Personal Communication.

Sharma, H.S.S. and Van Sumere, C.F. (1992). Enzyme Treatment of Flax. *The Genetic Engineer and Biotechnologist*, **March/April 1992**: 19-23.

Singh, B., Verma, A. and Gupta, M. (1998). Studies on Adsorptive Interaction Between Natural Fiber and Coupling Agents. *J. App. Polym. Sci.*, **70**: 1847-1858.

Sjöström, E. (1993). *Wood Chemistry: Fundamentals and Applications.* Academic Press, San Diego.

Snell, R., Hague, J. and Groom, L. (1997). Characterizing Agrofibers for Use in Composite Materials. *In: Proceedings of the 4th International Conference on Woodfiber-Plastic Composites, May 12-14, 1997, Madison, WI, USA.* Forest Products Society, Madison, WI, USA. pp. 5-11.

Sridhar, M.K., Basavarajappa, G., Kasturi, S.G. and Balasubramanian, N. (1982). Evaluation of Jute as a Reinforcement in Composites. *Indian Journal of Textile Research*, 7: 87-92.

Stanzl-Tschegg, S.E., Tschegg, E.K. and Teischinger, A. (1994). Fracture Energy of Spruce Wood after Different Drying Procedures. *Wood and Fiber Science,* **26**(4): 467-478.

Stanzl-Tschegg, S.E., Tan, D.M. and Tschegg, E.K. (1995). New Splitting Method for Wood Fracture Characterization. *Wood Sci. Technol.,* **29**: 31-50.

Stanzl-Tschegg, S.E., Tan, D.M. and Tschegg, E.K. (1996). Mode II Fracture Tests on Spruce Wood. *Mokuzai Gakkaishi,* **42**(7), 642-650.

Stephen, A.M. (1983). Other Plant Polysaccharides. *In: The Polysaccharides, Vol. 2. Ed. Aspinall, G.O.* Academic Press, New York. pp. 154-166.

Tang, R.C. and Hsu, N.N. (1973). Analysis of the Relationship Between Microstructure and Elastic Properties of the Cell Wall. *Wood and Fibre,* **5**(2): 139-149.

Timings, R.L. (1989). *Engineering Materials: Volume 1.* Longman, Harlow, UK.

Tufnol. (1991). *Engineering with Tufnol.* Tufnol Corporate Literature, October, 1991 (Publication No. 3386).

Tufnol. (1992). *Engineering Plastics and Composites.* Tufnol Corporate Literature, July 1992 (Publication No. 3442).

Turner, G.P.A. (1988). *Introduction to Paint Chemistry and Principles of Paint Technology: Third Edition.* Chapman and Hall, London.

Uma Devi, L., Bhagawan, S.S. and Thomas, S. (1997). Mechanical Properties of Pineapple Leaf Fiber-Reinforced Polyester Composites. *J. Appl. Polym. Sci.,* **64**: 1739-1748.

Van den Heuvel, P.W.J., Peijs, T. and Young, R.J. (1997). Failure Phenomenon in Two-Dimensional Multi-Fibre Microcomposites: 2. A Raman Spectroscopic Study of the Influence of Inter-Fibre Spacing on Stress Concentrations. *Comp. Sci. and Technol.,* **57**: 899-911.

Vilppunen, P., Solin, T. and Harmaa, K. (1992). Enzymatic Agro Fibre Treatment Process and Biological Waste Water Treatment. *Biomass for Energy, Industry and Environment, Proceedings of the 6th EC Conference, Athens, Greece, 1992.* pp. 1357-1359.

Vilppunen, P., Oksman, K., Mäentausta, Keskitalo, E. and Sohlo, J. (1999). Biotechnical Processing of Flax for Reinforced Composites. *In: Proceedings of the 5th International Conference on Woodfiber-Plastic Composites, May 26-27, 1999, Madison, WI, USA.* Forest Products Society, Madison, WI, USA. p. 309.

Voloshin, A.S. and Burger, C.P. (1983). Half-fringe Photoelasticity: A New Approach to Whole-Field Stress Analysis. *Experimental Mechanics, September, 1983*: 304-313.

Wardop, A.B. and Dadswell, H.E. (1947). Contributions to the Study of the Cell Wall. 5. The Occurrence, structure and Properties of Certain Cell Wall Deformations. Commonwealth of Australia C.S.I.R. Bulletin No. 221.

Weindling, L. (1947). *Long Vegetable Fibers : Manila, Sisal, Jute, Flax and Related Fibers of Commerce*. Columbia Univ. Press, New York.

Wells, H., Bowden, D.H., Macphail, I. and Pal, P.K. (1980). The Potential of Jute and Similar Bast Fibres as High Specific Stiffness Reinforcements. *In: 35th Annual Technical Conference, 1980 Reinforced Plastics/Composites Institute, The Society of the Plastics Industry, Inc.* Section 1-F. pp 1-7.

White, N.M. and Ansell, M.P. (1983). Straw-Reinforced Polyester Composites. *J. Mat. Sci.*, **18**: 1549-1556.

Williams, J.G. (1981). Fracture Mechanics of Non-Metallic Materials. *Phil. Trans. R. Soc. Lond. A*, **299**: 59-72.

Winfield, A.G. and Winfield, B.L. (1974). Reinforced Plastics in Low Cost Housing. *Advances in Chemistry Series, number 134: Fillers and Reinforcements for Plastics; American Chemical Society.* pp. 207-218.

Winfield, A.G. (1979). Jute Reinforced Polyester Projects for UNIDO/Government of India. *Plastics and Rubber International*, **4**(1): 23-28.

Zadorecki, P. and Flondin, P. (1986). Surface Modification of Cellulose Fibers III. Durability of Cellulose-Polyester Composites Under Environmental Ageing. *J. App. Polym. Sci.*, **31**: 1699-1707.

Zadorecki, P., Karnerfors, H. and Lindenfors, S. (1986). Cellulose Fibers as Reinforcement in Composites: Determination of the Stiffness of Cellulose Fibers. *Comp. Sci. Technol.*, **27**: 291-303.

Zadorecki, P. and Michell, A.J. (1989). Future Prospects for Wood Cellulose as Reinforcement in Organic Polymer Composites. *Polymer Composites*, **10**(2): 69-77.

Zimmerman, J.M. and Losure, N.S. (1998). Mechanical Properties of Kenaf Bast Fiber Reinforced Epoxy Matrix Composite Panels. *J. Advanced Materials.* **30**(2): 32-38.

Appendix 1 Summary of 'open-mould' processes.

Process	*Process parameters*	*Materials*	*Advantages*	*Disadvantages*
Hand laminating	V_f: 0.13-0.5. Size range: 0.25-2,000m^2 Process pressure: ambient. Process temperature: ambient.	Reinforcement: Most types can be used. Resins: Polyester, epoxy, vinylester, phenolic.	Low capital outlay. Secondary bonding. No size limit. Flexibility.	Operator dependent. Labour intensive. Low production rate. Poor weight and thickness control. Only one moulded face.
Spray-up	V_f: 0.13-0.21. Size range: 2-100m^2 Processing pressure: ambient. Processing temperature: ambient.	Reinforcement: chopped roving only. Resins: Polyester, vinylester.	Low material cost. High production rate. Low tooling cost. Large parts.	Very operator dependent. Very poor thickness control. Only one moulded face. Random reinforcement only.
Filament-winding	V_f: 0.55-0.7. Size range: 0.1-1,000 m^2 Processing pressure: ambient. Processing temperature: ambient.	Reinforcement: continuous rovings only. Resins: polyesters, epoxy, vinyl ester.	Excellent mechanical properties. High production rate. Good control of fibre orientation. Good thickness control. Good fibre content control. Good internal finish..	Limited range of shapes. Limited number of practical winding patterns.

(Adapted from Ball, 1994)

Appendix 2 Summary of 'closed-mould' proceses.

Process	*Process parameters*	*Materials*	*Advantages*	*Disadvantages*
Vacuum bag	V_f: 0.15-0.6. Size range: 0.5-20m^2 Processing pressure: 1 bar. Processing temp: Ambient.	Reinforcement: Most types. Resins: Most types. Fillers: Not recommended.	Low capital outlay. Low cost of tooling. Large components. Well suited to making sandwich panels.	Labour-intensive. Low production rate. Only one accurate surface.
Autoclave	V_f: 0.35-0.7. Size range: 0.25-5.0m^2 Processing pressure: Up to 10 bar. Processing temp: 140^{0}C.	Reinforcement: Unidirectional and woven prepregs. Resins: Epoxy. Fillers: No.	Very high quality. High fibre content. Low void content. Controlled cure.	Labour intensive. Slow. High capital investment.
Cold press moulding	V_f: 0.15-0.25. Size range: 0.25-5.0m^2 Processing pressure: 2-5 bar. Processing temp: 20-50^{0}C.	Reinforcement: Continuous strand mat/woven cloth. Resins: Polyester. Fillers: Up to 20% by volume.	Good surface on both sides. Good production rate. Accurate dimensions.	Limited by press size. Low fibre content.

(Adapted from Ball, 1994)

Appendix 2 continued.

Process	*Process parameters*	*Materials*	*Advantages*	*Disadvantages*
Hot press moulding	V_f: 0.12-0.4. Size range: 0.1-2.5m^2 Processing pressure: 50-150 bar. Processing temp: 130-150^{0}C.	Reinforcement: Usually pre-impregnated sheet moulding compound (SMC) or dough moulding compound (DMC). Resins: Polyester, epoxy, vinylester. Fillers: Up to 40%.	Very high production rate. Fine detail, close tolerance. Low cost. Long tool life.	Mechanical properties modest with SMC and DMC. Material flow causes property variability. High tooling cost.
Resin transfer moulding	V_f: 0.1-0.15. Size range: 0.25-5 m^2 Processing pressure: Max. 2 bar. Processing temperature: 20-50^{0}C.	Reinforcement: Continuous strand mat or chopped strand preform. Resins: Polyester, polyurethane, low viscosity epoxy. Fillers: Not recommended.	Good surface on both sides. Accurate dimensions. Wide range of part geometry. Reasonable production rate Sandwich construction possible.	Massive tooling. Low fibre content.
Vacuum-assisted resin injection	V_f: 0.15-0.35. Size range: 1.0-30 m^2 Processing pressure: Max. 2 bar. Processing temp: 15-30^{0}C.	Reinforcement: Continuous strand mat, woven cloths. Resins: Polyester, polyurethane. Fillers: Not recommended.	High fibre content. Large size. Low weight, low cost tooling. Full range of reinforcement.	One-shot process; modifications and repairs difficult. Production development usually needed on each mould.

(Adapted from Ball, 1994)

Appendix 3

Schematic representation of a non-woven felt manufacturing line

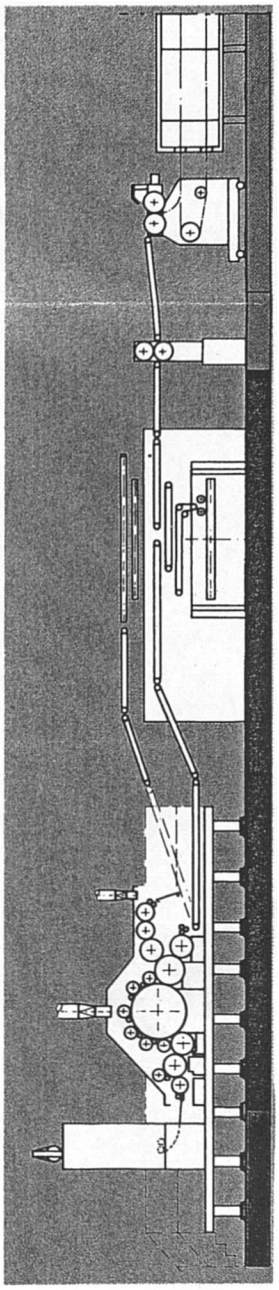

Appendix 4

Tensile test results

CSM glass fibre

No.	Max. Load (N)	Tens. Strength (MPa)	Auto. Mod. (GPa)	Young's Mod (GPa)	Proof Stress (MPa)	Strain at Break (mm/mm)
1	5905.50	62.20	8.35	9.09	55.10	0.0137
2	7031.80	78.40	7.80	8.48	59.70	0.0186
*3	6619.40	57.90	7.34	8.22	48.20	0.0328
4	6249.20	69.60	7.61	7.87	58.80	0.0156
5	6492.70	70.80	7.22	7.57	60.20	0.0163
6	7034.60	77.30	7.23	7.75	60.20	0.0195
7	6236.60	68.30	7.21	7.63	57.80	0.0167
8	6311.70	67.70	7.52	7.90	55.20	0.0170
9	6377.80	70.30	6.95	7.41	58.70	0.0171
10	7856.70	86.80	7.71	8.58	65.60	0.0198
11	6837.30	76.00	7.24	8.05	56.80	0.0191
12	7145.50	79.70	6.74	7.11	67.80	0.0178
Mean	6679.90	73.40	7.42	7.95	59.60	0.0174
SD	558.50	6.90	0.45	0.57	3.90	0.0018
CoV	8.40	9.50	6.00	7.21	6.60	10.4789
Min.	5905.50	62.20	6.74	7.11	55.10	0.0137
Max	7856.70	86.80	8.35	9.09	67.80	0.0198

Un-reinforced polymer

No.	Max. Load (N)	Tens. Strength (MPa)	Auto. Mod. (GPa)	Young's Mod (GPa)	Proof Stress (MPa)	Strain at Break (mm/mm)
3	3758.10	40.20	3.68	3.83	42.30	0.0133
5	5152.90	57.00	3.61	3.78	50.30	0.0204
6	4445.40	48.40	3.61	3.78	50.60	0.0164
7	4228.50	45.50	3.72	3.73	49.20	0.0153
8	4429.00	47.00	3.72	4.01	47.30	0.0163
9	4583.00	52.90	3.67	3.67	52.80	0.0168
10	5081.00	55.60	3.61	3.70	52.90	0.0195
11	4474.40	48.20	3.78	3.67	50.30	0.0016
12	4271.20	46.20	3.74	4.07	50.10	0.0154
14	4559.40	49.70	3.66	3.73	53.20	0.0169
Mean	4498.30	49.10	3.68	3.80	49.90	0.0166
SD	402.70	5.00	0.06	0.14	3.20	0.0021
CoV	9.00	10.20	1.56	3.64	6.50	12.3561
Min.	3758.10	40.20	3.61	3.67	42.30	0.0133
Max	5152.90	57.00	3.78	4.07	53.20	0.0204

2 layer jute reinforcement

No.	Max. Load (N)	Tens. Strength (MPa)	Auto. Mod. (GPa)	Young's Mod (GPa)	Proof Stress (MPa)	Strain at Break (mm/mm)
1	4360.40	48.20	6.39	6.67	42.20	0.0122
2	4443.60	46.00	6.26	6.42	44.00	0.0109
3	4553.30	48.30	6.68	7.70	44.30	0.0112
4	4604.80	48.30	6.26	6.48	44.40	0.0121
5	4263.70	44.90	6.58	7.13	44.10	0.0107
6	4545.10	48.70	6.43	6.68	46.80	0.0114
7	4308.90	45.20	6.63	6.82	42.50	0.0106
8	4431.00	46.20	6.37	6.71	42.90	0.0109
9	4313.00	45.50	6.40	6.52	45.70	0.0102
10	4443.90	46.20	6.36	6.59	42.10	0.0111
11	4129.50	44.00	6.14	6.39	46.30	0.0106
12	3929.10	41.70	6.34	6.37	45.30	0.0094
Mean	4360.50	46.10	6.40	6.65	44.20	0.0109
SD	191.50	2.10	0.16	0.25	1.60	0.0008
CoV	4.40	4.50	2.50	3.74	3.60	7.0523
Min.	3929.10	41.70	6.14	6.37	42.10	0.0094
Max.	4604.80	48.70	6.68	7.13	46.80	0.0122

4 layer jute reinforcement

No.	Max. Load (N)	Tens. Strength (MPa)	Auto. Mod. (GPa)	Young's Mod (GPa)	Proof Stress (MPa)	Strain at Break (mm/mm)
1	7004.50	72.10	8.56	9.20	53.00	0.0141
2	7299.40	72.30	8.04	8.67	44.40	0.0171
3	7337.30	71.90	8.36	8.95	47.00	0.0159
4	7125.00	70.10	8.66	9.28	54.10	0.0141
5	7550.40	75.80	8.84	9.30	58.90	0.0142
6	7785.90	78.50	8.54	9.19	56.30	0.0152
7	7428.90	75.60	8.50	9.20	54.10	0.0152
8	7461.40	72.00	9.10	9.87	50.10	0.0144
9	7209.30	74.20	8.86	9.61	56.90	0.0136
10	7470.70	71.60	8.99	9.79	54.90	0.0133
11	7429.30	74.20	8.49	8.95	56.50	0.0138
12	7642.00	75.00	8.61	9.21	58.00	0.0138
Mean	7395.30	73.60	8.63	9.25	53.70	0.0146
SD	218.00	2.40	0.29	0.35	4.50	0.0011
CoV	2.90	3.20	3.36	3.82	8.30	7.6116
Min.	7004.50	70.10	8.04	8.67	44.40	0.0133
Max.	7785.90	78.50	9.10	9.87	58.90	0.0171

6 layer jute reinforcement

No.	Max. Load (N)	Tens. Strength (MPa)	Auto. Mod. (GPa)	Young's Mod (GPa)	Proof Stress (MPa)	Strain at Break (mm/mm)
1	9252.90	74.40	9.09	9.87	54.70	0.0137
2	9819.90	78.40	9.14	9.78	53.70	0.0149
3	10464.10	83.90	8.46	9.63	45.60	0.0196
4	10450.10	85.00	8.65	9.20	52.90	0.0176
5	10192.80	83.30	9.19	9.97	49.80	0.0162
6	10510.50	87.70	9.14	9.76	53.30	0.0181
7	11002.40	85.90	8.85	9.88	53.40	0.0184
8	9878.80	77.90	8.45	9.23	50.90	0.0163
9	9735.00	78.70	9.31	10.03	49.80	0.0157
10	9800.40	80.80	8.89	9.57	47.10	0.0172
11	9193.60	72.90	8.65	9.11	49.50	0.0146
12	10746.60	85.40	9.16	10.37	51.30	0.0179
Mean	10087.30	81.20	8.92	9.70	51.00	0.0167
SD	568.30	4.80	0.30	0.38	2.80	0.0017
CoV	5.60	5.90	3.38	3.87	5.50	10.4829
Min.	9193.60	72.90	8.45	9.11	45.60	0.0137
Max.	11002.40	87.70	9.31	10.37	54.70	0.0196

3 layer hemp reinforcement

No.	Max. Load (N)	Tens. Strength (MPa)	Auto. Mod. (GPa)	Young's Mod (GPa)	Proof Stress (MPa)	Strain at Break (mm/mm)
1	3180.10	30.30	5.10	35.40	29.10	0.0077
2	3664.10	39.10	5.29	44.39	39.40	0.0096
3	3371.10	32.30	5.39	37.69	33.10	0.0082
4	3496.90	34.00	6.07	40.07	37.80	0.0086
5	3298.50	31.50	5.39	36.89	34.10	0.0085
6	3609.80	35.50	5.63	41.13	38.20	0.0094
7	3407.10	37.40	6.16	43.56	36.90	0.0087
8	3644.00	34.80	5.31	40.11	37.20	0.0101
9	3186.20	30.70	6.02	36.72	34.50	0.0084
10	3378.50	32.20	5.44	37.64	34.00	0.0084
11	3423.60	33.80	5.26	39.06	37.10	0.0092
Mean	3423.60	33.80	5.55	39.35	35.60	0.0088
SD	168.20	2.80	0.37	3.17	3.00	0.0007
CoV	4.90	8.20	6.58	14.78	8.30	7.7460
Min.	3180.10	30.30	5.10	35.40	29.10	0.0077
Max.	3664.10	39.10	6.16	45.26	39.40	0.0101

6 layer hemp reinforcement

No.	Max. Load (N)	Tens. Strength (MPa)	Auto. Mod. (GPa)	Young's Mod (GPa)	Proof Stress (MPa)	Strain at Break (mm/mm)
1	4478.20	49.10	7.47	7.88	43.70	0.0112
2	4979.30	55.00	8.23	8.75	47.30	0.0122
3	4959.90	57.20	7.45	7.80	45.80	0.0141
4	4848.40	54.40	7.48	7.78	44.90	0.0129
5	5026.50	54.70	8.06	8.56	44.20	0.0134
6	5219.00	57.80	8.43	8.90	43.20	0.0138
7	4845.60	54.90	8.45	8.95	47.80	0.0117
8	5187.90	54.60	9.45	10.29	45.50	0.0129
9	4908.50	55.80	7.79	8.60	40.80	0.0152
10	4925.60	56.00	8.68	9.23	45.40	0.0122
11	4152.30	47.00	7.56	8.15	40.10	0.0114
Mean	4866.50	54.10	8.10	8.63	44.40	0.0128
SD	306.80	3.50	0.63	0.74	2.40	0.0012
CoV	6.30	6.40	7.83	8.60	5.40	9.5432
Min.	4152.30	46.10	7.45	7.78	40.10	0.0112
Max.	5219.00	57.80	9.45	10.29	47.80	0.0152

9 layer hemp reinfocement

No.	Max. Load (N)	Tens. Strength (MPa)	Auto. Mod. (GPa)	Young's Mod (GPa)	Proof Stress (MPa)	Strain at Break (mm/mm)
1	8670.80	88.50	8.98	10.45	53.70	0.0214
2	8587.70	83.50	8.69	10.28	49.80	0.0206
4	8882.60	90.20	8.79	10.66	49.90	0.0234
5	8045.60	84.30	8.49	9.97	50.40	0.0209
6	8150.80	84.60	8.86	10.53	43.80	0.0216
8	9023.00	91.10	9.08	10.67	54.10	0.0226
9	8458.20	88.40	8.95	10.19	50.90	0.0204
10	7862.20	80.50	9.36	10.80	54.10	0.0176
11	7831.60	79.60	8.39	9.38	49.90	0.0196
12	7620.70	73.60	9.00	10.41	52.20	0.0172
13	8528.80	87.70	9.12	10.93	50.50	0.0211
Mean	8332.90	84.70	8.88	10.39	50.80	0.0206
SD	459.10	5.30	0.28	0.43	2.90	0.0019
CoV	5.50	6.20	3.19	4.16	5.70	9.1645
Min.	7620.70	73.60	8.39	9.38	43.80	0.0172
Max.	9023.00	91.10	9.36	10.93	54.10	0.0234

Appendix 5

THREE POINT FLEXURAL PROPERTIES

UN-REINFORCED POLYESTER RESIN

Specimen Number	Modulus (Man. Young) (MPa)	Modulus (Aut. Young) (MPa)	Stress at Yield (offset) (MPa)	Stress at Yield (Max. Load) (MPa)	Strain at Yield (Max. Load) (mm/mm)	Energy to Yield Point (J)	Energy to Break Point (J)
1	3394	3372	104.8	116.9	0.0392	0.875	1.158
2	3469	3404	103.5	111.6	0.0364	0.849	1.022
3	3284	3283	43.51	86.58	0.0279	0.5867	0.5867
4	3421	3340	106.5	112.6	0.037	0.9014	1.038
5	3583	3544	32.94	99.1	0.0305	0.7239	0.7239
6	3338	3376	106.6	109.6	0.0354	0.8843	0.9496
7	3400	3363	----------	97.67	0.0312	0.7322	0.7322
8	3492	3417	107.6	115.6	0.0378	0.9127	1.096
Mean:	3423	3387	----------	106.2	0.0344	0.8082	0.9133
SD:	93	76	----------	10.65	0.004	0.1156	0.2061

CSM GLASS FIBRE REINFORCED POLYESTER

Specimen Number	Modulus (Man. Young) (MPa)	Modulus (Aut. Young) (MPa)	Stress at Yield (offset) (MPa)	Stress at Yield (Max. Load) (MPa)	Strain at Yield (Max. Load) (mm/mm)	Energy to Yield Point (J)	Energy to Break Point (J)
1	6847	6826	117.8	160.5	0.0337	0.5826	3.078
2	6162	6281	106.3	148.2	0.0365	0.5151	2.266
3	7082	7242	147	186.4	0.0362	0.8279	3.285
4	6313	6269	105.3	147.9	0.036	0.4983	2.619
5	5613	6286	115.8	151.7	0.0357	0.5957	2.442
6	6028	6626	147.5	169.8	0.032	0.8931	2.631
7	6559	6774	138.3	179.1	0.0398	0.781	3.02
8	7190	7167	140.3	173.4	0.0339	0.7727	2.863
9	7203	6848	143.1	181.2	0.0371	0.8043	2.898
10	6578	6602	119.1	147.5	0.0313	0.5961	2.606
Mean:	6557	6692	128	164.6	0.0352	0.6867	2.771
SD:	534	350	16.8	15.2	0.0025	0.1433	0.313

2 LAYER JUTE REINFORCED POLYESTER

Specimen Number	Modulus (Man. Young) (MPa)	Modulus (Aut. Young) (MPa)	Stress at Yield (offset) (MPa)	Stress at Yield (Max Load) (MPa)	Strain at Yield (Max Load) (mm/mm)	Energy to Yield Point (J)	Energy to Break Point (J)
1	4995	4912	55.73	62.64	0.0172	0.179	0.3388
2	5059	4856	56.75	60.88	0.0168	0.1802	0.2712
3	5229	4900	59.64	72.11	0.0205	0.1971	0.3535
4	5104	4946	62.22	78.04	0.0218	0.2151	0.398
5	5134	4919	58.48	68.53	0.0193	0.1922	0.3928
6	4995	4747	58.32	64.84	0.0179	0.2049	0.3036
7	5149	4983	59.99	72.23	0.0193	0.2094	0.393
8	5049	4931	61.11	75.48	0.0209	0.2093	0.3592
Mean:	5089	4899	59.03	69.34	0.0192	0.1984	0.3513
SD	81	71	2.16	6.17	0.0018	0.0137	0.0456

4 LAYER JUTE REINFORCED POLYESTER

Specimen Number	Modulus (Man. Young) (MPa)	Modulus (Aut. Young) (MPa)	Stress at Yield (offset) (MPa)	Stress at Yield (Max Load) (MPa)	Strain at Yield (Max Load) (mm/mm)	Energy to Yield Point (J)	Energy to Break Point (J)
1	6926	6893	71.81	96.31	0.0215	0.237	0.8278
2	6946	6820	71.48	91.65	0.0199	0.2422	0.8157
3	7417	7129	75.96	97.84	0.02	0.2505	0.8186
4	6988	6911	74.23	104.9	0.0233	0.2639	0.9743
5	7091	6755	74.61	90.01	0.0196	0.2615	0.8317
6	7424	7054	74.18	94.72	0.02	0.2415	0.832
7	7134	7129	73.69	103.1	0.0223	0.2478	0.89
8	7182	7043	73.39	101.6	0.0223	0.2469	0.8721
Mean:	7139	6967	73.67	97.52	0.0211	0.2489	0.8578
SD:	196	142	1.47	5.38	0.0014	0.0095	0.054

6 LAYER JUTE REINFORCED POLYESTER

Specimen Number	Modulus (Man. Young) (MPa)	Modulus (Aut. Young) (MPa)	Stress at Yield (offset) (MPa)	Stress at Yield (Max Load) (MPa)	Strain at Yield (Max Load) (mm/mm)	Energy to Yield Point (J)	Energy to Break Point (J)
1	6578	7107	82.11	109.2	0.0228	0.3804	1.646
2	6784	6952	78.03	99.37	0.0206	0.3335	1.36
3	6585	7021	78	99.44	0.0209	0.3409	1.383
4	7030	7162	80.16	109.2	0.023	0.3566	1.576
5	7385	7220	83.96	108.6	0.0224	0.3712	1.578
6	7230	7162	83.15	109.4	0.0231	0.3778	1.422
7	6619	6996	79.54	103.8	0.0213	0.351	1.411
8	7067	7102	81.27	105.6	0.0222	0.3564	1.469
Mean:	6910	7090	80.78	105.6	0.022	0.3585	1.481
SD:	313	93	2.23	4.31	0.001	0.017	0.106

3 LAYER HEMP REINFORCEMENT

Specimen Number	Modulus (Man. Young) (MPa)	Modulus (Aut. Young) (MPa)	Stress at Yield (offset) (MPa)	Stress at Yield (Max Load) (MPa)	Strain at Yield (Max Load) (mm/mm)	Energy to Yield Point (J)	Energy to Break Point (J)
1	4297	4277	61.42	72.05	0.0255	0.2627	0.6447
2	4346	4182	47.31	59.31	0.0223	0.1762	0.475
3	4432	4296	49.2	53.77	0.0183	0.1861	0.3067
4	4568	4436	47.69	58.33	0.0195	0.1785	0.3608
5	4534	4420	52.59	65.27	0.0232	0.1983	0.4801
6	4965	4512	57.74	66.97	0.0229	0.229	0.4895
7	4993	4782	58.04	74.04	0.0242	0.2241	0.6641
8	4859	4433	52.78	63.09	0.0223	0.1993	0.4609
9	4784	4570	57.97	69.03	0.0235	0.233	0.5282
10	4264	4309	39.37	46.9	0.0162	0.1337	0.2321
Mean:	4604	4422	52.41	62.88	0.0218	0.2021	0.4642
SD:	277	172	6.67	8.44	0.0029	0.0365	0.1362

6 LAYER HEMP REINFORCED POLYESTER

Specimen Number	Modulus (Man. Young) (MPa)	Modulus (Aut. Young) (MPa)	Stress at Yield (offset) (MPa)	Stress at Yield (Max Load) (MPa)	Strain at Yield (Max Load) (mm/mm)	Energy to Yield Point (J)	Energy to Break Point (J)
1	5820	5615	61.84	77.52	0.0247	0.1967	0.8997
2	6173	6013	67.39	87.16	0.0246	0.2195	1.018
3	6090	5782	62.1	81.03	0.0276	0.1959	0.8148
4	6819	6481	70.23	100.6	0.0306	0.2365	1.318
5	6376	5971	62.57	79.11	0.0231	0.1939	0.8416
6	6335	6050	65.3	83.26	0.0253	0.2134	1.29
7	6138	5993	64.7	82.48	0.0241	0.2051	0.9707
8	6247	5863	66.77	87.02	0.027	0.2323	1.219
Mean:	6250	5971	65.11	84.77	0.0259	0.2117	1.047
SD:	287	252	2.94	7.24	0.0024	0.0167	0.2023

9 LAYER HEMP REINFORCED POLYESTER

Specimen Number	Modulus (Man. Young) (MPa)	Modulus (Aut. Young) (MPa)	Stress at Yield (offset) (MPa)	Stress at Yield (Max Load) (MPa)	Strain at Yield (Max Load) (mm/mm)	Energy to Yield Point (J)	Energy to Break Point (J)
1	7453	7599	77.82	119.9	0.0299	0.255	2.227
2	8096	7652	77.27	121.4	0.0311	0.2521	1.945
3	7896	8023	83.84	132.5	0.0309	0.2989	2.892
4	7809	7457	75.72	113.9	0.0278	0.2376	1.817
5	8033	7491	77.89	119.4	0.0301	0.2658	2.282
6	7126	7343	77.49	119.5	0.0303	0.262	2.11
7	8103	7710	81.05	124.5	0.0303	0.282	2.52
8	8079	7799	78.28	116.1	0.0266	0.2424	2.104
Mean:	7824	7634	78.67	120.9	0.0297	0.262	2.237
SD:	357	215	2.56	5.7	0.0016	0.0204	0.339

WORK OF FRACTURE IN THREE POINT FLEXURE

UN-REINFORCED POLYMER

Specimen No.	Energy to yield pt. (J)	Energy to break (J)	Specimen width (mm)	Specimen thick. (mm)	Work to yield pt (kJ m^{-2})	Work to fracture (kJ m^{-2})
1	0.875019	1.15782	15.44	4.35	13.0	17.2
2	0.848979	1.02153	15.49	4.35	12.6	15.2
3	0.58666	0.58666	15.45	4.37	8.7	8.7
4	0.901449	1.03797	15.23	4.37	13.5	15.6
5	0.723945	0.723945	15.21	4.34	11.0	11.0
6	0.884279	0.949618	15.11	4.36	13.4	14.4
7	0.73217	0.73217	15.12	4.35	11.1	11.1
8	0.912722	1.09642	15.53	4.34	13.5	16.3

Average	12.1	13.7
S.D.	1.7	3.0

CSM GLASS FIBRE REINFORCEMENT

Specimen No.	Energy to yield pt. (J)	Energy to break (J)	Specimen width (mm)	Specimen thick. (mm)	Work to yield pt (kJ m^{-2})	Work to fracture (kJ m^{-2})
1	0.582632	3.07837	15.42	4.23	8.9	47.2
2	0.515105	2.26645	15.41	4.23	7.9	34.8
3	0.827885	3.2853	15.51	4.23	12.6	50.1
4	0.49832	2.61907	15.08	4.22	7.8	41.2
5	0.595654	2.44169	15.31	4.23	9.2	37.7
6	0.893056	2.63053	15.5	4.23	13.6	40.1
7	0.78104	3.02032	15.39	4.23	12.0	46.4
8	0.772717	2.86307	15.43	4.27	11.7	43.5
9	0.804314	2.89847	14.96	4.25	12.7	45.6
10	0.596122	2.60553	15.15	4.24	9.3	40.6

Average	10.6	42.7
S.D.	2.2	4.7

2 LAYER JUTE REINFORCEMENT

Specimen No.	Energy to yield pt. (J)	Energy to break (J)	Specimen width (mm)	Specimen thick. (mm)	Work to yield pt (kJ m^{-2})	Work to fracture (kJ m^{-2})
1	0.179021	0.338751	14.8	4.07	3.0	5.6
2	0.180241	0.271242	14.61	4.04	3.1	4.6
3	0.197096	0.35354	14.63	3.98	3.4	6.1
4	0.215147	0.39796	14.79	4	3.6	6.7
5	0.192185	0.392758	14.84	4.03	3.2	6.6
6	0.204934	0.303609	15.2	4.09	3.3	4.9
7	0.209393	0.39302	15.16	4.14	3.3	6.3
8	0.209283	0.359163	14.94	3.98	3.5	6.0

Average	3.3	5.8
S.D.	0.2	0.8

4 LAYER JUTE REINFORCEMENT

Specimen No.	Energy to yield pt. (J)	Energy to break (J)	Specimen width (mm)	Specimen thick. (mm)	Work to yield pt (kJ m^{-2})	Work to fracture (kJ m^{-2})
1	0.236962	0.827776	14.57	4.45	3.7	12.8
2	0.242201	0.815688	15.09	4.45	3.6	12.1
3	0.250545	0.818609	14.64	4.42	3.9	12.7
4	0.263909	0.974316	15.21	4.46	3.9	14.4
5	0.261478	0.831654	15.1	4.44	3.9	12.4
6	0.241497	0.831979	14.49	4.44	3.8	12.9
7	0.247812	0.890019	14.8	4.47	3.7	13.5
8	0.246914	0.872082	14.7	4.47	3.8	13.3

Average	3.8	13.0
S.D.	0.1	0.7

6 LAYER JUTE REINFORCEMENT

Specimen No.	Energy to yield pt. (J)	Energy to break (J)	Specimen width (mm)	Specimen thick. (mm)	Work to yield pt ($kJ\ m^{-2}$)	Work to fracture ($kJ\ m^{-2}$)
1	0.380416	1.64587	15.36	5.48	4.5	19.6
2	0.333471	1.3598	14.65	5.51	4.1	16.8
3	0.340877	1.38308	15.05	5.52	4.1	16.6
4	0.356577	1.57631	15.04	5.52	4.3	19.0
5	0.371181	1.57814	14.78	5.44	4.6	19.6
6	0.377779	1.42159	15.15	5.43	4.6	17.3
7	0.351003	1.41145	14.92	5.52	4.3	17.1
8	0.3564	1.46921	14.79	5.47	4.4	18.2

Average	4.4	18.0
S.D.	0.2	1.2

3 LAYER HEMP REINFORCEMENT

Specimen No.	Energy to yield pt. (J)	Energy to break (J)	Specimen width (mm)	Specimen thick. (mm)	Work to yield pt ($kJ\ m^{-2}$)	Work to fracture ($kJ\ m^{-2}$)
1	0.262702	0.644653	15.33	4.29	4.0	9.8
2	0.176184	0.475014	15.83	4.32	2.6	6.9
3	0.186074	0.306663	15.68	4.3	2.8	4.5
4	0.178517	0.360779	16.49	4.3	2.5	5.1
5	0.198309	0.480099	15.64	4.3	2.9	7.1
6	0.22898	0.489481	15.79	4.29	3.4	7.2
7	0.224102	0.664134	15.72	4.29	3.3	9.8
8	0.19932	0.460878	15.73	4.3	2.9	6.8
9	0.233004	0.528154	15.86	4.31	3.4	7.7
10	0.13375	0.232052	16.16	4.31	1.9	3.3

Average	3.0	6.8
S.D.	0.6	2.1

6 LAYER HEMP REINFORCEMENT

Specimen No.	Energy to yield pt. (J)	Energy to break (J)	Specimen width (mm)	Specimen thick. (mm)	Work to yield pt (kJ m^{-2})	Work to fracture (kJ m^{-2})
1	0.196685	0.899712	15.51	3.89	3.3	14.9
2	0.219476	1.0183	15.53	3.96	3.6	16.6
3	0.195886	0.814831	15.69	3.87	3.2	13.4
4	0.236525	1.31838	15.77	4	3.7	20.9
5	0.19386	0.841579	15.72	3.91	3.2	13.7
6	0.213449	1.29001	15.65	4.06	3.4	20.3
7	0.205067	0.970656	15.61	3.94	3.3	15.8
8	0.232295	1.21864	15.64	4.13	3.6	18.9

Average	3.4	16.8
S.D.	0.2	2.9

9 LAYER HEMP REINFORCEMENT

Specimen No.	Energy to yield pt. (J)	Energy to break (J)	Specimen width (mm)	Specimen thick. (mm)	Work to yield pt (kJ m^{-2})	Work to fracture (kJ m^{-2})
1	0.254973	2.22665	15.13	4.2	4.0	35.0
2	0.252139	1.94536	15.09	4.21	4.0	30.6
3	0.298901	2.89195	15.52	4.33	4.4	43.0
4	0.23763	1.81671	14.64	4.18	3.9	29.7
5	0.265826	2.28223	15.31	4.24	4.1	35.2
6	0.262046	2.11012	14.97	4.27	4.1	33.0
7	0.281999	2.51992	15.44	4.3	4.2	38.0
8	0.242415	2.10441	14.69	4.2	3.9	34.1

Average	4.1	34.8
S.D.	0.2	4.2

Appendix 6

Results of Charpy impact strength tests

Unreinforced polymer

Specimen No.	Thick. (mm)	Width (mm)	Energy (J)	W. of F. (kJ m-2)
1	4.34.	9.81	0.39	9.04
2	4.35	9.74	0.38	8.85
3	4.33	9.83	0.44	10.34
4	4.34	9.76	0.19	4.49
5	4.35	9.78	0.45	10.46
6	4.35	9.92	0.39	8.92
7	4.31	9.20	0.25	6.18
8	4.36	9.98	0.45	10.23
9	4.36	10.05	0.27	6.16
10	4.34	9.75	0.55	13.00

Average	8.77
S.D.	2.52

CSM glass fibre ($V_f \sim 20\%$)

Specimen No.	Thick. (mm)	Width (mm)	Energy (J)	W. of F. (kJ m-2)
1	4.29	9.75	2.52	60.25
2	4.24	9.79	2.76	66.49
3	4.24	9.77	3.32	80.15
4	4.25	9.86	3.46	82.57
5	4.25	9.18	3.18	81.51
6	4.25	9.90	3.18	75.58
7	4.24	9.92	3.02	71.80
8	4.25	9.82	3.22	77.15
9	4.25	9.82	3.60	86.26
10	4.25	9.82	3.24	77.63

Average	75.94
S.D.	7.86

2 Layer jute (V_f ~ 19%)

Specimen No.	Thick. (mm)	Width (mm)	Energy (J)	W. of F. (kJ m-2)
1	4.03	9.33	0.24	6.38
2	4.05	9.95	0.26	6.45
3	3.95	9.73	0.25	6.50
4	3.96	10.07	0.28	7.02
5	3.98	10.26	0.28	6.86
6	3.97	10.24	0.26	6.40
7	4.10	10.04	0.25	6.07
8	4.00	10.73	0.28	6.52
9	3.99	9.99	0.28	7.02
10	3.96	9.95	0.25	6.34
11	3.97	9.74	0.24	6.21
12	3.97	10.48	0.26	6.25

Average	6.50
S.D.	0.31

4 Layer jute (V_f ~ 36%)

Specimen No.	Thick. (mm)	Width (mm)	Energy (J)	W. of F. (kJ m-2)
1	4.43	10.60	0.65	13.84
2	4.45	9.75	0.62	14.29
3	4.36	10.64	0.62	13.36
4	4.35	9.99	0.60	13.81
5	4.43	10.26	0.66	14.52
6	4.45	10.22	0.66	14.51
7	4.45	9.98	0.60	13.51
8	4.44	10.01	0.65	14.63
9	4.40	9.60	0.60	14.20
10	4.38	10.03	0.66	15.02
11	4.40	10.22	0.60	13.34
12	4.37	10.17	0.60	13.50

Average	14.05
S.D.	0.56

3 Layer hemp (V_f ~ 15%)

Specimen No.	Thick. (mm)	Width (mm)	Energy (J)	W. of F. (kJ m-2)
1	4.35	10.44	0.36	7.93
2	4.30	10.68	0.30	6.53
3	4.30	10.69	0.25	5.44
4	4.31	10.86	0.34	7.26
5	4.29	10.38	0.30	6.74
6	4.31	9.94	0.32	7.47
7	4.30	10.27	0.28	6.34
8	4.31	10.61	0.34	7.44
9	4.30	10.35	0.26	5.84

Average	6.78
S.D.	0.82

6 Layer jute (V_f ~ 40%)

Specimen No.	Thick. (mm)	Width (mm)	Energy (J)	W. of F. (kJ m-2)
1	5.46	10.82	1.22	20.65
2	5.54	10.98	1.06	17.43
3	5.49	9.76	0.84	15.68
4	5.54	10.01	1.06	19.11
5	5.54	9.67	1.06	19.79
6	5.49	10.38	0.96	16.85
7	5.43	9.92	0.80	14.85
8	5.54	10.53	1.06	18.17
9	5.53	10.17	0.94	16.71
10	5.35	10.33	0.84	15.20
11	5.42	10.16	1.00	18.16

Average	17.51
S.D.	1.88

6 Layer hemp (V_f ~ 31%)

Specimen No.	Thick. (mm)	Width (mm)	Energy (J)	W. of F. (kJ m-2)
1	3.92	9.90	0.62	15.98
2	3.94	10.09	0.60	15.09
3	3.88	10.36	0.70	17.41
4	3.89	10.37	0.68	16.86
5	3.85	10.37	0.72	18.03
6	4.01	10.53	0.68	16.10
7	3.96	10.38	0.58	14.11
8	3.91	9.67	0.74	19.57
9	4.07	10.88	0.74	16.71
10	3.90	10.15	0.56	14.15

Average	16.40
S.D.	1.71

9 Layer hemp (V_f ~ 44%)

Specimen No.	Thick. (mm)	Width (mm)	Energy (J)	W. of F. (kJ m-2)
1	4.18	10.43	1.32	30.28
2	4.23	10.22	1.08	24.98
3	4.19	9.90	1.00	24.11
4	4.27	10.33	1.28	29.02
5	4.29	10.59	1.08	23.77
6	4.19	10.40	1.16	26.62
7	4.24	10.37	1.18	26.84
8	4.19	10.18	1.14	26.73
9	4.32	10.27	1.44	32.46
10	4.26	10.32	1.14	25.93

Average	27.07
S.D.	2.76

Appendix 7

DETERMINATION OF PROVISIONAL VALUES FOR PLANE STRAIN FRACTURE TOUGHNESS - Kq

Laminate type: Unreinforced Resin

Specimen No.	"W" (mm)	"a" (mm)	"B" (mm)	"a/W"	f(a/W)	Fq (N)	Kq (MN m^-3/2)
1	15.18	7.86	8.44	0.518	2.819	57	0.611
2	14.84	8.20	8.45	0.553	3.170	47	0.585
3	15.17	8.13	8.44	0.536	2.995	55	0.627
4	15.20	7.95	8.44	0.523	2.868	60	0.653
5	15.20	8.05	8.46	0.530	2.932	59	0.655
6	15.17	8.03	8.46	0.529	2.929	55	0.612
7	15.16	7.97	8.40	0.526	2.894	57	0.631
8	14.51	8.01	8.53	0.552	3.165	46	0.586

Average	**0.620**
S.D.	**0.027**

Laminate type: CSM Glass Fibre

Specimen No.	"W" (mm)	"a" (mm)	"B" (mm)	"a/W"	f(a/W)	Fq (N)	Kq (MN m^-3/2)
1	15.20	8.54	6.59	0.562	3.276	577	9.183
2	14.50	8.20	6.67	0.566	3.319	517	8.840
3	15.19	8.21	6.60	0.540	3.041	678	10.013
4	15.27	8.24	6.57	0.540	3.032	645	9.466
5	15.12	8.38	6.77	0.554	3.189	433	6.582
6	15.27	8.10	6.66	0.530	2.940	735	10.317
7	15.25	8.32	6.68	0.546	3.095	528	7.793
8	15.24	8.39	6.73	0.551	3.148	660	9.846

Average	**9.005**
S.D.	**1.257**

Laminate type: 3 Layer Jute

Specimen No.	"W" (mm)	"a" (mm)	"B" (mm)	"a/W"	f(a/W)	Fq (N)	Kq (MN m^-3/2)
1	15.23	8.72	6.84	0.573	3.404	136	2.161
2	15.14	8.69	6.83	0.574	3.422	120	1.936
3	15.21	8.63	6.80	0.567	3.341	148	2.326
4	15.22	8.60	6.87	0.565	3.313	165	2.543
5	15.39	8.53	6.83	0.554	3.189	186	2.729
6	15.21	8.53	6.85	0.561	3.264	192	2.926
7	15.18	8.59	6.85	0.566	3.323	157	2.443
8	15.17	8.56	6.82	0.564	3.304	195	3.034

Average	**2.512**
S.D.	**0.375**

Laminate type: 6 Layer Jute

Specimen No.	"W" (mm)	"a" (mm)	"B" (mm)	"a/W"	f(a/W)	Fq (N)	Kq (MN m^-3/2)
1	15.09	8.19	7.01	0.543	3.065	288	4.076
2	15.31	8.28	7.01	0.541	3.045	316	4.347
3	15.66	8.30	6.99	0.530	2.936	359	4.616
4	15.25	8.26	7.02	0.542	3.053	307	4.254
5	15.23	8.05	7.01	0.529	2.922	344	4.577
6	15.28	8.31	6.99	0.544	3.076	332	4.642
7	15.32	8.22	7.01	0.537	3.001	294	3.982
8	15.33	8.16	7.04	0.532	2.958	320	4.251

Average	**4.343**
S.D.	**0.250**

Laminate type: 9 Layer Jute

Specimen No.	"W" (mm)	"a" (mm)	"B" (mm)	"a/W"	f(a/W)	Fq (N)	Kq (MN m^-3/2)
1	15.42	8.09	7.11	0.525	2.884	415	5.274
2	15.52	7.85	7.21	0.506	2.712	329	3.841
3	15.56	8.20	7.11	0.527	2.906	431	5.446
4	15.15	8.20	7.13	0.541	3.049	413	5.683
5	15.55	8.13	7.13	0.523	2.867	426	5.300
6	15.62	7.96	7.13	0.510	2.746	487	5.764
7	15.50	8.01	7.10	0.517	2.810	464	5.710
8	15.19	8.06	7.16	0.531	2.942	355	4.674

Average	**5.211**
S.D.	**0.656**

Laminate type: 5 Layer Hemp

Specimen No.	"W" (mm)	"a" (mm)	"B" (mm)	"a/W"	f(a/W)	Fq (N)	Kq (MN m^-3/2)
1	15.25	8.34	6.88	0.547	3.109	216	3.110
2	15.07	8.36	6.87	0.555	3.195	215	3.243
3	15.23	8.40	6.88	0.552	3.159	211	3.093
4	15.31	8.50	6.87	0.555	3.200	219	3.231
5	15.30	8.22	6.87	0.537	3.008	225	3.123
6	15.30	8.54	6.84	0.558	3.233	198	2.967
7	15.26	8.41	6.88	0.551	3.155	202	2.948
8	15.33	8.42	6.86	0.549	3.134	205	2.961

Average	**3.084**
S.D.	**0.117**

Laminate type: 10 Layer Hemp

Specimen No.	"W" (mm)	"a" (mm)	"B" (mm)	"a/W"	f(a/W)	Fq (N)	Kq (MN m^-3/2)
1	15.35	8.26	7.09	0.538	3.017	311	4.175
2	15.30	8.47	7.06	0.554	3.182	368	5.258
3	15.57	8.54	7.04	0.548	3.126	284	3.895
4	15.35	8.60	7.07	0.560	3.257	326	4.739
5	15.24	8.57	7.03	0.562	3.281	264	3.930
6	15.21	8.50	7.08	0.559	3.241	329	4.817
7	15.30	8.76	7.07	0.573	3.404	278	4.243
8	15.09	8.42	7.06	0.558	3.231	315	4.667

Average	**4.465**
S.D.	**0.480**

Laminate type: 15 Layer Hemp

Specimen No.	"W" (mm)	"a" (mm)	"B" (mm)	"a/W"	f(a/W)	Fq (N)	Kq (MN m^-3/2)
1	14.99	8.44	7.18	0.563	3.290	351	5.258
2	15.14	8.42	7.24	0.556	3.210	426	6.084
3	15.34	8.63	7.20	0.563	3.284	422	6.079
4	15.36	8.35	7.21	0.544	3.074	463	6.222
5	15.46	8.43	7.21	0.545	3.092	459	6.143
6	15.40	8.37	7.21	0.544	3.073	401	5.366
7	15.83	8.33	7.17	0.526	2.899	379	4.616
8	15.41	8.11	7.21	0.526	2.899	480	6.054

Average	**5.728**
S.D.	**0.581**

CRITICAL 'J' FRACTURE TOUGHNESS

LAMINATE TYPE: CAST POLYESTER RESIN

	Specimen Dimensions			Pk. Load Co-ords.		Co-ordinates for Initial Gradient Calculation				Total
No.	B (mm)	W (mm)	a (mm)	def. (mm)	L. (kN)	def.1 (mm)	L.1 (mm)	def.2 (mm)	L.2 (mm)	Work (J)
1	8.44	15.18	7.86	201.66	0.0567	201.54	-0.0034	201.66	0.0492	0.00381
2	8.45	14.84	8.2	0.3324	0.04685	0.244	0.0037	0.327	0.0416	0.00308
3	8.44	15.17	8.13	0.0233	0.05477	-0.052	0.0166	0.0097	0.0429	0.00387
4	8.44	15.2	7.95	0.3652	0.05974	0.237	0.0156	0.326	0.0563	0.00393
5	8.46	15.2	8.05	0.2782	0.05853	0.193	0.00786	0.285	0.0499	0.00378
6	8.46	15.17	8.03	0.2552	0.05517	0.158	0.0049	0.247	0.0447	0.00399
7	8.4	15.16	7.97	0.2295	0.05652	0.145	0.0072	0.232	0.0463	0.00355
8	8.53	14.51	8.01	0.3126	0.04631	0.192	0.0133	0.278	0.0446	0.00325

No.	a/W	f(a/W)	K (MPa m^0.5)	E (GPa)	"Ja" (Jm^-2)	Up (J)	"Jb" (Jm^-2)	"J. crit." (kJ m^-2)	Wk. of F. (kJ m^-2)
1	0.518	2.819	0.608	3.8	85	0.0001	5	0.09	0.06
2	0.553	3.170	0.583	3.8	79	0.0007	24	0.10	0.05
3	0.536	2.995	0.624	3.8	90	0.0004	12	0.10	0.07
4	0.523	2.868	0.650	3.8	98	0.0000	1	0.10	0.06
5	0.530	2.932	0.649	3.8	97	0.0000	1	0.10	0.06
6	0.529	2.929	0.613	3.8	87	0.0006	19	0.11	0.07
7	0.526	2.894	0.626	3.8	90	0.0000	0	0.09	0.06
8	0.552	3.165	0.590	3.8	80	0.0003	11	0.09	0.06

Average	88
S.D.	7

9	0.10	0.06
9	0.01	0.00

LAMINATE TYPE: CSM GLASS FIBRE (Vf ~ 0.21)

No.	Specimen Dimensions			Pk. Load Co-ords.		Co-ordinates for Initial Gradient Calculation				Total Work (J)
	B (mm)	W (mm)	a (mm)	def. (mm)	L. (kN)	def.1 (mm)	L.1 (mm)	def.2 (mm)	L.2 (mm)	
1	6.59	15.20	8.54	1.560	0.677	0.256	0.288	0.523	0.445	0.54961
2	6.67	14.50	8.20	2.240	0.555	1.141	-0.003	1.498	0.190	0.47357
3	6.60	15.19	8.21	1.644	0.775	0.060	0.177	0.451	0.434	0.67894
4	6.57	15.27	8.24	1.605	0.778	0.381	0.073	0.846	0.381	0.71965
5	6.77	15.12	8.38	1.666	0.671	0.467	0.103	0.870	0.337	0.57014
6	6.66	15.27	8.10	1.658	0.941	0.336	0.063	0.863	0.451	0.84312
7	6.68	15.25	8.32	1.666	0.795	0.198	0.021	0.721	0.360	0.76646
8	6.73	15.24	8.39	1.442	0.695	0.191	0.000	0.696	0.312	0.54100

No.	a/W	f(a/W)	K (MPa m^0.5)	E (GPa)	"Ja" (Jm^-2)	Up (J)	"Jb" (Jm^-2)	"J. crit." (kJ m^-2)	Wk. of F. (kJ m^-2)
1	0.562	3.276	10.774	7.97	12781	0.1599	7286	20.07	12.52
2	0.566	3.319	9.490	7.97	9915	0.1887	8981	18.90	11.27
3	0.540	3.041	11.445	7.97	14423	0.2219	9635	24.06	14.74
4	0.540	3.032	11.418	7.97	14354	0.2629	11384	25.74	15.58
5	0.554	3.189	10.200	7.97	11456	0.1824	7996	19.45	12.49
6	0.530	2.940	13.209	7.97	19209	0.2418	10126	29.34	17.66
7	0.546	3.095	11.734	7.97	15160	0.2789	12051	27.21	16.56
8	0.551	3.148	10.368	7.97	11835	0.1501	6511	18.35	11.74

Average	13642
S.D.	2856

9246	22.89	14.07
1939	4.24	2.39

LAMINATE TYPE: 3 LAYER JUTE (Vf ~ 0.16)

No.	Specimen Dimensions			Pk. Load Co-ords.		Co-ordinates for Initial Gradient Calculation				Total Work (J)
	B (mm)	W (mm)	a (mm)	def. (mm)	L. (kN)	def.1 (mm)	L.1 (mm)	def.2 (mm)	L.2 (mm)	
1	6.84	15.23	8.72	0.707	0.208	0.115	0.023	0.395	0.145	0.071
2	6.83	15.14	8.69	0.779	0.194	0.189	0.015	0.472	0.138	0.065
3	6.80	15.21	8.63	0.862	0.200	0.146	0.023	0.382	0.127	0.099
4	6.87	15.22	8.60	0.668	0.192	0.120	0.013	0.292	0.091	0.062
5	6.83	15.39	8.53	0.655	0.217	0.114	0.019	0.389	0.147	0.071
6	6.85	15.21	8.53	0.562	0.192	0.099	0.028	0.327	0.130	0.053
7	6.85	15.18	8.59	0.618	0.189	0.115	0.019	0.344	0.118	0.056
8	6.82	15.17	8.56	0.724	0.202	0.085	0.015	0.372	0.147	0.084

No.	a/W	f(a/W)	K (MPa m^0.5)	E (GPa)	"Ja" (Jm^-2)	Up (J)	"Jb" (Jm^-2)	"J. crit." (kJ m^-2)	Wk. of F. (kJ m^-2)
1	0.573	3.404	3.304	6.22	1540	0.0214	959	2.50	1.59
2	0.574	3.422	3.130	6.22	1382	0.0217	985	2.37	1.48
3	0.567	3.341	3.143	6.22	1394	0.0536	2397	3.79	2.21
4	0.565	3.313	2.959	6.22	1235	0.0214	939	2.17	1.36
5	0.554	3.189	3.184	6.22	1431	0.0204	871	2.30	1.52
6	0.561	3.264	2.926	6.22	1208	0.0118	516	1.72	1.16
7	0.566	3.323	2.941	6.22	1221	0.0147	651	1.87	1.24
8	0.564	3.304	3.143	6.22	1393	0.0396	1759	3.15	1.86

Average	**1351**
S.D.	**118**

1135	**2.49**	**1.55**
628	**0.68**	**0.34**

LAMINATE TYPE: 6 LAYER JUTE (Vf ~ 0.31)

No.	Specimen Dimensions			Pk. Load Co-ords.		Co-ordinates for Initial Gradient Calculation				Total Work (J)
	B (mm)	W (mm)	a (mm)	def. (mm)	L. (kN)	def.1 (mm)	L.1 (mm)	def.2 (mm)	L.2 (mm)	
1	7.01	15.09	8.19	0.942	0.336	0.232	0.042	0.565	0.244	0.156
2	7.01	15.31	8.28	0.864	0.338	0.146	0.038	0.467	0.244	0.148
3	6.99	15.66	8.30	0.944	0.383	0.206	0.032	0.513	0.252	0.199
4	7.02	15.25	8.26	0.785	0.345	0.100	0.041	0.402	0.246	0.143
5	7.01	15.23	8.05	0.881	0.358	0.152	0.039	0.491	0.272	0.173
6	6.99	15.28	8.31	0.887	0.353	0.181	0.065	0.500	0.266	0.171
7	7.01	15.32	8.22	0.846	0.340	0.089	0.063	0.445	0.292	0.181
8	7.04	15.33	8.16	0.726	0.341	0.062	0.065	0.402	0.288	0.148

No.	a/W	f(a/W)	K (MPa m^0.5)	E (GPa)	"Ja" (Jm^-2)	Up (J)	"Jb" (Jm^-2)	"J. crit." (kJ m^-2)	Wk. of F. (kJ m^-2)
1	0.543	3.065	4.755	8.39	2365	0.0629	2603	4.97	3.23
2	0.541	3.045	4.650	8.39	2261	0.0590	2394	4.66	3.00
3	0.530	2.936	4.925	8.39	2537	0.0967	3757	6.29	3.87
4	0.542	3.053	4.781	8.39	2390	0.0553	2253	4.64	2.91
5	0.529	2.922	4.763	8.39	2373	0.0798	3170	5.54	3.44
6	0.544	3.076	4.935	8.39	2547	0.0721	2961	5.51	3.51
7	0.537	3.001	4.606	8.39	2219	0.0911	3663	5.88	3.64
8	0.532	2.958	4.529	8.38	2148	0.0594	2352	4.50	2.93

Average	2355
S.D.	142

2894	5.25	3.32
592	0.66	0.35

LAMINATE TYPE: 9 LAYER JUTE (Vf ~ 0.47)

No.	Specimen Dimensions			Pk. Load Co-ords.		Co-ordinates for Initial Gradient Calculation				Total Work (J)
	B (mm)	W (mm)	a (mm)	def. (mm)	L. (kN)	def.1 (mm)	L.1 (mm)	def.2 (mm)	L.2 (mm)	
1	7.11	15.42	8.09	0.898	0.456	0.111	0.063	0.484	0.373	0.234
2	7.21	15.52	7.85	0.968	0.491	0.216	0.114	0.467	0.336	0.233
3	7.11	15.56	8.20	1.027	0.468	0.227	0.066	0.620	0.380	0.251
4	7.13	15.15	8.20	1.055	0.451	0.224	0.048	0.613	0.344	0.252
5	7.13	15.55	8.13	0.577	0.479	-0.111	0.090	0.269	0.399	0.209
6	7.13	15.62	7.96	0.534	0.503	-0.224	0.160	0.159	0.495	0.249
7	7.10	15.50	8.01	0.956	0.490	0.184	0.070	0.623	0.457	0.244
8	7.16	15.19	8.06	1.023	0.426	0.254	0.050	0.571	0.304	0.211

No.	a/W	f(a/W)	K (MPa m^0.5)	E (GPa)	"Ja" (Jm^-2)	Up (J)	"Jb" (Jm^-2)	"J. crit." (kJ m^-2)	Wk. of F. (kJ m^-2)
1	0.525	2.884	5.795	10.76	2739	0.1089	4179	6.92	4.49
2	0.506	2.712	5.732	10.76	2679	0.0967	3498	6.18	4.21
3	0.527	2.906	5.914	10.76	2852	0.1139	4355	7.21	4.80
4	0.541	3.049	6.206	10.76	3141	0.1183	4777	7.92	5.09
5	0.523	2.867	5.959	10.76	2896	0.0679	2568	5.46	3.95
6	0.510	2.746	5.953	10.76	2890	0.1044	3822	6.71	4.56
7	0.517	2.810	6.030	10.76	2965	0.1078	4055	7.02	4.59
8	0.531	2.942	5.609	10.76	2566	0.0978	3830	6.40	4.13

Average	2841		3885	6.73	4.48
S.D.	179		657	0.73	0.37

LAMINATE TYPE: 5 LAYER HEMP (Vf ~ 0.17)

No.	Specimen Dimensions			Pk. Load Co-ords.		Co-ordinates for Initial Gradient Calculation				Total Work (J)
	B (mm)	W (mm)	a (mm)	def. (mm)	L. (kN)	def.1 (mm)	L.1 (mm)	def.2 (mm)	L.2 (mm)	
1	6.88	15.25	8.34	1.121	0.27	0.429	0.0259	0.6	0.104	0.146
2	6.87	15.07	8.36	0.899	0.243	0.294	0.0255	0.47	0.102	0.119
3	6.88	15.23	8.4	1.021	0.241	0.256	0.069	0.408	0.141	0.117
4	6.87	15.31	8.5	0.932	0.25	0.128	0.056	0.264	0.12	0.125
5	6.87	15.3	8.22	0.88	0.26	0.112	0.05	0.288	0.136	0.115
6	6.84	15.3	8.54	1.047	0.247	0.232	0.056	0.45	0.147	0.131
7	6.88	15.26	8.41	0.788	0.206	0.17	0.041	0.352	0.121	0.078
8	6.86	15.33	8.42	0.73	0.238	0.028	0.052	0.161	0.114	0.099

No.	a/W	f(a/W)	K (MPa m^0.5)	E (GPa)	"Ja" (Jm^-2)	Up (J)	"Jb" (Jm^-2)	"J. crit." (kJ m^-2)	Wk. of F. (kJ m^-2)
1	0.547	3.109	3.887	6.22	2131	0.0662	2785	4.92	3.07
2	0.555	3.195	3.665	6.22	1895	0.0511	2216	4.11	2.58
3	0.552	3.159	3.533	6.22	1761	0.0557	2370	4.13	2.49
4	0.555	3.200	3.688	6.22	1919	0.0586	2505	4.42	2.67
5	0.537	3.008	3.609	6.22	1838	0.0458	1884	3.72	2.36
6	0.558	3.233	3.702	6.22	1933	0.0579	2505	4.44	2.83
7	0.551	3.155	3.006	6.22	1275	0.0297	1262	2.54	1.66
8	0.549	3.134	3.437	6.22	1667	0.0382	1614	3.28	2.09

Average	1802
S.D.	253

2143	3.94	2.47
515	0.75	0.44

LAMINATE TYPE: 10 LAYER HEMP (Vf ~ 0.30)

No.	Specimen Dimensions			Pk. Load Co-ords.		Co-ordinates for Initial Gradient Calculation				Total Work (J)
	B (mm)	W (mm)	a (mm)	def. (mm)	L. (kN)	def.1 (mm)	L.1 (mm)	def.2 (mm)	L.2 (mm)	
1	7.09	15.35	8.26	1.118	0.402	0.128	0.067	0.338	0.199	0.255
2	7.06	15.30	8.47	1.191	0.403	0.164	0.045	0.329	0.151	0.266
3	7.04	15.57	8.54	1.053	0.396	0.067	0.074	0.369	0.243	0.340
4	7.07	15.35	8.60	1.315	0.361	0.232	0.099	0.540	0.265	0.273
5	7.03	15.24	8.57	1.135	0.352	0.333	0.034	0.651	0.191	0.209
6	7.08	15.21	8.50	1.261	0.369	0.187	0.060	0.439	0.199	0.257
7	7.07	15.30	8.76	1.103	0.356	0.095	0.045	0.321	0.176	0.224
8	7.06	15.09	8.42	1.152	0.346	0.104	0.061	0.456	0.232	0.228

No.	a/W	f(a/W)	K (MPa m^0.5)	E (GPa)	"Ja" (Jm^-2)	Up (J)	"Jb" (Jm^-2)	"J. crit." (kJ m^-2)	Wk. of F. (kJ m^-2)
1	0.538	3.017	5.397	8.17	3128	0.1265	5031	8.16	5.07
2	0.554	3.182	5.758	8.17	3562	0.1396	5790	9.35	5.52
3	0.548	3.126	5.430	8.17	3167	0.1999	8078	11.24	6.87
4	0.560	3.257	5.247	8.17	2957	0.1521	6374	9.33	5.72
5	0.562	3.281	5.240	8.17	2949	0.0835	3562	6.51	4.46
6	0.559	3.241	5.403	8.17	3135	0.1336	5623	8.76	5.41
7	0.573	3.404	5.434	8.17	3172	0.1147	4960	8.13	4.84
8	0.558	3.231	5.126	8.17	2822	0.1048	4450	7.27	4.84

Average	**3112**
S.D.	**222**

5484	**8.60**	**5.34**
1356	**1.45**	**0.74**

LAMINATE TYPE: 15 LAYER HEMP (Vf ~ 0.42)

No.	Specimen Dimensions			Pk. Load Co-ords.		Co-ordinates for Initial Gradient Calculation				Total Work (J)
	B (mm)	W (mm)	a (mm)	def. (mm)	L. (kN)	def.1 (mm)	L.1 (mm)	def.2 (mm)	L.2 (mm)	
1	7.18	14.99	8.44	1.362	0.409	0.158	0.044	0.442	0.208	0.329
2	7.24	15.14	8.42	1.306	0.474	0.144	0.105	0.419	0.274	0.348
3	7.20	15.34	8.63	1.262	0.455	0.133	0.042	0.536	0.270	0.326
4	7.21	15.36	8.35	1.351	0.537	0.105	0.035	0.486	0.295	0.415
5	7.21	15.46	8.43	1.507	0.551	0.193	0.070	0.607	0.363	0.459
6	7.21	15.40	8.37	1.399	0.522	0.273	0.037	0.710	0.365	0.373
7	7.17	15.83	8.83	1.314	0.594	0.093	0.105	0.386	0.333	0.447
8	7.21	15.41	8.11	1.429	0.587	0.190	0.066	0.621	0.384	0.475

No.	a/W	f(a/W)	K (MPa m^0.5)	E (GPa)	"Ja" (Jm^-2)	Up (J)	"Jb" (Jm^-2)	"J. crit." (kJ m^-2)	Wk. of F. (kJ m^-2)
1	0.563	3.290	6.126	10.02	3287	0.1842	7832	11.12	7.00
2	0.556	3.210	6.770	10.02	4013	0.1652	6791	10.80	7.15
3	0.563	3.284	6.554	10.02	3762	0.1430	5921	9.68	6.75
4	0.544	3.074	7.216	10.02	4560	0.2037	8061	12.62	8.21
5	0.545	3.092	7.374	10.02	4763	0.2445	9648	14.41	9.06
6	0.544	3.073	6.985	10.02	4272	0.1915	7556	11.83	7.36
7	0.558	3.229	8.059	10.02	5688	0.2203	8778	14.47	8.91
8	0.526	2.899	7.404	10.02	4801	0.2415	9177	13.98	9.02

Average	**4393**
S.D.	**736**

7970	**12.36**	**7.93**
1237	**1.80**	**0.98**

Appendix 8

Details of Half-Fringe Photoelasticity system

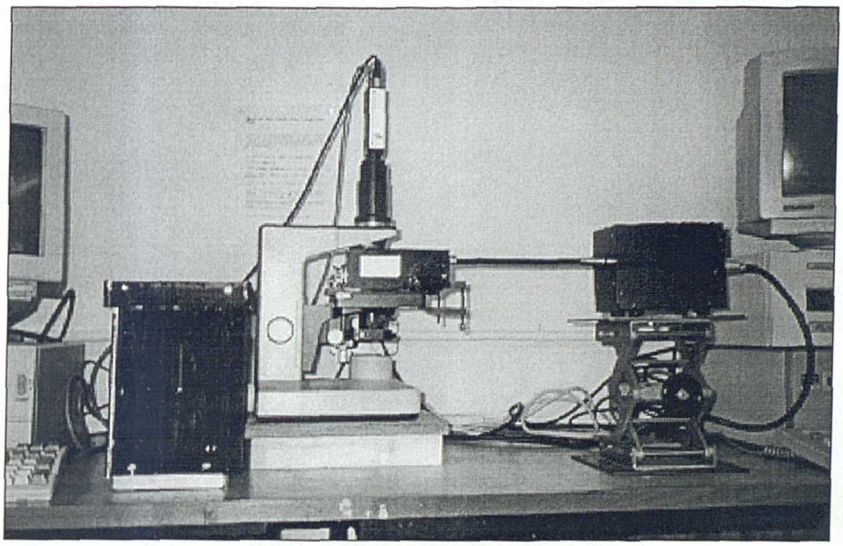

General arrangement of tensile rig set-up showing polariscope, 'Minimat', CCD unit, and stepper motor.

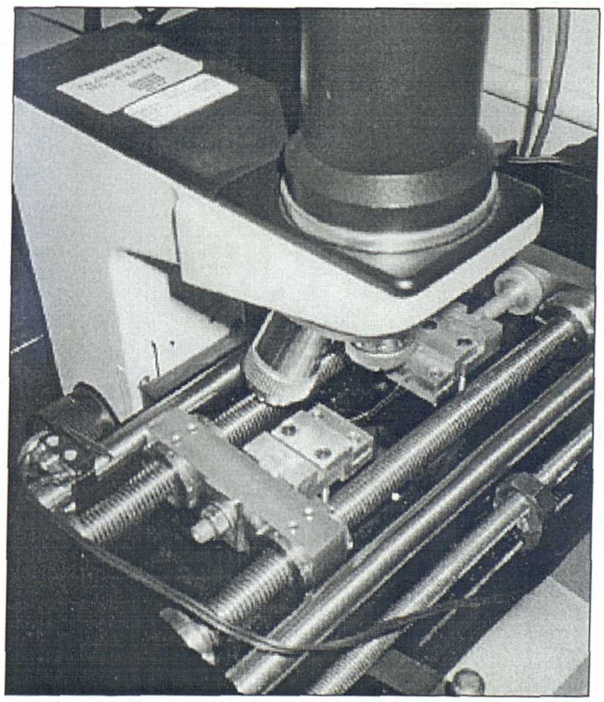

Details of tensile specimen clamping in the 'Minimat'.

Appendix 9

HFP Calibration: grey level versus principal stress difference plots.

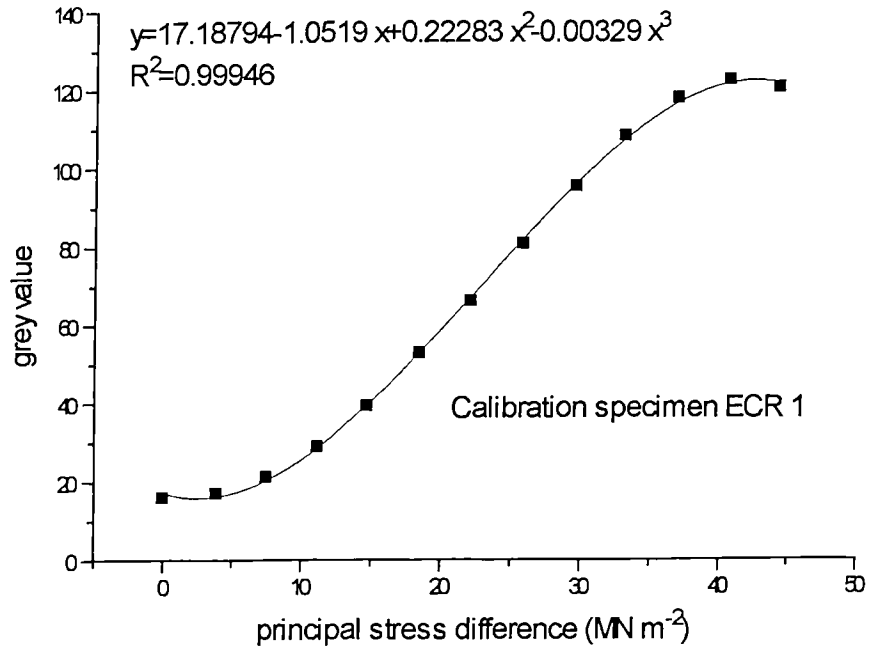

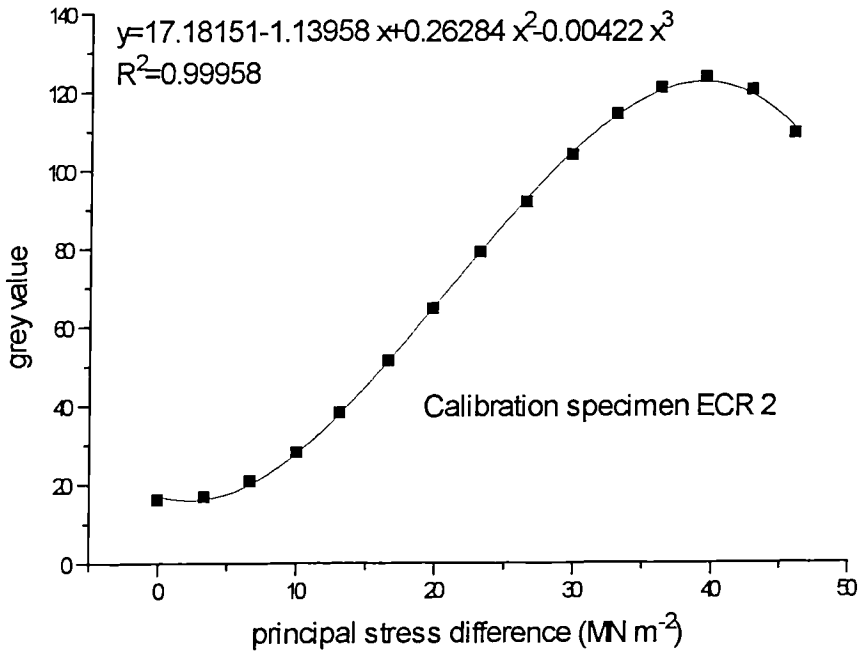

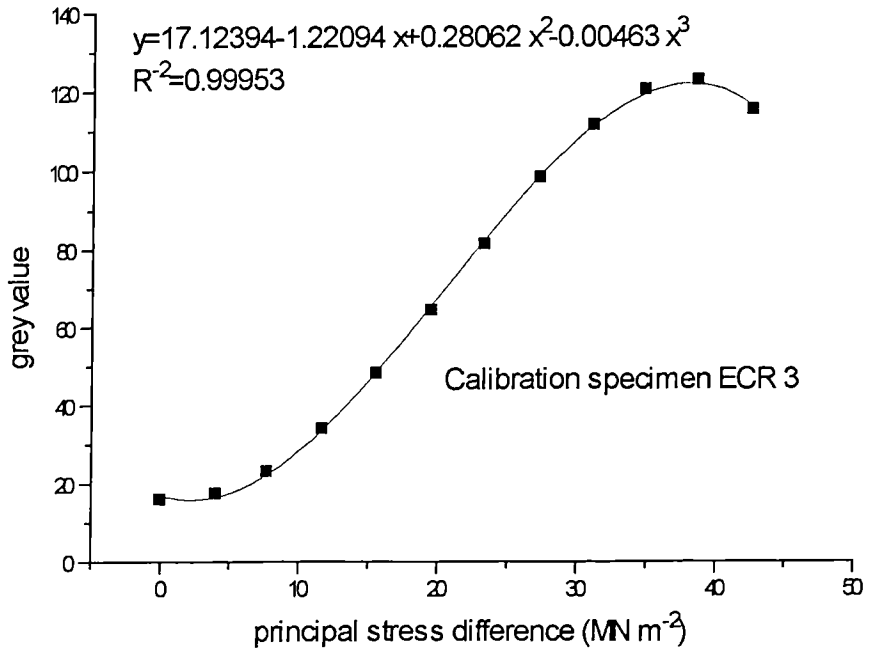
y=17.12394-1.22094 x+0.28062 x2-0.00463 x3
R-2=0.99953
Calibration specimen ECR 3
grey value
principal stress difference (MN m-2)
0
20
40
60
80
100
120
140
0
10
20
30
40
50

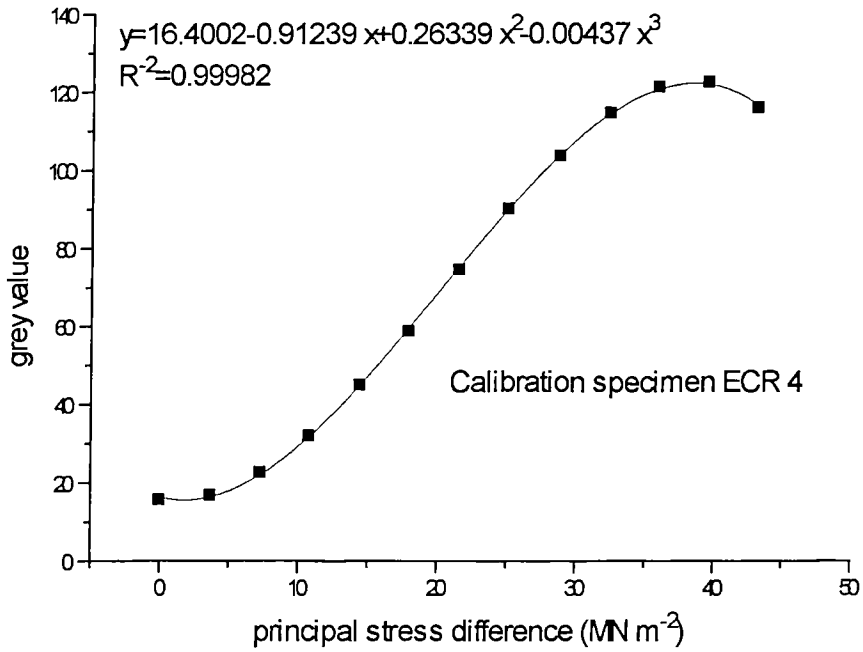
y=16.4002-0.91239 x+0.26339 x2-0.00437 x3
R-2=0.99982
Calibration specimen ECR 4
grey value
principal stress difference (MN m-2)
0
20
40
60
80
100
120
140
0
10
20
30
40
50

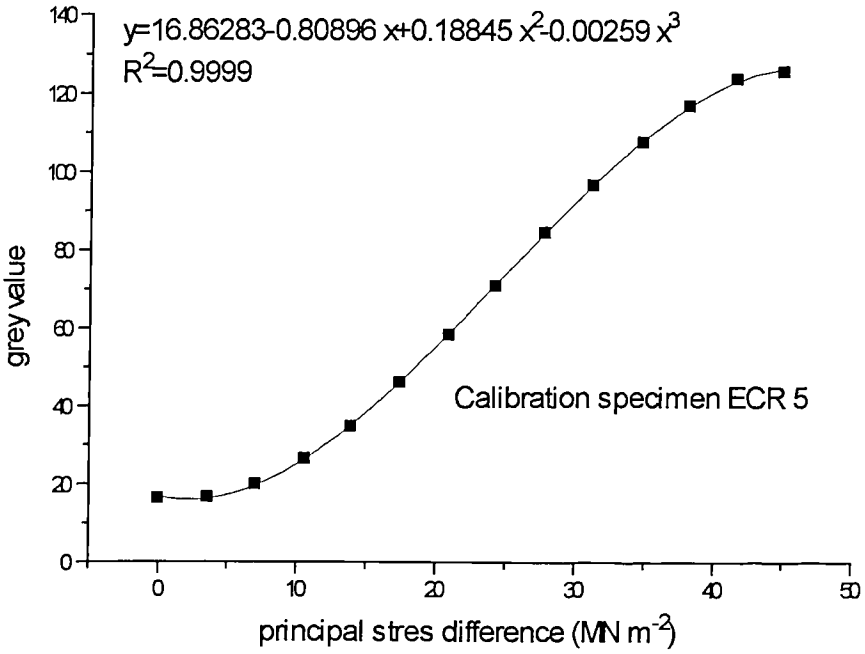
y=16.86283-0.80896 x+0.18845 x2-0.00259 x3
R2=0.9999
Calibration specimen ECR 5
grey value
principal stres difference (MN m-2)
0
20
40
60
80
100
120
140
0
10
20
30
40
50

CALIBRATION OF HALF FRINGE PHOTOELASTICITY SYSTEM

Derivation of material fringe value from regression curve analysis of stress versus grey level value plots

Regression curves in the form: **1st Derivative**

$y = ax^3 + bx^2 + cx + d$ $dy/dx = 3ax^2 + 2bx + c = 0$ (at maxima and minima)

Solution for x, where $Ax^2 + Bx + C = 0$, given by:

$x = (-B+/-(B^2 - 4AC)^{0.5})/2A$

Calibration regression curve functions:

$y = -0.00329x^3 + 0.22283x^2 - 1.0519x + 17.18794$ 1

$y = -0.00422x^3 + 0.26284x^2 - 1.13958x + 17.18151$ 2

$y = -0.00463x^3 + 0.28062x^2 - 1.22094x + 17.12394$ 3

$y = -0.00437x^3 + 0.26339x^2 - 0.91239x + 16.4002$ 4

$y = -0.00259x^3 + 0.18845x^2 - 0.80896x + 16.86283$ 5

Constants				First derivative constants			Stress @ Min-ima	Stress @ Max-ima	Z value Min.	Z value Max.	Spec-imen thick. (mm)	Mat. fringe val. (N/m)
a	b	c	d	A	B	C						
-0.003	0.22	-1.05	17.19	-0.010	0.446	-1.052	2.5	42.7	15.9	122.4	0.13	11090
-0.004	0.26	-1.14	17.18	-0.013	0.526	-1.140	2.3	39.2	15.9	122.2	0.14	10984
-0.005	0.28	-1.22	17.12	-0.014	0.561	-1.221	2.3	38.1	15.7	121.9	0.14	10668
-0.004	0.26	-0.91	16.40	-0.013	0.527	-0.912	1.8	38.4	15.6	122.3	0.14	10743
-0.003	0.19	-0.81	16.86	-0.008	0.377	-0.809	2.3	46.3	16.0	126.3	0.12	11102

Avg.	15.8	122.2	10914
S.D.	0.1	0.3	220

DETERMINATION OF LOG-LINEAR SENSITIVITY CURVE FOR VIDEO CAMERA (GAMMA FUNCTION)

Test specimen:
ECR1

Date of specimen manufacture: 02:02:99
Date of test:
03:12:99

load (N)	stress (MPa)	grey value (*Z* value)	min. grey value	max. grey value	adjusted *Z* value	adjusted max. *Z*	*Z*/Zmax	Npi	Sin(Npi)	Sin^2(Npi)	log (Z/Zmax)	log (sin^2Npi)
0.00	0.00	16.00	15.80	122.20	0.20	106.40	0.00	0.00	0.00	1.00	-2.73	0.00
1.05	3.85	17.20	15.80	122.20	1.40	106.40	0.01	0.14	0.14	0.02	-1.88	-1.70
2.03	7.46	21.40	15.80	122.20	5.60	106.40	0.05	0.28	0.27	0.07	-1.28	-1.13
3.03	11.17	29.00	15.80	122.20	13.20	106.40	0.12	0.41	0.40	0.16	-0.91	-0.79
4.00	14.73	39.40	15.80	122.20	23.60	106.40	0.22	0.54	0.52	0.27	-0.65	-0.57
5.01	18.45	52.80	15.80	122.20	37.00	106.40	0.35	0.68	0.63	0.40	-0.46	-0.40
6.00	22.08	66.20	15.80	122.20	50.40	106.40	0.47	0.82	0.73	0.53	-0.32	-0.28
7.03	25.86	80.90	15.80	122.20	65.10	106.40	0.61	0.96	0.82	0.67	-0.21	-0.18
8.05	29.63	95.40	15.80	122.20	79.60	106.40	0.75	1.09	0.89	0.79	-0.13	-0.10
9.00	33.13	108.20	15.80	122.20	92.40	106.40	0.87	1.22	0.94	0.88	-0.06	-0.05
10.04	36.97	117.70	15.80	122.20	101.90	106.40	0.96	1.37	0.98	0.96	-0.02	-0.02
11.06	40.70	122.40	15.80	122.20	106.60	106.40	1.00	1.50	1.00	1.00	0.00	0.00
12.04	44.31	120.30	15.80	122.20	104.50	106.40	0.98	1.64	1.00	1.00	-0.01	0.00
13.02	47.91	108.00	15.80	122.20	92.20	106.40	0.87	1.77	0.98	0.96	-0.06	-0.02

DETERMINATION OF LOG-LINEAR SENSITIVITY CURVE FOR VIDEO CAMERA (GAMMA FUNCTION)

Test specimen:
ECR2

Date of specimen manufacture: 02:02:99
Date of test:
03:12:99

load (N)	stress (MPa)	grey value (*Z* value)	min. grey value	max. grey value	adjusted *Z* value	adjusted max. *Z*	*Z*/*Z*max	Npi	Sin(Npi)	Sin^2(Npi)	log (Z/Zmax)	log (sin^2Npi)
0.00	0.00	16.10	15.80	122.20	0.30	106.40	0.00	0.00	0.00	1.00	-2.55	0.00
1.02	3.34	16.80	15.80	122.20	1.00	106.40	0.01	0.12	0.12	0.02	-2.03	-1.82
2.04	6.68	20.90	15.80	122.20	5.10	106.40	0.05	0.25	0.24	0.06	-1.32	-1.22
3.06	10.01	28.20	15.80	122.20	12.40	106.40	0.12	0.37	0.36	0.13	-0.93	-0.88
4.00	13.12	38.20	15.80	122.20	22.40	106.40	0.21	0.48	0.47	0.22	-0.68	-0.66
5.07	16.61	51.40	15.80	122.20	35.60	106.40	0.33	0.61	0.58	0.33	-0.48	-0.48
6.04	19.78	64.50	15.80	122.20	48.70	106.40	0.46	0.73	0.67	0.45	-0.34	-0.35
7.06	23.15	79.00	15.80	122.20	63.20	106.40	0.59	0.86	0.75	0.57	-0.23	-0.24
8.08	26.47	91.90	15.80	122.20	76.10	106.40	0.72	0.98	0.83	0.69	-0.15	-0.16
9.07	29.73	103.90	15.80	122.20	88.10	106.40	0.83	1.10	0.89	0.79	-0.08	-0.10
10.05	32.94	114.30	15.80	122.20	98.50	106.40	0.93	1.22	0.94	0.88	-0.03	-0.06
11.03	36.13	120.90	15.80	122.20	105.10	106.40	0.99	1.34	0.97	0.95	-0.01	-0.02
12.02	39.38	123.60	15.80	122.20	107.80	106.40	1.01	1.46	0.99	0.99	0.01	-0.01
13.05	42.75	120.30	15.80	122.20	104.50	106.40	0.98	1.58	1.00	1.00	-0.01	0.00

DETERMINATION OF LOG-LINEAR SENSITIVITY CURVE FOR VIDEO CAMERA (GAMMA FUNCTION)

Test specimen:
ECR3

Date of specimen manufacture: 02:02:99
Date of test:
03:12:99

load (N)	stress (MPa)	grey value (*Z* value)	min. grey value	max. grey value	adjusted *Z* value	adjusted max. *Z*	*Z*/*Z*max	Npi	Sin(Npi)	Sin^2(Npi)	log (Z/Zmax)	log (sin^2Npi)
0.00	0.00	16.00	15.80	122.20	0.20	106.40	0.00	0.00	0.00	1.00	-2.73	0.00
1.04	4.02	17.50	15.80	122.20	1.70	106.40	0.02	0.15	0.15	0.02	-1.80	-1.66
2.00	7.72	23.20	15.80	122.20	7.40	106.40	0.07	0.29	0.28	0.08	-1.16	-1.10
3.02	11.68	34.20	15.80	122.20	18.40	106.40	0.17	0.43	0.42	0.17	-0.76	-0.76
4.03	15.55	48.30	15.80	122.20	32.50	106.40	0.31	0.57	0.54	0.30	-0.52	-0.53
5.04	19.47	64.60	15.80	122.20	48.80	106.40	0.46	0.72	0.66	0.43	-0.34	-0.36
6.03	23.28	81.40	15.80	122.20	65.60	106.40	0.62	0.86	0.76	0.57	-0.21	-0.24
7.06	27.25	98.20	15.80	122.20	82.40	106.40	0.77	1.01	0.85	0.71	-0.11	-0.15
8.05	31.08	111.50	15.80	122.20	95.70	106.40	0.90	1.15	0.91	0.83	-0.05	-0.08
9.01	34.78	120.50	15.80	122.20	104.70	106.40	0.98	1.29	0.96	0.92	-0.01	-0.04
10.00	38.63	122.80	15.80	122.20	107.00	106.40	1.01	1.43	0.99	0.98	0.00	-0.01
11.03	42.59	115.30	15.80	122.20	99.50	106.40	0.94	1.57	1.00	1.00	-0.03	0.00
12.01	46.38	92.30	15.80	122.20	76.50	106.40	0.72	1.71	0.99	0.98	-0.14	-0.01

DETERMINATION OF LOG-LINEAR SENSITIVITY CURVE FOR VIDEO CAMERA (GAMMA FUNCTION)

Test specimen:
ECR4

Date of specimen manufacture: 02:02:99
Date of test:
03:12:99

load (N)	stress (MPa)	grey value (*Z* value)	min. grey value	max. grey value	adjusted *Z* value	adjusted max. *Z*	*Z*/*Z*max	Npi	Sin(Npi)	Sin^2(Npi)	log (Z/Zmax)	log (sin^2Npi)
0.00	0.00	15.90	15.80	122.20	0.10	106.40	0.00	0.00	0.00	1.00	-3.03	0.00
1.04	3.70	16.90	15.80	122.20	1.10	106.40	0.01	0.14	0.14	0.02	-1.99	-1.73
2.03	7.26	22.70	15.80	122.20	6.90	106.40	0.06	0.27	0.26	0.07	-1.19	-1.15
3.02	10.79	32.00	15.80	122.20	16.20	106.40	0.15	0.40	0.39	0.15	-0.82	-0.82
4.04	14.44	45.10	15.80	122.20	29.30	106.40	0.28	0.53	0.51	0.26	-0.56	-0.59
5.02	17.91	58.70	15.80	122.20	42.90	106.40	0.40	0.66	0.61	0.38	-0.39	-0.42
6.03	21.54	74.50	15.80	122.20	58.70	106.40	0.55	0.80	0.71	0.51	-0.26	-0.29
7.01	25.04	90.20	15.80	122.20	74.40	106.40	0.70	0.93	0.80	0.64	-0.16	-0.20
8.04	28.72	103.70	15.80	122.20	87.90	106.40	0.83	1.06	0.87	0.76	-0.08	-0.12
9.05	32.34	114.70	15.80	122.20	98.90	106.40	0.93	1.19	0.93	0.87	-0.03	-0.06
10.03	35.81	121.40	15.80	122.20	105.60	106.40	0.99	1.32	0.97	0.94	0.00	-0.03
11.04	39.43	122.50	15.80	122.20	106.70	106.40	1.00	1.46	0.99	0.99	0.00	-0.01
12.04	43.01	115.90	15.80	122.20	100.10	106.40	0.94	1.59	1.00	1.00	-0.03	0.00
13.01	46.47	99.30	15.80	122.20	83.50	106.40	0.78	1.72	0.99	0.98	-0.11	-0.01

DETERMINATION OF LOG-LINEAR SENSITIVITY CURVE FOR VIDEO CAMERA (GAMMA FUNCTION)

Test specimen:
ECR5

Date of specimen manufacture: 02:02:99
Date of test:
03:12:99

load (N)	stress (MPa)	grey value (*Z* value)	min. grey value	max. grey value	adjusted *Z* value	adjusted max. *Z*	*Z*/*Z*max	Npi	Sin(Npi)	Sin^2(Npi)	log (Z/Zmax)	log (sin^2Npi)
0.00	0.00	16.30	15.80	122.20	0.50	106.40	0.00	0.00	0.00	1.00	-2.33	0.00
1.04	3.58	16.70	15.80	122.20	0.90	106.40	0.01	0.13	0.13	0.02	-2.07	-1.76
2.04	7.04	20.10	15.80	122.20	4.30	106.40	0.04	0.26	0.26	0.07	-1.39	-1.18
3.06	10.58	26.50	15.80	122.20	10.70	106.40	0.10	0.39	0.38	0.15	-1.00	-0.84
4.02	13.89	34.90	15.80	122.20	19.10	106.40	0.18	0.51	0.49	0.24	-0.75	-0.62
5.03	17.40	46.20	15.80	122.20	30.40	106.40	0.29	0.64	0.60	0.36	-0.54	-0.44
6.04	20.90	58.20	15.80	122.20	42.40	106.40	0.40	0.77	0.70	0.49	-0.40	-0.31
7.01	24.25	70.70	15.80	122.20	54.90	106.40	0.52	0.90	0.78	0.61	-0.29	-0.21
8.02	27.74	84.30	15.80	122.20	68.50	106.40	0.64	1.03	0.85	0.73	-0.19	-0.14
9.03	31.21	96.60	15.80	122.20	80.80	106.40	0.76	1.15	0.91	0.84	-0.12	-0.08
10.06	34.77	107.60	15.80	122.20	91.80	106.40	0.86	1.28	0.96	0.92	-0.06	-0.04
11.03	38.15	116.90	15.80	122.20	101.10	106.40	0.95	1.41	0.99	0.97	-0.02	-0.01
12.04	41.63	123.70	15.80	122.20	107.90	106.40	1.01	1.54	1.00	1.00	0.01	0.00
13.01	44.98	125.50	15.80	122.20	109.70	106.40	1.03	1.66	1.00	0.99	0.01	0.00

Plots of $\log\left(\frac{Z}{Z_{max}}\right)$ versus $\log(\sin^2 N\pi)$ to yield camera sensitivity curve gamma

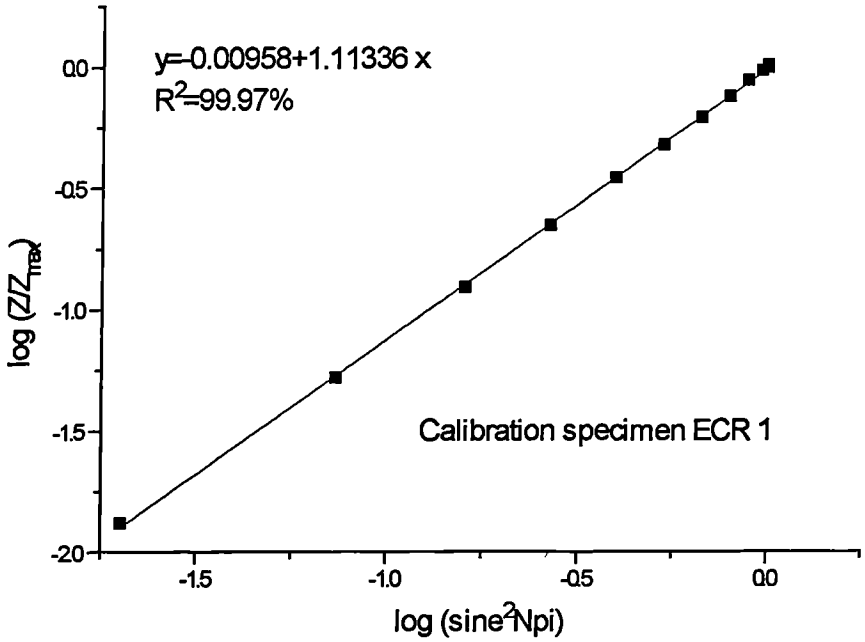

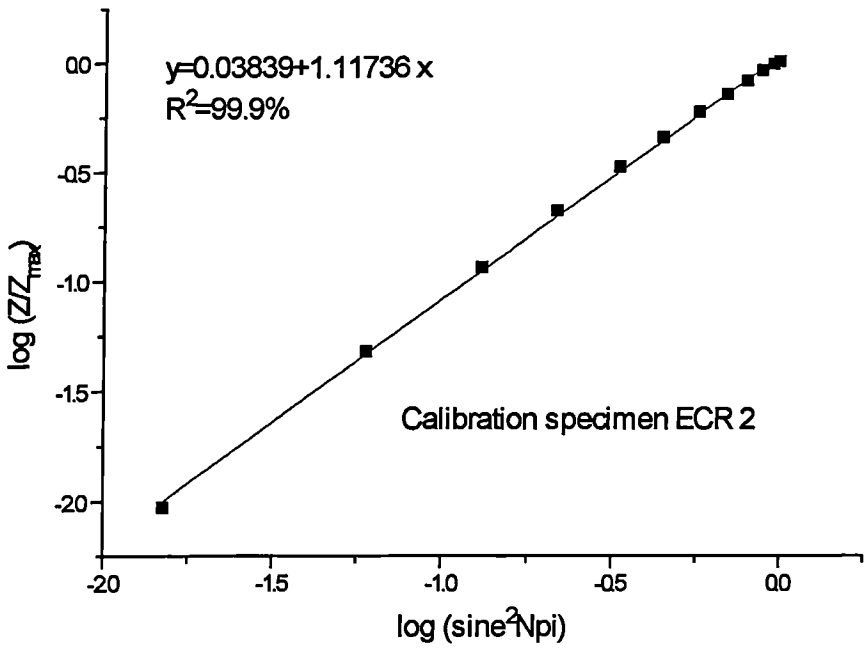

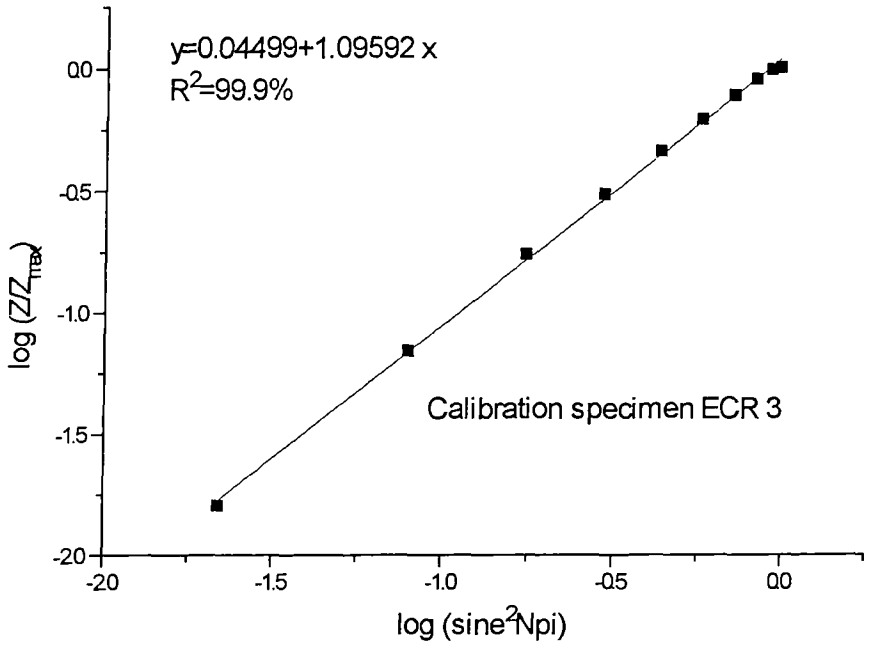
y=0.04499+1.09592 x
R2=99.9%
Calibration specimen ECR 3
log (Z/Zmax)
log (sine2Npi)
0.0
-0.5
-1.0
-1.5
-2.0

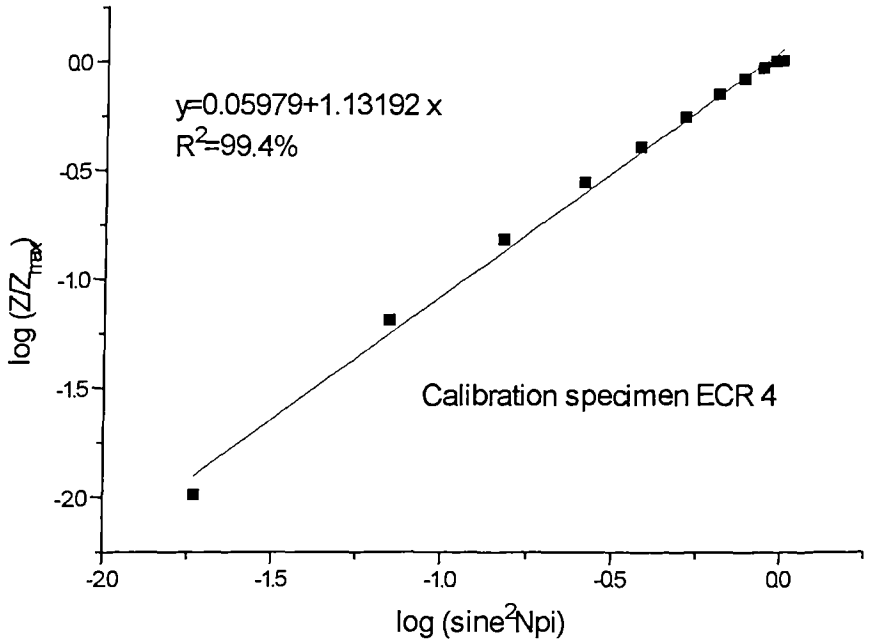
y=0.05979+1.13192 x
R2=99.4%
Calibration specimen ECR 4
log (Z/Zmax)
log (sine2Npi)
0.0
-0.5
-1.0
-1.5
-2.0

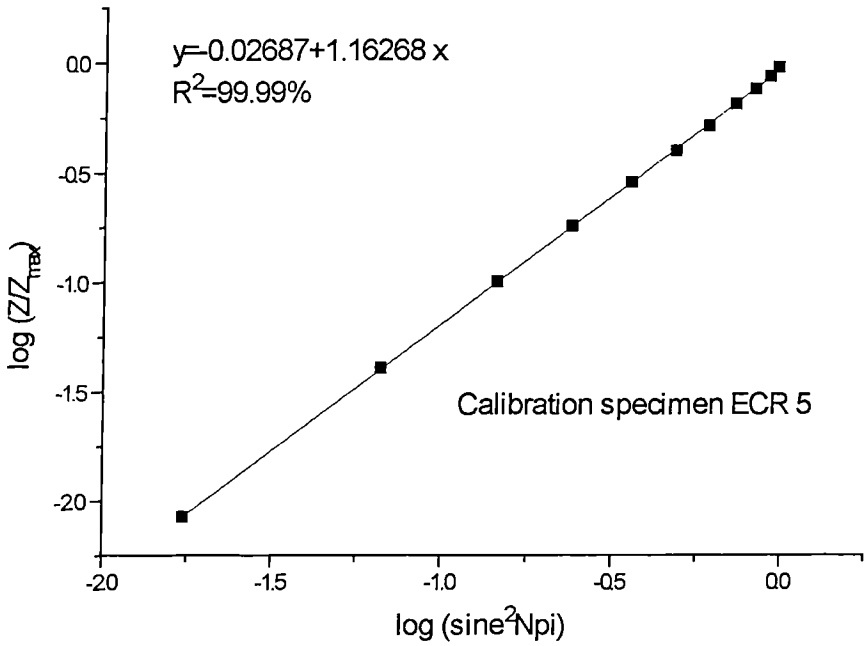

Derived value for Gamma

Specimen - 1	1.11
Specimen - 2	1.12
Specimen - 3	1.10
Specimen – 4	1.13
Specimen - 5	1.16

Average	1.12
S.D.	0.03

Contour maps of partial fringe orders around fibre micro-compressive defects